

**University of Alberta**

**Evaluation of New Co-Volume Mixing Rules for the Peng-Robinson  
Equation of State**

by

**Richard Anthony McFarlane**

A thesis submitted to the Faculty of Graduate Studies and Research  
in partial fulfillment of the requirements for the degree of Master of Science

in  
Chemical Engineering

Department of Chemical and Materials Engineering

Edmonton, Alberta

Fall 2007

*Between the acting of a dreadful thing  
And the first motion, all the interim is  
Like a phantasma, or a hideous dream:  
The Genius and the mortal instruments  
Are then in council; and the state of man,  
Like to a little kingdom, suffers then  
The nature of an insurrection.*

Marcus Junius Brutus Caepio in Julius Caesar, Act 2, Scene 1  
William Shakespeare

*Dedicated to*

*Andrea and my long-suffering (or not) friends*

---

## ABSTRACT

---

The Peng-Robinson cubic equation of state (CEOS) is widely used to predict thermodynamic properties of pure fluids and mixtures. The usual implementation of this CEOS requires critical properties of each fluid component and combining rules for mixtures. Determining critical properties for components of heavy asymmetric mixtures such as bitumen remains a challenge. Several group contribution (GC) methods were applied to determination of critical properties of molecular representations developed by Sheremata for Athabasca vacuum tower bottom (VTB). The Marrero-Gani GC method yielded estimated critical properties and boiling points superior to other methods evaluated. New mixing rules were developed and evaluated for computing co-volumes of asymmetric mixtures. The new mixing rules gave improved bubble point predictions for a binary mixture of n-paraffins. VTB critical properties from the Marrero-Gani GC method led to improved bubble point pressure and liquid density predictions using the classical van der Waals and newly developed mixing rules.

---

## ACKNOWLEDGEMENTS

---

I am grateful for the help and patient guidance of my co-supervisors Professors John Shaw and Murray Gray. They provided the necessary encouragement and enthusiasm, coloured with good humour, to keep me going.

Thanks to Professor Suzanne Kresta for helping me get through her course on fluid mechanics.

My colleagues in the Petroleum Thermodynamics group (Xiaohui Zhang, Bei Zhao, Khanh Tran, Martin Chodakowski, Vasek Lastovka, Michal Fulhem, Annemi Van Waeyenberghe and Nasser Sallamie) were a pleasure to work with. I am particularly grateful to Xiaohui for his kind assistance in helping me understand the operation of the x-ray view cell. Assistance of Andoni Austrich Senosian, visiting Ph.D. student from Instituto Mexicano del Petróleo, in helping to convert the view cell to low pressure operation is much appreciated.

I am grateful to my colleague Shauna Cameron (Alberta Research Council Inc.) for reviewing the draft of this thesis and pointing out my many grammatical mistakes and suggesting changes to make this work clearer. Any errors or ambiguities in this thesis are solely due to my inadequacies.

Feedback and suggestions from my colleagues in the Bitumen Upgrading Group is gratefully acknowledged. I am especially indebted to Jeff Sheremata for sharing his early results on molecular representations for Athabasca bitumen resid. Access to his early work was crucial to the direction and successful completion of this thesis.

The sponsors of the NSERC Industrial Research Chair in Petroleum Thermodynamics are acknowledged: Alberta Energy Research Institute, Computer Modelling Group Ltd., ConocoPhillips, Imperial Oil Resources Ltd., KBR/Halliburton, National Centre for Upgrading Technology, Natural Sciences and Engineering Research Council of Canada, Natural Resources Canada, NEXEN Inc., Petroleum Society of the Canadian Institute of Mining, Metallurgy and Petroleum, Shell Canada Ltd., and Syncrude Canada Ltd.

The sponsors of Syncrude/NSERC Industrial Research Chair in Advanced Upgrading of Bitumen are acknowledged: Alberta Energy Research Institute, Champion

Technologies, National Centre for Upgrading Technology, Natural Sciences and Engineering Research Council of Canada, Natural Resources Canada, and Syncrude Canada Ltd.

Thanks to Prof. Rafiqul Gani (Department of Chemical Engineering, Technical University of Denmark) for kindly providing a copy of the ProPred software which was extremely helpful in applying group contribution methods to the molecular representations produced by Jeff Sheremata.

I am grateful to my employer, Alberta Research Council Inc., for providing me with financial support and for accommodating my schedule while I pursued this degree. I am especially grateful to Dr. Doug Lillico (Manager, Heavy Oil and Oil sands) and Dr. Ian Potter (Vice-President of Energy) for their continued support throughout the past years.

Finally, I would like to thank Andrea for her love, patience, encouragement, and moral support during the past years while I completed my courses and this thesis.

---

## TABLE OF CONTENTS

---

<b>1.0</b>	<b>INTRODUCTION</b>	<b>1</b>
<b>1.1.</b>	<b>Background</b>	<b>1</b>
1.1.1.	<i>Importance of Phase Behaviour and Equations of State</i>	1
1.1.2.	<i>Utility of Cubic Equations of State</i>	4
<b>1.2.</b>	<b>Impetus for Current Study</b>	<b>6</b>
1.2.1.	<i>Production and Processing of Heavy Oil and Bitumen</i>	6
1.2.2.	<i>Critical Properties of Heavy Oil and Bitumen</i>	7
1.2.3.	<i>Size Asymmetry in Heavy Oil and Bitumen Mixtures</i>	9
1.2.4.	<i>Developments in Characterization of Bitumen Vacuum Tower Bottoms</i>	9
<b>1.3.</b>	<b>Objectives</b>	<b>10</b>
1.3.1.	<i>Bubble Point Pressure of Bitumen-Solvent Mixtures</i>	10
1.3.2.	<i>Density of Bitumen-Solvent Mixtures</i>	11
<b>2.0</b>	<b>REVIEW AND HYPOTHESIS</b>	<b>12</b>
<b>2.1.</b>	<b>Scope of Review</b>	<b>12</b>
<b>2.2.</b>	<b>Overview of Cubic Equations Of State</b>	<b>12</b>
2.2.1.	<i>Development of Cubic Equations of State</i>	12
2.2.1.1.	<i>Cubic Equation of van der Waals</i>	12
2.2.1.2.	<i>Relationship between van der Waals CEOS and Virial EOS</i>	16
2.2.1.3.	<i>Improvements to van der Waals Equation</i>	17
2.2.1.3.1.	<i>Redlich-Kwong</i>	18
2.2.1.3.2.	<i>Wilson</i>	19
2.2.1.3.3.	<i>Soave-Redlich-Kwong</i>	21
2.2.1.3.4.	<i>Peng-Robinson</i>	22
2.2.1.3.5.	<i>Twu-Sim-Tassone</i>	23
2.2.1.3.6.	<i>Schmidt-Wenzel</i>	24
2.2.1.3.7.	<i>Improvements to Alpha Functions</i>	25
2.2.2.	<i>Complexity: Ease of Use versus Accuracy</i>	28
<b>2.3.</b>	<b>More Complex Equations of States</b>	<b>31</b>
2.3.1.1.	<i>Quartic Equations of State</i>	32
2.3.1.2.	<i>Accounting for Association</i>	34
2.3.1.3.	<i>Equations of State Based on Perturbation Theory</i>	36
<b>2.4.</b>	<b>Parameters for CEOS</b>	<b>39</b>
2.4.1.	<i>Critical Property Measurements</i>	39
2.4.2.	<i>Properties from Correlations</i>	41
2.4.2.1.	<i>Critical Properties</i>	41
2.4.2.2.	<i>Acentric Factor</i>	46
2.4.3.	<i>Group Contribution Methods</i>	47
2.4.3.1.	<i>Joback-Reid Critical Properties</i>	47
2.4.3.2.	<i>Wilson-Jasperson Critical Properties</i>	48
2.4.3.3.	<i>Marrero-Gani Critical Properties</i>	49

2.4.3.4.	<i>Han-Peng Acentric Factor</i> .....	51
2.4.3.5.	<i>Constantinou-Gani-O'Connell Acentric Factor</i> .....	51
2.4.4.	<i>CEOS based on Group Contribution</i> .....	52
<b>2.5.</b>	<b>Cubic Equations of State for Mixtures</b> .....	<b>55</b>
2.5.1.	<i>van der Waals Mixing Rules</i> .....	55
2.5.2.	<i>Correspondence with Virial Equation of State</i> .....	58
2.5.2.1.	<i>Limitations and Pitfalls</i> .....	60
<b>2.6.</b>	<b>Challenges of Heavy Oil and Bitumen Mixtures</b> .....	<b>61</b>
2.6.1.	<i>Definition and Complexity of Heavy Oil Mixtures</i> .....	62
2.6.1.1.	<i>Characterization by Molecular Structure</i> .....	62
2.6.1.2.	<i>Characterization by Boiling Point</i> .....	63
2.6.2.	<i>Correlations for Critical Properties of Heavy Oil Components</i> .....	64
2.6.2.1.	<i>High Molecular Mass</i> .....	64
2.6.2.2.	<i>Aromaticity and Heteroatoms</i> .....	65
2.6.2.3.	<i>Association</i> .....	66
2.6.3.	<i>Size Asymmetry</i> .....	66
<b>2.7.</b>	<b>Approaches to Dealing with Heavy Oil and Bitumen Mixtures</b> .....	<b>67</b>
2.7.1.	<i>Alpha Functions</i> .....	67
2.7.2.	<i>Composition and Density Dependencies of Mixing Rules</i> .....	69
2.7.3.	<i>Excess Free Energy-Based Mixing Rules</i> .....	72
2.7.4.	<i>Binary Interaction Parameters</i> .....	73
2.7.4.1.	<i>Correlations</i> .....	73
2.7.5.	<i>Volume Translation</i> .....	77
2.7.6.	<i>Group Contribution Methods</i> .....	79
2.7.6.1.	<i>Critical Properties and CEOS</i> .....	79
2.7.6.2.	<i>Binary Interaction Parameters</i> .....	79
<b>2.8.</b>	<b>Hypothesis</b> .....	<b>81</b>
2.8.1.	<i>Rational for Investigation</i> .....	81
2.8.2.	<i>Basis for a New Mixing Rule</i> .....	82
2.8.3.	<i>Proposed Mixing Rules</i> .....	83
<b>2.9.</b>	<b>Outline of Investigation</b> .....	<b>85</b>
<b>3.0</b>	<b>EXPERIMENTAL</b> .....	<b>87</b>
<b>3.1.</b>	<b>X-Ray View Cell</b> .....	<b>87</b>
3.1.1.	<i>General Description</i> .....	87
3.1.2.	<i>Modifications</i> .....	89
<b>3.2.</b>	<b>Fluids Measured</b> .....	<b>92</b>
3.2.1.	<i>Athabasca Bitumen Vacuum Tower Bottoms</i> .....	92
3.2.2.	<i>N-Dodecane</i> .....	94
<b>3.3.</b>	<b>Vapour Pressure Measurement</b> .....	<b>94</b>
3.3.1.	<i>Sample Preparation and Measurement</i> .....	94
3.3.2.	<i>Temperature and Pressure Calibration</i> .....	94
<b>3.4.</b>	<b>Density Measurement</b> .....	<b>95</b>
3.4.1.	<i>Volumetric Calibration</i> .....	95



3.4.2. Property Calculations .....	98
<b>4.0 CRITICAL PROPERTIES FROM VAPOUR PRESSURE DATA.....</b>	<b>99</b>
<b>4.1. Analysis of Vapour Pressure Data.....</b>	<b>99</b>
<b>4.2. Analysis of N-Dodecane Data .....</b>	<b>100</b>
4.2.1. Consistency and Accuracy .....	101
4.2.2. Regression of Fluid Properties .....	107
<b>4.3. Analysis of VTB Data.....</b>	<b>111</b>
4.3.1. Consistency of Data .....	111
4.3.2. Regression of Fluid Properties .....	116
<b>4.4. Summary.....</b>	<b>119</b>
<b>5.0 EVALUATION OF THE GROUP CONTRIBUTION METHOD .....</b>	<b>121</b>
<b>5.1. Composition of Athabasca Residuum .....</b>	<b>121</b>
5.1.1. VTB Fractions from Supercritical Fluid Extraction .....	121
5.1.2. Molecular Representations for VTB.....	123
5.1.3. Regressed Composition for VTB .....	123
<b>5.2. Estimation of Critical Properties for VTB .....</b>	<b>126</b>
5.2.1. GC Methods for Very Large and Complex Molecules.....	127
5.2.2. Critical Properties .....	128
5.2.2.1. Marrero-Gani GC Method .....	128
5.2.2.2. Comparison with Joback and Reid.....	135
5.2.2.3. Comparison with Wilson-Jasperson .....	138
5.2.3. Boiling Point .....	140
5.2.3.1. Marrero-Gani and Joback-Reid GC Methods .....	140
5.2.3.2. Predicted and Measured Distillation Curves.....	141
5.2.4. Acentric Factor.....	141
5.2.5. Density of Model VTB .....	143
<b>5.3. Summary.....</b>	<b>146</b>
<b>6.0 PARTIAL MOLAR VOLUMES AT INFINITE DILUTION .....</b>	<b>148</b>
<b>6.1. Partial Molar Volume of Binary Mixtures .....</b>	<b>148</b>
6.1.1. Generalized Partial Molar Volume at Infinite Dilution .....	150
6.1.2. Calculation Methodology .....	151
<b>6.2. Results.....</b>	<b>152</b>
6.2.1. Two Constrained Critical Properties .....	153
6.2.2. Riazi-Daubert Constrained Critical Properties .....	155
<b>6.3. Summary.....</b>	<b>156</b>
<b>7.0 PREDICTION OF BUBBLE POINT PRESSURE.....</b>	<b>158</b>
<b>7.1. Bubble Point Pressure and Density.....</b>	<b>158</b>
7.1.1. Phase Equilibrium Calculations.....	158
<b>7.2. Ethane/n-Tetradecane Asymmetric Mixture .....</b>	<b>161</b>

<b>7.3. Bubble Point Pressure and Density of VTB/n-decane Mixtures.....</b>	<b>169</b>
7.3.1. 100 wt.% VTB .....	172
7.3.2. 90 wt.% VTB – 10 wt.% N-Decane .....	174
7.3.3. 10 wt.% VTB – 90 wt.% N-Decane .....	178
7.3.4. Sensitivity Analysis .....	180
<b>7.4. Summary.....</b>	<b>182</b>
7.4.1. Ethane/n-Tetratetracontane .....	182
7.4.2. VTB and VTB/n-decane .....	182
<b>8.0 SUMMARY, CONCLUSIONS AND RECOMMENDATIONS.....</b>	<b>185</b>
<b>8.1. Summary and Conclusions .....</b>	<b>185</b>
8.1.1. Introduction .....	185
8.1.2. Main Findings and Conclusions .....	186
<b>8.2. Recommendations .....</b>	<b>188</b>
<b>9.0 REFERENCES.....</b>	<b>190</b>
<b>APPENDIX 1 .....</b>	<b>203</b>
<b>APPENDIX 2 .....</b>	<b>220</b>
<b>APPENDIX 3 .....</b>	<b>224</b>
<b>APPENDIX 4 .....</b>	<b>243</b>
<b>APPENDIX 5 .....</b>	<b>288</b>
<b>APPENDIX 6 .....</b>	<b>311</b>
<b>APPENDIX 7 .....</b>	<b>321</b>

---

## LIST OF TABLES

---

Table 1-1	Definition of oil type by API gravity and density.....	6
Table 2-1	Comparison of the performance of six CEOS (from reference 34) .....	30
Table 2-2	Comparisons of the performance of four EOS (from reference 44).....	31
Table 3-1	Chemical and physical properties of VTB .....	93
Table 4-1	Summary of properties for n-dodecane obtained by regression of vapour pressure data. ....	108
Table 4-2	Summary of properties for n-dodecane obtained by regression of vapour pressure data from Dejoz et al. and densities obtained from the Guggenheim equation.....	109
Table 4-3	Tabulation of experimental vapour pressure and density measurements for VTB. ....	114
Table 4-4	Summary of properties for VTB obtained by regression of vapour pressure data. ....	117
Table 5-1	Summary of bulk properties for the ten supercritical fractions separated from VTB-C.....	122
Table 5-2	Composition of VTB used in the present study in terms of mass fractions of ten supercritically extracted (SCE) fractions and a narrow cut heavy vacuum gas oil (HVGO). ....	126
Table 5-3	GC methods and properties estimated using CAPEC's ProPred software package.....	127
Table 5-4	Results for GC method estimation of critical properties (Marrero-Gani) and acentric factors from Constantinou-Gani-O'Connell (CGO) and Ambrose and Walton (AW) for VTB representational molecules. ....	131
Table 5-5	Calculated molar average properties for model VTB.....	132
Table 5-6	Comparison of estimated density of model VTB fractions with measured values for SCE fractions and heavy vacuum gas oil (HVGO).....	145
Table 6-1	Summary of VTB properties derived from various sources .....	153
Table 6-2	Regressed properties for VTB from measured specific partial volume at infinite dilution in 1-methylnaphthalene and quinoline. Critical properties are constrained by Twu's correlations. ....	155
Table 6-3	Regressed properties for VTB from measured specific partial volume at infinite dilution in 1-methylnaphthalene and quinoline. Critical properties are constrained by Riazi and Daubert's correlations.....	156
Table 7-1	Forms of binary mixing parameters and values for a binary mixture of ethane and n-tetratetracontane. ....	162
Table 7-2	Average absolute error for prediction of bubble point pressure for ethane/n-tetratetracontane at 100°C by applying standard and proposed mixing rules.....	163
Table 7-3	Average absolute error for prediction of bubble point pressure for ethane/n-tetratetracontane at 150°C by applying standard and proposed mixing rules.....	163

Table 7-4	Co-volumes for the liquid phase ethane/n-tetratetracontane calculated using various mixing rules.....	166
Table 7-5	Values of the derivatives of mixing rules for ethane/n-tetratetracontane in the liquid phase.....	168
Table 7-6	Properties for a reduced component representation for VTB.....	171

---

## LIST OF FIGURES

---

Figure 1-1	Balances around an internal stage in a distillation column under total reflux.....	2
Figure 1-2	Effect of error in relative volatility on estimate of minimum number of equilibrium stages for a distillation column under total reflux.....	3
Figure 1-3	A simplified generic bitumen upgrader. ....	8
Figure 2-1	Comparison of calculated critical temperature using Riazi-Daubert correlation versus values from HYSYS-Aspen database. ....	45
Figure 2-2	Comparison of calculated critical pressure using Riazi-Daubert correlation versus values from HYSYS-Aspen database. ....	45
Figure 3-1	Simple schematic of x-ray view cell. ....	88
Figure 3-2	Illustration of x-ray image of VTB at 199.4°C and 21.0 kPa. ....	88
Figure 3-3	Simple P&ID for view cell with heated transducer. ....	91
Figure 3-4	High temperature simulated distillation curve for VTB. ....	93
Figure 3-5	Plot of x-ray image intensity versus pixel number in a line transecting the liquid-gas interface. ....	97
Figure 3-6	Volume calibration curve for x-ray view cell from 70 to 105 mL. ....	97
Figure 4-1	Flowchart for determining critical properties from regression of vapour pressure data. ....	100
Figure 4-2	Plot of ln(vapour pressure) vs. 1/temperature for n-dodecane .....	102
Figure 4-3	Analysis of n-dodecane vapour pressure using Oonk's arc method with reference pressure and temperature of 1 atmosphere and 500K, respectively.....	103
Figure 4-4	Comparison between experimental vapour pressures and those calculated from the data of Dejoz <i>et al.</i> ....	105
Figure 4-5	Trend absolute per cent deviation between experimental and calculated vapour pressure (using data of Dejoz <i>et al.</i> ) versus temperature. ....	105
Figure 4-6	Comparative analysis of n-dodecane vapour pressure data using Oonk's arc method with reference pressure and temperature of 1 kPa and 298.15K, respectively.....	106
Figure 4-7	Measured density of n-dodecane vs. temperature. ....	106
Figure 4-8	Measured density of n-dodecane vs. density calculated from correlation using Guggenheim equation.....	107
Figure 4-9	Comparison of experimentally determined density for n-dodecane with that calculated by the Peng-Robinson CEOS using critical properties from Riazi-Daubert correlation (average absolute relative deviation: 15.2%). ....	110
Figure 4-10	Comparison of experimentally determined density for n-dodecane with that calculated by the Peng-Robinson CEOS using critical properties from Twu correlation (average absolute relative deviation: 15.2%). ....	110
Figure 4-11	Vapour pressure of VTB showing effect of pressure drop due to condensation in pressure transducer and connecting tubing.....	111

Figure 4-12	Vapour pressure of VTB from two series of measurements on the same sample where pressure drops due to condensation was eliminated.....	112
Figure 4-13	Density of VTB versus temperature. ....	114
Figure 4-14	Comparison between vapour pressure data for VTB used in the present study and that used by Schwarz <i>et al.</i> ....	115
Figure 4-15	Comparison between density data for VTB used in the present study and that used by Schwarz <i>et al.</i> .....	116
Figure 4-16	Comparison of experimentally determined density for VTB with that calculated by the Peng-Robinson CEOS using critical properties from Riazi-Daubert correlation (average absolute relative deviation: 10.7%). ....	118
Figure 4-17	Comparison of experimentally determined density for VTB with that calculated by the Peng-Robinson CEOS using critical properties from Twu correlation (average absolute relative deviation: 26.0%). ....	118
Figure 5-1	Comparison of high temperature simulated distillation curve for VTB used in the present study and that separated by supercritical extraction by Chung and coworkers.....	124
Figure 5-2	High temperature simulated distillation curves (from left to right) for narrow cut heavy vacuum gas oil (HVGO) and supercritically extracted fractions 1 through 10.....	125
Figure 5-3	High temperature simulated distillation curves for VTB used in the present study and that for a model based on the ten supercritically extracted (SCE) fractions and a narrow cut heavy vacuum gas oil (HVGO).....	125
Figure 5-4	Critical temperature estimated by the Marrero-Gani GC method versus molecular weight of the representational molecules for VTB.....	133
Figure 5-5	Critical pressure estimated by the Marrero-Gani GC method versus molecular weight of the representational molecules for VTB.....	133
Figure 5-6	Critical volume estimated by the Marrero-Gani GC method versus molecular weight of the representational molecules for VTB.....	134
Figure 5-7	Critical compressibility factor, calculated from critical properties estimated by the Marrero-Gani GC method, versus molecular weight of the representational molecules for VTB.....	134
Figure 5-8	Comparison of critical temperatures estimated by the Joback-Reid and Marrero-Gani GC methods versus molecular weight of the representational molecules for VTB.....	136
Figure 5-9	Comparison of critical pressures estimated by the Joback-Reid and Marrero-Gani GC methods versus molecular weight of the representational molecules for VTB.....	136
Figure 5-10	Comparison of critical volumes estimated by the Joback-Reid and Marrero-Gani GC methods versus molecular weight of the representational molecules for VTB.....	137
Figure 5-11	Critical compressibility factor, calculated critical properties estimated by the Joback-Reid GC method, versus molecular weight of the representational molecules for VTB. ....	137

Figure 5-12	Comparison of critical temperatures estimated by the Wilson-Jasperson and Marrero-Gani GC methods versus molecular weight of the representational molecules for VTB. ....	139
Figure 5-13	Critical compressibility factor, calculated critical properties estimated by the Wilson-Jasperson GC method, versus molecular weight of the representational molecules for VTB.....	139
Figure 5-14	Comparison of normal boiling points estimated by the Joback-Reid and Marrero-Gani GC methods versus molecular weight of the representational molecules for VTB.....	140
Figure 5-15	Comparison of measured high temperature simulated distillation curve for VTB and that calculated from the model comprised of molecular representations and a narrow boiling range heavy vacuum gas oil. ....	141
Figure 5-16	Comparison of acentric factors estimated by the Constantinou-Gani- O'Connell and the GC method and Ambrose-Walton correlation versus molecular weight of the representational molecules for VTB. ....	144
Figure 5-17	Acentric factor vs. molecular weight for simple aromatics from the HYSYS 3.2 database. ....	144
Figure 5-18	Plot of critical compressibility factor calculated from acentric factor versus that calculated from critical properties estimated from the Marrero-Gani GC method. ....	145
Figure 6-1	Flowchart for determining critical properties from regression of specific partial molar volume data.....	152
Figure 6-2	Comparison between the measured specific partial volume of VTB and that predicted by the model using the composite van der Waals and Lee and Sandler mixing rule. ....	154
Figure 7-1	Calculation methodology for bubble point pressure.....	160
Figure 7-2	Comparison of bubble point pressure predictions and data of Gasem <i>et al.</i> with simple mixing rules for mixtures of ethane and n-tetratetracontane at 100°C. ....	164
Figure 7-3	Comparison of bubble point pressure predictions and data of Gasem <i>et al.</i> with composite mixing rules for mixtures of ethane and n-tetratetracontane at 100°C.....	164
Figure 7-4	Comparison of vapour pressures for VTB measured to those predicted from the selected mixing rules. ....	173
Figure 7-5	Comparison of liquid phase densities for VTB measured to those predicted from the selected mixing rules. ....	173
Figure 7-6	Comparison of measured bubble point pressures for 89.95 wt.% VTB mixture with n-decane (data of Zhang) to prediction from the selected mixing rules. ....	175
Figure 7-7	Comparison of measured bubble point pressure or 89.95 wt.% VTB mixture with n-decane (data of Zhang) to prediction from the van der Waals mixing rules and vapour pressure of pure n-decane.....	175
Figure 7-8	Comparison of measured liquid densities for 89.95 wt.% VTB mixture (data of Zhang) with n-decane to prediction from the selected mixing rules. ....	177

Figure 7-9	Comparison of measured bubble point pressures for 89.95 wt.% VTB mixture with n-decane (data of Zhang) to prediction from the selected mixing rules and a single-component representation for VTB. ....	177
Figure 7-10	Comparison of measured liquid densities for 89.95 wt.% VTB mixture with n-decane (data of Zhang) to prediction from the selected mixing rules and a single-component representation for VTB. ....	178
Figure 7-11	Comparison of measured bubble point pressures for 10.03 wt.% VTB mixture with n-decane (data of Zhang) to prediction from the selected mixing rules. ....	179
Figure 7-12	Comparison of measured liquid densities for 10.03 wt.% VTB mixture with n-decane (data of Zhang) to prediction from the selected mixing rules. ....	180
Figure 7-13	Comparison of the seventy and twenty-component representations for VTB for prediction of bubble point pressure with van der Waals mixing rules for 89.95 wt.% VTB mixture with n-decane (data of Zhang). ....	181
Figure 7-14	Comparison of the seventy and twenty-component representations for VTB for prediction of liquid phase density with van der Waals mixing rules for 89.95 wt.% VTB mixture with n-decane (data of Zhang). ....	181



---

## NOMENCLATURE

---

### Notations

<b>a</b>	Cubic equation of state term corresponding to attractive forces
<b>b</b>	Co-volume for cubic equation of state corresponding to repulsive forces
<b>GC</b>	Group contribution method
<b>f</b>	Fugacity
<b>F<sub>i</sub></b>	Molar flow rate
<b>G</b>	Gibbs molar free energy
<b>H</b>	Molar enthalpy
<b>K</b>	K value (x/y)
<b>K<sub>eq</sub></b>	Equilibrium constant
<b>k<sub>ij</sub></b>	Binary interaction parameter
<b>L</b>	Liquid
<b>m<sub>ij</sub></b>	Binary mixing parameter
<b>n</b>	Moles
<b>P</b>	Pressure
<b>R</b>	Gas constant
<b>SG</b>	Specific gravity
<b>SRK</b>	Soave-Redlich-Kwong (equation of state)
<b>T</b>	Temperature
$\bar{V}_i$	Partial molar volume
$\bar{V}_i^{\infty}$	Partial molar volume at infinite dilution
$\bar{v}_i^{\infty}$	Specific partial volume at infinite dilution
$\underline{V}_t$	Total volume of the system (extensive property)
<b>v</b>	Molar volume
<b>V</b>	Vapour or molar volume
<b>VLE</b>	Vapour-liquid equilibrium
<b>x<sub>i</sub></b>	Molefraction in the liquid phase

$y_i$	Molefraction in the vapour phase
$z_i$	Molefraction in the feed
$Z$	Compressibility factor
<b>Subscripts</b>	
$i$	$i^{\text{th}}$ component
$c$	Critical condition
<b>mix</b>	Mixture
$r$	Reduced property, ratio at current condition to that at critical condition
<b>Superscripts</b>	
$\infty$	Infinite dilution

### Greek Symbols

$\alpha$	alpha-function; temperature dependent part of attractive parameter
$\alpha_{AB}$	Relative volatility ( $K_A/K_B$ )
$\mu$	Chemical potential
$\xi$	Fraction of feed in the vapour phase
$\rho$	Density
$\varphi$	Fugacity coefficient
$\omega$	Acentric factor, Pitzer acentric factor, acentricity

### Abbreviations

<b>CEOS</b>	Cubic equation of state
<b>EOS</b>	Equation of state
<b>GC</b>	Group contribution
<b>HTSD</b>	High temperature simulated distillation
<b>HVGO</b>	Heavy vacuum gas oil
<b>NMR</b>	Nuclear magnetic resonance
<b>PR</b>	Peng - Robinson (cubic equation of state)
<b>PVT</b>	Pressure-volume-temperature; phase space

<b>SCE</b>	Supercritical extraction
<b>SCO</b>	Synthetic crude oil
<b>SG</b>	Specific Gravity
<b>SRK</b>	Soave-Redlich-Kwong (cubic equation of state)
<b>TARE</b>	Total absolute relative error
<b>vdW</b>	van der Waals (cubic equation of state or mixing rule)
<b>VLE</b>	Vapour-liquid equilibrium
<b>VLLE</b>	Vapour-liquid-liquid equilibrium
<b>VTB</b>	Athabasca bitumen vacuum tower bottoms

---

## 1.0 INTRODUCTION

---

### 1.1. BACKGROUND

#### 1.1.1. *Importance of Phase Behaviour and Equations of State*

Efficient design of chemical processes depends on a good understanding of phase behaviour and the ability to predict thermodynamic properties such as pressure, density, enthalpy, entropy, and heat capacity of pure fluids and mixtures<sup>1</sup>. All of these thermodynamic properties can be derived from equations of state (EOS) and fundamental thermodynamic relationships. For the past 134 years, since van der Waals proposed the first equation of state that could successfully predict liquid-vapour phase behaviour<sup>2</sup>, development and modification of equations of state have been active areas of research<sup>3</sup>. Despite such efforts, an equation of state that can accurately predict the phase behaviour and thermodynamic properties of a wide variety of fluids over a wide range of conditions remains elusive. However, many equations of state can be used to fit experimentally observed phase behaviour using inputs based on measured or correlated properties of the pure components such as critical temperature and pressure. Once fitted, such equations of state can be used to predict phase behaviour over a range limited by that of the fitted data.

In the design, analysis, and operation of even the simplest chemical processes involving more than one phase, an equation of state that can give reliable predictions over a wide range of pressures, temperatures, and compositions can be essential. The importance of phase behaviour is not only manifested in the operation of chemical plants but in seemingly unrelated areas such as: (a) oil and gas production and transportation, and (b) planetary geochemistry (e.g., water on Mars and gas-liquid-solid phase behaviour on the surface Jupiter). The current work represents part of an ongoing effort to improve the performance of equations of state that can lead to efficient designs for heavy oil and bitumen production, transportation, and processing.

One simple example of the importance of accurate phase behaviour predictions for unit design can be illustrated by an examination of the balances around the feed stage of a distillation column (Figure 1-1). At each equilibrium stage in the column, the relative proportion of a component in the vapour phase to that in the liquid phase (i.e., K-value)

is an important parameter that can be calculated using an equation of state. For distillation of a binary mixture of components A and B, where A is the more volatile component, the relative volatility,  $\alpha_{AB}$ , determines how easily the components can be separated using vapour-liquid equilibrium (VLE) and is related to the K-values:

$$\alpha_{AB} = \frac{K_A}{K_B} \quad (1.1)$$

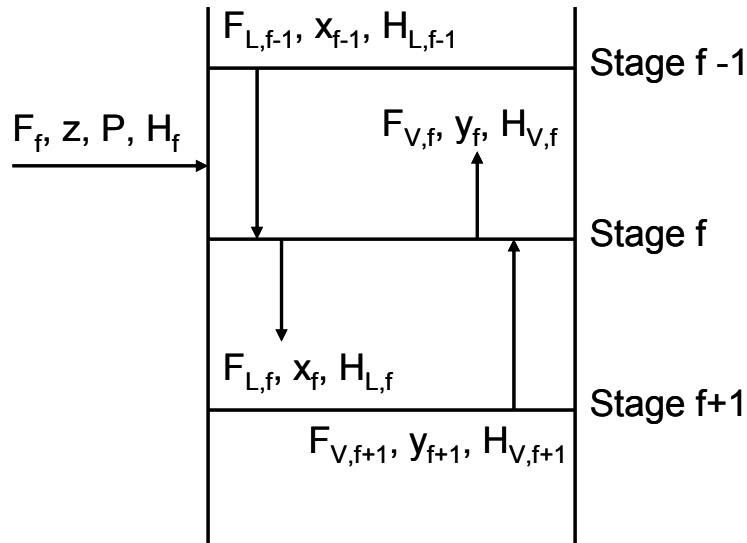


Figure 1-1 Balances around an internal stage in a distillation column under total reflux.

For the optimum design of a distillation tower, the minimum number of equilibrium stages required to achieve separation of component A and B to a specified purity is a useful guide. The minimum number of equilibrium stages to achieve specified compositions in the reboiler ( $x_{A,R}$ ) and condenser ( $x_{A,C}$ ) can be estimated using the Fenske equation:

$$\text{Min. Number of Stages} = \frac{\ln \left[ \frac{x_{AC}(1-x_{AR})}{x_{AR}(1-x_{AC})} \right]}{\ln(\alpha_{AB})} \quad (1.2)$$

Figure 1-2 provides some insights into how errors in the relative volatility calculated from an equation of state might result in over- or under-estimation of the minimum number of stages. Note that this example is for large values of relative volatility. As the relative volatility gets closer to unity, e.g., for separation isomers or homologues, the impact of errors on the number of stages becomes more significant.

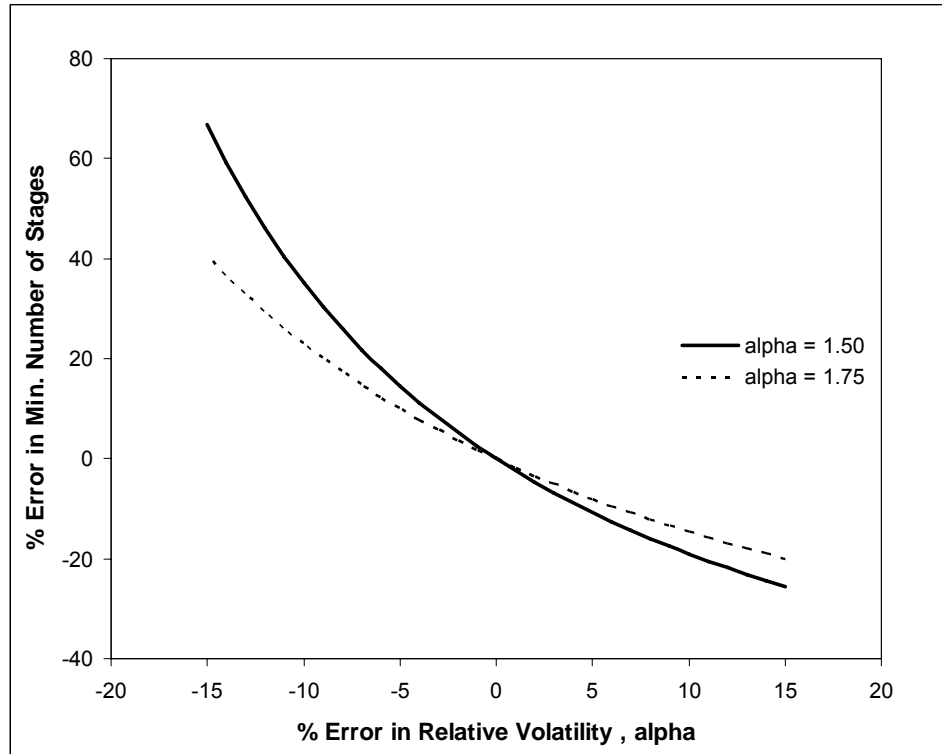


Figure 1-2 Effect of error in relative volatility on estimate of minimum number of equilibrium stages for a distillation column under total reflux.

The Fenske relationship, equation (1.2), has built in assumptions regarding the independence of relative volatility from temperature and composition. Nevertheless, in practice, this type of result implies that unless empirical data are available, the choice and accuracy of the equation of state can lead to under-design and poor performance or over-design and waste of capital resources. In either case, the process will not operate as designed. In any chemical plant, there are many equilibrium processes whose design and operations can be understood through the use of an appropriate equation of state. Similarly, in heavy oil and bitumen recovery, transportation and conversion, variations

of pressure, temperature, and composition can have profound effects on phase behaviour and thereby process operations. Improved equations of state can, therefore, contribute to better process design, improved operation, and greater efficiency in the use of raw materials, equipment, and capital in the energy and chemicals industries.

### 1.1.2. Utility of Cubic Equations of State

The van der Waals (vdW) cubic equation of state (CEOS) was the first equation of state that was able to successfully predict, at least qualitatively, vapour-liquid equilibrium phase behaviour:

$$P = \frac{RT}{v-b} - \frac{a}{v^2} \quad (1.3)$$

The van der Waals CEOS contains only two parameters, 'a' and 'b', the attractive energy and co-volume parameters, respectively, and is classed as a two-parameter CEOS. Both of these parameters can be calculated from critical temperature ( $T_c$ ) and pressure ( $P_c$ ) which are widely tabulated for simple molecules. For pure fluids, the van der Waals CEOS has an easy analytical solution. For fluid mixtures, mixing rules are required to calculate the overall attractive energy and co-volume parameters. The simplest mixing rules are the so-called van der Waals mixing rules which are the geometric mean mixing rule for the attractive term and the linear mixing rule for the co-volume:

$$a_{mix} = \sum_i \sum_j x_i x_j \sqrt{a_{ii} a_{jj}} \quad (1.4)$$

$$b_{mix} = \sum_i x_i b_i \quad (1.5)$$

Early successful modifications to improve the predictive capabilities of the van der Waals EOS have included making 'a' temperature dependent along with the introduction of a third molecular parameter in the form of the acentric factor ( $\omega$ ). Still further improvements were made for polar, associating and heavier hydrocarbons by

the introduction of the binary interaction parameter and composition or density dependence to the geometric means mixing rule in equation(1.4). Rarely, the linear mixing rule has been modified by using geometric or other types of averages as well as other adjustable parameters similar to the binary interaction parameter for the energy term. Despite such modifications, the most widely used cubic equations of state still only required knowledge of three critical properties ( $T_c$ ,  $P_c$  and  $\omega$ ) for the pure fluid which can be obtained by measurements (tabulated for many simple pure fluids) or by correlation (e.g., those based on normal boiling point and specific gravity).

CEOS remain the most widely used types of equation of state due to their mathematical simplicity and the ease with which the molecular parameters (critical properties) required to solve them can be obtained or estimated. The mathematical simplicity makes it easy to implement the cubic equation of state in routine as well as complex iterative calculations to estimate phase behaviour and other properties of fluids in designs for large integrated chemical plants. Such mathematical simplicity was important when computers were not as powerful as those available today where even simple handled calculators could be used to solve CEOS. More importantly, the availability of critical properties for components from established databases and the ease of calculation of these parameters for newly synthesized simple components mean that cubic equation of states can be applied to almost any mixtures or component encountered in any chemical process in any industry.

Of course, there are limitations to the application of CEOS, which will be discussed in the following chapter, but CEOS still have much wider applicability than any other extant equation of state. Newer and more complex equations of state, which can be handled by today's more power computers and that can give more accurate predictions for some phase behaviour and thermodynamic properties, have been and continue to be developed. In this regard, the popularity of CEOS poses a dilemma for the chemical engineering community for the development of new processes and new chemistry while at the same time meeting increasing requirements for efficiency in design and operation. One approach to dealing with this dilemma is to accept the popularity of CEOS and try to continuously improve them for application to new challenges such as bitumen processing.



## 1.2. IMPETUS FOR CURRENT STUDY

### 1.2.1. Production and Processing of Heavy Oil and Bitumen

World production of crude oils, arbitrarily defined in terms of gravity and viscosity (Table 1-1; see for example Gray<sup>4</sup> and Speight<sup>5</sup>), increasingly includes heavy and extra-heavy oils such as bitumen as production of conventional light and medium crudes decline. Athabasca bitumen is on its way to being the dominant source of liquid hydrocarbons produced in Western Canada. In Alberta, Athabasca bitumen already represents more than 50% of total oil production and this proportion will increase since the production of light, medium, and heavy crudes from the Western Sedimentary Basin continues to decline since peak production was achieved in 1998. It is estimated that by 2015 about 3 million barrels per day of synthetic crude oil (SCO) will be produced from Athabasca bitumen<sup>6</sup>. Phase behaviour and thermodynamic properties of heavy oil and bitumen are extremely important for production<sup>7</sup>, pipeline transportation<sup>8</sup>, upgrading<sup>9</sup>, and refining.

**Table 1-1 Definition of oil type by API gravity and density**

<b>Oil Type</b>	<b>°API Gravity</b>	<b>Density (kg/m<sup>3</sup>)</b>	<b>Viscosity (cP)</b>
<b>Light</b>	<b>&gt; 31.1</b>	<b>870</b>	<b>&lt; 10</b>
<b>Medium</b>	<b>22.3 - 31.1</b>	<b>920 - 870</b>	<b>10 - 100</b>
<b>Heavy</b>	<b>10 - 22.3</b>	<b>920 - 1000</b>	<b>100 - 10,000</b>
<b>Extra-heavy or Bitumen</b>	<b>&lt;10</b>	<b>&gt;1000</b>	<b>&gt; 10,000</b>

*In situ* bitumen recovery processes that are based on injection of steam or solvents rely on complex phase behaviours between steam, solvent, and oil components in the reservoir, well bore, and at the surface handling facilities. Phase behaviour of the oil itself can range from simple gas-liquid to gas-liquid-solid behaviour and the presence of immiscible water adds an additional layer of complexity. In the case of pipeline transportation of heavy oil and bitumen, diluents in the form of light hydrocarbons such as natural gas condensates are added to dilute the viscous crude. The presence of these diluents, intermingling with other crudes in transit as well as the conditions in the pipelines and intermediate storage can lead to liquid-liquid or solid-liquid phase

behaviours which can have deleterious impact on the transportation infrastructure and pipeline scheduling.

A simplified outline of a generic bitumen upgrader is shown in Figure 1-3. During the upgrading, naphtha-diluted Athabasca bitumen from the recovery process undergoes a series of physical separations prior to being subjected to conversion processes which ultimately lead to the production of synthetic crude oil (SCO). The diluted bitumen is first distilled in an atmospheric unit to recover the naphtha diluent which is recycled back to recovery processes. The topped bitumen is then sent to a vacuum distillation unit where the operating pressure may be about 3 to 5 kPa and the reboiler temperature about 350°C. Light and heavy gas oil cuts are recovered and sent to hydrotreaters while the residue or vacuum tower bottoms (VTB) is sent to cokers or residue hydrocrackers, depending on the upgrader configuration. VTB typically amounts to about 50 wt.% of Athabasca bitumen.

#### *1.2.2. Critical Properties of Heavy Oil and Bitumen*

Generally, the increasing density and viscosity of heavy crudes and bitumen compared to light and medium crude oils, is due to increasing molecular weights and aromatic carbon, sulphur, oxygen, and nitrogen contents<sup>4, 5, 10</sup>. These properties of heavy oil and bitumen also correlate with components (distillate fractions) having much higher boiling point compared to those in light crudes. The critical properties can be difficult or impossible to measure for heavy oil and bitumen fractions due to thermal reactions that can occur below their high critical temperatures or even below their boiling points. Estimation of critical properties can also be problematic and subject to large errors since most of the correlations and group contribution methods for estimating such properties have been developed for light crudes with lower densities, boiling points, and molecular weights. These challenges are further exacerbated when a large portion of the heavy oil or bitumen cannot be separated by distillation, due to high boiling points and thermal reactivity. Without fractionation, these heavy components cannot be characterized to provide input data for correlations to determine critical properties. In the case of Athabasca bitumen, this means that about 50% of the crude cannot be accurately described to provide reliable input properties for a cubic equation of state.

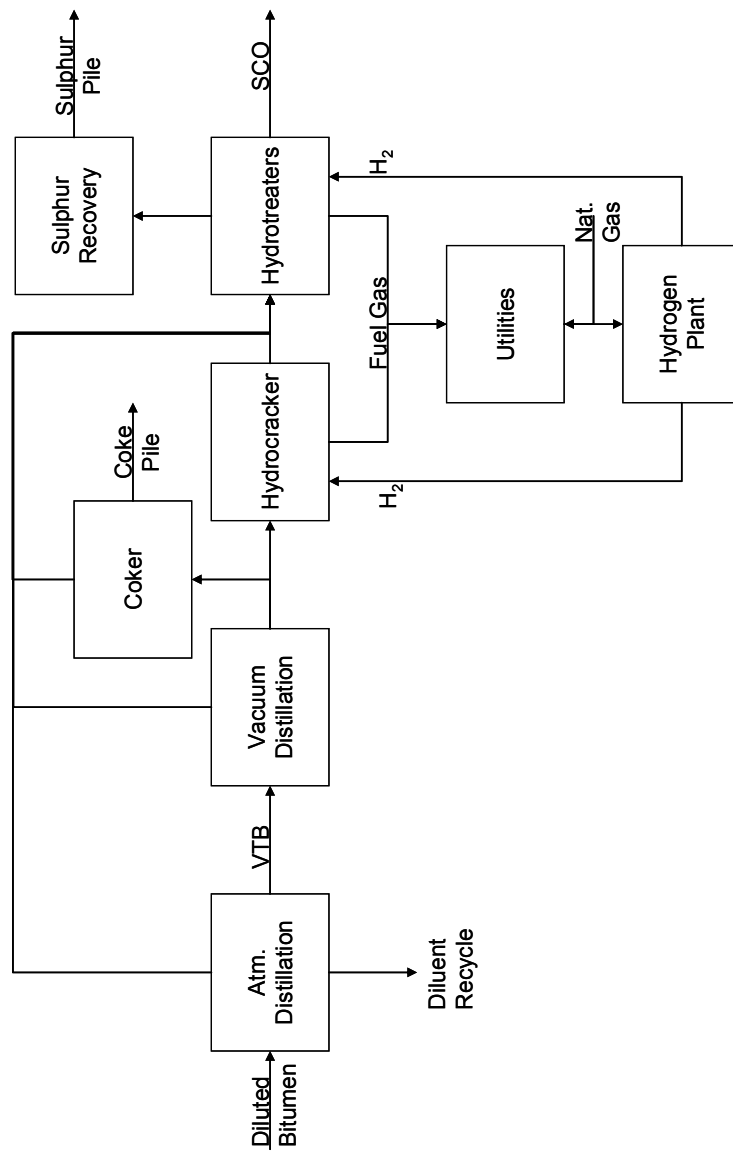


Figure 1-3 A simplified generic bitumen upgrader.

### 1.2.3. Size Asymmetry in Heavy Oil and Bitumen Mixtures

Compared to light and medium crudes, heavy oil and bitumen encompass molecules having a much wider boiling range, and therefore, a broader distribution of molecular sizes. The size asymmetry between small and large molecules, leads to more complex phase behaviours<sup>11</sup> which are poorly predicted by cubic equations of state. The high levels of aromatics and heteroatoms also make heavy oil and bitumen mixtures asymmetric in terms of polarity. The higher degree of aromaticity and content of polar heteroatoms (oxygen and nitrogen) can lead to molecular associations which are difficult to handle using cubic equations of state that have no built-in ability to handle associative interactions dependent on molecular orientation.

Over many years, cubic equations of state have been refined to allow good estimates and predictions for light to medium crude oils. More accurate predictions of phase behaviour for Athabasca bitumen are desired for development of new and efficient processes and enhancement of the operability and efficiency of existing processes. To date, refinements to address shortcomings of CEOS with respect to size and polarity asymmetry have mainly focused on the attractive term and mostly neglected the repulsive or co-volume term. Based on the underlying relationships between co-volume and molecular size, and the wide asymmetry in molecular sizes of components in Athabasca bitumen, a new focus on the co-volume term in CEOS is warranted.

### 1.2.4. Developments in Characterization of Bitumen Vacuum Tower Bottoms

Being able to predict the phase behaviour and thermodynamic properties of VTB is clearly important to all aspects of bitumen production, transportation as diluted bitumen, and conversion to SCO. Fortunately, much more data is becoming available about the properties of VTB. Chung *et al.*<sup>12</sup> separated Athabasca bitumen vacuum tower bottoms into ten fractions by n-pentane supercritical fluid extraction. These fractions have been extensively characterized in terms of physical and molecular properties<sup>13, 14</sup>. Some of these physical properties can be used with various correlations to predict critical properties ( $T_c$ ,  $P_c$  and  $\omega$ ) required for a cubic equation of state. Recently, Sheremata *et al.*<sup>15, 16</sup> used these analytical data along with NMR molecular structural information to develop optimized molecular representations of VTB. With such

molecular representations it is now possible to use group contribution methods to estimate the critical properties of VTB for input to an equation of state. It is also fortuitous that recent development in group contribution (GC) methods by Marrero and Gani<sup>17</sup> now allow us to estimate critical properties for such large and complex molecules. Thus, we have a choice between two methodologies (correlations and GC methods) to obtain critical properties of VTB. With such data, it becomes possible to carry out calculations to predict the phase behaviour of fluid mixtures containing VTB.

### 1.3. OBJECTIVES

The overall objective of this work was to investigate some alternate mixing rules for the co-volume parameter of size-asymmetric mixtures of Athabasca bitumen vacuum tower bottoms. One of the most widely used equations of state which has been applied to the phase behaviour of hydrocarbons is the Peng-Robinson CEOS<sup>18</sup>. This equation of state has its roots in the van der Waals CEOS but differs in the form of the attractive energy term. Although the Peng-Robinson CEOS has the same general weaknesses of all such CEOS, it generally leads to physically reasonable solutions. Therefore, Peng-Robinson CEOS was chosen as the equation of state for evaluation of some new alternate mixing rules for the co-volume parameter.

#### 1.3.1. *Bubble Point Pressure of Bitumen-Solvent Mixtures*

The ability to accurately predict component vapour pressure is a necessary although not sufficient, criterion for cubic equations of state to also accurately predict vapour-liquid equilibrium (VLE) as well as other types of phase behaviours and thermodynamic properties<sup>19</sup>. Thus, one objective of this work was to measure the vapour pressure of Athabasca bitumen vacuum tower bottoms and to compare this result to estimates obtained from the Peng-Robinson equation of state using van der Waals mixing rules with critical properties derived either from correlation of physical properties or molecular group contribution methods. The second, but related, objective was to investigate the performance of some alternate mixing rules for the co-volume term to improve the predicted vapour pressure. As a further evaluation of the estimated critical properties and performance of the mixing rules, predicted and previously reported experimental values for bubble pressures for VTB-n-decane mixtures were compared.

### 1.3.2. *Density of Bitumen-Solvent Mixtures*

The density of a fluid mixture can be an important variable in chemical engineering processes such as gravity separation, blending, and pumping. In general, cubic equations of state show large deviations in fluid densities at high pressures and conditions close to the critical point of the fluid<sup>20</sup>. For the Peng-Robinson CEOS, the error in density prediction increases with increasing molecular size even for pure fluids. For example, Riazi and Mansoori<sup>21</sup> report that, using the Peng-Robinson CEOS, the average absolute deviation for the estimated density was 4.5% for methane but increased to 44.4% for n-tetracontane (n-C<sub>40</sub>H<sub>82</sub>). An investigation of the ability of alternative mixing rules to improve the predictions for liquid phase densities of VTB was the final objective of this work.

---

## 2.0 REVIEW AND HYPOTHESIS

---

### 2.1. SCOPE OF REVIEW

This work is mainly focused on cubic equations of state (CEOS) and more specifically the one developed by Peng and Robinson. Other types of equations of state (EOS) are reviewed and discussed to the extent that they shed some insight on the development, use, and limitations of CEOS. The reviews of development, limitations and applications of EOS presented in this chapter draw on several excellent treatises on these subjects. One of the more recent comprehensive reviews is an excellent two-part monograph edited by Sengers *et al.* titled: *Equations of State for Fluids and Fluid Mixtures*. Details and examples of the applications of equations of state are provided in a comprehensive text: *The Properties of Gases and Liquids* by Poling, Prausnitz, and O'Connell<sup>22</sup>. Additional details on these subjects are drawn from a number of published papers and these are referenced where applicable.

### 2.2. OVERVIEW OF CUBIC EQUATIONS OF STATE

#### 2.2.1. Development of Cubic Equations of State

##### 2.2.1.1. Cubic Equation of van der Waals

As noted in the introduction in Chapter 1, the van der Waals CEOS (2.1) was the first to successfully qualitatively predict vapour-liquid equilibrium phase behaviour.

$$P = \frac{RT}{v-b} - \frac{a}{v^2} \quad (2.1)$$

The first term on the right hand side is called the repulsive term while the second is the attractive term. This exact form of the repulsive term is common to most cubic equations of state, even those being developed today. The parameter 'b' is the co-volume or repulsive parameter and relates to the volume occupied by the molecules themselves which, in effect, reduces the amount of the total volume (V) in which the molecules are free to move. The parameter 'a' is the energy parameter and relates to the attractive

forces between the molecules. Both 'a' and 'b' in vdW CEOS can be calculated from critical temperature and pressure ( $T_c$  and  $P_c$ ) which are widely tabulated for many simple molecules. Given values of the critical temperature and pressure for any fluid, the van der Waals CEOS can be solved analytically.

Certain key aspects regarding CEOS can be illustrated by considering their behaviour at the critical point. The mathematical form of the parameters 'a' and 'b' for CEOS is usually found by applying it at the critical point with the following constraints:

$$\left(\frac{\partial P}{\partial v}\right)_{T_c} = \left(\frac{\partial^2 P}{\partial v^2}\right)_{T_c} = 0; \text{ for } v = v_c \quad (2.2)$$

At the critical point, there are three identical roots which can be expressed in terms of compressibility factor,  $Z$ :

$$\text{Compressibility : } Z = \frac{Pv}{RT} = \frac{P}{\rho RT}$$

Define :

$$A = \frac{aP}{R^2 T^2}; B = \frac{bP}{RT}$$

For van der Waals EOS :

$$Z = \frac{1}{1 - \frac{B}{Z}} - \frac{A}{B} \cdot \frac{B}{Z} = \frac{Z}{Z - B} - \frac{A}{Z} \quad \rightarrow \quad Z^3 - (B + 1)Z^2 + AZ - AB = 0$$

Roots at the critical point :

$$(Z - Z_c)^3 = 0$$

$$\therefore Z^3 - 3Z_c Z^2 + 3Z_c^2 Z - Z_c^3 = Z^3 - (B + 1)Z^2 + AZ - AB$$

Solve for A, B then  $Z_c$ ,  $a_c$  and  $b_c$  :

For the van der Waals CEOS this leads to:

$$Z_c = \frac{3}{8} \quad (2.3)$$



$$a_c = \frac{27R^2T_c^2}{64P_c} \quad (2.4)$$

$$b_c = \frac{RT_c}{8P_c} \quad (2.5)$$

Although calculated at the critical point, the values of  $a_c$  and  $b_c$  are treated as being reasonable but not exact for all points in PVT space. Trebble<sup>23</sup> has pointed out that the value of  $b_c$  has a strong influence on the asymptotic behaviour of the critical isotherm as it approaches high pressure. Trebble speculates that it should be possible to calculate optimum values of  $b_c$  from the shape of the critical isotherms just as the Pitzer acentric factor (see later section for discussion) is related to the shape of the vapour-liquid equilibrium curve. Note also that for a two parameter CEOS like van der Waals with two derivative constraints (2.2), the CEOS is completely constrained to follow a path along the critical isotherm so that the critical compressibility factor will be fixed by the CEOS. The above analysis to determine the values of  $Z_c$ ,  $a_c$ , and  $b_c$  can be carried out in the same manner for all CEOS. This leads to five general observations regarding two-parameter CEOS:

1. Each CEOS assumes that all fluids have exactly the same critical compressibility factor ( $Z_c$ ) which is not true.
2. The form of each two-parameter CEOS determines the value of  $Z_c$ .
3. CEOS are constrained at the critical point but this constraint does not imply accurate PVT properties at the critical point since  $Z_c$  is assumed constant for all fluids.
4. Unless otherwise modified, the co-volume and energy parameters are assumed to be constant for each component and determined by their values at the critical point. Thus, the overall co-volume and energy terms of a mixture depend only on composition.
5. The use of the critical constraints to fix the values of the attractive and co-volume parameters, at least at the critical point, fixes the form of the critical

isotherm, but it is known that the form of the isotherm varies for different components.

One consequence of a fixed critical compressibility factor is that, for pure fluids whose actual  $Z_c$  differs significantly from this fixed value, their predicted molar densities will also differ significantly from measured values. Most typical hydrocarbons have  $Z_c$  ranging from 0.24 to 0.29; however, there is a wider range when hydrocarbons containing heteroatoms are considered. For van der Waals CEOS with  $Z_c$  of 0.375,  $V_c$  is over-predicted. This implies that the entire saturated liquid line, from triple point to the critical point, could be translated in molar volume proportional to the difference in  $Z_{c,EOS}$  and  $Z_{c,actual}$ . Therefore, for the van der Waals CEOS, molar volumes will be over-predicted, i.e., liquid densities are under-predicted.

As noted above, CEOS are inherently inaccurate near the critical point. Both the saturation curve and the critical isotherm exhibit anomalous behaviour near the critical point. As noted by Sandler<sup>24</sup> CEOS do not obey the following, as well as other, scaling laws:

$$\mathbf{Lim}_{T \rightarrow T_c} (v^g - v_c) \approx (T - T_c)^\beta; \mathbf{Lim}_{T \rightarrow T_c} (v^L - v_c) \approx (T - T_c)^\beta$$

$$\beta = 0.32 \pm 0.01$$

$$\mathbf{Lim}_{v \rightarrow v_c} |P - P_c| \sim (v^g - v_c)^\delta$$

$$\delta = 4.8 \pm 0.2$$

All two-parameter CEOS typically give  $\beta = 0.25$  and  $\delta = 3.0$  which is a reflection of the limitations of their functional forms.

Despite the foregoing, one of the virtues of van der Waals CEOS is that it does not generally lead to physically unreasonable solutions compared to some other forms of CEOS. For example, some CEOS may lead to negative molar volumes (negative densities) only at hyperbaric pressures while some CEOS give negative molar volumes even at low to moderate pressures. This behaviour limits the range of temperature and pressure over which some CEOS can be applied. This has been mathematically

illustrated by Deiters<sup>25</sup> for four CEOS including van der Waals and Peng-Robinson CEOS. Whereas Peng-Robinson CEOS can lead to negative solutions for molar volume under some conditions, van der Waals CEOS only leads to positive values. Other characteristics and limitations of CEOS after discussed in the following sections.

#### 2.2.1.2. Relationship between van der Waals CEOS and Virial EOS

About twelve years after van der Waals developed his CEOS, Thiessen<sup>26</sup> proposed an infinite power series based on inverse molar volume to represent the compressibility factor of a fluid. The virial EOS can be considered a Maclaurin expansion of the ideal gas equation and, as such, represents the deviation of the real fluid from ideal gas behaviour:

$$Z = 1 + \frac{B}{v} + \frac{C}{v^2} + \frac{D}{v^3} + \dots \quad (2.6)$$

The parameters B, C, and D are known as the second, third, and fourth virial coefficients, respectively. The virial EOS has its basis in statistical mechanics and the virial coefficients, B, C, and D, are related to interactions between two, three, and four molecules, respectively.

The virial EOS is not widely used because each virial coefficient is molecular specific and a function of inverse temperature. The second virial coefficient is known for most simple molecules and less data is available regarding the third virial coefficient, however, generalized correlations have been developed for both the second and third virial coefficients. The absence of information on higher virial coefficients means that there is a remainder term for the series and this may represent a source of significant error. Additionally, the virial EOS is exact for gases but not for liquids where the molecular interactions are more complex.

The relationship between van der Waals CEOS and the virial EOS can be determined by expressing the van der Waals equation in terms of compressibility factor (Z) and expanding it as a Maclaurin series around zero density.

$$Z_{vdW} = \frac{1}{1 - \frac{b}{v}} - \frac{a}{vRT} = \frac{1}{1 - b\rho} - \frac{a\rho}{RT} \quad (2.7)$$

Expanding  $Z_{vdW}$  as a Maclaurin series:

$$Z_{vdW} = 1 + \left(b - \frac{a}{RT}\right) \frac{1}{v} + \left(\frac{2b^2}{2!}\right) \frac{1}{v^2} + \left(\frac{2 \cdot 3b^2}{3!}\right) \frac{1}{v^3} + \dots = 1 + \sum_{i=1}^{\infty} \left(\frac{b}{v}\right)^i - \frac{a}{RT} \quad (2.8)$$

By comparing equations (2.6) and (2.8), the relationship between the attractive energy parameter 'a', co-volume 'b' and the virial coefficients becomes obvious. This relationship becomes important when CEOS are applied to mixtures.

Although van der Waals CEOS could qualitatively represent vapour-liquid phase behaviour, it was not grounded in statistical mechanics and its accuracy was not very good. For almost the first fifty years of the twentieth century, the virial EOS, and its variants, gradually supplanted van der Waals CEOS even though obtaining the third and higher virial coefficient was difficult and also limited the accuracy of the virial EOS. Enthusiasm for the virial EOS started to wane as it became increasingly important to have a simple analytical means to calculate fugacities for equilibrium calculations required for process design. Attention turned back to CEOS because of their simplicity in this regard. The original van der Waals CEOS itself is still used for qualitative assessment of phase behaviour because it does not lead to physically unreasonable solutions unlike some more modern and sophisticated CEOS.

### 2.2.1.3. Improvements to van der Waals Equation

One of the first improvements to vdW CEOS was proposed by Clausius in 1881 (see Chapter 4 in Sengers *et al.*). He replaced the  $v^2$  term in the denominator of the attractive term by  $(v + c)^2$ . Later Bertholet (*ibid.*) proposed making 'a' temperature dependent by replacing it with  $a/T$ . It is worth noting that even with these early modifications of van der Waals CEOS, researchers were initially proposing changes to the attractive term leaving the repulsive term untouched. Subsequent developments of CEOS took two paths: (i) new forms for a temperature dependent attractive parameter,  $a(T)$  for existing

CEOS, and (ii) completely new forms for the denominator of the attractive term (giving new values of  $Z_c$ ) and by necessity a new form to  $a(T)$ . Some of these developments are discussed below. All of the two-parameter ( $a$  and  $b$ ) CEOS can be written in the general form:

$$P = \frac{RT}{v-b} - \frac{a}{(v+ub)(v+wb)} \quad (2.9)$$

For the van der Waals CEOS,  $u$  and  $w$  are both equal to zero. Note that the values of  $u$  and  $w$  will determine the value of the critical compressibility.

#### 2.2.1.3.1. Redlich-Kwong

The first widely adopted modification to van der Waals CEOS was proposed by Redlich and Kwong<sup>27</sup> for fluids composed of small non-polar molecules. They noted that at high pressures, the molar volume of all gases is practically independent of temperature and approaches a limiting value which is approximately 26% of the critical volume. On the other hand, in the low pressure limit, the second virial coefficient varied approximately with inverse temperature raised to the 3/2 power (see equations (2.6) and (2.8)). With these two observations in mind, Redlich and Kwong proposed the following CEOS:

$$P = \frac{RT}{v-b} - \frac{a}{T^{1/2}v(v+b)} \quad (2.10)$$

where ' $a$ ' and ' $b$ ' have similar meanings as in the vdW CEOS and their forms can be determined in the same way. Note that for the Redlich-Kwong CEOS,  $Z_c$  is now 1/3 which is closer to  $Z_c$  of typical hydrocarbons compared to that from van der Waals CEOS. The Redlich-Kwong CEOS provided improved predictions for gases above their critical temperature compared to that obtained from van der Waals CEOS. However, this CEOS was still not sufficiently accurate for simultaneous predictions of the properties of gas and liquid. The form of the attractive parameter ' $a$ ', was not powerful enough to reproduce the vapour pressure curve since Redlich and Kwong had focused

their attention on constraining the molar volume at high temperatures. Also, the prediction of molar volumes of liquids was still not accurate enough partly due to the fact that  $Z_c$  was still high compared to that for typical hydrocarbons. Nevertheless, like the work of van der Waals, the work of Redlich and Kwong inspired others to continue trying to improve CEOS.

#### 2.2.1.3.2. *Wilson*

Although there were other proposed changes to the Redlich-Kwong CEOS, it would be 15 years before the next major advance in the development of CEOS was first proposed by Wilson<sup>28</sup> in 1964. The original van der Waals and Redlich-Kwong CEOS were constrained at the critical point (see equation (2.2)) which is the extreme temperature limit of the vapour-liquid equilibrium line. Wilson proposed to modify the attractive parameter 'a' to provide a better prediction of vapour pressure by matching the slope of the vapour-liquid line between the normal boiling point and the critical point. This was partly achieved by replacing the Redlich-Kwong  $T^{-0.5}$  term with what become known as the alpha-function:

$$P = \frac{RT}{v-b} - \frac{a(T)}{v(v+b)}$$

where :

$$a(T) = a_c \alpha(T) \tag{2.11}$$

Here,  $a_c$  denotes the temperature independent part of the attractive parameter and is equivalent to  $a(T_c)$  and is determined as illustrated earlier for the van der Waals CEOS. The Wilson alpha-function is given by:

$$\alpha(T) = T_r \left[ 1 + (1.57 + 1.62\omega)(T_r^{-1} - 1) \right]$$

where :

$$T_r = \frac{T}{T_c} \tag{2.12}$$

The variable  $\omega$  is Pitzer's acentric factor, discussed below, and is defined as:

$$\omega = -\log \left[ \frac{P}{P_c} \right]_{T_r=0.7} - 1 \quad (2.13)$$

The value of  $Z_c$  in Wilson's CEOS is the same as that for the Redlich-Kwong CEOS and the values of 'a' and 'b' are those at the critical point. Note that the Wilson alpha function has a value of one at the critical point and can have negative values above the critical temperature. The attractive parameter ( $a(T)$ ) should always be positive, therefore,  $\alpha(T)$  should always be positive. Theoretically, the alpha function should decrease smoothly with temperature and should ultimately be zero at infinite temperature. The alpha-function was not expressed in the form shown in equation (2.12) in Wilson's original publication but it is the result of generalizing the slopes of the vapor-liquid line near the critical point for pure components.

The use by Wilson of the acentric factor as a third molecular parameter in the equation of state was an inspired choice. The earlier work of Pitzer<sup>29</sup> showed that the acentric factor accounted for interactions of the non-central parts of non-spherical molecules. Whereas simple fluids such as argon, krypton, xenon, and methane had acentric factors close to zero, non-spherical molecules had acentric factors greater than zero. Pitzer intuited that as a result, such an acentric interaction would manifest itself in the reduced vapour pressure versus reduced temperature curve. Simple fluids had a reduced vapour pressure of exactly 0.1 at a reduced temperature of 0.7. The acentric factor is a measure of the slope of this curve for non-spherical molecules. The acentric factor is the result of applying the principle of corresponding state so that all fluids would follow the same curve for simple fluids and have a reduced vapour pressure of 0.1 at 0.7 reduced temperature. Pitzer's acentric factor thus provided the constraint that Wilson was seeking; the acentric factor constrained the slope of the vapour pressure curve. In this way Wilson was able to obtain improved vapour pressure predictions which he hoped would lead to overall improvements to phase behaviour predictions. However, Wilson's CEOS only gave reasonable slope of the vapour pressure curve close

to the critical point but this did not guarantee good predictions remote from the critical point, i.e., closer to the triple point or boiling point. For this reason, Wilson's CEOS was not good enough to provide reliable predictions and was therefore not widely adopted.

#### 2.2.1.3.3. *Soave-Redlich-Kwong*

Following in the footsteps of Wilson, Soave<sup>30</sup> proposed an alternate alpha-function in 1972, which received more widespread attention and resulted in the CEOS being more widely adopted as a tool for predicting vapour-liquid equilibrium of non-polar fluids. Soave's alpha-function for the Redlich-Kwong CEOS also relied on acentric factor:

$$\alpha(T) = \left[ 1 + (0.480 + 1.57\omega - 0.17\omega^2)(1 - T_r^{1/2}) \right]^2 \quad (2.14)$$

Soave's alpha function was developed by considering the linear plots of  $\alpha(T)^{1/2}$  versus  $T_r^{1/2}$  between a reduced temperature of 0.7 and the critical point and generalizing the values of the slope between these two points in terms of the acentric factor. Soave's alpha-function constrained the Redlich-Kwong CEOS to give the correct vapour pressure between a reduced temperature of 0.7 and the critical point. Thus, Soave's alpha function represents an improvement on Wilson's CEOS which only matched the slope of the vapour pressure curve near the critical point. Like Wilson's alpha function, Soave's alpha function has a value of one at the critical point but it remains positive at all temperatures.

With Soave's alpha-function applied to the Redlich-Kwong CEOS, it became known as the SRK CEOS. The SRK CEOS could be applied to non-polar molecules (except carbon dioxide) to provide good predictions of vapour pressures for reduced temperatures from approximately 0.6 up to the critical temperature. The SRK CEOS is restricted to non-polar molecules with acentric factors less than 0.6, i.e., smaller than n-tridecane and was, therefore, not applicable to heavy hydrocarbons. It should again be noted that  $Z_c$  is still 1/3 for the SRK CEOS and therefore the molar volumes of fluids with  $Z_c$  significantly different from this will not be accurately predicted.



#### 2.2.1.3.4. Peng-Robinson

The development of the Peng-Robinson (PR) CEOS proceeded in a similar manner to the SRK CEOS but with one important difference. Peng and Robinson recognized that the  $Z_c$  from the SRK being 1/3 was not very close to typical hydrocarbons. They proposed to modify the denominator of the attractive term in the CEOS to achieve a more reasonable value for  $Z_c$  of 0.3074 which was much closer to that for typical hydrocarbons:

$$P = \frac{RT}{v-b} - \frac{a(T)}{v(v+b)+b(v-b)} \quad (2.15)$$

Using the new form of the CEOS, and experimental vapour pressure data, Peng and Robinson calculated the values of  $\alpha(T)$ . Following the linear relation between  $\alpha(T)^{1/2}$  vs.  $T_r^{1/2}$  found by Soave, Peng and Robinson developed a correlation which covered the region between the normal boiling point and the critical point. It is interesting to note that Peng and Robinson actually achieved Wilson's original vision of matching the slope of the vapor-liquid line between the boiling point and critical point. What Wilson lacked was a way of linearizing this slope and so he had only used the terminal slope near the critical point. The Peng-Robinson alpha-function is given by:

$$\alpha(T) = \left[ 1 + \kappa \left( 1 - T_r^{1/2} \right) \right]^2 \quad (2.16)$$

where :  $\kappa = 0.37464 + 1.54226\omega - 0.26992\omega^2$

The form of Peng and Robinson's alpha-function is the same as that of Soave, only the coefficients are different. This is because Soave only considered two points of the vapour-liquid line at  $T_r$  of 0.7 and 1 in developing his function, whereas Peng and Robinson consider the entire vapour-liquid line between the normal boiling point and the critical point which is an important refinement. With its more refined alpha function, the PR CEOS provided improved vapour pressure predictions. The more realistic value for  $Z_c$ , for this CEOS, also gave improved predictions for molar volumes. Thus, the PR

CEOS achieved improved accuracy while maintaining the simplicity of the SRK CEOS in requiring only three molecular properties for each component.

#### 2.2.1.3.5. *Twu-Sim-Tassone*

Although no two-parameter (a and b) CEOS can predict the liquid densities of all components better than any other two-parameter CEOS, Twu *et al.*<sup>31</sup> proposed a new CEOS that reportedly give the optimal liquid densities for heavy hydrocarbon and polar components. The Twu-Sim-Tassone CEOS has a  $Z_c$  of 0.2963 which is lower than that for any of the previous CEOS:

$$P = \frac{RT}{v-b} - \frac{a(T)}{(v+3b) + (v-0.5b)} \quad (2.17)$$

Twu *et al.* indicate that, compared to the SRK and PR CEOS, the Twu-Sim-Tassone CEOS provided more accurate predictions of molar volumes for polar components and hydrocarbons larger than n-octane. The SRK CEOS was superior for molar volumes of methane while PR CEOS was superior for n-propane to n-heptane. For predictions of vapour pressures of hydrocarbons and polar components, the Twu-Sim-Tassone CEOS was found to yield better predictions than either PR or SRK CEOS. The alpha function for the Twu-Sim-Tassone CEOS has an entirely different form from those mentioned so far and is discussed in a later section of this review:

$$\alpha(T) = \alpha^{(0)} + \omega(\alpha^{(1)} - \alpha^{(0)})$$

where :

$$\alpha^{(0)} = T_r^{N^{(0)}(M^{(0)}-1)} e^{L^{(0)}(1-T_r^{N^{(0)}M^{(0)}})} \quad (2.18)$$

$$\alpha^{(1)} = T_r^{N^{(1)}(M^{(1)}-1)} e^{L^{(1)}(1-T_r^{N^{(1)}M^{(1)}})}$$

Note that compared to other alpha-functions, the present one is linearly dependent on acentric factor and exponentially dependent on reduced temperature. In this alpha function, L, M, and N have been generalized for all components to one set of numerical

coefficients for conditions below the critical point and another set above the critical point.

#### 2.2.1.3.6. Schmidt-Wenzel

As noted above, a more realistic value for  $Z_c$  can lead to improved estimates for molar volumes. If, in addition to 'a' and 'b', a third parameter is introduced into the CEOS, then the critical compressibility factor can be made component dependent. For example, Lee and Kesler<sup>32</sup> have correlated critical compressibility factors with acentric factors:

$$Z_c = 0.2905 - 0.085\omega \quad (2.19)$$

Considering the relationships between the apparent critical compressibility factor of CEOS having constant  $Z_c$ , Schmidt and Wenzel<sup>33</sup> proposed a simple three-parameter CEOS with a component dependent critical compressibility factor:

$$P = \frac{RT}{v-b} - \frac{a(T)}{v^2 + ubv + wb^2}$$

where :

$$u + w = 1$$

$$w = -3\omega \quad (2.20)$$

Note that for this equation of state the co-volume is now a function of three properties of the pure component ( $T_c$ ,  $P_c$ , and  $\omega$ ). The forms of co-volume and attractive parameter can both be found by applying the critical condition as previously discussed. The alpha function is slightly more complex than that for the SRK CEOS:

$$\alpha(T) = \left[ 1 + \kappa \left( 1 - T_r^{1/2} \right) \right]^2 \quad (2.21)$$

where:

$$\begin{aligned}\kappa &= \kappa_0 + \frac{(5T_r - \kappa_0 - 1)^2}{70} & T_r \leq 1 \\ \kappa &= \kappa_0 + \frac{(4 - \kappa_0)^2}{70} & T_r > 1 \\ \kappa_0 &= 0.465 + 1.347\omega - 0.528\omega^2\end{aligned}$$

For pure components with acentric factors up to 0.5, the CEOS of Schmidt and Wenzel predicted liquid molar volumes to within 2% of measured values which was better than either the SRK or PR CEOS. The deviations in predictions become larger as the temperature approached  $T_c$ , which is typical of CEOS of the van der Waals type. Vapour pressure predictions for the PR and Schmidt and Wenzel CEOS have approximately the same accuracy and both are better, in this respect, than from the SRK CEOS.

#### 2.2.1.3.7. Improvements to Alpha Functions

With the improved accuracy of the Soave-Redlich-Kwong (SRK) and Peng-Robinson (PR) CEOS, more attention was given to the alpha function in an effort to increase the accuracy over a wider PVT space (e.g., supercritical region and low  $T_r$  for SRK) as well as for polar and heavy hydrocarbons (large acentric factors). This area has been well summarized by Sengers *et al.*<sup>3</sup> and only a few highlights are given here. It should be stressed that each alpha-function is developed for specific equations of state, using the methodology as discussed above, and cannot be used interchangeably.

Attempts have also been made to make the co-volume temperature dependent in a similar way to the attractive energy term. Temperature dependent co-volume terms have been found to adversely affect derivative properties such as heat capacities. For example, Trebble and Bishnoi<sup>34</sup> have shown that some combinations of temperature dependent  $a(T)$  and  $b(T)$  for three-parameter CEOS can lead to negative heat capacities in the single phase regions. Subsequently, Salim and Trebble<sup>35</sup> concluded that any temperature dependence of the co-volume term in vdW-type CEOS would lead to anomalies in thermodynamic properties of pure components at some extreme conditions. Further consideration of temperature dependent co-volume terms is beyond the scope of this review.

Alpha functions which can be applied to polar or even associating components have been proposed. Robinson *et al.*<sup>36</sup> modified their original alpha function to obtain better predictions for hydrocarbons with acentric factors greater than 0.5:

$$\alpha(T) = \left[ 1 + \kappa \left( 1 - T_r^{1/2} \right) \right]^2$$

$$\omega \leq 0.491$$

$$\kappa = 0.37464 + 1.54226\omega - 0.26992\omega^2 \quad (2.22)$$

$$\omega \geq 0.491$$

$$\kappa = 0.379642 + 1.48503\omega - 0.164423\omega^2 + 0.016666\omega^3$$

Stryjek and Vera<sup>37</sup> proposed a modification of the alpha function for the Peng-Robinson CEOS which was not only a function of acentric factor but also included an empirical parameter characteristic of the pure component. This empirical parameter is obtained from regression of the vapour pressure curve for the pure component. The value in  $\kappa$  for equation (2.22) is now given by:

$$\kappa = \kappa_0 + \kappa_1 \left( 1 + T_r^{1/2} \right) \left( 0.7 - T_r \right)$$

where :

$$\kappa_0 = 0.378893 + 1.4897153\omega - 0.17131848\omega^2 - 0.0196554\omega^2 \quad (2.23)$$

$$\kappa_1 : \text{empirical parameter for a pure component}$$

This alpha function is applicable to heavy hydrocarbons with moderate polarity. The polarity of the component is basically incorporated in the component specific parameter  $\kappa_1$ . Since this empirical parameter is not generalized, it introduced additional complexity to the CEOS since we now require four molecular parameters:  $T_c$ ,  $P_c$ ,  $\omega$ , and  $\kappa_1$ .

For the van der Waals CEOS, Soave<sup>38</sup> proposed an alpha function applicable to hydrocarbons with acentric factors between 0 and 1 that was similar in form to the alpha function proposed by Robinson *et al.* with cubic dependence on acentric factor:

$$\alpha(T) = \left[ 1 + \kappa \left( 1 - T_r^{1/2} \right) \right]^2$$

where:  $\kappa = 0.4998 + 1.5928\omega - 0.19563\omega^2 + 0.025\omega^3$  (2.24)

for:  $0 \leq \omega \leq 1$

For polar hydrocarbons, Soave proposed a second alpha function with two component specific empirical constants (m and n) derived from correlation of pure component vapour pressure data:

$$\alpha(T) = 1 + m(1 - T_r) + n(T_r^{-1} - 1)$$

$m, n$ : empirical parameters for a pure component (2.25)

Androulakis *et al.*<sup>39</sup> proposed an alpha function with three adjustable parameters for a modified van der Waals CEOS to account for the behaviour of polar and non-polar components:

$$\alpha(T) = 1 + d_1 \left( 1 - T_r^{2/3} \right) + d_2 \left( 1 - T_r^{2/3} \right)^2 + d_3 \left( 1 - T_r^{2/3} \right)^3$$

$d_1, d_2, d_3$ : empirical parameters for a pure component (2.26)

While this alpha function resulted in improved vapour predictions from triple point to critical point, the use of three empirical parameters which have not been generalized, e.g., in terms of acentric factor, increases the computational complexity.

As noted above, the alpha function should decrease smoothly with increasing temperature and reach a limiting value of zero at infinite temperature. All of the alpha functions presented above contravene this principle. The decrease of  $\alpha(T)$  with increasing temperature from triple point to critical point leads to reasonably good predictions but above the critical point the increase in  $\alpha(T)$  with increasing temperature can lead to poor predictions. In order to provide smooth decrease of alpha functions with increasing temperature, alpha functions have been proposed with exponential dependence on temperature. The most recent of these is that of Twu *et al.*<sup>40</sup> who

proposed an alpha function for the Peng-Robinson CEOS with a linear dependence on acentric factor and an exponential dependence on reduced temperature:

$$\alpha(T) = \alpha^{(0)} + \omega(\alpha^{(1)} - \alpha^{(0)})$$

where :

$$\alpha^{(0)} = T_r^{N^{(0)}(M^{(0)}-1)} e^{L^{(0)}(1-T_r^{N^{(0)}M^{(0)}})} \quad (2.27)$$

$$\alpha^{(1)} = T_r^{N^{(1)}(M^{(1)}-1)} e^{L^{(1)}(1-T_r^{N^{(1)}M^{(1)}})}$$

The parameters L, M, and N were generalized and have different values below and above the critical temperature. The above alpha function is applicable only to non-polar components including heavy hydrocarbon, at least up to an acentric factor of 1. Compared to either the original or Stryjek and Vera alpha function, Twu's alpha function for the PR CEOS yields better predictions of hydrocarbon vapour pressures between the triple point and critical point. However, for polar components, component-specific values of L, M, and N are required, thereby increasing the complexity of the computation.

### 2.2.2. Complexity: Ease of Use versus Accuracy

The CEOS discussed above were developed to provide improved predictions of phase behaviour compared to previous versions. The improvements have, to a large extent, been driven towards predictions of vapour pressure and molar volume. Subsequent improvements extended these CEOS to heavier hydrocarbon (larger acentric factors) and polar components. CEOS are also utilized for calculations of enthalpy, entropy, heat capacity, and other thermodynamic properties required for process engineering. It has been observed, however, that good vapour pressure predictions do not necessarily lead to good prediction of departure functions (e.g., enthalpy, Helmholtz energy, entropy) and derivative properties (e.g., heat capacities, compressibilities, speed of sound, Joule-Thompson coefficient). For example, Mathias and Klotz<sup>41</sup> have illustrated that while the PR CEOS with the original or Stryjek and Vera alpha functions

can provide good predictions of vapour pressures, there can be substantial errors in its predictions of constant pressure heat capacities.

In their recent work developing a three-parameter EOS, Cismondi and Mollerup<sup>42</sup> applied renewed emphasis to the earlier observations that the limitations of all CEOS like SRK and PR are a consequence of their two-parameter density dependence which is also related to their unique critical compressibility for all fluids. All purely two-parameter CEOS show a unique PVT behaviour in terms of reduced variables and therefore, can be considered as corresponding state model. The inclusion of a temperature dependent attractive energy parameter and acentric factor make the CEOS more component specific, i.e., no longer completely a corresponding state model. However, because calculated molar volumes still only depends on the two parameters of the CEOS and is independent of the alpha function, the ratio of saturated densities,  $\rho_L^{sat} / \rho_V^{sat}$ , is a universal function of  $P_r^{sat} / T_r$  for the CEOS. The phase behaviours of components that do not follow this relationship are not well predicted by the CEOS. Cismondi and Mollerup show that at higher densities and pressures the predictions for compressibility and fugacity coefficient from two-parameter CEOS become worse. Nevertheless, it must be noted that the two-parameter CEOS provides reasonably good prediction for critical compressibility and fugacity at lower densities and pressures and also provides the correct trends for these properties with increasing pressure and density.

Treble and Treble and Bishnoi have compared the performance of ten CEOS which included those with two, three, and four parameters and which were developed between 1972 and 1986. Two of these three-parameter CEOS included temperature dependent co-volumes, the shortcomings of which have been briefly mentioned above. The comparison dataset included seventy-five pure components ranging from argon through n-octane, including polar components and acentric factors up to 0.635 for n-propanol. Table 2-1 summarizes the average absolute deviations for predictions of vapour pressure, saturated liquid molar volume, saturated vapour molar volume, and single phase volume for six of these CEOS. The results demonstrate that the PR represented a significant improvement over the SRK CEOS. Considering the additional complexity of the three- and four-parameter CEOS, the subsequent incremental



improvements were relatively small compared to that achieved by the PR CEOS. Absolute average deviations from predictions of all ten CEOS are presented by Trebble and Bishnoi. The same study also reported that compared to other CEOS, PR produced fairly accurate enthalpy and heat capacity predictions which were always physically reasonable. In a later study, Salim and Trebble<sup>43</sup> compared their own improved four-parameter CEOS to the PR and found that it gave comparable results for thermodynamic properties which included: second virial coefficient, internal energy, enthalpy, entropy, isobaric and isochoric heat capacities, speed of sound, and Joule-Thompson coefficient. These results illustrate why the PR CEOS continues to be popular among process engineers.

**Table 2-1 Comparison of the performance of six CEOS (from reference 34)**

Property	Adachi-Lu-Sugie	Patel-Teja	Heyen	Schmidt-Wenzel	PR	SRK
Year developed	1983	1982	1981	1980	1976	1972
Number of parameters	4	3	3	3	2	2
Co-volume b(T)	No	No	Yes	No	No	No
	<b>% Average Absolute Deviation</b>					
Vapour Pressure	1.37	1.54	5.00	1.27	1.39	1.74
Saturated liquid molar volume	7.81	7.91	2.20	8.4	8.58	17.64
Saturated vapour molar volume	5.32	5.41	9.60	5.34	5.34	5.81
Single phase volume	3.78	3.90	5.36	4.16	4.96	7.05

Satyro<sup>44</sup> developed a new EOS based on so-called significant structure theory which in its generalized form requires critical properties ( $T_c$  and  $V_c$ ), acentric factor and dipole moments. The performance of this new EOS was compared to two CEOS (PR and an enhanced SRK) and the EOS of Lee and Kesler which is based on corresponding states. The version of the SRK CEOS used in this comparison was enhanced in two ways: (a) by the inclusion of volume translation (see later section of this chapter) to improve predictions for saturated liquid molar volumes and (b) use of the alpha function of Mathias and Copeman<sup>45</sup> which included two component specific parameters. The comparison data set included 277 pure components from the DIPPR (Design Institute for

Physical Property Data) database<sup>46</sup>. Average absolute deviations for non-generalized and generalized forms of this new EOS compared to other CEOS are given Table 2-2. The PR CEOS, with a generalized alpha function, performs just as well as the generalized new EOS. The SRK CEOS is superior to the PR but this is because it has been enhanced by volume translation and component specific parameters in the alpha function. The PR CEOS would likely perform just as well if it were also enhanced in these ways.

**Table 2-2 Comparisons of the performance of four EOS (from reference 44)**

Property	CEOS % Average absolute deviation				
	New EOS <sup>a</sup>	Generalized New EOS	PR	SRK <sup>b</sup>	Lee Kesler
Vapour Pressure	1.53	3.77	1.69	2.23	5.48
Saturated liquid molar volume	3.34	5.19	6.43	3.46	5.35
Enthalpy of vaporization	2.76	3.40	2.71	3.23	2.86
Isobaric heat capacity	2.39	8.18	8.16	2.62	6.60
Critical isotherm molar volume <sup>c</sup>	3.67	-	9.06	3.34	4.43

(a) New EOS with component specific parameters. See Satyro

(b) SRK enhanced with volume translation and component specific parameters

(c) A small subset of pure components (16) was used for this property compared to the set (277) used for other properties.

Despite modifications, the most widely used two-parameter cubic equations of state only require knowledge of three properties ( $T_c$ ,  $P_c$ , and  $\omega$ ) for the pure fluid which can be obtained from compilations (tabulated for many simple pure fluids), direct measurement, or by way of correlations of simple physical properties (e.g., normal boiling point and specific gravity). Two-parameter CEOS, such as the Peng-Robinson CEOS, have comparable accuracy compared to more complex CEOS, such as those with up to four parameters and component specific variables. Depending on the complexity of the problem being solved and the precision required, there is therefore a trade-off involved in the selection of an appropriate EOS.

### 2.3. MORE COMPLEX EQUATIONS OF STATES

The very simplicity of CEOS have limitations built into them which many researchers have attempted to address by the use of modified alpha functions to account for polarity and large acentric factors for heavy hydrocarbons. These modifications

include alternative alpha functions with additional parameters which may be pure component specific or in some cases have been generalized, e.g., using the acentric factor. Other modifications include the creation of multi-parameter CEOS with as many as five parameters compared to the conventional two parameters ('a' and 'b') for the simple CEOS. Some of these multi-parameter CEOS were discussed above in comparison to well-known two-parameter CEOS such as Peng-Robinson and Soave-Redlich-Kwong. In this section, some examples of more complex EOS, having a sounder theoretical base than simple CEOS, are discussed including those that deal with polar associating components.

#### 2.3.1.1. *Quartic Equations of State*

Quartic EOS are based on the generalized van der Waals theory which treats the attractive and repulsive terms separately. Although, the repulsive and attractive terms in the vdW CEOS has no theoretical basis, the separation of these terms does have a sound theoretical basis. Most EOS based on generalized van der Waals theory have in common the use of various forms and approximations of the Carnahan-Starling<sup>47</sup> repulsive term for hard spheres. Like cubic EOS, quartic EOS can be solved analytically. Quartic EOS yield up to four distinct solutions and, for positive pressures, one of the four real roots is negative and can be discarded or there is only one real and positive root.

One of the first quartic EOS was developed by Kubic<sup>48</sup> for large chain-like molecules encountered in the petrochemical and polyolefin industries. Two of the four generalized parameters in Kubic's EOS are functions of temperature. On average, for pure component vapour pressures and molar volumes of vapour and liquids, Kubic's EOS represents only a modest improvement over PR CEOS. For some mixtures evaluated, the PR CEOS was clearly superior to Kubic's EOS.

For PVT behaviour of pure components, Soave<sup>49</sup> proposed a quartic EOS with five parameters which could be reduced to three parameters yet still yield good predictions over a range of conditions spanning the triple point to critical point. The repulsive part of Soave's EOS was developed from the van der Waals CEOS but modified to behave like the Carnahan-Starling repulsive term in a simpler form proposed previously by

Scott<sup>50</sup>. The attractive term was a generalized form of the attractive term for a CEOS. For PVT behaviour of polar components, Soave's quartic EOS was found to be superior to the PR and RK CEOS. For light, non-polar hydrocarbons (e.g., methane to benzene), the PR CEOS gave similar accuracy to that from Soave's quartic EOS.

Shah *et al.*<sup>51</sup> proposed a generalized quartic EOS for pure non-polar components in which a two-part repulsive term was developed from molecular simulations. The first part of the repulsive term was very similar to the vdW repulsive term. The attractive term was derived empirically by regression with experimental compressibilities and the repulsive term. This quartic EOS was more accurate than the PR CEOS for density predictions particularly at high pressures and supercritical temperatures. For liquid densities in the sub-critical region, the quartic EOS was superior to PR CEOS. However, for saturated liquid densities of non-polar hydrocarbons such as n-paraffins, the performance of the PR CEOS approached that of the quartic equation as the chain length increased from methane to n-octane. This quartic equation was also reportedly superior for other properties such as isobaric heat capacity, Joule-Thompson coefficient, and speed of sound, but this conclusion was based on a very limited data set.

Many quartic EOS are not constrained at the critical points (equation (2.2)) because there is no explicit solution as their form is too complex for derivation of the analytical expression satisfying the critical criteria. An exception to this is Soave's quartic EOS. Due to the absence of a critical point constraint, predictions from some of these quartic EOS may overshoot the critical point considerably. For example, Anderko points out (in Chapter 4 in Sengers *et al.*) that this lack of constraint at the critical point actually makes these quartic EOS perform better than if they were so constrained and, therefore, comparisons to critically constrained CEOS are unfair and should be treated cautiously. Over-predicting the critical point may lead to qualitatively incorrect behaviour in process simulations (predicting two-phase behaviour instead of supercritical behaviour) and this can be a serious disadvantage when using quartic EOS. These properties of quartic EOS are yet another set of reasons why CEOS such as PR and SRK retain their widespread popularity.

### 2.3.1.2. Accounting for Association

Thus far, the tendency for association of polar molecules has been dealt with indirectly by modifying the alpha function as proposed by Stryjek and Vera, Soave, and Androulakis for polar hydrocarbons. For multi-component mixtures, which will be discussed in a later section, various mixing rules have been proposed to partially deal with associating behaviour. Molecular association can also be dealt with explicitly in two ways:

1. Solving simultaneously the equations for chemical equilibria and phase equilibria for all species in the mixture
2. Incorporation of association into an EOS by solving the chemical equilibrium equations and then deriving an equation of state with the association behaviour built in.

For the simultaneous equations approach, it is necessary to assume the form of the associated species that are present (dimers, trimers, tetramers, etc.,) and generally this will be as few as possible. If a continuously linear association model was assumed (i.e., continuously higher multimers) the number of equations to define the system would approach infinity. For mixtures, if association between different molecules in the mixture was assumed, they are usually restricted to dimers because it is impossible to obtain all the parameters for mixed associating species from binary data. With the above simplifications, equilibrium constants for the associations can then be expressed in terms of component mole fractions, pressure and fugacity coefficients. For chemical equilibria we have:

$$iM_j \rightarrow M_i$$
$$K_{eq_{M_i}} = \frac{x_i \phi_i}{x_j^i \phi_j^i P^{i-1}} \quad (2.28)$$

and for phase equilibria:

$$f_i^{phase1}(T, P, x) = f_i^{phase2}(T, P, x) \quad (2.29)$$

The major shortcoming of this approach is the need to arbitrarily select and limit the number of associating species. Since there are no clear rules for selecting the associating species, trial and error is required to determine which ones are required to represent the phase equilibrium. This makes this approach cumbersome and inefficient. Additionally, this approach is not easily extended to mixtures containing more than one associating component.

A second approach for dealing with association is to incorporate it directly in the EOS. This approach overcomes some of the shortcomings of the simultaneous equations approach. An example of this approach is given by Heidemann and Prausnitz<sup>52</sup> who used a generalized van der Waals EOS which separates the attractive and repulsive terms. The Carnahan-Starling repulsive term for a hard sphere along with the Redlich-Kwong attractive term expressed in terms of reduced density formed their EOS. By judicious selection of a mixing rule to determine co-volume and attractive terms for the multimers from that of the monomers, significant simplifications could be achieved. Further simplification resulted from the assumption that the equilibrium constants for association to form multimers were independent of the degree of association. With these assumptions, the resulting EOS was found to be explicitly independent of association:

$$P = \frac{n_A}{n_o} \frac{RT\xi}{v} \left( \frac{1 + \xi + \xi^2 + \xi^3}{(1 - \xi)^3} \right) - \frac{a}{b^2} \left( \frac{\xi^2}{(1 - 4\xi)} \right)$$

where:

$$\xi = \frac{b}{v} \tag{2.30}$$

$n_A$  : total moles of multimers

$n_o$  : total moles of monomer in the absence of association

This EOS has an implicit dependence on association through the ratio of the total number of moles of multimers ( $n_A$ ) to the total number of moles of monomer ( $n_o$ ) in the absence of association which is in turn dependent on the equilibrium constant for association. This approach is also easily applied to mixtures containing more than one

associating component. The above ratio can be expressed in a very simplified form when only one component in the mixture is associating.

Incorporating association explicitly in the EOS is computationally simpler than the approach of simultaneous equations for chemical and phase equilibria with trial and error choice of the associated species. The approach using an EOS incorporating association has been extended to other choices for the repulsive and attractive terms in the generalized van der Waals EOS. Similarly, with the simultaneous equations for chemical and phase equilibria, any suitable EOS may be employed. Both of the above association models require five parameters for each associating component: (1) enthalpy, and (2) entropy of association to determine the temperature dependence of association and, (3) the critical temperature, (4) critical pressure and (5) acentric factor of the monomer.

#### *2.3.1.3. Equations of State Based on Perturbation Theory*

Perturbation theory provides the basis for a more modern family of EOS. In its application to EOS, perturbation theory basically involves a Taylor series expansion of a property of the fluid around the known properties of a reference fluid, e.g., an ideal gas or a hard sphere fluid. A useful fluid property for this application to EOS is the Helmholtz energy since the derivative with respect to volume leads directly to the EOS. One of the more important EOS developed in the past twenty years using this approach is based on the so-called statistical associating fluid theory (SAFT) developed by Chapman *et al.*<sup>53, 54</sup> and subsequently Huang and Radosz<sup>55</sup>. The SAFT approach was developed to capture the effects of non-spherical, chain-like molecular shape and molecular association. Thus SAFT is an EOS with association incorporated directly just like the generalized van der Waals EOS of Heidemann and Prausnitz discussed in the previous section.

In the SAFT model, molecules are considered to be made up of a specific number of segment attached together to form chains. These molecular chains can be associated with each other through multiple sites, the number of which is not constrained. The SAFT equation uses the Helmholtz energy as the fundamental fluid property and an ideal gas

reference fluid. The SAFT equation can be expressed in terms of the residual Helmholtz energy ( $A^{res}$ ):

$$A^{res} = A - A^{ig} = A^{seg} + A^{chain} + A^{assoc} \quad (2.31)$$

The association term ( $A^{assoc}$ ) is given by a theory developed by Wertheim (see Chapman *et al.*<sup>54</sup> and references therein) which relates the residual Helmholtz energy ( $A^{res}$ ) due to association to monomer density which Chapman and co-workers modified and extended to apply to mixtures of spheres and chains. Chains are formed by strong covalent bonds between segments. The chain term ( $A^{chain}$ ) was developed by Chapman *et al.* from Wertheim's theory by replacing the bonds due to molecular association, which forms multimers, by covalent bonds to form chains. The segment Helmholtz energy ( $A^{seg}$ ) is itself based on perturbation theory and uses hard spheres as a reference fluid with Carnahan-Starling repulsive interaction with a dispersion force as a perturbation.

For application of SAFT, characteristic parameters are required for segment, chains, and the association between chains. Segments (hard spheres) interact to form chains which grow into chains by interacting with other segment according to set rules. The segment interaction is governed by a Leonard-Jones potential. Thus, molecules are defined in terms of the number of segments per chain molecule ( $m$ ,  $m = 1$  for spherical molecule), hard sphere diameter ( $\sigma$  or volume,  $v$ ) and the segment-segment interaction energy ( $u$ ). These three pure component parameters are considered to be temperature independent. Thus, for a non-associating fluid, SAFT results in a three-parameter EOS. Association between pure components is governed by a square-well potential. The association energy ( $\epsilon^{A-B}$ ) and a parameter characterizing the association volume for segments ( $k^{A-B}$ ) are also required.

The three pure component parameters can be determined by regression of pure component vapour pressures and liquid densities. Values for the three parameters for several classes of pure components have been tabulated by Huang and Radosz. Correlations based on molar mass have also been developed. In principle, these



parameters could be calculated from the molecular properties of pure components but this approach was not used by Huang and Radosz perhaps because interpretation of some parameters such as the number of segments in a molecular chain and estimation of equivalent hard-sphere diameters for segments are not straightforward for non-spherical, non-symmetric components.

For application to non-associating mixtures, the van der Waals mixing rules (equations (1.4) and (1.5)) are used to determine the three temperature independent parameters ( $m$ ,  $\sigma$ , and  $u$ ). This approach is only valid for Leonard-Jones interacting spheres of similar size. This does not necessarily invalidate the SAFT approach since the mixing rules are only applied to the non-associating part of the fluid and strong non-ideality caused by association is dealt with by another part of the SAFT EOS.

The SAFT model has been evaluated for a number of systems including: pure alkanes and mixtures of alkanes, gas solubility in alkanes (including  $H_2$ ), methanol, acetic acid, bitumen- $CO_2$ - $n$ -decane mixtures, asphaltenes, and polymer solutions among others. Ting *et al.*<sup>56</sup> compared the performance of PR and SAFT EOS for modeling VLE of binary asymmetric mixtures of  $n$ -alkanes. When the SAFT EOS parameters were regressed from vapour pressure and liquid densities, SAFT EOS and PR CEOS gave similar results for VLE predictions but the PR CEOS was better at predicting the vapour phase compositions and behaviour in the critical region. Both SAFT and PR EOS over-predicted the critical composition but SAFT yielded better predictions for the more asymmetric systems where the critical region has less impact on phase behaviour. The advantage of SAFT EOS compared to PR CEOS is that it can yield reasonable predictions for these asymmetric mixtures of  $n$ -alkanes using the correlations for the SAFT parameter as developed by Huang and Radosz even with the binary interaction parameter ( $k_{ij}$ , required to handle mixtures; see later section) set equal to zero. In contrast, the binary interaction parameter  $k_{ij}$  for the PR CEOS was not well behaved and varied widely and non-linearly with temperature so that the PR CEOS cannot yet be considered truly predictive.

## 2.4. PARAMETERS FOR CEOS

This section deals only with the so-called two-parameter CEOS such as Peng-Robinson and Soave-Redlich-Kwong CEOS. Critical temperature and pressure as well as the Pitzer acentric factor are the required pure component properties for solving the two-parameter CEOS. The accuracy of values for these properties can greatly affect the accuracy of phase behaviour predictions given by a CEOS. For example, Voulgaris *et al.*<sup>57</sup> showed that even a 1% error in critical temperature can lead to an error of 16% in predicted vapour pressures of n-decane. A similar error in either acentric factor or critical pressure leads to relatively smaller errors in vapour pressure of n-decane of approximately 1% and 3%, respectively. In contrast to their impacts on vapour pressures, errors in critical properties and acentric factor lead to an order of magnitude smaller error for saturated liquid density of n-decane. Voulgaris *et al.* observes that the impact of these errors on predicted properties increases as molar mass increases which does not bode well for predictions involving heavy hydrocarbons such as bitumen. The following sections briefly discuss how critical properties can be measured and estimated.

### 2.4.1. Critical Property Measurements

Critical temperature and pressure of some pure components can be determined experimentally provided that the components are thermally stable at the critical conditions. For heavier hydrocarbons (heavier than C<sub>20</sub>), with very high critical temperatures but correspondingly low critical pressures, direct measurements are not possible due to thermal cracking of the hydrocarbons above about 500°C or even as low as 350°C for more reactive hydrocarbons. Critical properties can also be obtained indirectly from other measurements, e.g., by regression of vapour pressure data.

The acentric factor is a derived property related to the curvature of the VLE line and requires that the critical temperature and pressure are known. By definition, the acentric factor is given by:

$$\omega = -\log \left[ \frac{P^{sat}}{P_c} \right]_{T_r=0.7} - 1 \quad (2.32)$$

If the saturation pressure at the reduced temperature is not known then correlations, discussed below, are available to estimate it.

Ambrose and Young<sup>58</sup> have reviewed the methods used to determine critical properties. The typical method for experimentally determining critical temperature and pressure is based on the observation of the meniscus between the liquid and gas phases. As the critical temperature is approached from the sub-critical region, the meniscus disappears at the critical point. This method is only reliable if the pure component is thermally stable around the critical conditions.

When the pure component is thermally unstable, short duration measurements at the critical conditions are employed. As demonstrated by Teja *et al.*<sup>59</sup>, critical temperature can be determined by a method based on rapid heating of a sealed tube with extrapolation to account for the small amount of decomposition. Teja and co-workers also developed a short residence time flow method that can be used to obtain both critical temperature and critical pressure.

Indirect measurements of critical properties include those based on the discontinuity in physical properties at the critical point. For example, Ribeiro *et al.*<sup>60</sup> developed a method based on the measurement of the speed of sound. As the critical point is approached, the isothermal compressibility ( $k_T$ , equation (2.33)) tends to infinity and the speed of sound ( $c$ , equation (2.34)) in the fluid decreases and is more strongly attenuated. This method is particularly useful for mixtures.

$$k_T^{-1} = \rho \left( \frac{\partial P}{\partial \rho} \right)_T \quad (2.33)$$

$$c = \sqrt{\frac{C_p}{C_v} \left( \frac{\partial P}{\partial \rho} \right)} \quad (2.34)$$

Critical properties and acentric factors for many pure components are tabulated in a number of sources. The DIPPR database provides an extensive compilation of data that has been evaluated for suitability for thermodynamic calculations. The text by Poling,

Prausnitz, and O'Connell is another useful source of experimentally determined critical properties drawn from the TRC Thermodynamic Tables<sup>61</sup>.

#### 2.4.2. Properties from Correlations

A number of correlations have been developed for prediction of critical temperature and pressure. Ideally, these correlations should be based on measurements that encompass the range of applicability. As was already discussed, for hydrocarbons such as n-paraffins, measurements can be made up to n-eicosane before thermal stability of the n-paraffin makes the measurements unreliable. For hydrocarbons heavier than n-eicosane critical properties need to be estimated by, for example, regression of vapour pressure data or from theoretical considerations. As a final resort, correlations can be employed outside the range of data on which they are based. Riazi<sup>62</sup> provides an excellent review of the many correlations developed for prediction of critical properties.

##### 2.4.2.1. Critical Properties

The correlations typically used for prediction of critical properties have a weak theoretical basis and should be considered as being purely empirical. For a homologous series of hydrocarbons, correlations are based on single properties such as carbon number, molecular mass, or normal boiling point. The typical form of these correlations is:

$$\ln(\theta_{\infty} - \theta) = a - b\Omega^c$$

where:

$$\begin{array}{ll} \theta & \text{--critical property} \\ \theta_{\infty} & \text{--limiting critical property} \\ \Omega & \text{--carbon number, molar mass or boiling point} \\ a, b, c & \text{--coefficients} \end{array} \quad (2.35)$$

The use of normal boiling point becomes problematic for very heavy hydrocarbons because of the potential for thermal reactions. Fortunately, critical temperature and pressure tend towards limiting values as carbon number and molecular mass increases. The limiting value of critical temperature is usually taken as limiting the boiling point.

Some of these correlations have limiting values which may not be reasonable or lack theoretical support. Using measured critical data and a modified Flory theory for the free energy of linear chain molecules, Tsonopoulos and Tan<sup>63</sup> were able to fit the measured data and define limiting critical properties for n-paraffins. Unlike some correlations which result in a limiting critical pressure of zero absolute pressure, Tsonopoulos and Tan predict a limiting value of 0.268 MPa. The limiting value of the critical properties is one of the main differences between various correlations and the source of most of the variability in the predictions for critical properties of heavy hydrocarbons.

For petroleum distillates, average boiling points and specific gravities are readily available. The distillate fraction may be further subdivided into molecular class (e.g., paraffins, isoparaffins, naphthenes, and aromatics). Many correlations for estimating critical properties of distillate fractions have been developed which require only normal boiling point and specific gravity for the entire fraction or for each molecular class within each fraction. These critical properties are more accurately called pseudo-critical properties. Kesler and Lee<sup>64</sup> developed widely used correlations for critical properties with six coefficients for calculation of critical temperature and ten coefficients for calculation of critical pressure. These correlations are still used in some process simulators.

Riazi and Daubert<sup>65</sup> produced the first widely accepted simple correlations having the form:

$$\theta = aT_b^n SG^m$$

where :

$$\begin{array}{ll} \theta & \text{--critical property} \\ T_b & \text{--normal boiling point} \\ SG & \text{--specific gravity} \\ a, n, m & \text{--coefficients} \end{array} \quad (2.36)$$

This correlation has been adapted for a wide variety of hydrocarbon families by regression of the coefficients with experimental data for each family. One problem with

correlations of this form is that they can be inconsistent. Three independent correlations are used to determine critical temperature, pressure, and volume whereas all critical properties are related to each other through molecular structure and interactions. Another issue with correlations of this form is that there is no obvious limiting value as boiling point and specific gravity increases. Exceptions to these inconsistencies include the correlations developed by Twu<sup>66</sup> for heavy oils and coal-tar liquids with specific gravities up to 1.44 and normal boiling points up to 715°C. The correlations developed by Twu use the critical properties of n-paraffins as a reference. These correlations still require normal boiling point and specific gravity as input. The normal boiling point is used to calculate critical properties for a reference n-paraffin. These reference critical properties are then used with specific gravity to solve iteratively for the inter-related critical properties of the real fluid.

Riazi and Daubert<sup>67</sup> point out that the two parameter correlations, in the form of equation (2.36), are only suitable for non-polar hydrocarbons and even then have limited accuracy. For hydrocarbon containing heteroatoms (S, O, N) and polar functional groups, a third parameter is necessary. For improved predictions of critical properties of pure hydrocarbons (paraffins, olefins, naphthenes, and aromatics) Riazi and Daubert<sup>67</sup> proposed a new correlation of the form:

$$\theta = a \cdot \exp(b\theta_1 + c\theta_2 + d\theta_1\theta_2) \cdot \theta_1^e \theta_2^f$$

where :

$\theta$	–critical property	(2.37)
$\theta_1$	–normal boiling point	
$\theta_2$	–specific gravity	
$a, b, c, d, e, f$	–coefficients	

Although boiling point and specific gravity are the normal input properties for using equation (2.37), Riazi and Daubert also provided correlations for other pairs of properties such as boiling point and carbon-to-hydrogen ratio, and molar mass and specific gravity. Critical properties predicted using equation (2.37) were compared to those predicted using the correlations developed by Twu and Kesler and Lee. A data set

of 138 pure compounds with normal boiling points from 27 to 343°C and molar mass of 70 to 300 g/mole was used for the comparison. The correlation of Riazi and Daubert was only slightly better than that of Twu which in turn was only slightly better than that of Lee and Kesler. The comparison with Twu's correlation may be somewhat unfair since Riazi and Daubert's correlation was optimized for lighter hydrocarbons with boiling points up to 343°C while Twu's correlations were developed especially for heavy hydrocarbons with boiling points up to 715°C.

Figure 2-1 and Figure 2-2 show calculated versus reference values for critical temperature and pressure, respectively for various types of hydrocarbons. The critical temperature and pressures were calculated using equation (2.37) with coefficients taken from Riazi and Daubert. Reference values were taken from HYSYS - Aspen database<sup>68</sup>. The compounds used included n-alkanes from C<sub>4</sub> to C<sub>30</sub>, substituted and unsubstituted aromatics from benzene to pyrene and sulphur compounds including mercaptans (thiols), sulphides and thiophenes ranging from ethylthiol to 1-octadecythiol. While good predictions of critical temperatures are obtained for n-alkanes, there are significant under- and over-predictions for sulphur and aromatic compounds. The predictions of critical pressures using equation (2.37) show large scatter for high critical pressures and for lower molar mass sulphur compounds and aromatics. For both predicted critical temperature and pressure, there was a broad range (up to 7% for T<sub>c</sub> and 30% for P<sub>c</sub>) in average absolute relative error for the different types of hydrocarbons. For sulphur-containing compounds and aromatics, there was no tendency for increase or decrease in error for either T<sub>c</sub> or P<sub>c</sub> with increasing boiling point. In contrast, the predicted critical temperatures for n-alkanes showed almost a constant absolute average relative error (~ 1%) whilst the error in predicted critical pressures tended to increase with increasing boiling point and was 18% for triacontane.

The use of correlations based on boiling point and specific gravity may have another source of inaccuracy when the normal boiling point is above 350°C. In order to avoid decomposition, such components are distilled under reduced pressure. The distillation pressure and temperature are then converted to an atmospheric equivalent using the correlation developed by Maxwell and Bonnell<sup>69</sup>. However, Gray *et al.*<sup>70</sup> suggest that the

error in conversion to an atmospheric equivalent boiling point, especially for aromatic compounds, may have a significant effect on the calculated critical properties.

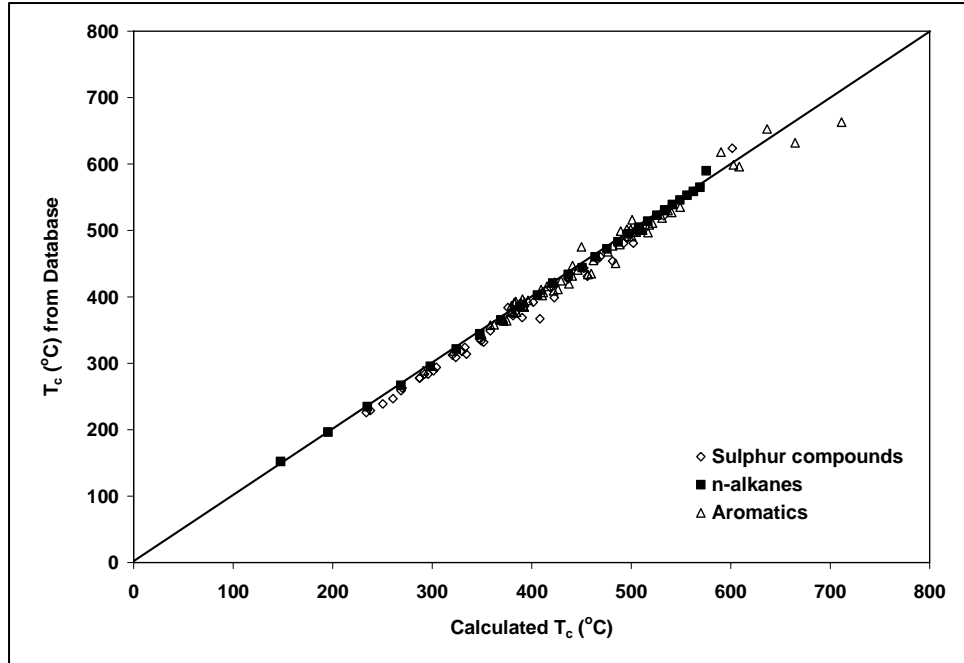


Figure 2-1 Comparison of calculated critical temperature using Riazi-Daubert correlation versus values from HYSYS-Aspen database.

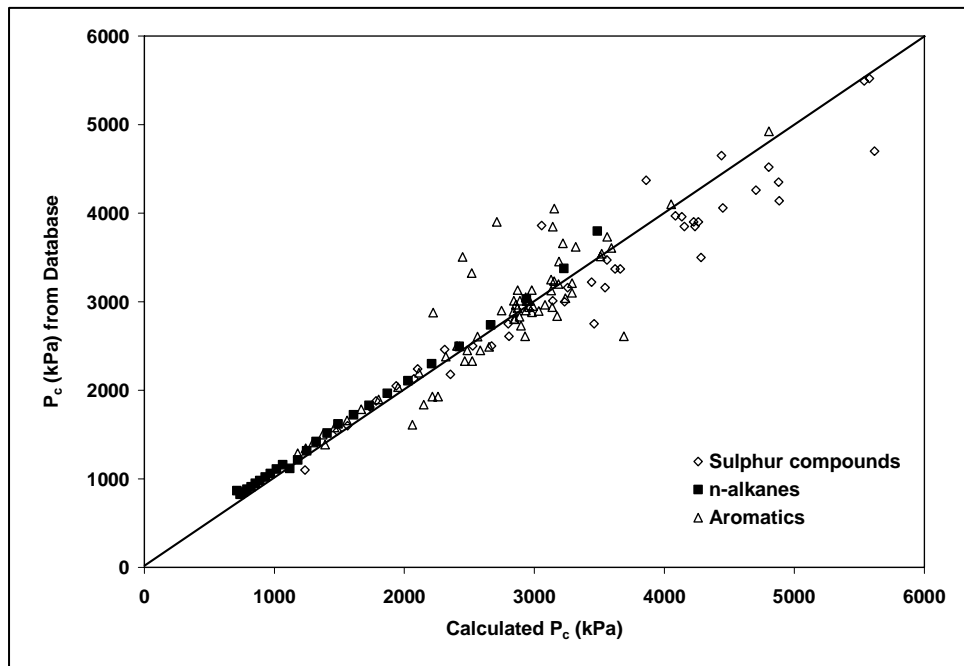


Figure 2-2 Comparison of calculated critical pressure using Riazi-Daubert correlation versus values from HYSYS-Aspen database.



#### 2.4.2.2. Acentric Factor

All of the widely used correlations for acentric factor require that the critical temperature and pressure be known. In addition, either a vapour pressure datum or normal boiling point must also be known. Thus, in cases where critical properties are also estimated using correlations, these errors may be magnified in the estimated acentric factor. Only a few of the more widely used correlations, which are discussed in greater detail by Poling *et al.*, are reviewed here.

The Lee-Kesler method requires the normal boiling point and critical properties, and is recommended for reduced boiling points ( $T_{b,r} = T_b/T_c$ ) less than 0.8 or molar mass less than 300 g/mole. It is based on Pitzer's definition, equation (2.13), with vapour pressure from the correlation by Lee and Kesler.

The method developed by Edmister is a more simple method which is also based on Pitzer's definition but uses the so-called shortcut method for estimation of vapour pressure. The use of the shortcut vapour pressure means that Edmister's correlation is suitable only when  $T_{b,r}$  is above 0.5 and the critical pressure is high enough so that ideal gas behaviour can be assumed for the vapour, i.e., it may not be suitable for heavy hydrocarbons with low critical pressures.

Poling *et al.* recommend the method of Ambrose and Walton<sup>71</sup> as being the most accurate. This method is based on a two-parameter equation for estimation of vapour pressure of n-paraffins based on the principle of corresponding states:

$$\ln\left(\frac{P_{sat}}{P_c}\right) = f^{(0)} + \omega f^{(1)} + \omega^2 f^{(2)}$$

where :

$$f^{(0)}, f^{(1)}, f^{(2)} - \text{functions of } T_c \text{ and } T_{sat}$$
(2.38)

For a database of 330 compounds, with acentric factors up to 0.954 for 1-eicosanol and molar mass up to 488.07 g/mole for eicosafuorononane, and including both polar and non-polar compounds, the average absolute deviation was 2.4%. The difference in error

by excluding the quadratic term was small so that with the removal of this term equation (2.38) could be made explicit for the acentric factor.

### 2.4.3. Group Contribution Methods

Group contribution (GC) methods for estimation of critical properties based on molecular composition and structure can in principle provide better results than correlations based on bulk properties because they intrinsically include molecular interactions which determine such properties. However, like bulk property based correlations, GC methods are developed by regression with data for components with low measurable critical properties. Thus, application to heavy hydrocarbons often involves applying these methods beyond the range of the data on which they are based. A few of the more widely used and more accurate GC methods for determination of critical properties are discussed. Two GC methods developed for estimation of acentric factors are also discussed.

#### 2.4.3.1. Joback-Reid Critical Properties

Joback and Reid<sup>72</sup> developed a GC method for estimating critical temperature, pressure, and volume as well as other properties such as enthalpy of vaporization and isobaric heat capacity. Essentially two levels of contributions are considered with atoms comprising the first order level of contribution and small groups (41 in all) comprising the second order level. The groups used are small and include no more than four atoms. This GC method does not include the effects of molecular geometry and, therefore, cannot distinguish between the properties of isomers. Estimated critical temperature and pressure are given by equations (2.39) and (2.40), respectively.

$$T_c(K) = T_b \left[ 0.584 + 0.965 \left( \sum_k N_k(tc_k) \right) - \left( \sum_k N_k(tc_k) \right)^2 \right]^{-1} \quad (2.39)$$

$$P_c(bar) = \left[ 0.113 + 0.0032N_{atoms} - \sum_k N_k(pc_k) \right] \quad (2.40)$$

where:

$N_k$ : number of groups of  $k^{\text{th}}$  type

$t_{ck}$ : contribution to  $T_c$  by  $k^{\text{th}}$  group  
 $p_{ck}$ : contribution to  $P_c$  by  $k^{\text{th}}$  group  
 $N_{\text{atoms}}$ : number of atoms in molecule

Several important points should be noted with regards to the above equations. The estimation of critical temperature requires that the normal boiling be known and, if not measurable, be estimated in some other way. This need to estimate boiling points for heavy hydrocarbons is a shortcoming of this GC method. The GC method for critical temperature assumes that, for small molecules, the critical temperature is approximately 1.7 times the normal boiling point. With this correlation, as molecular size increases, critical temperature first approaches the boiling point then increases before becoming negative for very large molecules. Thus, the Joback-Reid GC method is not consistent and physically reasonable for prediction of  $T_c$  for heavy hydrocarbons. Prediction of critical pressure does not require that any bulk property be known. This GC method for critical pressure predicts a limiting critical pressure of close to 0.11 bar for very large n-paraffins. The limiting value for critical pressure of very large molecules is uncertain but may be close to zero. Thus, the Joback-Reid GC method may be more reliable for predicting critical pressure than for critical temperature, especially for very large molecules.

Poling *et al.* have reported that for over three hundred molecules with molar mass up to 488.07 g/mole (eicosfluorononane), the average absolute error for estimating  $T_c$  and  $P_c$  was 6.7K (1.2%) and 2.2 bar (5.9%), respectively. The impacts of error in  $T_c$  and  $P_c$  in prediction of vapour pressure and liquid density were discussed above.

#### 2.4.3.2. Wilson-Jasperson Critical Properties

The GC method of Wilson and Jasperson<sup>73</sup> for  $T_c$  and  $P_c$  is based on the number of rings, atoms, and groups. Essentially two levels of contributions are considered. Atoms constitute the first order level and rings and a few small groups (14 in all) comprise the second order level. Due to its simplicity, this GC method is not capable of distinguishing the critical properties of isomers. Like the Joback-Reid GC method, the Wilson-Jasperson GC method requires that the normal boiling point be known and, for estimating  $P_c$ ,  $T_c$  must be known. While the dependence of  $P_c$  on  $T_c$  introduces a degree of molecular

consistency, errors in estimating  $T_c$  will be transferred to estimation of  $P_c$ . Critical properties are estimated as follows:

$$T_c(K) = T_b \left[ 0.04827 - 0.019846N_r + \sum_k N_k(tc_k) + \sum_j M_j(tc_j) \right]^{-0.2} \quad (2.41)$$

$$P_c(\text{bar}) = 0.0186233T_c \left[ -0.96601 + e^Y \right] \quad (2.42)$$

$$Y = -0.00922295 - 0.0290403N_r + 0.041 \left( \sum_k N_k(pc_k) + \sum_j M_j(pc_j) \right)$$

where:

$N_k$ : number of atoms of  $k^{\text{th}}$  type

$M_j$ : number of groups of  $j^{\text{th}}$  type

$tc_k$ : contribution to  $T_c$  by  $k^{\text{th}}$  group

$pc_k$ : contribution to  $P_c$  by  $k^{\text{th}}$  group

$N_r$ : number of rings

The GC method of Wilson and Jasperson shows that  $T_c$  tends toward  $T_b$  as molecular size increases, then decreases for very large molecules but does not go to zero or become negative for large molecules without many rings. In this respect, the GC method of Wilson-Jasperson is more consistent than that of Joback-Reid. Like the Joback-Reid GC method, the limiting value of  $P_c$  for very large molecules is close to zero. Using the same database to evaluate the GC methods of Joback-Reid and Wilson-Jasperson, Poling *et al.* found that both GC methods had similar accuracy.

#### 2.4.3.3. Marrero-Gani Critical Properties

One of the more recent developments in GC methods for critical properties has been the use of more complex groups that can, in principle, distinguish between the properties of isomers. Marrero and Gani have proposed a GC method for estimation of critical properties as well as normal boiling and melting points and enthalpies for phase transitions. In this GC method, three levels of group contribution are considered. The first order level of contribution is composed of small groups that are able to describe a wide variety of organic compounds. First order groups are used to describe the entire molecule. A total of 182 first order groups have been defined. The second order groups

are more complex than the first order groups and include geometric considerations that can be used to distinguish isomers for a range of molecular classes from paraffins to aromatics. Second order groups need not describe the entire molecule and the groups may overlap in some parts of the molecules. A total of 122 second order groups have been defined. Finally, third order groups were created to better describe polycyclic systems such as fused aromatic and non-aromatic rings as well as rings joined together by chains. A total of 66 third order groups have been defined. The equations for estimating critical temperature (K) and pressure (bar) have the following forms:

$$\exp(T_c/231.239) = \sum_i N_i(tc_i) + \sum_j M_j(tc_j) + \sum_k O_k(tc_k) \quad (2.43)$$

$$(P_c - 5.9827)^{-\frac{1}{2}} - 0.108998 = \sum_i N_i(pc_i) + \sum_j M_j(pc_j) + \sum_k O_k(pc_k) \quad (2.44)$$

where:

$N_i, M_j, O_k$ : number of 1<sup>st</sup>, 2<sup>nd</sup> and 3<sup>rd</sup> order groups

$tc_i, tc_j, tc_k$ : 1<sup>st</sup>, 2<sup>nd</sup> and 3<sup>rd</sup> order group contributions to  $T_c$

$pc_i, pc_j, pc_k$ : 1<sup>st</sup>, 2<sup>nd</sup> and 3<sup>rd</sup> order group contributions to  $P_c$

The Marrero-Gani GC method does not require that the normal boiling point be known and neither does the estimation of critical pressure depend on critical temperature. The explicit independence of critical pressure from critical temperature appears to create an inconsistency but this is probably overcome by the complexity of the groups considered in this method. The Marrero-Gani GC method has a limiting value of critical pressure of 5.99 bar. This limiting value for  $P_c$  is higher than the 2.68 bar calculated from theoretical considerations by Tsonopoulos and Tan<sup>63</sup> for large n-paraffins.

Marrero and Gani have developed and evaluated their GC method using 2,000 compounds ranging from  $C_3$  to  $C_{60}$  drawn from the CAPEC database<sup>74</sup>. The average absolute errors for  $T_c$  and  $P_c$  were compared for the Marrero-Gani and Joback-Reid GC methods using a subset of the CAPEC database consisting of about 570 compounds. For estimation of  $T_c$ , the average absolute error was 11.0K (2.1%) for Joback-Reid versus 4.9K

(0.9%) for Marrero-Gani. In the case of estimated  $P_c$ , the average absolute error was 2.45% for Joback-Reid versus 0.74% for Marrero-Gani. Given the similar performance of the Wilson-Jasperson and Reid-Joback GC methods, it appears that the Marrero-Gani GC method may be the most reliable one to use for estimating critical properties. An additional advantage of the Marrero-Gani GC method is that its complexity allows distinction between isomers whereas the more simple GC methods cannot make this distinction.

#### 2.4.3.4. Han-Peng Acentric Factor

Han and Peng<sup>75</sup> developed a GC method for estimation of the acentric factors for hydrocarbons except methane and those containing boron, silicon, or halogens. The database used to develop the correlation included 219 compounds including n-paraffins up to n-eicosane. The GC method can be represented as:

$$\omega = 0.004423 \left[ \ln \left( 3.3063 + \sum_i N_i \varepsilon_i \right) \right]^{3.651} \quad (2.45)$$

where:

$N_i$ : number of group of the  $i^{\text{th}}$  type

$\varepsilon_i$ : contribution from group of  $i^{\text{th}}$  type

The contributions of some groups such as ring structures are complicated by corrections that depend on the number of groups in the ring. The Platt numbers (total number of pair of carbons three bonds apart) of paraffinic structure and corresponding n-paraffin must be determined for other group contributions. For the 60 paraffins in the database used for developing the correlation, the average absolute deviation was 1.2%. The correlation was not evaluated with an independent dataset nor was the error reported for other types of hydrocarbons.

#### 2.4.3.5. Constantinou-Gani-O'Connell Acentric Factor

A more comprehensive GC method, in comparison to that of Han and Peng, for estimation of acentric factor was proposed by Constantinou, Gani and O'Connell<sup>76</sup>. The GC method considers first order contributions from relatively simple groups that can be

used to represent most molecules including those containing halogens. Second order contributions from more complex groups provide geometric considerations which may distinguish some isomers although Constantinou, Gani and O'Connell do not make this claim. The GC method for estimating acentric factor is given by the following equation:

$$\omega = 0.4085 \left[ \ln \left( \sum_i N_i \varepsilon_{1i} + A \sum_j M_j \varepsilon_{1j} + 1.1507 \right) \right]^{0.5050} \quad (2.46)$$

where:

$N_i, M_j$ : number of 1<sup>st</sup> and 2<sup>nd</sup> order groups

$\varepsilon_{1i}, \varepsilon_{1j}$ : 1<sup>st</sup> and 2<sup>nd</sup> order group contributions to  $\omega$

A: 0 or 1 depending on whether or not there is a defined 2<sup>nd</sup> order contribution

The application of the Constantinou-Gani-O'Connell GC method is straightforward with the exception that not all of the groups listed have assigned contributions because the database used in development of the method was not sufficient to extract a good estimate of their contribution. The average absolute relative error for estimation of the acentric factor for hydrocarbons (C and H only) was 2.5% which is similar to the error reported by Han and Peng. For hydrocarbons with heteroatoms substitution, the error ranged up to 4.4%. Poling *et al.* have reported that for 80 molecules evaluated, the average absolute relative error for estimating acentric factor was 11.98%.

#### 2.4.4. CEOS based on Group Contribution

As an alternative to estimating critical properties and then calculating the two parameters (co-volume and attractive energy parameter) for the CEOS, GC methods have been incorporated directly into the CEOS. Such methods are not yet in widespread use in, for example, process simulators. One example of this type of GC method which has been recently refined is discussed.

A group contribution-based form of the Peng-Robinson CEOS has been developed by Coniglio *et al.*<sup>77</sup> and further refined and simplified by Crampon and coworkers<sup>78</sup>. The later GC method provides contributions from 19 groups which encompass alkanes, naphthenes, aromatics, alkenes, and alkynes. The co-volume, 'b', is calculated from a GC

method developed by Bondi for the van der Waals volume ( $V^*$ ) but using methane as a reference:

$$b = b_{CH_4} \frac{V^*}{V_{CH_4}^*}$$

where :

$$b_{CH_4} = 26.80 \text{ cm}^3 \text{ mol}^{-1}$$

$$V_{CH_4}^* = 17.12 \text{ cm}^3 \text{ mol}^{-1}$$
(2.47)

The van der Waals volume ( $V^*$ ) for a component is given by GC:

$$V^* = \sum_i N_i V_i$$

where :

$$N_i : \text{number of groups of the } i^{\text{th}} \text{ type}$$

$$V_i : \text{contribution of the } i^{\text{th}} \text{ group}$$
(2.48)

The attractive energy parameter, 'a', is temperature dependent and can also be estimated by the GC method:

$$a(T) = a(T_b) \exp \left[ \begin{array}{c} (1.80546m + 0.21887) \left( 1 - \left( \frac{T}{T_b} \right)^{0.4} \right) \\ - (-0.11113m + 0.03502) \left( 1 - \left( \frac{T}{T_b} \right)^{2.5} \right) \end{array} \right]$$

where :

$$m : \text{shape factor from GC method}$$
(2.49)

Note that the temperature dependence of the attractive energy parameter is expressed as a "reduced" normal boiling point which, therefore, must be known. If the normal boiling point is not known or cannot be measured then it can be estimated from another GC method developed by Coniglio and Nouviaire<sup>79</sup> or, alternatively, the method of Marrero



and Gani discussed above. The value of  $a(T_b)$  is found through iteration using the Peng-Robinson equation of state to match the vapour pressure at the normal boiling point, i.e., 1 atmosphere. The so-called shape factor,  $m$ , is stated to be characteristic of the molecular shape and is calculated from a group contribution method:

$$m = 0.23269S^{(S^{0.6}+0.5)} + 0.08781\ln(S) + 0.59810 \quad (2.50)$$

$$S = \sum_j M_j S_j$$

where :

$M_j$  : number of groups of the  $j^{\text{th}}$  type

$S_j$  : contribution of the  $j^{\text{th}}$  group

(2.51)

The estimation of the co-volume and  $a(T)$  are based on a linear sum of contributions which is identical in form to the linear vdW mixing rule for the co-volume.

The average absolute errors for estimating vapor pressures for alkanes, cycloalkanes and aromatics were evaluated for the GC method of Crampon *et al.* and they were compared with the original GC method of Coniglio *et al.* The errors were slightly greater with Crampon's method but still within the range of experimental error, i.e., about 1%. For alkanes up to n-triacontane and aromatics up to 1-phenyl-naphthalene, the GC methods of Coniglio's and Crampon's provided a significant improvement over the Peng-Robinson CEOS using critical parameters estimated from GC methods. However, it must be noted that the GC methods used for estimation of critical properties used in the PR CEOS were those of Ambrose<sup>80</sup> and may not represent the best choice for estimating such properties.

The original GC method of Coniglio *et al.* developed for the Peng-Robinson CEOS was recently evaluated by Van Waeyenberghe<sup>81</sup>. For pure fluids (toluene, cyclooctane, n-eicosane, and pyrene), very similar vapour pressure estimates were obtained from the GC-based PR and critical properties-based PR CEOS and both results were in good agreement with experimental data. For binary mixtures (hexane/hexadecane and

benzene/ethylbenzene), the GC-based PR gave slightly better agreement with the experimental data than the critical property-based PR CEOS.

Van Waeyenberghe also applied the GC-based PR CEOS to estimation of the vapour pressure of Athabasca vacuum tower bottom (VTB) alone and with 90 wt.% and 50 wt.% n-decane. The vapour pressure of pure VTB was grossly underestimated by the GC-based PR CEOS; however, reasonably good agreement was obtained with VTB and 90 wt.% mixture of n-decane. The estimated vapour pressure for the mixture of VTB and 50 wt.% decane was not in good agreement with the experimental data. The poor agreement in this case was explained by the presence a second liquid phase which could not be accounted for in the Van Waeyenberghe's calculations.

## 2.5. CUBIC EQUATIONS OF STATE FOR MIXTURES

For application of CEOS to fluid mixtures, mixing rules are required to calculate the overall attractive energy and co-volume parameters (the 'a' and 'b' terms, respectively), for example, in the van der Waals CEOS given by equation (2.1). The choice of mixing rules can have significant effects on the predictions from CEOS. Depending on whether the mixture consists of molecules of similar types and size, and are polar or non-polar, one mixing rules may give better predictions than another. This section is devoted to the most commonly employed mixing rules, the so-called van der Waals mixing rules. Other examples of mixing rules are discussed in subsequent sections.

### 2.5.1. *van der Waals Mixing Rules*

The original mixing rules proposed by van der Waals were fairly simple and were comprised of the geometric mean mixing rule for the attractive term and the linear mixing rule for the co-volume:

$$a_{mix} = \left( \sum_i x_i \sqrt{a_i} \right)^2 \quad (2.52)$$

$$b_{mix} = \sum_i x_i b_i \quad (2.53)$$

These mixing rules worked well for mixtures of similar hydrocarbons, however, for dissimilar hydrocarbons the errors in predictions could be large. The mixing rules were subsequently modified by the introduction of new parameters to account for the interactions between dissimilar molecules. These modifications gave rise to the so-called classical or van der Waals mixing rules commonly used in CEOS:

$$a_{mix} = \sum_i \sum_j x_i x_j a_{ij} \quad (2.54)$$

$$b_{mix} = \sum_i \sum_j x_i x_j b_{ij} \quad (2.55)$$

The terms  $a_{ij}$  and  $b_{ij}$  are given the following combining rules:

$$a_{ij} = (a_i a_j)^{\frac{1}{2}} (1 - k_{ij}) \quad (2.56)$$

$$b_{ij} = 0.5(b_i + b_j)(1 - l_{ij}) \quad (2.57)$$

where:

$$k_{ij} = k_{ji}; l_{ij} = l_{ji}$$

$$k_{ii} = 0; l_{ii} = 0$$

The parameters  $k_{ij}$  and  $l_{ij}$  in equations (2.56) and (2.57) are the so-called binary interaction parameters and are entirely empirical in nature. If both  $k_{ij}$  and  $l_{ij}$  are set equal to zero then equations (2.54) and (2.55) are reduced to the original van der Waals rules, equations (2.52) and (2.53), respectively. It is important to note that the use of the binary interaction parameters means that the CEOS is now no longer fully predictive even when the critical properties and acentric factors are known for each component in the mixture.

The cross terms,  $a_{ij}$  and  $b_{ij}$ , can take a number of forms besides those of the classical van der Waals mixing rules shown above. Among other forms for  $b_{ij}$  and  $a_{ij}$  are:

1. Lorentz rule derived from consideration of the additivity of collision diameters and which has been used by Radosz *et al.*<sup>82</sup> for asymmetric

mixtures of hydrogen and hydrocarbons up to n-hexadecane and diphenylmethane:

$$b_{ij} = \frac{1}{8} \left( b_i^{\frac{1}{3}} + b_j^{\frac{1}{3}} \right)^3 \quad (2.58)$$

2. Geometric mean rule proposed by Good and Hope<sup>83</sup> from theoretical considerations and which is identical to the van der Waals mixing rule for the energy parameter:

$$b_{ij} = \sqrt{b_i b_j} \quad (2.59)$$

3. The Lee and Sandler<sup>84</sup> rule developed on theoretical grounds for molecules :

$$b_{ij} = \left( \frac{b_i^{\frac{2}{3}} + b_j^{\frac{2}{3}}}{2} \right)^{\frac{3}{2}} \quad (2.60)$$

4. The Berthelot mixing rule:

$$a_{ij} = (a_i a_j)^{\frac{1}{2}} \frac{b_{ij}}{(b_i b_j)^{\frac{1}{2}}} \quad (2.61)$$

Kontogeorgis and co-workers<sup>85</sup> have examined the performance of the classical, Lorentz, geometric mean and Lee-Sandler co-volume mixing rules along with the classical and Berthelot mixing rules for the energy parameter. This study of various asymmetric mixtures of n-paraffins concluded that the combination of the two classical van der Waals mixing rules worked best. Furthermore, optimization of the binary interaction parameter for the co-volume term,  $l_{ij}$  in equation (2.57) with  $k_{ij}$  equal zero, resulted in better agreement with experimental data compared to optimization of the binary interaction parameter for the energy parameter,  $k_{ij}$  in equation (2.56) with  $l_{ij}$  equal

zero. The later result tends to emphasize the importance of size asymmetry for the mixing rule for co-volume.

### 2.5.2. Correspondence with Virial Equation of State

As discussed above, the virial equation of state, which is based on statistical mechanics, is exact for gases but does not provide good correspondence to liquid phase behaviour. In the low density limit, CEOS and the virial EOS should yield the same result for a gas. This concept has been applied to relate the attractive and co-volume terms from a CEOS to the coefficients of the virial EOS. This was demonstrated above for the van der Waals CEOS. Comparing equations (2.6) and (2.8) it can be seen that the second and higher virial coefficients are related to the two parameters from the CEOS:

$$B = b - \frac{a}{RT} \quad (2.62)$$

$$C = b^2; D = b^3 \dots \quad (2.63)$$

Since it is known that the second virial coefficient accounts for most of the deviation from ideal gas behaviour, its compositional dependence can be used to develop a set of mixing rules having a basis in statistical mechanics. Hall *et al.*<sup>86</sup> have shown that for a binary mixture, the compositional dependence of all virial coefficients is quadratic provided that all cross-terms ( $B_{12}$ ,  $C_{12}$ ,  $D_{12}$ , etc.) have no compositional dependence. This is certainly true for the second virial coefficient. Furthermore McGregor *et al.*<sup>87</sup> has shown that this can also be true of the third virial coefficient. It therefore follows that:

$$B_{mix} = \sum_i \sum_j x_i x_j B_{ij} \quad (2.64)$$

$$C_{mix} = \sum_i \sum_j x_i x_j C_{ij} \quad (2.65)$$

From equations (2.64) and (2.65) it follows that  $a_{mix}$  and  $b_{mix}$  will be given by the following relationships:

$$b_{mix} - \frac{a_{mix}}{RT} = \sum_i \sum_j x_i x_j \left( b_{ij} - \frac{a_{ij}}{RT} \right) \quad (2.66)$$

$$b_{mix}^2 = \sum_i \sum_j x_i x_j b_{ij}^2 \quad (2.67)$$

Hall *et al.* have shown that if  $B_{ij}$  is the arithmetic average of  $B_{ii}$  and  $B_{jj}$  and,  $a_{mix}$  and  $b_{mix}$  are mutually independent, then the original van der Waals mixing rule can be reproduced independent of the choice of CEOS used in the above derivation. If  $a_{mix}$  and  $b_{mix}$  are not mutually independent, then more complex mixing rules are obtained which are CEOS specific.

The mixing rule for the second virial coefficient and its relationship with the attractive energy and co-volume parameters have been used as justification for the van der Waals mixing rules. Placing this limitation on the mixing rules has been questioned since CEOS are applied to both the liquid and vapour phase while the virial EOS is only applicable to the gas phase. Some researchers therefore contend that limitations on mixing rules derived from the virial EOS should not be rigidly applied by limiting the mixing rules to having a quadratic dependence on composition (see equations (2.54), (2.55), and (2.64)). Indeed, some mixing rules with higher compositional dependence have been shown to work better for some mixtures than the van der Waals mixing rules. However, Orbey and Sandler<sup>88</sup> have pointed out that the fugacity coefficient of a component in a mixture, which is required for phase behaviour calculations, integrates the compositional dependence of pressure from zero density up to the density of the mixture. Thus, if the compositional dependence at zero pressure, i.e., the lower boundary condition, is violated the CEOS model becomes theoretically inconsistent and also introduces a potential source of error in the prediction of phase behaviour. Where the mixing rules with higher than quadratic compositional dependence work well, they may do so only for some systems in limited regions of PVT space.

Another approach to explaining the success (or legitimizing) the van der Waals mixing rule (e.g., Harismiadis *et al.*<sup>89</sup>) is to show that they can be derived from statistical

mechanics for hard spheres with pair-wise interaction represented by a Lennard-Jones potential ( $u_{ij}$ ):

$$u_{ij} = 4\varepsilon_{ij} \left[ \left( \frac{\sigma_{ij}}{r} \right)^{12} - \left( \frac{\sigma_{ij}}{r} \right)^6 \right] \quad (2.68)$$

where:

$u_{ij}$ : interaction energy

$\varepsilon_{ij}$ : characteristic energy; depth of the potential energy well

$\sigma_{ij}$ : characteristic distance; distance between centers of interacting spheres for energy

$r$ : distance between interacting spheres

From the application of conformal theory, whereby a single hypothetical fluid is used to represent the properties of a real fluid (in this case the Lennard-Jones fluid consisting of hard spheres), the characteristic energy and distance of this so-called one-fluid (1-f) can be expressed as:

$$\sigma_{1-f}^3 = \sum_i \sum_j x_i x_j \sigma_{ij}^3 \quad (2.69)$$

$$\varepsilon_{1-f} \sigma_{1-f}^3 = \sum_i \sum_j x_i x_j \varepsilon_{ij} \sigma_{ij}^3 \quad (2.70)$$

Tenuous relationships between the attractive energy parameter 'a' and  $\varepsilon\sigma^3$  and the co-volume 'b' and  $\sigma^3$  have been invoked to lend support to the van der Waals mixing rule. However, there is no direct relationship between the attractive term in a CEOS and the attractive part of an intermolecular potential. Also, real molecules are not hard spheres.

#### 2.5.2.1. Limitations and Pitfalls

Even after modifications to the original van der Waals mixing rules (equations (2.52) and (2.53)) through the inclusion of binary interaction parameters, they are only applicable to moderately non-ideal mixtures (see for example Sengers *et al.* Chapter 9). It

is worth noting that CEOS have the same shortcomings when applied to mixtures as were discussed regarding their application to pure components.

In most applications of the mixing rules,  $l_{ij}$  is set equal to zero while  $k_{ij}$  is obtained from regression of experimental data. Even with the use of the binary interaction parameters, predicted phase behaviour for mixtures of molecules of very dissimilar sizes or types may not correlate well with experimental data. Additionally, while  $k_{ij}$  can be close to zero for nearly ideal mixtures of hydrocarbons, setting  $k_{ij}$  equal to zero does not correspond to treating the mixture as an ideal solution since this does not result in the expression for Gibbs excess energy of mixing being zero (see Chapter 9 by Sandler and Orbey in Sengers *et al.*). Indeed, setting  $k_{ij}$  to zero can lead to incorrect predictions of phase behaviour. This latter point again emphasizes that such CEOS is no longer fully predictive when applied to mixtures. The binary interaction parameter,  $k_{ij}$ , is typically a function of temperature but, as a parameter regressed from experimental data, it may not follow a consistent trend with temperature and may be either positive or negative.

## 2.6. CHALLENGES OF HEAVY OIL AND BITUMEN MIXTURES

Heavy oil and bitumen can be differentiated from light conventional and medium heavy crude oils by their density (or API gravity) and viscosity. However, these differences in physical properties that distinguish crude oils are merely manifestations of the differences in composition. A simplified molecular theory of viscosity<sup>90</sup> indicates that viscosity is exponentially related to boiling point and inversely related to molar volume. Gray has developed a correlation for the density of heavy oils which shows that density decreases with increasing hydrogen content but increases with increasing nitrogen and sulphur content:

$$\rho = 1033 - 13.69H + 13.85S + 115.7N \quad (2.71)$$

where:

$\rho$ : density is in kg/m<sup>3</sup>

H, S, N: hydrogen, sulphur, and nitrogen contents in wt. %



The fundamental differences between heavy oil or bitumen and light to medium crude oils are the higher boiling point and heteroatom content of the former. As previously discussed, in the case of Athabasca bitumen, about 50% of the oil has a boiling point above 525°C in comparison to light crude oils which typically have boiling points only up to about 350°C.

## 2.6.1. *Definition and Complexity of Heavy Oil Mixtures*

### 2.6.1.1. *Characterization by Molecular Structure*

In the growing field of petroleomics, efforts are being made to define heavy oils in terms of the molecular structures of individual components and thereby obtain good predictions of properties and phase behaviours. This is proving to be challenging for crude oils due to the large number of molecules that can be present in a single sample. The large numbers of molecules require that new procedures be developed just to handle the large amount of molecular data. For example, Rodgers and co-workers<sup>91</sup> have reported that in the polar fraction which accounts for only 10 wt.% of a crude oil, there are over 17,000 distinct molecules. Gray and Strausz<sup>92</sup> provide some examples of the types of molecular structures that can be found in heavy oils.

Rather than attempting to identify every molecule in a crude oil fraction, Sheremata *et al.*<sup>15, 16</sup> have taken a simpler and more utilitarian approach. In characterizing ten supercritically separated fractions of Athabasca bitumen vacuum bottoms, Sheremata and co-workers have used a Monte Carlo method to construct the minimum set of molecules which are consistent with elemental composition, molecular weight, and structural data from NMR. It was found that six molecules were required to describe each fraction and that, therefore, only sixty molecules were required to account for the molecular structural and physical properties of the vacuum bottoms which represents 50 wt.% of Athabasca bitumen. With such molecular representations, group contribution methods such as those developed by Marrero and Gani can be used to determine critical properties and acentric factor for calculating parameters for a CEOS.

### 2.6.1.2. Characterization by Boiling Point

Even the limited molecular representations derived from chemical analysis as demonstrated by Sheremata *et al.*<sup>15, 16</sup> cannot yet be considered a routine procedure for heavy oil. Characterization of heavy oils for estimation of critical properties is still done on the basis of boiling point distribution from atmospheric and vacuum distillation. Crude oils and distillate fraction are complex mixtures of thousands of components that have an essentially continuous boiling point distribution. To conveniently and properly represent the oil and distillate so that their phase behaviours can be modeled in, for example, a distillation tower, two approaches are commonly used. The first approach is to characterize the crude oil or crude oil fractions in terms of pseudo-components defined by an average boiling point or hydrocarbon type (e.g., paraffinic, olefinic, naphthenic, or aromatics). Correlations such as those based on boiling point and specific gravity can then be used to calculate critical properties. A second approach is the so-called continuous mixture approach where the oil is described by a continuous distribution function with respect to molecular mass, boiling point, or some other measurable property. This approach only works well when the oil consists of one type of hydrocarbon, for example, paraffins.

In the case of heavy oils and bitumen, which include a significant fraction which can be separable by conventional distillation, gas chromatographic techniques can be used to estimate boiling points up to 750°C. This technique called high temperature simulated distillation<sup>93</sup> uses a correlation between the retention times of n-paraffins up to C<sub>100</sub> to estimate the boiling points of crude oil mixtures. The predicted boiling points of heavy oils and bitumen from this technique are only as good as the correlations used to determine them and whether the oil components, which may include aromatics and heteroatoms, behave like n-paraffins on the gas chromatographic column. Heavy oils and bitumen may have material that boil above 750°C. Whether a conventional or simulated distillation is used to characterize the oil, by assuming a log normal distribution for carbon number, the boiling point distribution curve can be extended to the temperature corresponding to 100% of the heavy oil or bitumen.

### 2.6.2. *Correlations for Critical Properties of Heavy Oil Components*

As already mentioned above, crude oils can be characterized by a number of methods that allow one to determine critical properties and acentric factors for a CEOS. If the crude is defined in terms of molecular structure, then group contribution methods can be employed. If the crude oil is defined by boiling point and specific gravity, simple correlations based on these properties can be used. In the case of heavy oils and bitumen, it has already been indicated that non-distillable residues present a challenge. If there is no measurable boiling point then correlations for critical properties based on such measurements are impossible. If boiling points for non-distillable residues representing a large fraction of the crude (e.g., 50 wt.% in the case of Athabasca bitumen) are determined by extrapolation, this would be unreasonable and the results may not be reliable. Even if reliable molecular structure and boiling points are available, heavy oils and bitumen still represent a challenge because GC methods and correlations are generally developed for lighter distillable hydrocarbons.

#### 2.6.2.1. *High Molecular Mass*

Group contribution methods requiring molecular structure and correlations utilizing boiling point and specific gravity are based on low boiling distillate having low critical temperatures and high critical pressures. Some of the challenges of measuring and estimating critical properties for heavy hydrocarbons were discussed above. The relationships used for estimating critical properties are properly used only in the range of actual measurement, i.e., critical temperatures up to about 350°C. Heavy crudes and bitumen will have a substantial fraction boiling between 350 and 525°C and perhaps an even larger fraction boiling above 525°C. Some boiling point and specific gravity correlations can be applied to hydrocarbons with molecular weights up to 700 g/mole corresponding to a C<sub>50</sub> paraffin. Many correlations however are only valid for molecular weights up to about 300 g/mole (equivalent to C<sub>22</sub> paraffin) which correspond approximately to the heaviest fraction from atmospheric distillation. The residue fraction, including asphaltenes, may have molecular weights as high as 5,000 g/mole although this high value may be due to associative behaviour. Other fractions of the non-asphaltenic portion of Athabasca vacuum bottoms may have molecular weights<sup>94</sup> up to 1,200 g/mole. The molecular weights of such bitumen fractions are well beyond

the range of all of the previously discussed correlations and group contribution methods.

#### 2.6.2.2. Aromaticity and Heteroatoms

It should be noted that many boiling point and specific gravity correlations are heavily based on critical properties of the homologous series of n-paraffins. One clear example of this is the correlations developed by Twu for heavy hydrocarbons where the underlying reference compounds consist entirely of n-paraffins. Even with the inclusion of other hydrocarbon types, the data on which the correlations are based are usually relatively small, typically two hundred to three hundred compounds. Group contribution methods, by necessity, cover a wide range of hydrocarbons but may be based on a relatively small database of reliable critical properties. The group contribution method of Marrero and Gani, which is based on data from about two thousand compounds, may be one of the few exceptions to this.

The above shortcomings were demonstrated with the Riazi-Daubert correlation for n-paraffins, aromatics, and sulphur-containing hydrocarbons. The results shown in Figure 2-1 and Figure 2-2 illustrate that while there is good correspondence between predicted and measured critical properties for n-paraffins, there are significant errors in predictions for aromatics and sulphur-containing hydrocarbons. For example, the average absolute error in predicted critical temperature was 0.8% for n-paraffins, 2.4% for aromatics, and 3.7% for sulphur-containing compounds. As noted before, Voulgaris *et al.* have shown that even a 1% error in critical temperature can lead to a 16% error in vapour pressure prediction. Thus, in applying correlations such as those discussed earlier to heavy crudes containing aromatics and heteroatoms, there will be a significant degree of uncertainty in the predictions due to unknown level of error in the estimated critical properties and acentric factor. One way to resolve these errors is to use measured data for these heavy crudes to regress critical properties or to adjust the binary interaction parameters. Another approach involves the use of group contribution methods provided that the molecular structures are known.

### 2.6.2.3. Association

Heavy oils and bitumen contain polar hydrocarbons which may associate in the liquid phase. Asphaltenes are a solubility class of hydrocarbons that are known to associate in heavy oil and bitumen under a wide range of process conditions. The main driving force for the association of asphaltenes appears to be their poor solubility due to stronger intermolecular interactions compared to asphaltene-oil/solvent interactions<sup>95</sup>. Yarranton<sup>96</sup> has suggested that asphaltene molecules may associate via  $\pi - \pi$ , acid-base, and hydrogen bonding in a manner similar to polymerization in aggregates of three to six molecules. The strong tendency of asphaltenes to associate makes their characterization difficult.

For a long time there was no general agreement on what the molecular weight of asphaltenes might be and suggested values range from 500 to 5,000 g/mole depending on the technique used in its measurement<sup>97</sup>. Led by Mullins and co-workers<sup>98</sup>, there is an emerging consensus that the molecular weight may be around 750 g/mole. However, more recent work by Qian and co-workers<sup>99</sup> indicate an asphaltene molecular weight of 1238 g/mole. Due to their strong association and thermal reactivity, it is unlikely that a boiling point can be measured for asphaltenes so a  $T_b/SG$  correlation cannot be used. Data on the structure of asphaltenes are still emerging and models are being developed. Until a well-defined structure is resolved for asphaltenes a group contribution method cannot be used to estimate critical properties. Even if critical properties can be estimated, strong intermolecular association of asphaltenes will complicate the calculation of phase behaviour using standard CEOS.

### 2.6.3. Size Asymmetry

Heavy oils and bitumens contain hydrocarbons which span the range from light distillates to heavy non-distillable residue. This wide range in hydrocarbon boiling points and corresponding range in molecular size make heavy oils and bitumens asymmetric mixtures. The asymmetry of heavy oil mixtures has a profound effect on phase behaviour so that even at low temperatures liquid-liquid phase behaviour may occur<sup>100</sup>. These asymmetric mixtures cannot be considered ideal with respect to use of van der Waals mixing rules for CEOS. It has been suggested that the van der Waals

mixing rules may be adequate for pairs of molecules that have up to an eightfold difference in volume. However, this conclusion is based on hard sphere molecules but real molecules are not hard spheres.

## 2.7. APPROACHES TO DEALING WITH HEAVY OIL AND BITUMEN MIXTURES

The application of CEOS to predict the phase behaviour of heavy oils and bitumens faces many challenges. These challenges include obtaining critical properties to estimate parameters for the CEOS, the nature of the alpha function, and choice of appropriate mixing rules for asymmetric mixtures. This section discusses a few of the solutions proposed for dealing with the challenges posed by heavy oil and bitumen mixtures.

### 2.7.1. Alpha Functions

Alpha functions generalized by acentric factors are determined typically by analysis of component specific  $\alpha(T)$  obtained from vapour pressure data for pure components with a particular CEOS. The numerical coefficients in these types of alpha functions are therefore CEOS specific. The focus of this discussion is limited to generalized alpha functions where coefficients have been determined specifically for the Peng-Robinson CEOS which will be used in the present study.

The original PR alpha function, equation (2.16), was developed for relatively small hydrocarbons with acentric factors up to 0.49 corresponding to n-decane. This original alpha function was later modified by Robinson and co-workers to cover a much wider range of acentric factors up to a value of 2 (equation (2.22)).

$$\alpha(T) = \left[ 1 + \kappa \left( 1 - T_r^{1/2} \right) \right]^2 \quad (2.16)$$

$$\text{where : } \kappa = 0.37464 + 1.54226\omega - 0.26992\omega^2$$

$$\alpha(T) = \left[ 1 + \kappa \left( 1 - T_r^{1/2} \right) \right]^2$$

$$\omega \leq 0.491$$

$$\kappa = 0.37464 + 1.54226\omega - 0.26992\omega^2 \quad (2.22)$$

$$\omega \geq 0.491$$

$$\kappa = 0.379642 + 1.48503\omega - 0.164423\omega^2 + 0.016666\omega^3$$

Stryjek and Vera proposed an alpha function with a substance specific parameter that was able to give reasonable predictions for non-ideal polar and associated mixtures. However, Stryjek and Vera required a non-symmetric binary interaction parameters,  $k_{ij} \neq k_{ji}$ . Thus, essentially two additional parameters are required with the Stryjek and Vera approach for predictions for polar, associating mixtures. The range of applicable acentric factors was not given by Stryjek and Vera so the applicability of their alpha function to associating heavy hydrocarbons is not known.

Twu *et al.* have proposed a radically different form for the alpha function which has exponential dependence on reduced temperature. Their form of the alpha function was generalized with acentric factors up to 0.95 corresponding to n-eicosane. However, it is claimed that the form of this alpha function provides better predictions with heavy hydrocarbons because of its linear dependence on acentric factor so it may be valid for even heavier molecules with higher acentric factors.

$$\alpha(T) = \alpha^{(0)} + \omega(\alpha^{(1)} - \alpha^{(0)})$$

where :

$$\alpha^{(0)} = T_r^{N^{(0)}(M^{(0)}-1)} e^{L^{(0)}(1-T_r^{N^{(0)}M^{(0)}})} \quad (2.27)$$

$$\alpha^{(1)} = T_r^{N^{(1)}(M^{(1)}-1)} e^{L^{(1)}(1-T_r^{N^{(1)}M^{(1)}})}$$

One potential issue with this exponential form of the alpha function is that while it may provide good predictions for vapour pressure, it may exhibit unreasonable behaviour for derivative properties such as isobaric heat capacities. Diedrich and coworkers<sup>101</sup> have shown that the PR CEOS with the Twu alpha function gave reasonable isobaric heat capacities at moderate to high temperatures but poor agreement at low temperature. However, the agreement could be improved by simultaneously fitting the coefficients of the alpha function to vapor pressure and enthalpy of vaporization.

### 2.7.2. Composition and Density Dependencies of Mixing Rules

Many systems of interest to chemical engineers are polar associating mixtures, such as those involving alcohols or organic acids combined with other hydrocarbons. Bitumen and heavy oils also contain polar and associating molecules. The behaviour of polar and associating systems is not well predicted by the classical van der Waals mixing rules and simple alpha functions. One alternative alpha function for polar associating mixtures was discussed above. Some alternative mixing rules have also been proposed for such mixtures.

Some investigators argue that, like the second virial coefficient for mixtures, the compositional dependence of the mixing rule for the attractive energy parameter should be quadratic in nature. Composition dependent mixing rules in general depart from this quadratic dependence. This departure from a quadratic dependence on composition may incorrectly influence the calculated fugacity coefficient at very low pressures and thereby equilibrium predictions. Despite such potential limitations, several mixing rules have been proposed with higher than quadratic dependence on composition.

Stryjek and Vera introduced two companion mixing rules to their alpha function for the attractive energy term for polar associating mixtures. The two mixing rules had two binary interaction coefficients and were referred to as a "Van Laar"-type and a "Margules"-type due to the similarities in terms for the Van Laar and Margules equations for fitting excess Gibbs energy of liquid mixtures. The Margules and Van Laar type mixing rules are, respectively:

$$a_{mix} = \sum_i \sum_j x_i x_j (a_{ii} a_{jj})^{0.5} (1 - x_i k_{ij} - x_j k_{ji}) \quad (2.72)$$

$$a_{mix} = \sum_i \sum_j x_i x_j (a_{ii} a_{jj})^{0.5} \left( 1 - \frac{k_{ij} k_{ji}}{x_i k_{ij} - x_j k_{ji}} \right) \quad (2.73)$$

Note that the binary coefficient  $k_{ij}$  is not equal to  $k_{ji}$  in this case. However, if the binary interaction coefficients are equal, then both mixing rules reduce to the classical van der Waals mixing rule. For various alcohol-hydrocarbon and acetone-hydrocarbon



mixtures, the Van Laar-type mixing rule was found to give the best performance of the two mixing rules.

Panagiotopoulos and Reid<sup>102</sup> proposed a mixing rule which, for binary mixtures, was mathematically identical to the Mragules-type mixing rule of Stryjek and Vera:

$$a_{mix} = \sum_i \sum_j x_i x_j (a_{ii} a_{jj})^{0.5} (1 - k_{ij} + (k_{ij} - k_{ji}) x_i) \quad (2.74)$$

This mixing rule was later modified to achieve a quadratic dependence on composition in the low density limit in agreement with the quadratic dependence of the second virial coefficient for mixtures:

$$a_{mix} = \sum_i \sum_j x_i x_j (a_{ii} a_{jj})^{0.5} (1 - k_{ij}) + \frac{b_{mix}}{vRT} \sum_i \sum_j x_i x_j (x_i \lambda_{ij} + x_j \lambda_{ji})$$

where :

$$k_{ij} = k_{ji} \text{ and } \lambda_{ij} = -\lambda_{ji} \quad (2.75)$$

Note that there are now two binary interaction parameters. With the PR CEOS, this version of the Panagiotopoulos and Reid mixing rule gave qualitatively correct predictions for a ternary mixture of carbon dioxide-n-butanol-water at moderate temperature and pressure in both the three and four phase regions.

Sandoval *et al.*<sup>103</sup> proposed a mixing rule with three binary parameters ( $k_{ij}$ ,  $k_{ji}$  and  $l_{ij}$ ) for the Peng-Robinson CEOS with Stryjek and Vera alpha function:

$$a_{mix} = \sum_i \sum_j x_i x_j (a_{ii} a_{jj})^{0.5} (1 - \bar{k}_{ij} + x_i \Delta k_{ij} - x_j \Delta k_{ji} - l_{ij} (x_i - x_i^2 + x_j - x_j^2)) \quad (2.76)$$

The parameters  $\bar{k}_{ij}$  and  $\Delta k_{ij}$  were related to  $k_{ij}$  and  $k_{ji}$ . This mixing rule was evaluated for prediction of vapour-liquid equilibria for ternary mixtures. Twelve ternary systems and the three binary pairs for each ternary system were used in the evaluation of these mixing rules. These systems include highly polar components (e.g., water, alcohols,

acetone, acetonitrile, methylacetate, chloroform) as well as non-polar components (e.g., hexane, cyclohexane, benzene, heptane, and toluene). The Sandoval mixing rule gave better predictions than the original Panagiotopoulos and Reid mixing except for the binary pair of acetone-water.

Michelsen and Kistenmacher<sup>104</sup> identified two shortcomings of the above compositionally dependent mixing rules. The first was that these mixing rules were not invariant if an individual component was divided into two identical sub-components. That is to say, if for a binary mixture with molefractions  $x_1$  and  $x_2$ , the first component was divided into two identical components with molefractions  $x_{1a}$  and  $x_{1b}$ , with  $x_{1a}$  plus  $x_{1b}$  equal to  $x_1$ , the mixing rules would give different values for  $a_{mix}$ . This would lead to different phase behaviour and properties for what are compositionally identical mixtures. A second shortcoming for mixing rules, like that proposed by Sandoval *et al.*, was that as the number of components increased, the importance of the  $l_{ij}$  term decreased and vanished in the limit of continuous thermodynamic EOS.

Mathias and co-workers<sup>105</sup> proposed a modification of the first Panagiotopoulos and Reid mixing rule, equation (2.74), which overcomes the shortcomings identified by Michelsen and Kistenmacher:

$$a_{mix} = \sum_i \sum_j x_i x_j (a_{ii} a_{jj})^{0.5} (1 - k_{ij}) + \sum_i x_i \left[ \sum_j x_j (a_{ii} a_{jj})^{\frac{1}{6}} (k_{ij} - k_{ji})^{\frac{1}{3}} \right]^3 \quad (2.77)$$

Mathias *et al.* compared the performances of the Panagiotopoulos and Reid mixing rule and this Mathias-Klotz-Prausnitz mixing rule. They found that for binary systems both mixing rules gave identical results. However, for ternary mixtures the Panagiotopoulos and Reid mixing rule gave erroneous phase behaviour predictions compared to the Mathias-Klotz-Prausnitz mixing rule.

Density dependent mixing rules have also been proposed to give better predictions for polar asymmetric mixtures as well as to overcome the limitations of compositionally dependent mixing rules. Despite having a sounder theoretical basis than the above compositionally dependent binary interactions, density dependent mixing rules perform

no better and contribute no additional information to the present discussion. Anderko<sup>106</sup> has reviewed some of these mixing rules and commented on their cost, benefits and limitations.

### 2.7.3. Excess Free Energy-Based Mixing Rules

For predictions involving polar and associating mixtures, mixing rules based on excess free energy of mixing show great promise. Mixing rules based on excess Gibbs or Helmholtz energy of mixing represent a more recent approach to the development of mixing rules. The attraction of using this approach is that the excess energy directly reflects the degree of ideality or non-ideality of the mixture and builds this right into the mixing rule. It is now more common that excess energy mixing rules are based on excess Helmholtz energy which is almost independent of pressure compared to excess Gibbs energy.

The excess Helmholtz energy of mixing, like other thermodynamic properties, can be derived from the CEOS:

$$A_{mix}^E(T, P, x) = A_{mix}(T, P, x) - A_{mix}^{ig}(T, P, x) - \sum_i x_i (A_i(T, P) - A_i^{ig}(T, P)) \quad (2.78)$$

If experimental data are available or a model can be used to calculate the excess Helmholtz (e.g. van Laar equation with activity coefficients) then an equality can be created with the right hand side of equation (2.78). Since both excess Gibbs and Helmholtz energies depend on pressure whereas activity coefficients are independent of pressure, the above equality is exact only at one pressure. It is common to have a reference at either zero or infinite pressure for this equality by making appropriate adjustment to the right hand side of equation (2.78). The final step in obtaining the mixing rule is to force  $a_{mix}$  and  $b_{mix}$  to adhere to the quadratic dependence on composition as shown by their relationship to the second virial coefficient shown in equation (2.66).

Apart from their greater complexity, the major weakness of mixing rules based on excess free energy relationships, is the need for accurate prediction or good

experimental data for free energy of mixing. While this approach appears to work for smaller molecules, it has not been demonstrated for large molecules such as those found in bitumen. Additionally, data for excess free energy of mixing and on which models for its predictions are based are applicable to systems at high reduced temperatures. Phase behaviour for heavy oil and bitumen mixtures are generally of most interest at low reduced temperatures.

#### 2.7.4. Binary Interaction Parameters

The original van der Waals mixing rule for the attractive energy parameter was modified to include a binary interaction parameter ( $k_{ij}$ ) to better correspond with experimental data. Most mixing rules for the attractive energy parameters, that have as their basis the classical van der Waals mixing rules, include one or more binary interaction parameters. These binary interaction parameters are empirical coefficients and are typically derived from regression of experimental data for vapour pressure data for a binary mixture using a specific CEOS. Binary interaction parameters are, therefore, CEOS specific and not transferable from one CEOS to another. Even when the binary interaction parameter is given in the form of a generalized correlation it remains specific to the CEOS for which the regression was carried out to obtain  $k_{ij}$ .

Since heavy oil and bitumen are usually described in terms of pseudo-components based on boiling point, it is not practical to determine binary interaction parameters by regression of experimental data. In the absence of these binary interaction parameters it may be tempting to set them equal to zero. As noted earlier, setting binary interaction parameters equal to zero does not mean the mixture is treated as ideal. The expression for excess Gibbs energy of the binary mixture does not go to zero when, for example,  $k_{12}$  is set to zero for the classical van der Waals mixing rule. Indeed, Orbey and Sandler<sup>107</sup> have pointed out that setting  $k_{ij}$  may lead to unreasonable phase behaviour or non-convergence of CEOS calculations for phase behaviour.

##### 2.7.4.1. Correlations

A number of simple correlations have been developed for predictions of binary interaction parameters ( $k_{ij}$ ) for various equations of state. Most of these correlations have been generalized in terms of molecular properties such as critical properties, acentric

factor, or molecular weight. A few correlations have been developed for some systems which show that  $k_{ij}$  can be correlated with temperature or pressure.

It is important to stress that correlations for  $k_{ij}$  based on regression of data do not necessarily indicate that there is theoretical basis for the parameters in the correlations. Depending on the dataset and its accuracy,  $k_{ij}$  can be determined independent of temperature or as a function of temperature. Similarly, depending on the pressure and temperature range of data,  $k_{ij}$  can be determined as a function of pressure but independent of temperature. Regressions for determination of  $k_{ij}$  for a particular data can represent a balance between convenience and accuracy.

Stryjek<sup>108</sup> demonstrated that there was a linear relationship between the binary interaction parameters and temperature for the SRK CEOS. Correlations for  $k_{ij}$  for mixtures of methane, ethane, or propane with n-paraffin up to n-decane took the form:

$$k_{ij} = k_{ij}^0 + k_{ij}^T (T - 273.15) \quad (2.79)$$

Values for  $k_{ij}^0$  and  $k_{ij}^T$  were tabulated by Stryjek for the various binary pairs. Voros and Tassios<sup>109</sup> have shown that  $k_{ij}$  for binary mixtures of carbon dioxide, argon, or nitrogen with hydrocarbons can be correlated with pressure or density. Unfortunately, neither Stryjek or Voros and Tassios have generalized the correlation for  $k_{ij}$  in terms of molecular properties such as critical properties.

Nishiumi and co-workers<sup>110</sup> developed a correlation to predict binary interaction parameters using the PR CEOS for binary mixtures involving different series of hydrocarbons and non-hydrocarbons:

$$m_{ij} = (1 - k_{ij}) = 1.041 + 0.110|\omega_i - \omega_j| - 0.0403 + 0.0367|\omega_i - \omega_j|\frac{V_{ci}}{V_{cj}} \quad (2.80)$$

This correlation gave values for  $m_{ij}$  within 0.7% of the optimized value for the binary mixtures investigated.

For the PR CEOS, a generalized correlation for  $k_{ij}$  based on critical temperature and critical compressibility was proposed by Gao *et al.*<sup>111</sup> for binary mixture of methane with n-paraffins up to n-decane as well as other simple hydrocarbons:

$$k_{ij} = 1 - \left[ \frac{2(T_{ci}T_{cj})^{0.5}}{(T_{ci} + T_{cj})} \right]^{0.5(Z_{ci} + Z_{cj})} \quad (2.81)$$

When used with the PR CEOS, this correlation considerably improved predictions for bubble point pressures and vapour phase compositions compared to setting  $k_{ij}$  to zero. For asymmetric mixtures, e.g., methane-n-nonane, the average absolute deviation was 3.23% and 0.54% for bubble point pressure and vapour phase composition, respectively.

Kordas *et al.*<sup>112</sup> have produced generalized correlations for  $k_{ij}$  in the Peng-Robinson CEOS for binary mixtures of methane and n-paraffins up to n-tetratetracontane based solely on acentric factor. The correlation used depends on whether the second component is heavier than n-eicosane:

$$\begin{aligned} nC_n \leq nC_{20} : \\ k_{ij} &= -0.13409\omega + 2.28543\omega^2 - 7.61455\omega^3 + 10.46565\omega^4 - 5.2351\omega^5 \\ nC_n > nC_{20} : \\ k_{ij} &= -0.04633 - 0.04367 \ln(\omega) \end{aligned} \quad (2.82)$$

The reason for the use of two correlations was a discontinuity in  $k_{ij}$  versus carbon number. For carbon numbers up to 16,  $k_{ij}$  was positive whereas for carbon numbers higher than 16  $k_{ij}$  was negative. For isomers and cycloalkanes up to  $C_6$ , the same correlation used for n-paraffins up to n- $C_{20}$  gave good predictions. Kordas *et al.* compared the predicted bubble point pressure using  $k_{ij}$  from their correlation to that from using correlations developed by Gao *et al.* and Nishiumi *et al.* and found that these

correlations gave errors above 10% when the second component was heavier than n-pentadecane.

Chueh and Prausnitz<sup>113</sup> have proposed a correlation for  $k_{ij}$  for hydrocarbon-hydrocarbon mixtures whose form is widely used. The correlation is generalized in terms of critical volume and therefore reflects the difference in size of the binary interacting components:

$$k_{ij} = A \left\{ 1 - \left[ \frac{2(V_{ci}V_{cj})^{\frac{1}{6}}}{(V_{ci})^{\frac{1}{3}} + (V_{cj})^{\frac{1}{3}}} \right]^B \right\} \quad (2.83)$$

Chueh and Prausnitz originally specified the coefficients A and B as 1 and 3, respectively. In many cases, the coefficient B often has a value of 6 and A is regressed to match VLE data. With this correlation,  $k_{ij}$  is always positive and increases smoothly with increasing critical volume ratio between  $i^{\text{th}}$  and  $j^{\text{th}}$  components.

Pedersen *et al.*<sup>114</sup> proposed a correlation for  $k_{ij}$  for the SRK CEOS based only on molecular weight (MW) for components in a North Sea Oil:

$$k_{ij} = 0.00145 \frac{MW_i}{MW_j} \quad (2.84)$$

*where* :  $M_i \geq M_j$

Katz and Firoozabadi<sup>115</sup> proposed a correlation for  $k_{ij}$  for binary mixtures with methane which minimized the deviation between experimental bubble points and those calculated using the PR CEOS. This correlation for  $k_{ij}$  for methane-hydrocarbon mixtures was based solely on specific gravity of the heavier hydrocarbon:

$$k_{CH_4j} = 0.14SG_j - 0.0688 \quad (2.85)$$

It is worth pointing out that another approach taken by Gao *et al.*<sup>111</sup> requires a different type of binary interaction parameter. For the PR and SRK CEOS, Gao and co-workers proposed a new alpha function and cross-terms ( $a_{ij}$  and  $b_{ij}$ ) for the van der Waals mixing rules:

$$a_{ij} = \left( \frac{a_i^{N_{ij}} + a_j^{N_{ji}}}{2} \right)^{1/N_{ji}} \quad (2.86)$$

$$b_{ij} = \left( \frac{b_i^{M_{ij}} + b_j^{M_{ji}}}{2} \right)^{1/M_{ji}} \quad (2.87)$$

The value of  $N_{ij}$  was generalized for some binary systems using acentric factor. The value of  $M_{ij}$  was equal to one for both PR and SRK CEOS. A relationship was also given between  $k_{ij}$  for  $a_{\text{mix}}$  and  $l_{ij}$  for  $b_{\text{mix}}$  in the classical van der Waals mixing rules.

#### 2.7.5. Volume Translation

It has been noted that two-parameter CEOS fail to accurately predict liquid molar volumes while simultaneously accurately predicting VLE behaviour. A method, termed volume translation, for improving the predictions of the molar volume was first proposed by Martin<sup>116</sup> and subsequently extended by Peneloux and co-workers<sup>117</sup> for the SRK CEOS. The so-called volume translation approach basically involves shifting the volume prediction from the CEOS by either a fixed or variable (e.g., as a function of temperature) amount  $c_i$ :

$$c_i = v^{CEOS} - v^{\text{exp}t} \quad (2.88)$$

With this volume translation, the SRK CEOS can be re-written as:



$$P = \frac{RT}{v+c-b} - \frac{a(T)}{(v+c)(v+c+b)} \quad (2.89)$$

Unless experimental molar volumes are available for use with equation (2.88), the Rackett equation can be used as suggested by Peneloux *et al.* Of course, the molar volumes of the vapour phase are also shifted but since the volume shift applied is relatively small in comparison to the molar volume of the gas, its effect is well within experimental error for the vapour. The volume translation technique can lead to greatly improved prediction of molar volume. Peneloux *et al.* have shown that, for pure fluids, binary, ternary, and petroleum fluid mixtures, the volume translated SRK provided substantial improvement over the PR CEOS for predicting molar volumes. Peneloux and co-workers also provided a group contribution method for estimating the Rackett parameter ( $Z_{RA}$ ) which in the original Rackett equation was exactly equal to the critical compressibility factor.

Volume translation as developed by Peneloux *et al.* can be applied to any of the CEOS previously discussed. The inclusion of volume correction, as in equation (2.89), does not create a new CEOS since the CEOS could be solved in its initial form and then the volume translation applied. This is because volume translation does not alter predictions for vapour pressures, phase envelope, entropy, heat capacities and other properties which are therefore termed invariant. Volume translation does alter molar volume, enthalpy, sound velocity, and Joule-Thomson coefficient. Thus, the use of volume translation creates an inconsistent model for phase behaviour since a different model is used for translated properties compared to untranslated properties. Leibovici<sup>118</sup> has discussed the properties derived from CEOS which are variant or invariant with respect to the parameters of the equation of state. Leibovici also provides the necessary equations for shifting back properties such as enthalpy, velocity of sound, and Joule-Thomson coefficient which have been shifted by volume translation.

Chou and Prausnitz<sup>119</sup> have proposed an additional refinement to volume translation for prediction in the critical region using the SRK CEOS. An additional volume translation is included which is dependent on the bulk modulus:

$$v^{\text{expt}} = v^{\text{CEOS}} - c_i - \frac{RT_c}{P_c} (Z_c^{\text{CEOS}} - Z_c^{\text{expt}}) \left( \frac{0.35}{0.35 + \frac{1}{RT_c} \left( \frac{\partial P}{\partial \rho} \right)_{T_c}} \right) \quad (2.90)$$

The additional volume translation term improves molar volumes in the critical region compared to the original SRK and volume translated SRK CEOS. However, the inclusion of the bulk modulus, which is itself a function of the CEOS, means that other properties such as fugacity and consequently VLE predictions are affected by this translation term. The invariances discussed above do not necessarily apply in this case.

#### 2.7.6. Group Contribution Methods

Many properties of heavy oils and bitumen, such as critical properties, are difficult to determine directly. Correlations developed for estimating the properties of light conventional oil are often not applicable to heavy oil and bitumen. Group contribution can be particularly useful for heavy oil mixtures provided representative molecular structures can be found to describe these mixtures.

##### 2.7.6.1. Critical Properties and CEOS

The use of group contribution (GC) methods to predict critical properties was discussed in an earlier section. Poling *et al.* suggest that the GC methods of Gani and co-workers<sup>17, 76</sup> are currently among the most accurate for estimating critical properties.

The need to determine critical properties can be bypassed entirely if a GC method based CEOS is used. Examples of such a CEOS include those developed by Coniglio and co-workers<sup>77, 78, 79</sup>. One form of the GC-based CEOS of Coniglio *et al.* was recently evaluated by van Waeyenberghe and found to give reasonable predictions for bubble point pressure and liquid molar volume when volume translation was used.

##### 2.7.6.2. Binary Interaction Parameters

More recently, Jaubert and co-workers<sup>120</sup> have been developing a GC method for temperature dependent binary interaction parameters ( $k_{ij}$ ) for the Peng-Robinson CEOS. Unlike most correlations for  $k_{ij}$  discussed above, which are usually developed for a

particular set of binary pairs, e.g., methane plus n-paraffins, this method is completely general so long as the molecules are composed of hydrogen and carbon only. Additionally, only the critical properties and acentric factor, which are also needed for calculating CEOS parameters, are required. The GC method calculates  $k_{ij}$  using group contributions, temperature, energy parameter ( $a_{ii}$ ), and co-volume ( $b_{ii}$ ) of the molecule:

$$k_{ij}(T) = \frac{-\frac{1}{2} \sum_{k=1}^{N_{gi}} \sum_{l=1}^{N_{gl}} (\alpha_{ik} - \alpha_{jk})(\alpha_{il} - \alpha_{jl}) A_{kl} \left(\frac{298.15}{T}\right)^{\left(\frac{B_{kl}}{A_{kl}} - 1\right)} - \left(\frac{\sqrt{a_i(T)}}{b_i} - \frac{\sqrt{a_j(T)}}{b_j}\right)^2}{2 \frac{\sqrt{a_i(T)a_j(T)}}{b_i b_j}} \quad (2.91)$$

where:

$N_{gi}$ : Total number of groups in  $i^{\text{th}}$  molecule

$\alpha_{ik}$ : Number of  $k^{\text{th}}$  type groups divided by  $N_{gi}$

$A_{kl}$ : First contribution for interaction of  $k^{\text{th}}$  and  $l^{\text{th}}$  type groups

$B_{kl}$ : Second contribution for interaction of  $k^{\text{th}}$  and  $l^{\text{th}}$  type groups

$A_{kl} = A_{lk}$ ;  $B_{kl} = B_{lk}$

$A_{kk} = B_{kk} = 0$

Although formidable in appearance, the above expression can be readily incorporated into a CEOS calculation for phase behaviour predictions. The values of  $k_{ij}$  calculated by this method can be either positive or negative.

The inclusion of a temperature dependent term in the estimation of the binary interaction parameter appears to lead to improved predictions over a wide temperature range for bubble points, dew points, and critical loci. Additionally, Jaubert and Mutelet indicate that improved VLE predictions obtained with the temperature-dependent binary interaction parameter and the classical van der Waals mixing rules support the conclusion that these mixing rules are applicable to highly asymmetric mixtures. If true, this GC method may be of tremendous advantage in predicting phase behaviour for asymmetric heavy oil mixtures. Unfortunately, the GC method of Jaubert and co-workers is only applicable to paraffinic, naphthenic and aromatic hydrocarbons but not those with heteroatoms. Also, no information is yet available on the impact of the use of this GC method for  $k_{ij}$  on the prediction of derivative properties.

## 2.8. HYPOTHESIS

The foregoing review reveals that substantial efforts have been taken to try to improve the accuracy of EOS for predictions of phase behaviour and phase properties. Following the success of the van der Waals CEOS there have been many improvements to the form and sophistication of the inputs for the two-parameter CEOS. In the recent past, it has been suggested that improvements to CEOS have reached the point of diminishing returns. The limitations imposed by the cubic form on the prediction of molar volumes have been reached by use of methods such as volume translation or a multi-parameter CEOS. The emerging consensus appears to be that EOS with a firm theoretical basis, such as statistical thermodynamic approach of SAFT, are required to achieve improved predictions for polar and associating fluids. Despite this, CEOS still remain firmly entrenched for most engineering calculations with the exception of niche applications such as polymer systems where EOS such as SAFT appears to be best suited. Thus, continued improvement of the two-parameter form of CEOS is justified.

### 2.8.1. *Rational for Investigation*

Much of the efforts in improving the performance of two-parameter CEOS have focused on three areas:

1. Alpha functions
2. Mixing rule for the energy parameter
3. Estimation of parameters such as critical properties

Two of the above areas of improvements deal directly with the attractive energy part of the CEOS and have resulted in major improvements in the quality and accuracy of predictions. The repulsive part of the CEOS has remained unaltered since proposed by van der Waals 134 years ago. Efforts to alter the repulsive term have not met with success. Attempts to make the co-volume term, in the repulsive part of the CEOS, temperature dependent have been shown to have adverse effects on predictions of derivative properties such as heat capacities. Increasing size asymmetry and polarity of hydrocarbons has been accounted for in the form of the alpha function and mixing rule for the attractive term. It is believed that size asymmetry should be addressed in the

repulsive term. It appears that only limited attention has been given to the mixing rule for the co-volume term. Since changing the form of the repulsive term has met with absolutely no encouraging success, it is proposed to modify the mixing rule for the co-volume term.

If one is to develop a new mixing rule, it would be useful to have some guidelines which avoid past mistakes and provide mixing rules that are practical to use. Solorzano-Zavala *et al.*<sup>121</sup> have summarized some useful criteria for mixing rules:

1. Be simple
2. Have few parameters
3. Be invariant to division of a component into identical subcomponents
4. Predict VLE for binary and multi-component systems equally well
5. Provide good predictions of other properties such as enthalpy and heat capacity
6. Predict well liquid-liquid and liquid-liquid-vapour equilibria

It would be beyond the scope of the present thesis to verify that any proposed mixing rule meets all of these criteria. Nevertheless, by keeping these criteria in mind they serve to set some boundaries on perceived claims for the applicability of any proposed mixing rules.

### 2.8.2. *Basis for a New Mixing Rule*

In the development of his cubic equation of state, van der Waals considered the co-volume as representing the finite space occupied by the molecules themselves which decreased the free volume for molecules, increased the collisions with the wall, and therefore increased pressure. While the co-volume has a relatively small impact on gas phase calculations, it has a more significant impact on the liquid phase where the molecules are much closer together. The classical van der Waals notion regarding the volume occupied by the molecules fails at high densities because it does not account for the overlapping of parts of the excluded volume of the molecules. The Carnahan-

Starling repulsive term provides a more accurate expression for the excluded volume at all densities but still considers the molecules as spheres. However, most molecules, and certainly heavy oil molecules, are not spherical.

Substituting the van der Waals repulsive term with the Carnahan-Starling repulsive term in a two-parameter CEOS would destroy the cubic nature of the equation which makes CEOS attractive to use in the first place. However, it may be possible to retain the cubic form of the two-parameter EOS but use alternative mixing rules to compensate for the weakness of the co-volume term itself. The use of a mixing rule in this way would obviously not improve the situation for pure components provided that such mixing rules are invariant to splitting a single pure component into several subcomponents.

### 2.8.3. Proposed Mixing Rules

To our knowledge, mixing rules that have been proposed for the co-volume term generally involved changing the form of cross term,  $b_{ij}$ , to have a single power-law dependence on  $b_i$ , e.g.,  $b_i^{\frac{1}{2}}$ ,  $b_i^{\frac{1}{3}}$ , and  $b_i^{\frac{2}{3}}$ . These mixing rules may perform better than the classical van der Waals mixing rule under some circumstances but do not appear to be universally applicable to mixtures with a high degree of asymmetry. Furthermore, these mixing rules do not reduce to the van der Waals linear mixing rule for symmetric mixtures.

In contrast to conventional mixing rules, it is proposed to combine the arithmetic mean form of  $b_{ij}$  and a second form of  $b_{ij}$  in such a way that it reduces to the classical van der Waals mixing rule for a symmetric mixture. In addition to the criteria proposed by Solorzano-Zavala *et al.* for a new mixing rule, the following guidelines are proposed:

1. Flexible combining rule for both symmetric and asymmetric mixtures
2. Maintain quadratic compositional dependence for co-volume mixing rule
3. Reduces to van der Waals mixing rule for symmetric mixture
4. Any new binary interaction parameter should not be compositionally dependent and ideally should be symmetric, i.e.,  $l_{ij} = l_{ji}$

5. Any binary interaction parameters should be calculable from critical properties

On the basis of the above criteria, the proposed mixing rule, therefore, takes the following form:

$$b = \sum_i \sum_j (x_i x_j [(1 - m_{ij}) b_{ij} + m_{ij} b_{ij}^*])$$

where :

$$b_{ij} = \frac{1}{2}(b_i + b_j) \tag{2.92}$$

In the above mixing rule,  $m_{ij}$  can be considered as a binary mixing parameter used to proportion the overall mixing rule based on the van der Waals linear mixing rule, given by  $b_{ij}$ , and that based on a second mixing rule, given by  $b_{ij}^*$ . In the simplest case the binary mixing parameter should be symmetric, i.e.,  $m_{ij} = m_{ji}$  and should be related to the size of the molecules to account for the size asymmetry of the mixture. One exemplary form for  $m_{ij}$  is the following:

$$m_{ij} = \frac{(b_i - b_j)^2}{(b_i^2 + b_j^2)} \tag{2.93}$$

This form of  $m_{ij}$  emphasizes the difference in size between the  $i^{\text{th}}$  and  $j^{\text{th}}$  molecule. Alternative expressions for  $m_{ij}$  compare the geometric and arithmetic mean sizes, respectively:

$$m_{ij} = 1 - \frac{2(b_i b_j)^{\frac{1}{2}}}{(b_i + b_j)} \tag{2.94}$$

$$m_{ij} = \frac{abs(b_i - b_j)}{(b_i + b_j)} \quad (2.95)$$

With the above forms of  $m_{ij}$ , it can be seen that as the molecules become more similar in size, given by co-volume terms, the proposed mixing rule reduces to the van der Waals mixing rule.

For the second part of the mixing rule we propose to investigate three different possibilities for  $b_{ij}^*$ :

1. Lorentz term, equation (2.58)
2. Geometric mean term, equation (2.59)
3. Lee and Sandler term, equation (2.60)

Although each of these mixing rules has been previously investigated, no information could be found which would indicate that a composite mixing rule, as represented by equation (2.92), has ever been investigated.

## 2.9. OUTLINE OF INVESTIGATION

The performance of individual and composite mixing rules for the co-volume will be compared with the classical van der Waals mixing rule when applied to asymmetric mixtures of small solvents with Athabasca bitumen vacuum tower bottoms (VTB). These comparisons will be made with three different experimental datasets for VTB:

1. Partial molar volume at infinite dilution as a function of temperature for VTB in various solvents (Maham *et al.*<sup>122</sup>)
2. Bubble pressure and density as functions of temperature for VTB in n-decane (Zhang<sup>123</sup>)
3. Vapor pressure and density of VTB versus temperature (current work)



Measurements of partial molar volume at infinite of VTB in various solvents can be used to regress properties (e.g., average boiling point, specific gravity, and critical properties) of the VTB treated as a single component. Although the treatment of a complex oil mixture such as VTB as a single component is not strictly correct, this approach attempts to determine the extent to which this approximation can be made when the data are regressed with different mixing rules. It would be desirable to also carry out the above regression with VTB as a multi-component mixture, however, the data set available from Maham *et al.* is too small to attempt this.

Sheremata has provided sixty molecular representations for VTB. Critical properties and normal boiling points for these sixty representations or fractions can be determined using the GC method of Marrero and Gani. Using these estimated critical properties, acentric factors can be estimated using the correlation of Ambrose and Walton. Critical properties for VTB can also be estimated using the correlation of Twu with measured boiling point distribution from high temperature simulated distillation and specific gravity as inputs. Zhang has investigated the phase behaviour of VTB-n-decane mixtures in great detail including pressure, temperature, and phase densities under VLE behaviour as well as under LLE and VLLE behaviour. Using the two sets of critical data estimated from GC methods and boiling point correlations, bubble pressures will be determined for VTB-n-decane mixtures at conditions where no second liquid phase should be present. The performance of the various mixing rules for such bubble pressure predictions will be estimated. Also, the effect of the methods used for estimation of critical properties will also be examined.

The vapour pressure of pure VTB will also be determined as part of this work. An identical approach to that used for bubble pressures above will be used to assess the mixing rules and estimated critical properties.

---

## 3.0 EXPERIMENTAL

---

### 3.1 X-RAY VIEW CELL

#### 3.1.1. General Description

The x-ray view cell apparatus used in this work was capable of providing a visual image and record of the phase behaviour (individual phase volumes and apparent density) from about 20°C and 0 kPa up to 450°C and 27.5 MPa. Detailed descriptions of this equipment and its capabilities have been previously reported by Abedi *et al.*<sup>124</sup> and only a brief overview is provided here.

The general experimental set-up and basic components of the x-ray view cell are shown in Figure 3-1. The x-ray source is a Phillips MCN-165, tungsten-target producing bremsstrahlung x-rays within a nominal energy range from 5 to 160 keV. Typically, the x-ray source is operated at 50 kilovolts and 30 miliamperes. A lead pinhole produces an approximation of an x-ray point source. The cylindrical beryllium cell has a nominal volume of 245 mL depending on the arrangement of internals (mixers, spacers, flexible bellows, etc.). The volume of the gas phase can be adjusted by the use of a flexible nickel bellows at the top of the cell. Beryllium has good x-ray transparency and excellent mechanical strength for use at moderately high temperatures and pressures. The major caution in using beryllium metal is that the oxide is extremely toxic. However, the beryllium is not readily oxidized under the conditions employed. An x-ray camera is used to observe real-time images of the fluids and their behaviour in the cell. Still images can be captured for later processing to determine phase volumes, phase densities, and to maintain a record of experiments. A typical still image is shown in Figure 3-2 for VTB at 199.4°C and 21.0 kPa. The liquid meniscus is visible as a lighter region between the liquid and gas phase regions.

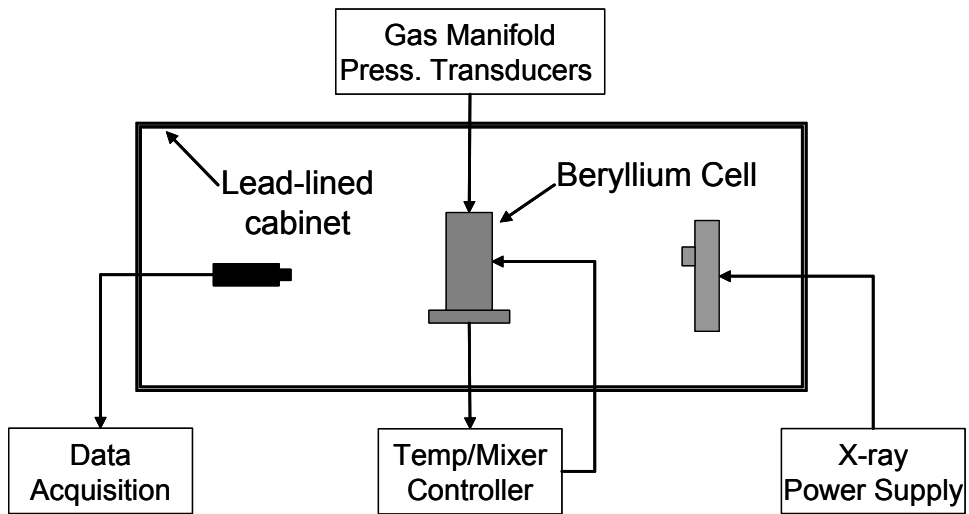


Figure 3-1 Simple schematic of x-ray view cell.

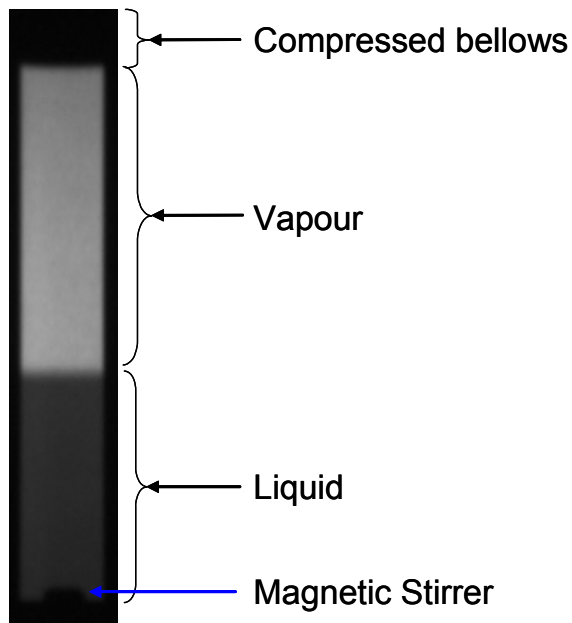


Figure 3-2 Illustration of x-ray image of VTB at 199.4°C and 21.0 kPa.

### 3.1.2. *Modifications*

The x-ray view cell was designed to be sealed and operated at high pressures. Early efforts to operate this system under vacuum to obtain vapour pressure data were not successful. Two major issues were identified which made such operations difficult:

1. The cell was prone to leakage under vacuum due to the nature of the seals employed, and
2. Due to vapour condensation, there was a significant pressure drop between the cell and the pressure transducer.

The issue of cell leakage under vacuum was addressed by changing the main seals on the beryllium cell. The seals initially in place were Flexitalic seals composed of spiral wound nickel and graphite in an outer retaining stainless steel ring. These seals operated by permanently deforming when the closure torque was applied to seal the cell. Replacement of the seals with custom-made Kalrez 7075 seals (AR Thompson Group, Edmonton) which had an upper operating temperature limit of 327°C. The new seals consisted of a Kalrez o-ring with an outer retaining ring of stainless steel. The Kalrez seals deformed significantly but reversibly when the cell was sealed. The new Kalrez seals worked much better than the previous ones because the Kalrez o-ring could be highly deformed to the slightly pitted sealing surfaces of the beryllium cell. The Kalrez o-rings could be used safely at temperatures up to 310°C and still maintained a good seal and were reusable.

The pressure transducer used to measure the vapour pressure in the view cell was connected by approximately 50 cm of 0.158 cm (OD) stainless steel tubing. Condensation of vapour in this line could have caused a pressure drop between the view cell and transducer. When the tubing and dead volume of the transducer were eventually filled with condensed liquid the pressure drop was eliminated. The total dead volume of the tubing and transducer was estimated at about 1.5 mL. Since the typical volume charged to the view cell is about 80 mL, the dead volume for condensed vapour can represent almost 2 vol.% of the liquid charge. While the elimination of the pressure drop by filling with condensed vapour was acceptable for a pure fluid it was not acceptable for a multi-component system such as bitumen. In the case of bitumen, much of the condensed

liquid filling the dead volume would be the most volatile components which would have the greatest contribution to vapour pressure. Condensing these components in the dead volume removes this fluid from the vapour liquid equilibrium so that the total composition of fluid in the cell would be altered from that initially charged. Additionally, since density measurements required that the mass of liquid in the cell be known, the loss of liquid to the dead volume would contribute at least a 2% error to this measurement.

To overcome the effects of pressure drop, it was decided that the transfer line should be heated to about 5°C above the temperature in the view cell to avoid condensation of vapour. This also meant that the pressure transducer would have to be heated 5°C above the temperature of the view cell. Unfortunately, most low pressure transducers are not operable above 80°C. A silicon-on-sapphire pressure transducer (0 - 15 psia) with temperature compensation to 260°C was obtained from Sensonetics (Huntington Beach, California). The stated static stability at 21°C was 0.25% of full scale. Thermal zero shift and sensitivity were both specified as  $\pm 0.031\%$  of full scale.

The connecting tubing between the view cell and transducer was wrapped with heat tape and insulated. A thermocouple was placed in contact with the transducer to monitor and control its temperature. Figure 3-3 shows a P&ID diagram for the system as used. Ideally, the transducer and view cell should be heated in the same furnace. The Sensonetics pressure transducer was equipped with a high temperature cable so it could be placed in the same furnace as the view cell. Unfortunately, the design of the furnace housing did not allow for placing both the pressure transducer and the view cell inside.

The view cell included a notched insert at the bottom of the cell where small amounts of any second liquid phase could settle and thereby be readily observed during phase behaviour studies. This insert was found to trap small amounts of gases which were sufficient to make this insert float out of position when the view cell was evacuated. This insert was removed and therefore the calibration curve for liquid volume in the cell versus height at the bottom of the meniscus has to be re-determined. The insert also served as a reference for correcting x-ray images for the slight variation in x-ray source intensity from test to test. Without this reference reliable measurements

of the apparent density of the liquid phase were not possible. A safe operating procedure for this cell, pressure manifold and x-ray source is given in Appendix 1.

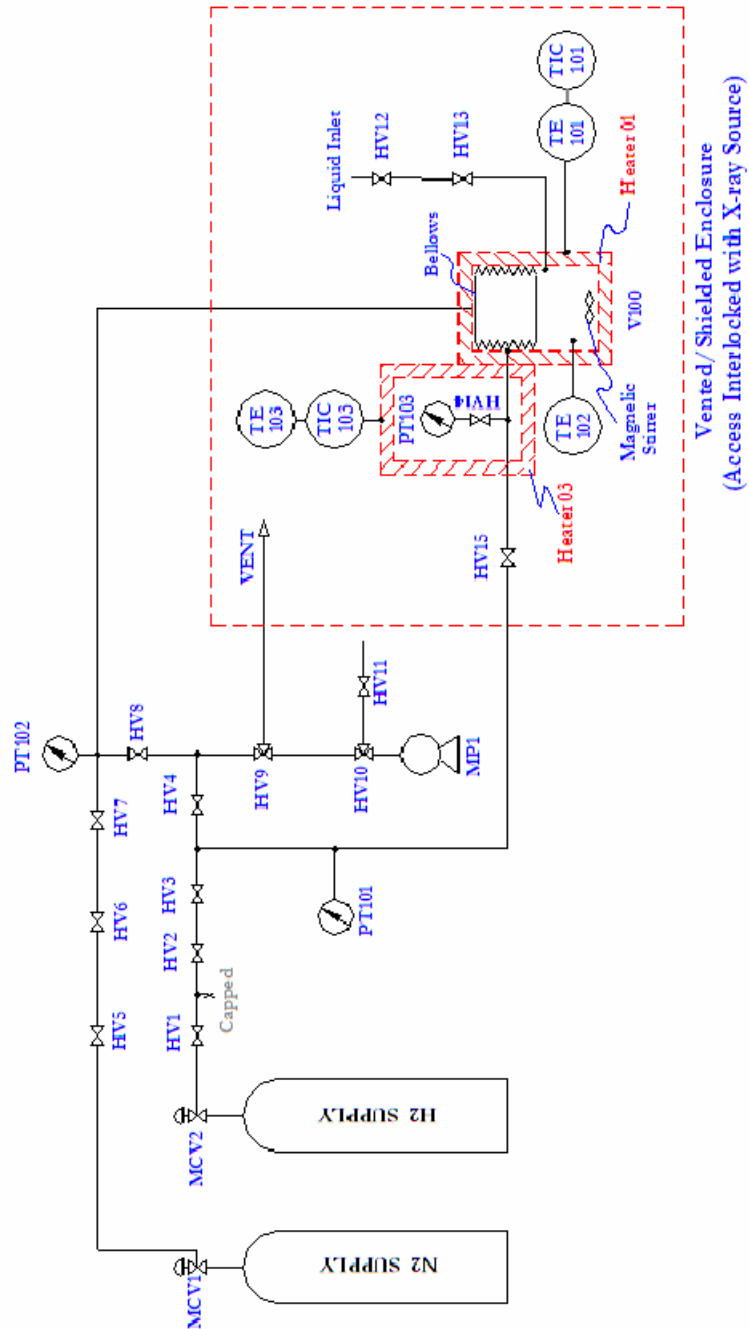


Figure 3-3 Simple P&ID for view cell with heated transducer.

## 3.2. FLUIDS MEASURED

### 3.2.1. Athabasca Bitumen Vacuum Tower Bottoms

The sample of Athabasca bitumen vacuum tower bottoms (VTB) used in this work was previously supplied by CANMET. Some chemical and physical properties of this sample are summarized in Table 3-1. The high temperature simulated distillation curve is shown in Figure 3-4. The initial boiling point from simulated distillation of VTB was 448°C. The weight average boiling was 610°C for the fraction of VTB with boiling point below 750°C.

Saturates, aromatics, resins and aromatics (SARA) content, elemental composition and metals content were taken from data of Zou<sup>125</sup>. Molecular weight was determined by vapour pressure osmometry in o-dichlorobenzene at the National Centre for Upgrading Technology (NCUT) in Devon, Alberta. Toluene insolubles (solids) were determined by dilution of about 9 g of VTB in 45 g of toluene and centrifuging the sample at 18,000g for 24 hours. This process was considered sufficient to remove all particles with diameter smaller than 0.4 microns. The sediment was washed and centrifuged three times with about 65 g of toluene.

Water in VTB was determined by Karl Fisher titration using a Cou-Lo Compact Karl Fisher Titrator (GR Scientific, Bedfordshire, UK). For this analysis, a stock solution of toluene/iso-propanol at a mass ratio of 10:1 was prepared. A portion of this stock solution (67.14 g) was mixed with 18.73 g of VTB. To determine the relatively low amount of water in VTB, an abnormally large sample size (1.0 mL) was used for Karl Fisher analysis. Due to this large sample size the Karl Fisher reagent had to be replaced after each pair of analyses of blank and sample. For the analysis, a 1.0 mL sample of the stock solution was analyzed to determine the blank reading. Next a 1.0 mL sample of the VTB solution was injected. The results for the sample with VTB were corrected for the contributions from the toluene and iso-propanol as given by the blank and the water content of VTB could then be calculated.

**Table 3-1 Chemical and physical properties of VTB**

Property	Value
Density @ 15.6°C	1.052
Molecular Weight (o-DCB†) (g/mole)	1048
Toluene insolubles (wt.%)	1.65
Moisture (wt.%)	0.081
<b>Viscosity (cP):</b>	
160°C	683
200°C	133
<b>Hydrocarbon type (wt.%)</b>	
Saturates	6.8
Aromatics	41.99
Resins	19.04
Asphaltenes	32.18
<b>Elemental composition (wt.%):</b>	
Carbon	81.66
Hydrogen	9.54
Sulphur	6.87
Nitrogen	0.065
<b>Metals (ppmw):</b>	
Nickel	137
Vanadium	344

† o-dichlorobenzene

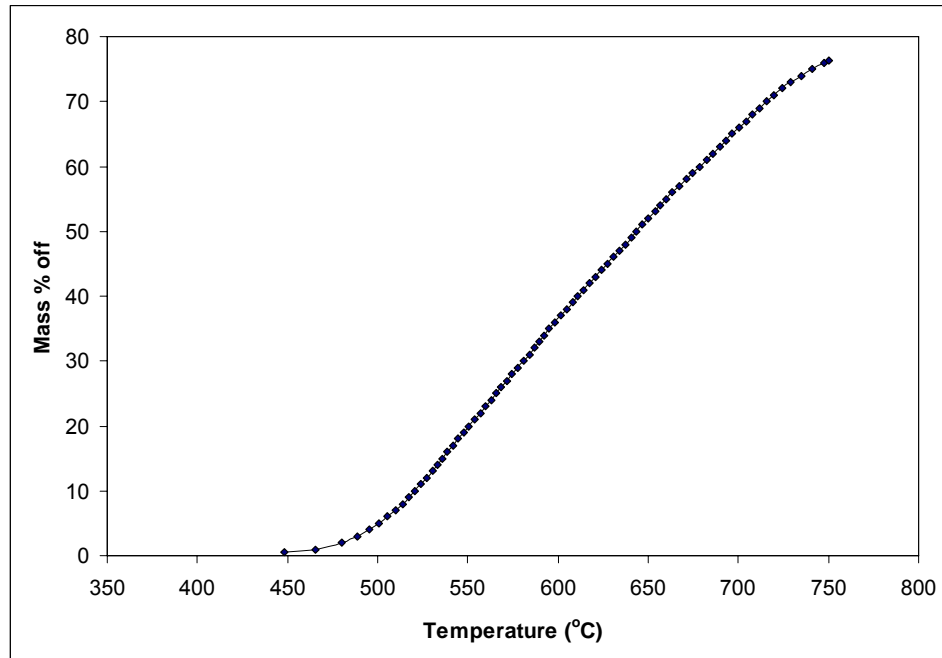


**Figure 3-4 High temperature simulated distillation curve for VTB.**



### 3.2.2. *N-Dodecane*

Anhydrous n-dodecane with a stated purity of  $\geq 99.3$  wt.% was obtained from Sigma-Aldrich. The purity confirmed by GC analysis was 99.30 wt.%. The impurities appear to be mainly isomers of n-dodecane. Isomers of C<sub>14</sub> and C<sub>6</sub> represented 0.07 wt.% and 0.03 wt.%, respectively, of the sample. The sample had no measurable water content.

## 3.3. VAPOUR PRESSURE MEASUREMENT

### 3.3.1. *Sample Preparation and Measurement*

After a known mass of sample was charged to the view cell, it was evacuated with a mechanical vacuum pump to about 0.02 kPa. Trapped air and moisture were removed by prolonged evacuation while stirring the liquid. The sample was degassed until the pressure did not decrease any further. For n-dodecane, the sample was degassed at approximately 75°C for about 1 hour. The vapour pressure at this temperature was low enough ( $\sim 0.6$  kPa) so that any mass loss was well within experimental error.

In the case of VTB, the sample was first slowly evacuated at 25°C for about 30 minutes so that fine particles of the solid sample were not removed by entrainment. The VTB was then heated to about 150°C, with constant stirring, while the view cell was isolated from the vacuum pump. The sample was then slowly evacuated so as to maintain a low level of bitumen foam in the cell. Once foaming ceased, the sample was evacuated with continued stirring at about 150°C until no more gas evolution was evident in the form of bubbles when stirring was momentarily halted. This was achieved after about 30 minutes.

### 3.3.2. *Temperature and Pressure Calibration*

The absolute accuracy of the thermocouple measuring the temperature of the view cell was checked with a thermocouple calibration furnace (Hart 9122, Hart Scientific: a Division of Fluke Instruments). The resulting calibration curve (see Appendix 2) was used to correct the measured temperatures. A quadratic fit was used to interpolate temperature corrections at each measured temperature. The average absolute relative error for the quadratic fit was 0.02% with the maximum error being 0.07% at 250°C.

Even though an overall average error was specified for the pressure transducer, it was desirable to know the actual error in pressure measurement as a function of temperature, particularly above the 260°C compensation limit specified by the manufacturer. The actual error in pressure measurement was estimated by measurement of the shift in pressure reading as a function of temperature under vacuum of  $10^{-4}$  kPa and at ambient atmospheric pressure read from a mercury barometer. The actual pressure span (ambient atmospheric pressure minus  $10^{-4}$  kPa) was compared to the measured span at each temperature between 18 and 325°C. The zero and ambient pressure offsets were fitted to temperature and these were then used to calculate corrected pressure at each temperature. This method of pressure correction at each temperature was based on the assumption that the correction at each temperature was a fixed percentage of the indicated pressure which is given by the error in span determined as a function of temperature. Curves showing the difference between the instrumental zero and ambient pressure readings and the actual values as functions of temperature are given in Appendix 2. The resulting correction factor for measured pressure as a function of transducer temperature is also given in Appendix 2.

### **3.4. DENSITY MEASUREMENT**

#### *3.4.1. Volumetric Calibration*

As noted above, due to the removal of part of the internals of the view cell, a new calibration curve for volume versus height was required. The calibration was done at ambient pressure and known temperature by incrementally adding a known mass of n-dodecane to the view cell and then recording an x-ray image. From image analysis, the pixel position at the interface was found with respect to the bottom of the view cell as a reference position. Since the mass and density of n-dodecane added was known, a plot of volume versus pixel number (height) was obtained. This curve could be used to calculate the volume of any liquid in the cell based on the height of the interface.

Figure 3-5 shows a plot of the x-ray intensity versus pixel number along a line from the bottom of the view cell to the top of the view cell. The position of the interface was taken as the point where the first derivative of intensity was greatest. The position of the bottom of the view cell was found in a similar manner but this was found to be

unchanged from image to image. The volume of n-dodecane incrementally added to the view cell was determined from the known mass of the increment and fluid density calculated using the Guggenheim equation with coefficients for n-dodecane from Stephan and Hildwein<sup>126</sup>:

$$\rho = MW \left[ a_1 (1 - T_r)^{\frac{1}{3}} + a_2 (1 - T_r)^{\frac{2}{3}} + a_3 (1 - T_r) + a_4 (1 - T_r)^{\frac{4}{3}} + a_5 (1 - T_r)^{\frac{5}{3}} + V_c^{-1} \right] \quad (2.96)$$

where:

$a_i$ :  $i^{\text{th}}$  Guggenheim coefficients

$MW$ : molecular weight

$V_c$ : critical volume

The resulting calibration curve for liquid volume versus pixel number is given in Appendix 2. The calibration in the low volume region (20 – 70 mL) is subject to error due to parallax caused by the divergent beam of x-ray passing through the lower part of the cell which is at a high angle with respect to the plane of the pinhole. Since all tests start with about 80 mL of liquid in the cell, only points between 70 and 105 mL were used to create the final calibration curve.

Since there are a finite number of pixels corresponding to height of the liquid in the view cell, there is an uncertainty of one half of a pixel in the position of the liquid interface at the top and bottom of the view cell. One pixel was estimated to correspond to 0.855 mL. The error in the density was estimated, therefore, from the error in measured volume of 0.855 mL due to the height of a single pixel, i.e., the sum of the half pixel errors at the bottom and top of the liquid.

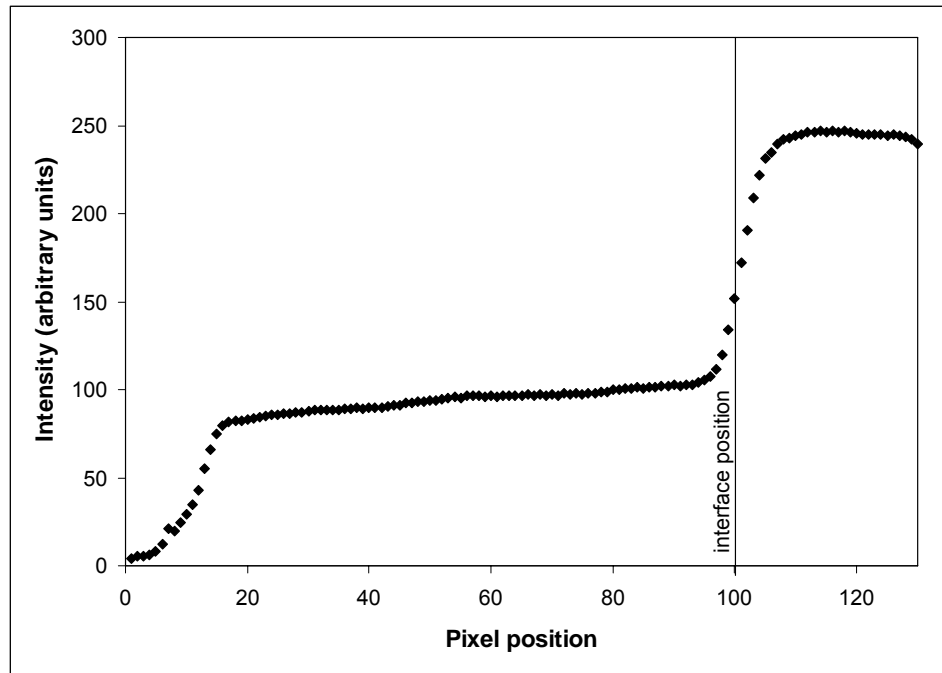


Figure 3-5 Plot of x-ray image intensity versus pixel number in a line transecting the liquid-gas interface.

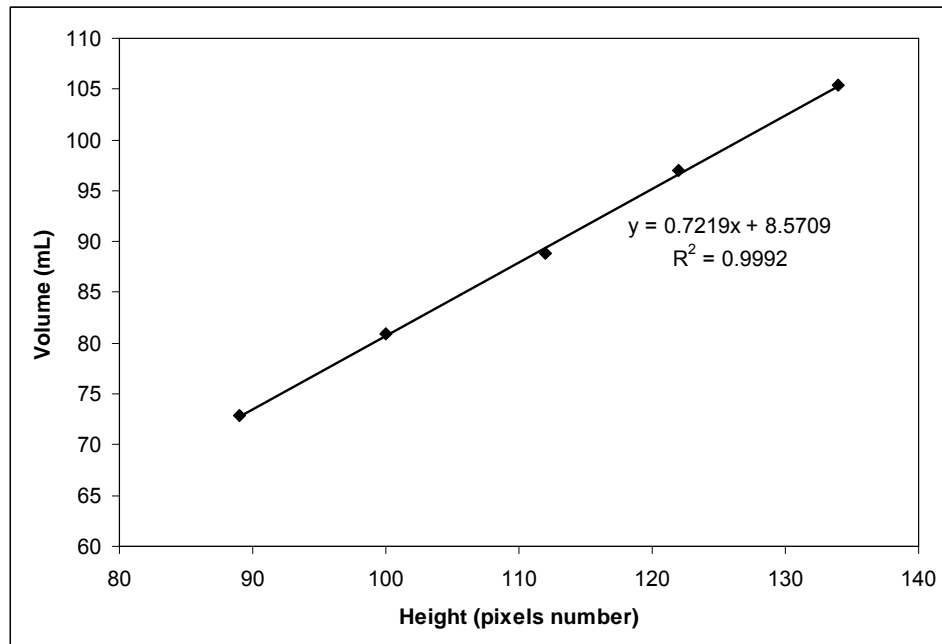


Figure 3-6 Volume calibration curve for x-ray view cell from 70 to 105 mL.

### 3.4.2. *Property Calculations*

The results of measurements using the x-ray view cell were tabulated as measured temperature, pressure, and pixel height at the liquid interface. Temperature was corrected using the calibration curve for the thermocouple. The measured pressure was first corrected to adjust for the zero offset due to temperature and then the final correction factor from a temperature correction curve was applied. The density of the liquid phase was calculated from the known mass of liquid originally charged to the view cell and the volume calculated using the calibration curve in Figure 3-6. For experiments involving n-dodecane, the mass of fluid in the liquid phase was corrected for that in the vapour phase. The dead volume of the system was estimated as 250 mL and the volume occupied by vapour was the dead volume minus liquid volume. By application of the ideal gas law the amount of n-dodecane in the gas was estimated. A similar correction was not applied for experiments with VTB since the vapour pressures measured were low, less than 25 kPa.

---

## 4.0 CRITICAL PROPERTIES FROM VAPOUR PRESSURE DATA

---

### 4.1. ANALYSIS OF VAPOUR PRESSURE DATA

Vapour pressure and liquid density as a function of temperature were measured for n-dodecane and Athabasca vacuum tower bottoms (VTB). With a good quality data set, any CEOS can be used for a regression of critical properties, acentric factor, and also molecular weight if it is not known. In carrying out such regressions, it is important to note that all of the above molecular properties are not mutually independent. While no single unifying equation necessarily combines all of these properties they are, in fact, related through a unique molecular structure and composition.

Various correlations that could be used to estimate critical properties and acentric factor were discussed in Chapter 2. Among these correlations are those based on normal boiling point and specific gravity such as those proposed by Riazi and Daubert for prediction of critical properties. Riazi provided coefficients for a correlation, equation(2.37), which is suitable for all types (paraffins, cycloparaffins, and aromatics) of heavy hydrocarbons spanning the range of C<sub>6</sub> to C<sub>50</sub> and these are given in Appendix 3. A correlation of the form of equation (2.37) was also proposed by Riazi for prediction of molecular weights for heavy hydrocarbon with boiling points from 27 to 580°C and the coefficients for this correlation are also given in Appendix 3.

Correlations developed by Riazi *et al.* for each critical property are mutually independent, i.e., no interdependence of critical temperature, pressure, and volume. In contrast, critical properties derived from the correlations developed by Twu are all mutually inter-dependent through their relationship to an equivalent hypothetical n-paraffin. The correlations developed by Twu also include prediction for molecular weights of heavy hydrocarbons.

The correlation for acentric factor developed by Ambrose and Walton is based on normal boiling point, critical temperature, and critical pressure. This correlation therefore provides a value for acentric factor which will be consistent with critical properties derived by either of the previously discussed correlations.

The above correlations were used to constrain the regression for critical properties from vapour pressure and density data for n-dodecane and VTB. An outline of the

iterative procedure for calculating the optimum values of normal boiling point and specific gravity, which provides critical properties that lead to the best agreement with experimental data, is shown in Figure 4-1. The Matlab code used is given in Appendix 3.

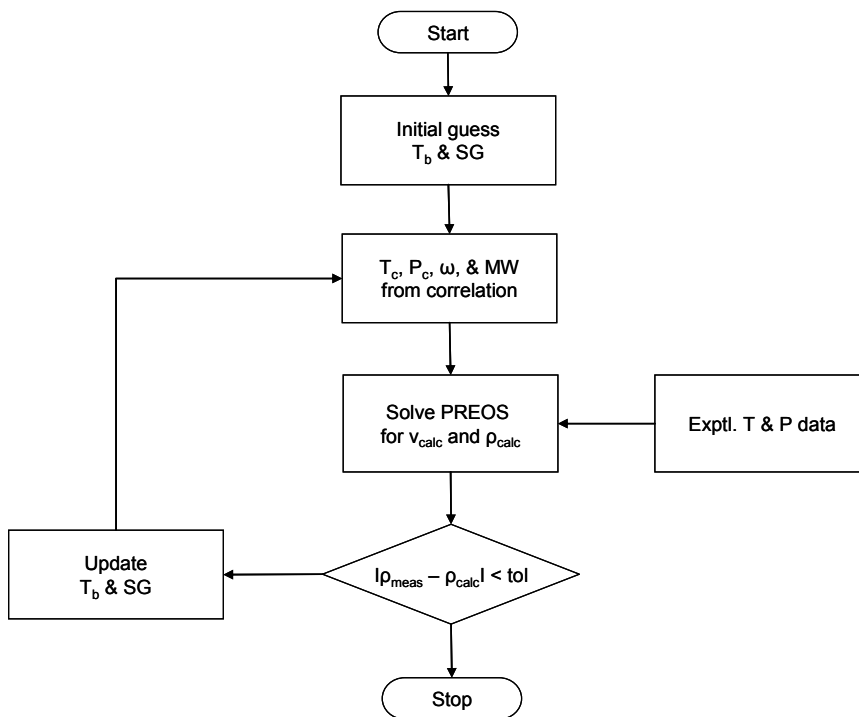


Figure 4-1 Flowchart for determining critical properties from regression of vapour pressure data.

#### 4.2. ANALYSIS OF N-DODECANE DATA

The vapour pressure of n-dodecane was measured at temperatures from 22.5 °C to 221.0°C corresponding to vapour pressures ranging from 0.33 kPa to 109.34 kPa. Two series of measurements were taken. After the first series, the sample was cooled to about 22°C and re-evacuated with the mechanical vacuum pump for 30 minutes, and then again at 75°C for 30 minutes prior to the start of the second series of data collection. The second set of vapour pressure measurements were taken approximately at the mid-point of the temperature interval for the first set of measurements.

#### 4.2.1. Consistency and Accuracy

The vapour pressure and density of n-dodecane as a function of temperature were measured to determine the accuracy to which these types of measurements could be made with the current experimental arrangement in comparison to literature data. It was assumed that the degree of internal consistency and errors in measuring density and vapour pressure for n-dodecane would provide an estimate of the maximum consistency and minimum errors for the same measurements for VTB whose properties are unknown.

The typical method of checking the consistency of vapour pressure data is to plot the logarithm of vapour pressure versus reciprocal absolute temperature. Such a plot is shown in Figure 4-2. The experimental data appears to show good consistency and reproducibility at higher temperatures, gives the expected straight line, and extrapolates close to the true boiling point for n-dodecane. The straight line behaviour follows from the Clausius-Clapeyron equation, (4.1), which includes the assumptions that: (a) the heat of vaporization is constant over the range of the data and (b) the vapor pressure is sufficiently low so that it behaves as an ideal gas.

$$d \ln P = \frac{-\Delta H_{vap}}{R} d\left(\frac{1}{T}\right) \quad (4.1)$$

Integration from a reference state with vapour pressure  $P_{ref}$ , the Clausius-Clapeyron equation becomes:

$$\ln\left(\frac{P}{P_{Ref}}\right) = \frac{-\Delta H_{vap}}{R} \left(\frac{1}{T} - \frac{1}{T_{Ref}}\right) \quad (4.2)$$



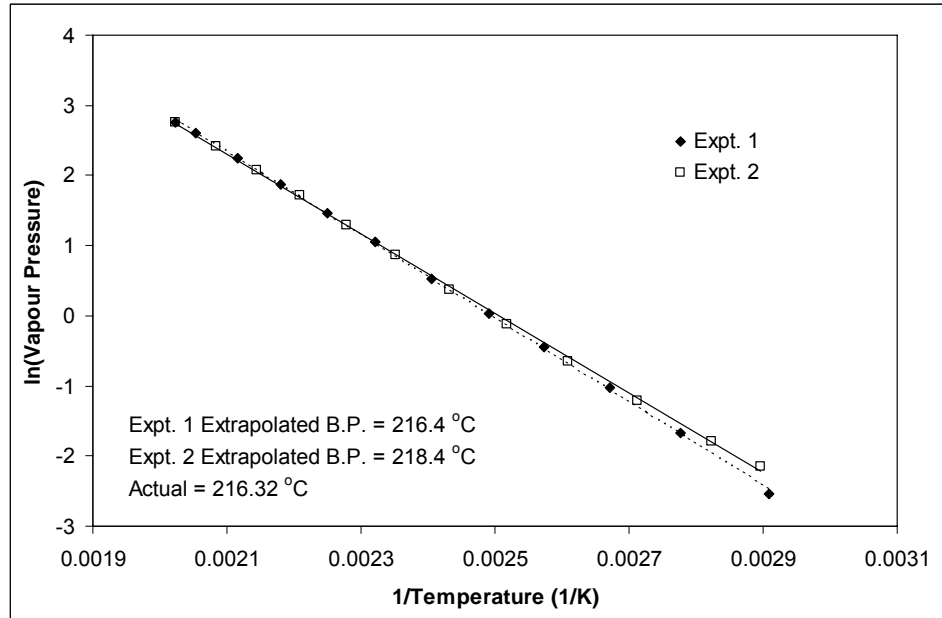


Figure 4-2 Plot of  $\ln(\text{vapour pressure})$  vs.  $1/\text{temperature}$  for n-dodecane

Despite the above approximations, the “straight line” is actually slightly concave downwards. In order to better assess vapour pressure data, Oonk *et al.*<sup>127</sup> have proposed a method of analysis that preserves and emphasizes the curvature due to changes in the heat of vaporization. The method involves the addition of a linear contribution in reciprocal temperature to the  $\ln(P)$  term:

$$\ln(f_p) = \ln\left(\frac{P}{P_{Ref}}\right) - \alpha + \frac{\beta}{T} \quad (4.3)$$

The terms  $\alpha$  and  $\beta$  are chosen so that the absolute value  $|\ln(f_p)|$  is close to zero at the extrema of the data set. When  $\ln(f_p)$  versus  $1/T$  is plotted, the result is a symmetrical arc if the data set is consistent. The curve along which the internally consistent data lie for the given value of  $\alpha$  and  $\beta$  is found by using the thermodynamic relationship for low pressure VLE derived by Oonk *et al.*:

$$\begin{aligned}
R \ln(P/P_{\text{Ref}}) = & -\Delta G_{\text{vap}}^{\theta} / \theta + \Delta H_{\text{vap}}^{\theta} (1/\theta - 1/T) + \\
& \Delta C_{p,\text{vap}}^{\theta} (\theta/T - 1 + \ln(T/\theta)) + \\
& (\theta/2) (\partial(\Delta C_{p,\text{vap}}^{\theta}) / \partial T) (T/\theta - \theta/T - 2 \ln(T/\theta) + \dots)
\end{aligned}
\tag{4.4}$$

where  $\theta$  corresponds to the reference temperature for  $P_{\text{ref}}$ . Substituting equation (4.4) in equation (4.3) gives the arc on which the experimental data should lie for the given values of  $\alpha$  and  $\beta$ . The results are shown for the present data in Figure 4-3. The greatest deviation between the experimental data and the predicted arc is for the low temperature data where the measured vapour pressure is also low. The deviations at low vapour pressure are an indication of the accuracy of the pressure transducer but the effect of impurities in n-dodecane cannot be discounted.

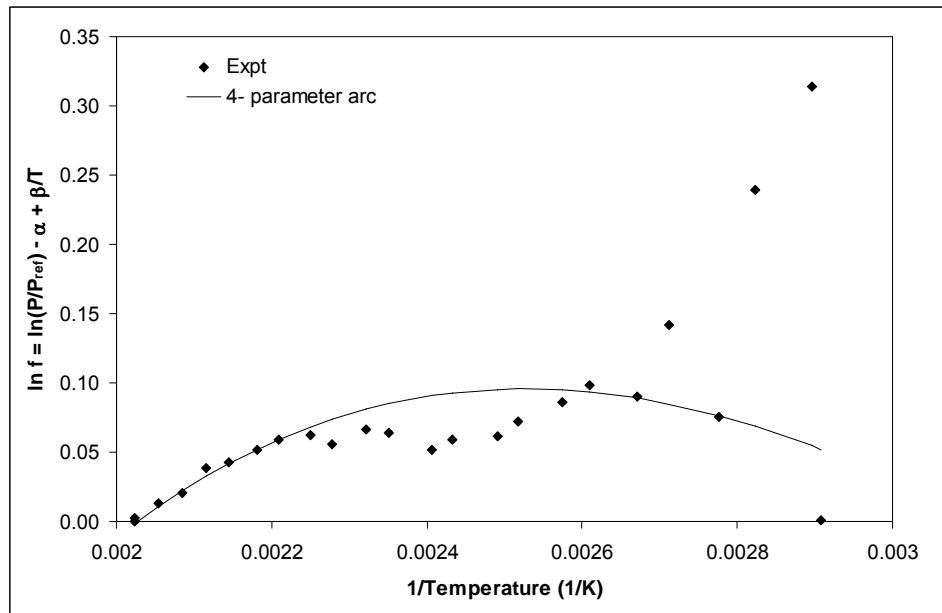


Figure 4-3 Analysis of n-dodecane vapour pressure using Oonk's arc method with reference pressure and temperature of 1 atmosphere and 500K, respectively.

Dejz and co-workers have published vapour pressure data for n-dodecane. In order to compare the data from Dejz *et al.*<sup>128</sup> with the present data, the former was fitted to equation(4.4). The fitted parameters reproduced the data of Dejz *et al.* with an average absolute relative error of 0.37%. These parameters were then used to calculate vapour

pressure at the same temperatures as the current experimental data set. The resulting comparison of the two data sets is shown in Figure 4-4. The trend in absolute per cent deviation as a function of temperature at which the vapour pressure was measured is shown in Figure 4-5. At low temperatures, the measured vapour pressures have large positive deviations from that calculated from the data of Dejoz, whereas at higher temperature, the deviations are smaller and positive. The average absolute relative deviation between the two data sets was 10.9%. The error was less than 10% when the measured vapour pressure was above than 4 kPa. The average deviation was larger than would be expected for the pressure transducer with a stated static accuracy of 0.25% of full scale. The trend in absolute deviation with temperature tends to indicate that the contribution of temperature sensitivity of the transducer to the overall deviation is less than about 3%, i.e., similar to the error at high temperatures where the impact of temperature on the pressure transducer would be greatest. In contrast, the absolute accuracy of the transducer at low pressures may be the main source of errors at low temperatures. The conclusion regarding accuracy of the transducer at low pressures is not absolutely certain because impurities in n-dodecane could also contribute to deviations in the low vapour pressure measured at low temperatures. The deviations at low pressure are also evident, as shown in Figure 4-6, when the data of Dejoz *et al.* and the present data are plotted together using the arc method.

The consistency of density data was assessed by plotting the measured density as a function of temperature (Figure 4-7) and by comparing with densities calculated by the Guggenheim correlation (Figure 4-8). The error bars on the measured data correspond to the estimated combined errors due to mass of fluid in the vapour phase and instrumental error due to image resolution. The distinct steps in the data are due to the resolution of the digital images from which the height of the liquid meniscus and thereby liquid volumes are calculated. In comparison to data from the Guggenheim correlation, the average absolute deviation was 0.95%.

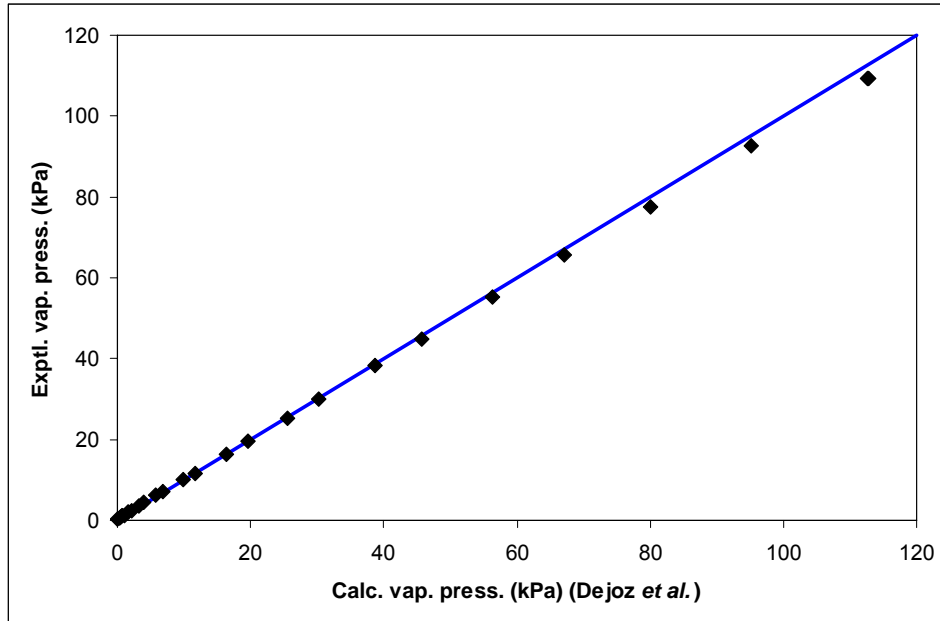


Figure 4-4 Comparison between experimental vapour pressures and those calculated from the data of Dejoz *et al.*

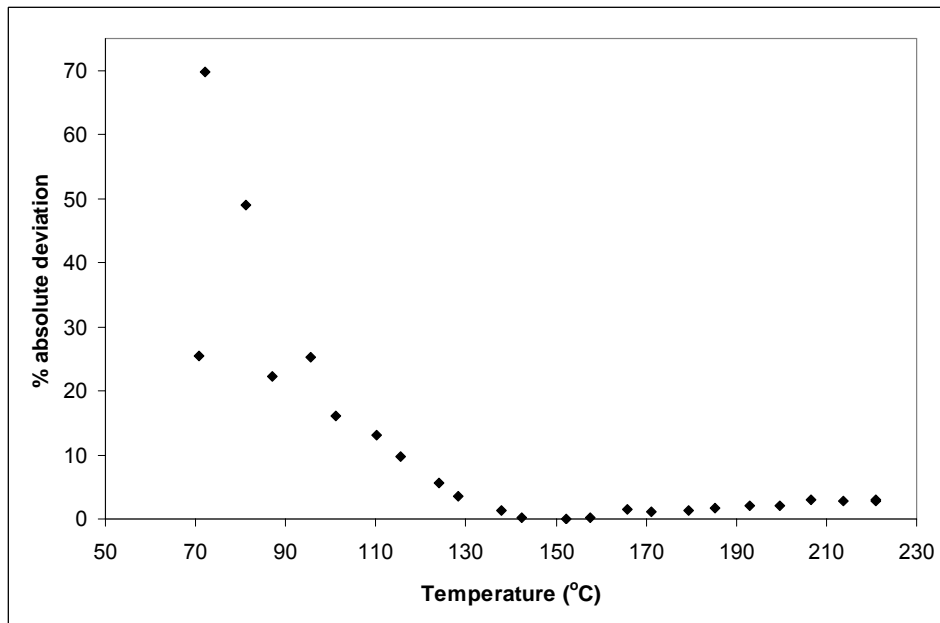


Figure 4-5 Trend absolute per cent deviation between experimental and calculated vapour pressure (using data of Dejoz *et al.*) versus temperature.

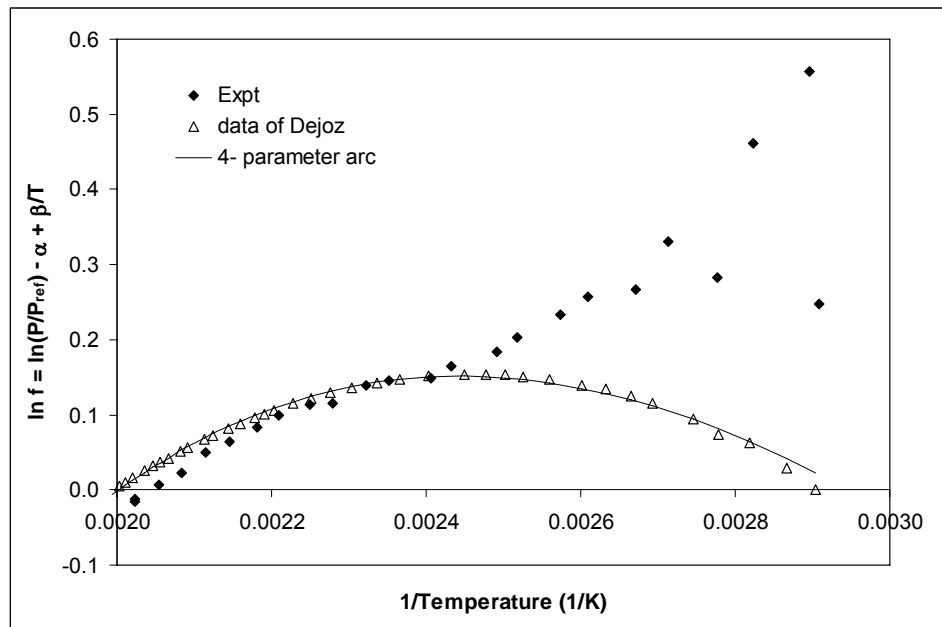


Figure 4-6 Comparative analysis of n-dodecane vapour pressure data using Oonk's arc method with reference pressure and temperature of 1 kPa and 298.15K, respectively.

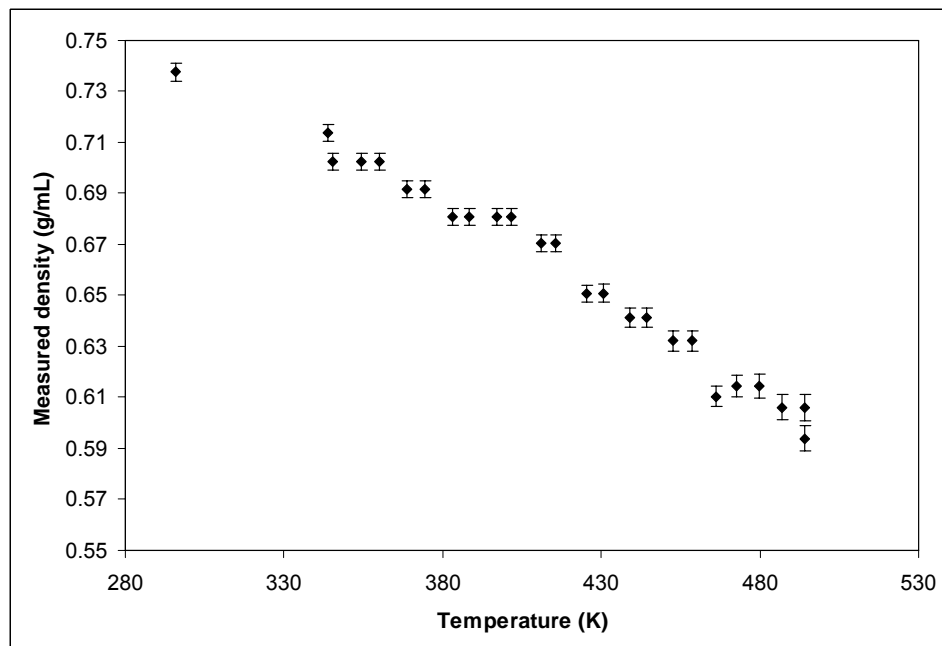


Figure 4-7 Measured density of n-dodecane vs. temperature.

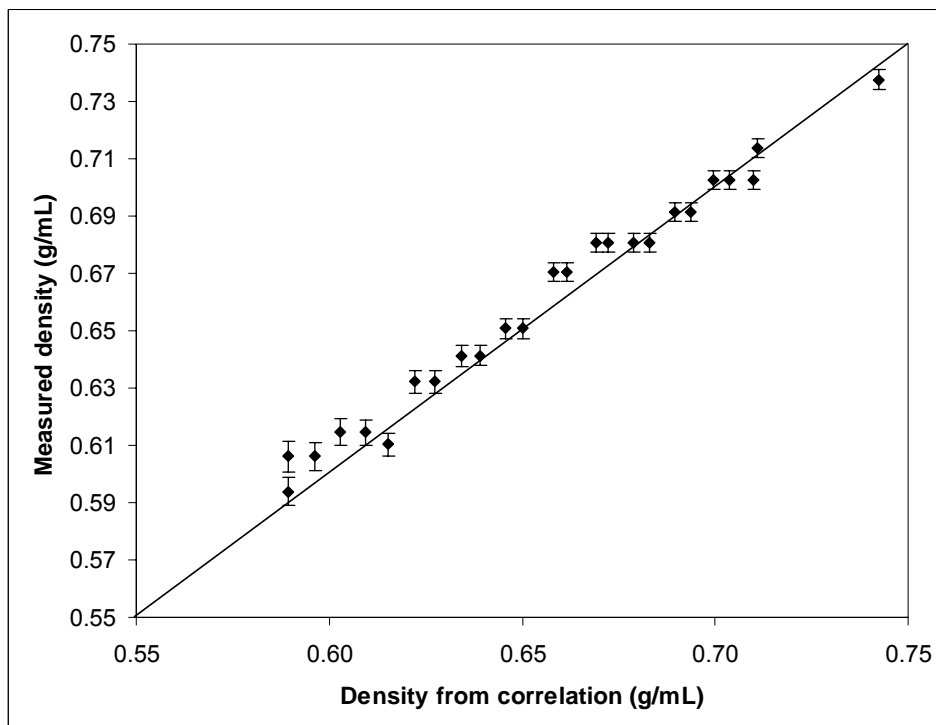


Figure 4-8 Measured density of n-dodecane vs. density calculated from correlation using Guggenheim equation.

#### 4.2.2. Regression of Fluid Properties

In spite of the errors in low pressure data, the complete experimental data set was regressed using the Peng-Robinson CEOS. Critical properties were constrained as discussed above using correlation based on normal boiling point and specific gravity. The results are summarized in, Table 4-1, Figure 4-9, and Figure 4-10. The average absolute deviation between the experimental liquid densities and those calculated by the Peng-Robinson CEOS was 15.2% when using either the Riazi-Daubert or Twu derived critical properties.

**Table 4-1 Summary of properties for n-dodecane obtained by regression of vapour pressure data.**

Property	T <sub>b</sub> /SG Correlation						DIPPR Database
	Riazi-Daubert			Twu			
	Optimum	95% Confidence Limits		Optimum	95% Confidence Limits		
T <sub>c</sub> (K)	651.87	641.84	661.80	654.21	643.81	664.53	658
P <sub>c</sub> (kPa)	2172.8	2268.4	2082.0	2329.3	2421.0	2242.1	1820.0
V <sub>c</sub> (m <sup>3</sup> /kmole)	0.623	0.597	0.650	0.584	0.557	0.612	0.755
Acentric factor	0.4649	0.4407	0.4894	0.4274	0.4071	0.4479	0.576385
MW (g/mole)	156.75	149.28	164.50	147.14	140.65	153.82	170.335
T <sub>b</sub> (K)	468.19	457.13	479.24	464.18	453.37	474.99	489.473
SG	0.7827	0.7792	0.7862	0.8006	0.7966	0.8046	0.7463*

\* From Guggenheim correlation

Molecular weight and normal boiling point were under-estimated while specific gravity was over-estimated. The critical temperature determined from the regression of vapour pressure data and constrained by either the Riazi-Daubert or Twu correlation differed from the value in the DIPPR data base by 0.93% and 0.58%, respectively. The estimated critical pressure using either correlation was considerably higher than the value from the DIPPR database, with absolute errors of 19.4% and 28.0% with Riazi-Daubert and Twu correlations, respectively. The estimated acentric factors differed by similar amounts as estimated critical pressure from DIPPR values. As noted in Chapter 2, Voulgaris *et al.* reported that a 1% absolute error in critical temperature leads to an absolute error of 16% in predicted vapour pressures of n-decane, whereas a similar error in either acentric factor or critical pressure leads to relatively smaller absolute errors in vapour pressure of n-decane of approximately 1 and 3%, respectively. The errors in the estimated critical properties and acentric factor in the present case are consistent with the higher sensitivity of CEOS calculation to critical temperature compared to critical pressure and acentric factor.

The differences in properties obtained from the regression with the Riazi-Daubert and Twu critical property constraints reflect the intrinsic differences of the correlations themselves. For n-dodecane, the Riazi-Daubert correlations result in better correspondence with accepted properties from the DIPPR database. That the regressions

using both critical property constraints lead to the same average absolute deviations between measured and calculated reflect the limitations of the data set.

The measured density was chosen as dependent variable for these regressions. The shortcomings of the Peng-Robinson and other CEOS for prediction of liquid phase densities were discussed at length in Chapter 2. We could have chosen density as the independent variable; however, the stepped behaviour of measured density versus temperature as shown in Figure 4-7 caused unmanageable instabilities and convergence problems in the regression. Even with a consistent data set made up of vapour pressure data from Dejoz *et al.* and densities from the Guggenheim equation, the deviations of the values of regressed critical properties from those in the DIPPR database are no better than those obtained with the present data. In some cases the deviations are worse. The deviations of estimated critical properties from the accepted values represent the best compromise which minimizes the error in densities calculated by the Peng-Robinson CEOS and reflect the limitations of the correlations for critical properties and the CEOS.

**Table 4-2 Summary of properties for n-dodecane obtained by regression of vapour pressure data from Dejoz et al. and densities obtained from the Guggenheim equation.**

Property	Correlation		DIPPR
	Riazi-Daubert	Twu	Database
<b>T<sub>c</sub> (K)</b>	640.94	642.72	658
<b>P<sub>c</sub> (kPa)</b>	2253.4	2398.0	1820.0
<b>V<sub>c</sub> (m<sup>3</sup>/kmole)</b>	0.598	0.561	0.755
<b>Acentric factor</b>	0.4422	0.4102	0.576385
<b>MW (g/mole)</b>	149.28	141.02	170.335
<b>T<sub>b</sub> (K)</b>	456.89	453.28	489.473
<b>SG</b>	0.7766	0.7933	0.7463*



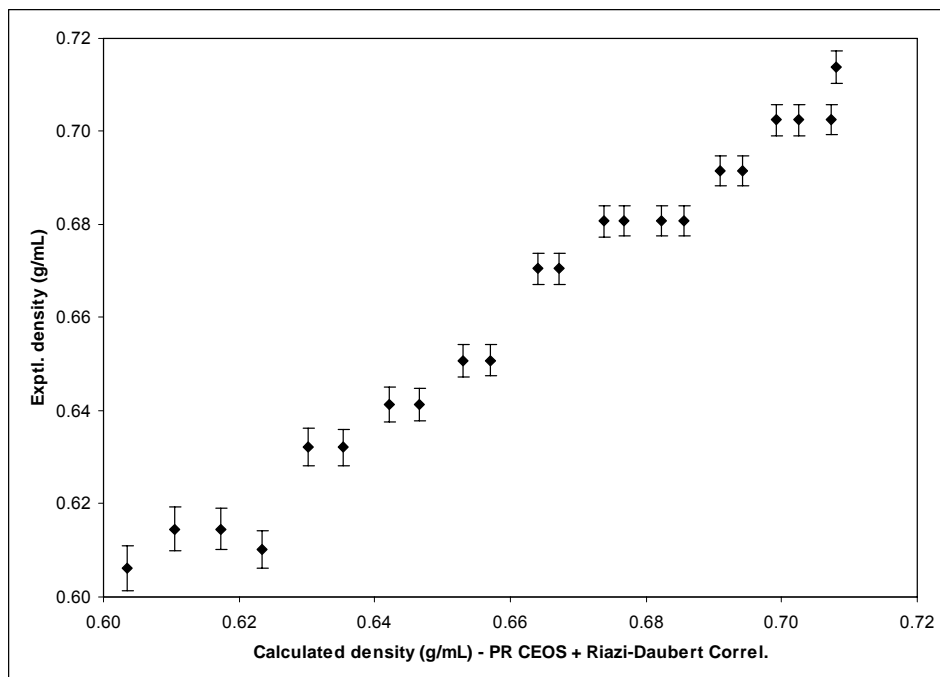


Figure 4-9 Comparison of experimentally determined density for n-dodecane with that calculated by the Peng-Robinson CEOS using critical properties from Riazi-Daubert correlation (average absolute relative deviation: 15.2%).

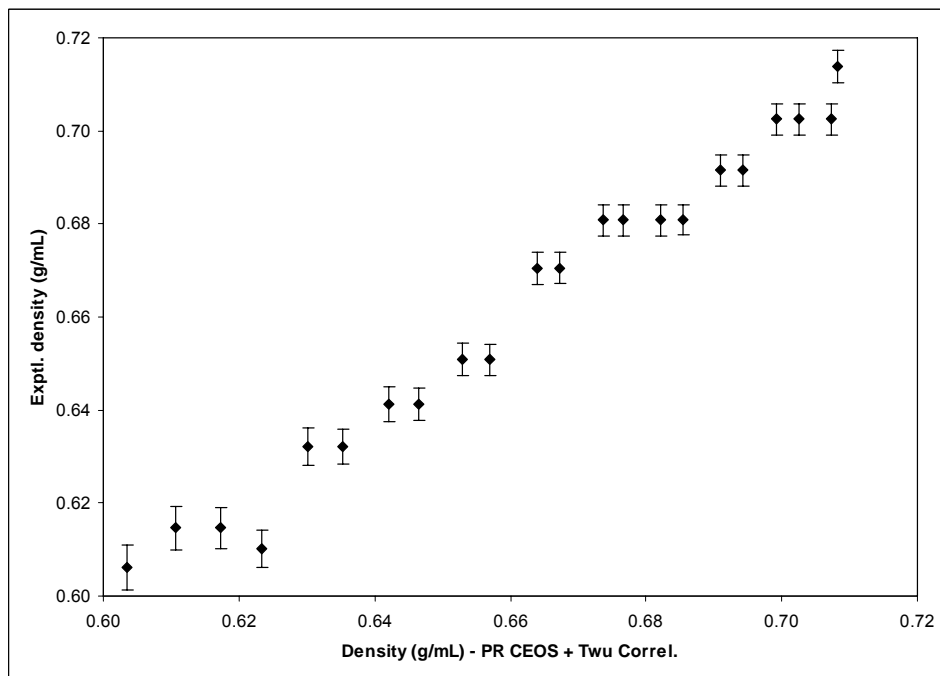


Figure 4-10 Comparison of experimentally determined density for n-dodecane with that calculated by the Peng-Robinson CEOS using critical properties from Twu correlation (average absolute relative deviation: 15.2%).

### 4.3. ANALYSIS OF VTB DATA

The vapour pressure of VTB was measured between 150 and 300°C. Three series of measurements were undertaken. The same sample of VTB was used for all three series of measurements.

#### 4.3.1. Consistency of Data

In the first series, the temperature of the pressure transducer was maintained at about 5°C above the fluid temperature until the transducer temperature reached 250°C at which point the temperature of the transducer was no longer increased as the fluid temperature increased. This was done because the manufacturer specified 260°C as the upper limit of temperature compensation for the pressure transducer. Once the temperature of the fluid exceeded the temperature of the transducer and the connecting tubing, there was a change in slope of the  $\ln(P)$  vs.  $1/T$  curve attributable to a pressure drop due to condensation in the tubing and transducer (Figure 4-11). It was also observed that as the temperature was being increased above 150°C, small bubbles periodically detached from the stir bar. The number and size of bubbles first decreased with increasing temperature but then started to increase with increasing temperature above 255°C.

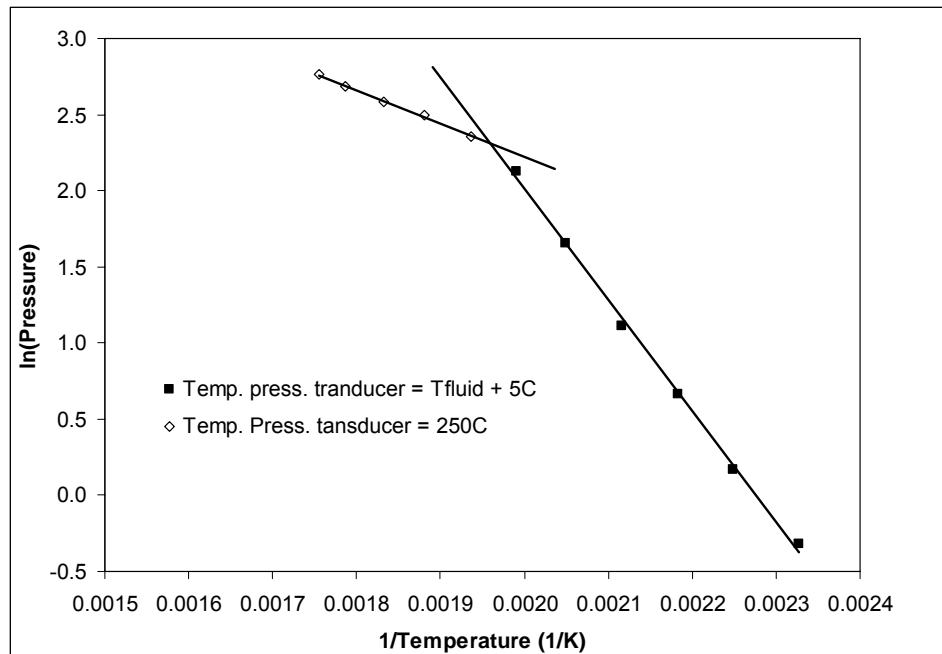


Figure 4-11 Vapour pressure of VTB showing effect of pressure drop due to condensation in pressure transducer and connecting tubing.

In preparing for the second series of measurements, the sample was again evacuated at about 150°C to remove all traces of dissolved gas. It was surprising to observe the vigorous foaming of the liquid due to gas removal and the faint odour of sulphur from the discharge of the mechanical pump. For this second series of measurements, the temperature of the pressure transducer and connecting tubing was maintained about 5°C above the fluid temperature for the entire measurement range to a final fluid temperature of 300°C. Although no gas bubbles were observed below 250°C, once the temperature was above 250°C, small bubbles of gas were observed at steady intervals. Upon cooling the sample and evacuating the cell, vigorous foaming was once again observed indicating some light components, and a sulphurous odour was again detected. The same observations were made for the third and final series of measurements as for the second series. The results of these last two series of measurements are plotted in Figure 4-12. Although pressure drops due to condensation is believed to have been eliminated, there was significant scatter in the vapour pressure data of VTB compared to data for n-dodecane. Part of the scatter may be attributed to the accuracy of the pressure transducer in measuring the low vapour pressures for VTB (0.5 to 20 kPa) with the transducer heated from 155 to 305°C.

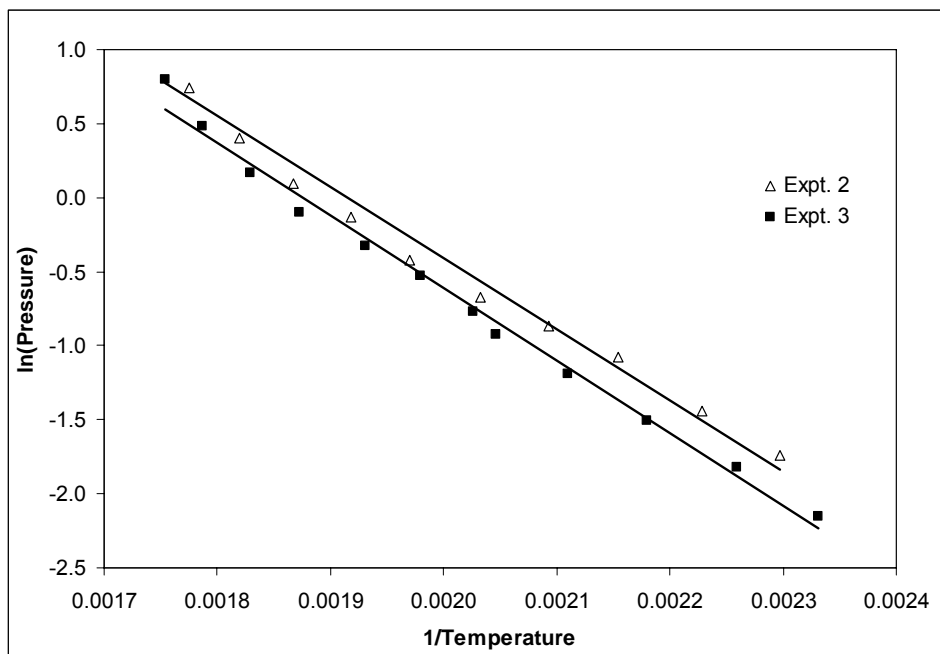


Figure 4-12 Vapour pressure of VTB from two series of measurements on the same sample where pressure drops due to condensation was eliminated.

The above observations indicate that VTB may be more reactive than previously thought. Under normal conditions, the rate of reaction appears slow and is not readily detectable. Under near vacuum conditions and with the ability to observe the fluid using x-ray imaging, even small numbers of gas bubbles 2 to 3 millimeters in diameter can be observed. The amount of gas appears to diminish slightly with each temperature cycle indicating a slight diminution of thermal reactivity. The occurrence of the thermal reaction means that evolved gas contributed to the measured pressure so that vapour pressures were over-estimated. Furthermore, due to reaction, the liquid phase composition is being altered, even if only to a minor extent, so that it intrinsically would have a different vapour pressure after each temperature cycle. The extrapolated normal boiling point was 465°C and 481°C for series 2 and 3, respectively. The higher value for the extrapolated boiling point from the series 3 data may be indicative of the change in composition due to thermal reactions and/or perhaps the influence of the evolved gas which is not as prevalent in series 3 compared to series 2. Certainly, we can conclude that each of the three series of measurements reflected similar but different fluid compositions. These points should be borne in mind when considering these results.

Figure 4-13 shows a plot of the density of VTB versus temperature. The estimated instrumental error due to resolution of the x-ray image is given by the error bar. Within the limits of experimental error, the three sets of measurement agree with each other. This is not surprising since the extent of thermal reactions during these measurements was unlikely to be sufficient to alter the density significantly. As noted in Chapter 2, the relationship between density and elemental composition proposed by Gray would require significant thermal removal of sulphur to alter the fluid density. Vapour pressure and density data for all three series of measurements are tabulated in Table 4-3.

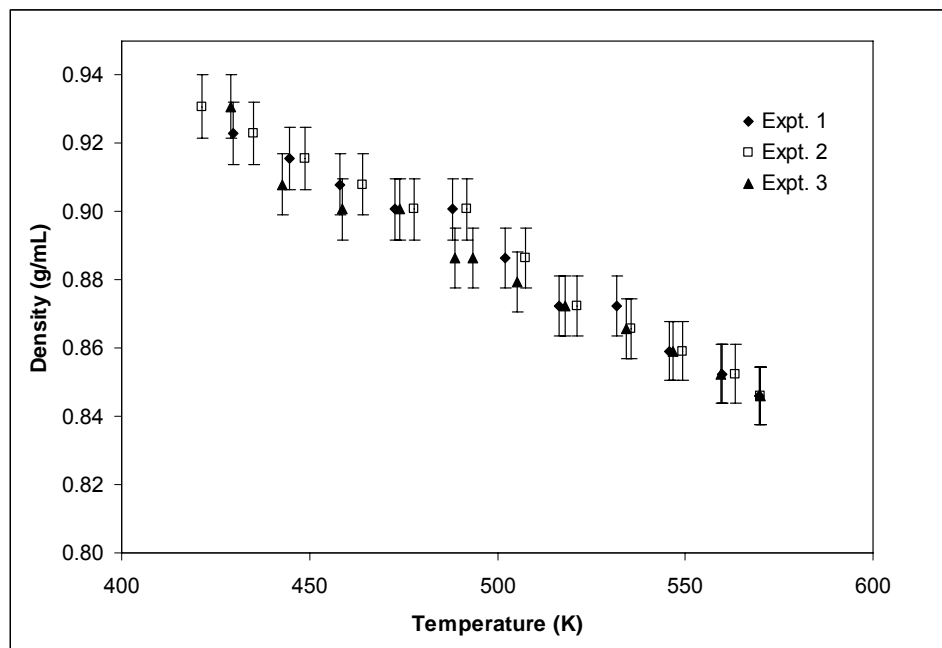


Figure 4-13 Density of VTB versus temperature.

Table 4-3 Tabulation of experimental vapour pressure and density measurements for VTB.

Series 1			Series 2			Series 3		
Press. (kPa)	Temp. (°C)	Density (g/mL)	Press. (kPa)	Temp. (°C)	Density (g/mL)	Press. (kPa)	Temp. (°C)	Density (g/mL)
5.0	156.6	0.923	0.5	148.1	0.931	0.8	155.8	0.931
8.1	171.4	0.915	1.2	162.1	0.923	1.1	169.5	0.908
13.4	185.0	0.908	1.6	175.7	0.915	1.5	185.7	0.901
21.0	199.4	0.901	2.3	191.1	0.908	2.1	200.8	0.901
36.1	214.8	0.901	2.9	204.8	0.901	2.7	215.6	0.886
57.8	229.0	0.886	3.5	218.8	0.901	3.2	220.3	0.886
72.5	243.1	0.872	4.5	234.4	0.886	4.1	232.0	0.879
83.8	258.7	0.872	6.0	248.2	0.872	5.0	244.8	0.872
91.3	272.6	0.859	7.6	262.4	0.866	6.2	261.0	0.866
100.7	286.8	0.852	10.3	276.3	0.859	8.2	273.5	0.859
109.0	296.7	0.846	14.5	290.2	0.852	11.2	286.4	0.852
-	-	-	20.1	296.8	0.846	15.3	297.0	0.846

There are no reference data with which to compare the present data set. Schwarz *et al.*<sup>129</sup> have measured the vapour pressure and density of an Athabasca bitumen vacuum residue produced by Syncrude Canada. Vapour pressure was measured using an ebulliometer while density was determined using a glass pycnometer. The vapour

pressure and density of VTB obtained in the present study was compared to those obtained by Schwarz *et al.* in Figure 4-14 and Figure 4-15, respectively. The vapour pressures measured by Schwarz and co-workers were lower than those obtained in the present study over a similar temperature range. The data of Schwarz *et al.* yields a steeper negative slope which indicates a higher heat of vaporization compared to that from the present data. The present data indicate an extrapolated normal boiling point of 465°C and 481°C for series 2 and 3, respectively. In contrast, the extrapolated normal boiling point from the data of Schwarz and co-workers was 406°C. The comparison of density data shows good consistency despite the differences in vapour pressure because the density was not as sensitive to slight differences in compositions.

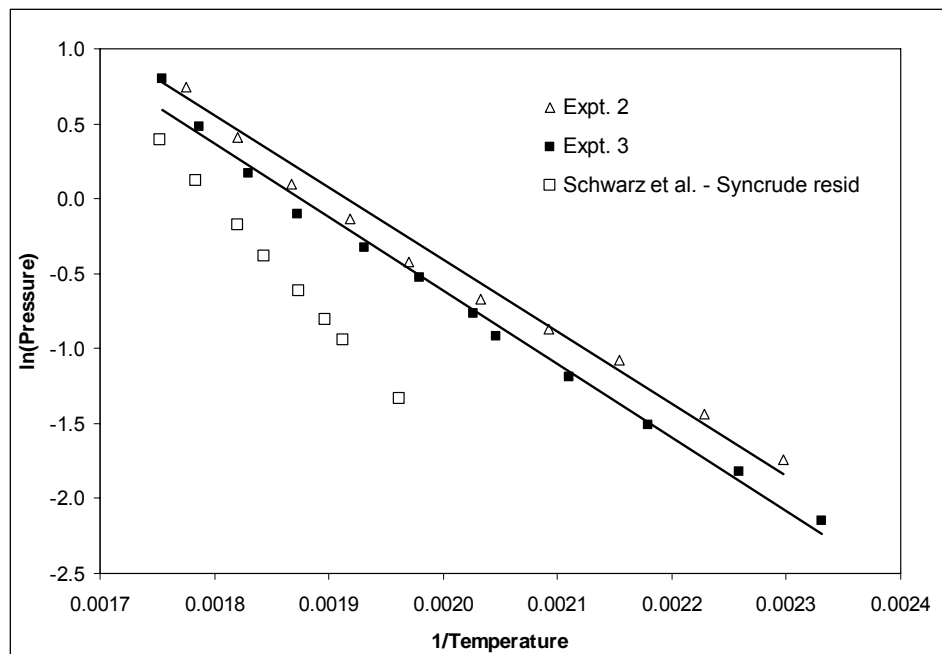


Figure 4-14 Comparison between vapour pressure data for VTB used in the present study and that used by Schwarz *et al.*

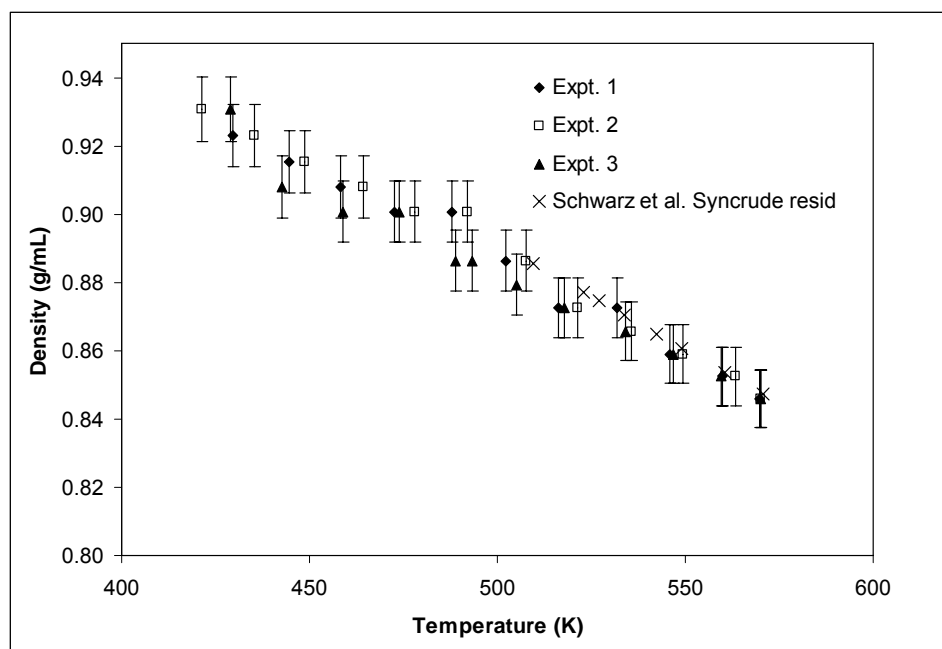


Figure 4-15 Comparison between density data for VTB used in the present study and that used by Schwarz *et al.*

The molar average heats of vaporization can be obtained from the slope of the plots shown in Figure 4-14. For the VTB used in this work the estimated heat of vaporization is 39.9 and 40.7 kJ/mole from experiments 2 and 3, respectively, whereas for the sample used by Schwarz and co-workers<sup>129</sup> it is 68.4 kJ/mole. For a homologous series, the heat of vaporization should increase with molecular weight and boiling point. The correspondence between boiling point and heats of vaporization for experiments 2 and 3 is consistent with this trend. Schwarz *et al.* do not provide detailed analysis for the sample used which would allow a comparison to VTB used in the present study.

#### 4.3.2. Regression of Fluid Properties

As was done for the vapour pressure and density data for n-dodecane, the data for VTB (Series 2 and 3) were regressed while constraining critical properties using the Riazi-Daubert or Twu correlations. The regressed properties are shown in Table 4-4 and the model predictions for density are compared to experimental values in Figure 4-16 and Figure 4-17.

For the regression constrained by the Riazi-Daubert correlations for critical properties, the predicted boiling point of 378°C was well below either the 448°C initial boiling point of VTB or the 610°C mass average boiling point of the 76.3 wt.% of VTB which boils below 750°C. The under-prediction of boiling point by regression means that critical temperature will be under-predicted while critical pressure will be over-predicted. The regressed molecular weight was also much lower than what would be expected for heavy oil even without associating asphaltenes. The measured molecular weight of VTB by vapour pressure osmometry was 1048 g/mole. Even if the limiting value of asphaltenes molecular weight was taken as 750 g/mole, the high asphaltenes content of 32.2 wt.% of VTB would indicate that the molecular weight should be higher than values of 304 g/mole obtained by regression. An identical conclusion was also reached from an examination of the regression constrained by the Twu correlations. A further complication with regression constrained by the Twu correlation was that it can lead to unrealistic values as shown by complex values within the 95% confidence limits for critical properties.

The vapour pressure of VTB can be predicted using critical properties derived from high temperature simulated distillation (HTSD) data and specific gravity. This was done with HYSYS version 3.2 process simulator using Twu's correlation for critical properties and the Peng-Robinson CEOS. Vapour pressures appear to be severely under-estimated by this procedure, yielding a maximum vapour pressure of 0.011 kPa at 297°C compared to experimental data of 15.3 kPa of 297°C. This result implies that VTB behaves as a more volatile fluid than indicated by its HTSD curve.

**Table 4-4 Summary of properties for VTB obtained by regression of vapour pressure data.**

Property	T <sub>b</sub> /SG Correlation					
	Riazi-Daubert			Twu		
	Optimum	95% Confidence Limits		Optimum	95% Confidence Limits	
T <sub>c</sub> (K)	828.85	814.23	843.20	1010.47	627.24	1408.52
P <sub>c</sub> (kPa)	1783.1	1911.7	1662.9	2197.6	3728.1	complex
V <sub>c</sub> (m <sup>3</sup> /kmole)	1.096	0.994	1.209	0.864	0.220	1.852
Acentric factor	1.0104	0.9401	1.0849	0.7719	0.0139	complex
MW (g/mole)	303.56	280.65	328.01	289.75	71.03	complex
T <sub>b</sub> (K)	651.19	631.83	670.55	761.29	376.58	1146.00
SG	0.9337	0.9326	0.9348	1.1667	7.0558	9.3892



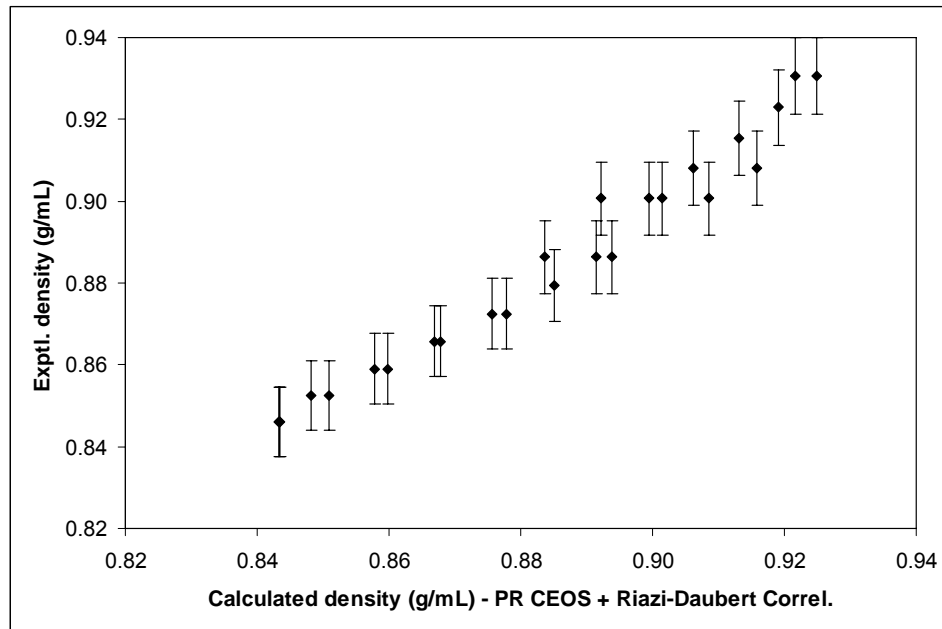


Figure 4-16 Comparison of experimentally determined density for VTB with that calculated by the Peng-Robinson CEOS using critical properties from Riazi-Daubert correlation (average absolute relative deviation: 10.7%).

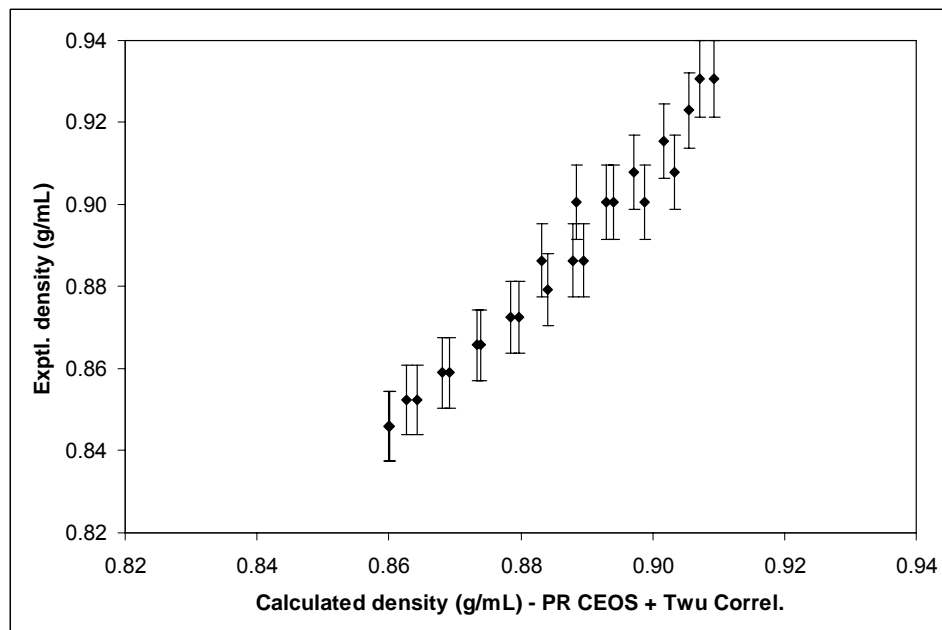


Figure 4-17 Comparison of experimentally determined density for VTB with that calculated by the Peng-Robinson CEOS using critical properties from Twu correlation (average absolute relative deviation: 26.0%).

#### 4.4. SUMMARY

The vapour pressure of VTB was measured from 150 to 300°C. During these measurements, there was clear visual evidence of the thermal reaction of VTB when the temperature was above 250°C. One product of the thermal reaction of VTB was volatile hydrocarbons which increased the measured vapour pressure. These vapour pressure measurements were achieved with relatively small vapour volumes and so represent a lower limit for actual bubble point pressures.

Critical properties ( $P_c$ ,  $T_c$ ,  $V_c$ ), acentric factor, molecular weight, normal boiling point, and specific gravity of VTB were obtained from regression of the VTB vapour pressure data. The regression was constrained by the use of property correlations (Riazi-Daubert and Twu) based on normal boiling point and specific gravity. Without such constraints, a unique solution could not be obtained since the critical properties are not independent variables but are dependent on the given molecular structure.

The regressed critical properties were not consistent with expectations for high boiling, high molecular weight, and asymmetric VTB mixture even though these properties led to good correspondence with measured data.

The questionable values for estimated critical properties, boiling points, and molecular weights obtained from regression of vapour pressure and density data for VTB may be a consequence of the following factors:

1. VTB is a multi-component mixture that is not well represented as a single component, e.g., the fluid mixture is highly non-ideal and associating.
2. Correlations based on boiling point and specific gravity are not suitable for heavy high molecular weight mixtures.
3. The Peng-Robinson CEOS under-predicts molar densities of liquids and may not provide good predictions for size asymmetric and association heavy oils. Since CEOS are not accurate for predicting liquid densities, regressions involving liquid density data may lead to unreasonable critical properties.
4. Vapour pressures used for the regression may be over-predicted due to liberation of light gas products from thermal reactions.

These results demonstrate that good prediction of vapour pressure and liquid molar volume does not imply accurate critical properties. The unreasonable nature of these regressed critical properties makes the accuracy of other phase behaviour predictions and derived properties obtained through calculations with them doubtful despite their good correspondence with vapour pressure data.

---

## 5.0 EVALUATION OF THE GROUP CONTRIBUTION METHOD

---

### 5.1. COMPOSITION OF ATHABASCA RESIDUUM

As previously discussed, critical properties and acentric factors are essential molecular properties for determining parameters for solving cubic equations of state (CEOS). For heavy oil and bitumen fractions, these properties are typically estimated from correlations based on average normal boiling point and specific gravity. Such correlations have significant shortcomings when applied to high molecular weight hydrocarbons which may be highly aromatic and contain heteroatoms such as sulphur, nitrogen, and oxygen. In such cases, group contribution (GC) methods may offer more reliable estimates of molecular properties. Since it is at present impractical to define all the molecular species in a heavy oil or bitumen fraction, average representative structures must be defined in order to apply such group contribution methods.

Of all the GC methods discussed in Chapter 2, the method developed by Marrero and Gani appears to be the most promising one for estimating normal boiling point and critical properties for heavy oil and bitumen fractions. The group contribution method of Constantinou, Gani and O'Connell also shows potential to yield good estimates of acentric factor. Estimates of acentric factor can also be obtained, using the correlation developed by Ambrose and Walton, from critical properties and normal boiling point derived from the GC method of Marrero and Gani. In this section these methods are applied and examined for prediction of normal boiling point, acentric factor, and critical properties of fractions derived from Athabasca bitumen vacuum tower bottoms (VTB).

#### 5.1.1. VTB Fractions from Supercritical Fluid Extraction

A sample of Athabasca vacuum tower bottoms (VTB-C) was separated into ten fractions by Chung and co-workers<sup>12, 13, 14</sup> by extraction with supercritical n-pentane. These ten fractions have been described and characterized in great detail by Chung and co-workers and some of the properties pertinent to this study are summarized in Table 5-1. All data in Table 5-1 were reported by Gray *et al.* except for densities and properties of VTB-C which were reported by Rahimi and co-workers<sup>130</sup>. It should be

**Table 5-1 Summary of bulk properties for the ten supercritical fractions separated from VTB-C.**

Fraction #	Yield (wt.%)	MW (g/mole)	Density (g/mL)	Elemental composition (wt.%)				Ni (ppm)	V (ppm)	SARA Analysis (wt.%)			
				C	H	S	N			Saturates	Aromatics	Resins	Asphaltenes
1	12.7	506	0.9745	84.5	11.50	4.10	3080	12.8	30.7	26.86	57.23	15.91	0
2	9.8	755	0.9930	83.5	11.15	4.64	4100	21.3	48.7	16.42	62.41	21.17	0
3	7.6	711	1.0061	83.5	10.95	5.01	4330	30.1	69.8	9.68	65.70	24.62	0
4	10.6	799	1.0228	84.0	10.55	5.47	5070	44.8	101	4.1	66.73	29.17	0
5	6.5	825	1.0427	83.0	10.25	6.27	6160	71.1	166	1.36	63.86	34.78	0
6	4.4	948	1.0543	84.0	10.05	5.74	6810	89.7	221	0.68	53.35	45.97	0
7	3.3	1134	1.0646	83.0	9.80	6.12	7370	123	300	0.57	45.40	54.03	0
8	2.6	1209	1.0678	83.0	9.70	5.99	7530	138	355	0.28	45.91	53.81	0
9	2.1	1517	1.0736	82.5	9.50	6.29	7900	162	409	0	40.76	59.24	0
10	40.4	4185	-	78.5	8.00	6.51	10500	339	877	0	2.19	9.38	88.03
VTB	100	1191	1.0868	82.7	9.00	6.50	4600	148	364	6.3	33.00	29.40	31.4

noted that the mass balances for the elements in the ten fractions are not consistent with the composition of VTB-C given in Table 5-1.

#### 5.1.2. *Molecular Representations for VTB*

Sheremata and Sheremata *et al.* have employed analytical data to develop quantitative molecular representations of all ten fractions from supercritical separation of VTB-C. Elemental and molecular weight data were employed along with molecular structural information from  $^1\text{H}$  and  $^{13}\text{C}$  nuclear magnetic resonance spectroscopy to create the representations. It was found that six molecules were sufficient to represent each VTB-C fraction. These molecular representations, compositions, and mole fraction are summarized in Appendix 4.

#### 5.1.3. *Regressed Composition for VTB*

Chung *et al.* employed a +524°C vacuum residue (VTB-C) in their work which was different from the VTB used in the present study which contained more heavy vacuum gas oil. The differences between the two samples of VTB are evident when the respective high temperature simulated distillation (HTSD) curves are compared in Figure 5-1. It can be observed that the present VTB contains a significant concentration of lower boiling components compared to the sample (VTB-C) separated by Chung *et al.* Note that high temperature simulated distillation (HTSD) curves for each of the ten fractions from Gray<sup>131</sup> were combined to produce the curve for the original feed.

Despite the forgoing differences, the sample of VTB used in the present study can be defined according to the relative concentrations of supercritically extracted fractions of Chung and co-workers. Since there was a significant concentration of lower boiling components in the present sample of VTB, these were accounted for by inclusion of a heavy vacuum gas oil cut, derived from Athabasca bitumen along with the ten supercritically extracted fractions. The HTSD curves for all ten supercritically extracted fractions and the HVGO are shown in Figure 5-2. Analytical properties of this HVGO are summarized in Appendix 4. The composition of the VTB was estimated in terms of the eleven components using a non-linear regression solver built into Microsoft Excel. The relative proportions of supercritically extracted fractions 2 through 10 were constrained to have the same relative proportion as in the sample separated by Chung

and co-workers. The proportions of HVGO and fraction 1 were varied to minimize the average absolute relative difference over the entire boiling range to 0.09%. The results are shown graphically in Figure 5-3 and tabulated in Table 5-2.

The sample of VTB used in this study was found to contain 32.18 wt.% of n-pentane asphaltenes (Table 3-1). The model of VTB summarized in Table 5-2 includes 30.55 wt.% of fraction 10 which, from Table 5-1, has 88.03 wt.% of asphaltenes. These data imply that the model VTB includes only 26.9 wt.% of asphaltenes, which is less than the asphaltenes content of true VTB of 32.18 wt.%. However, as noted earlier, a mass balance of elemental compositions for the ten fractions was not consistent with the composition of the parent VTB given in Table 5-1 so the above difference with the present sample of VTB may not be significant. Additionally, asphaltene contents of heavy crudes are subject to significant experimental variability.

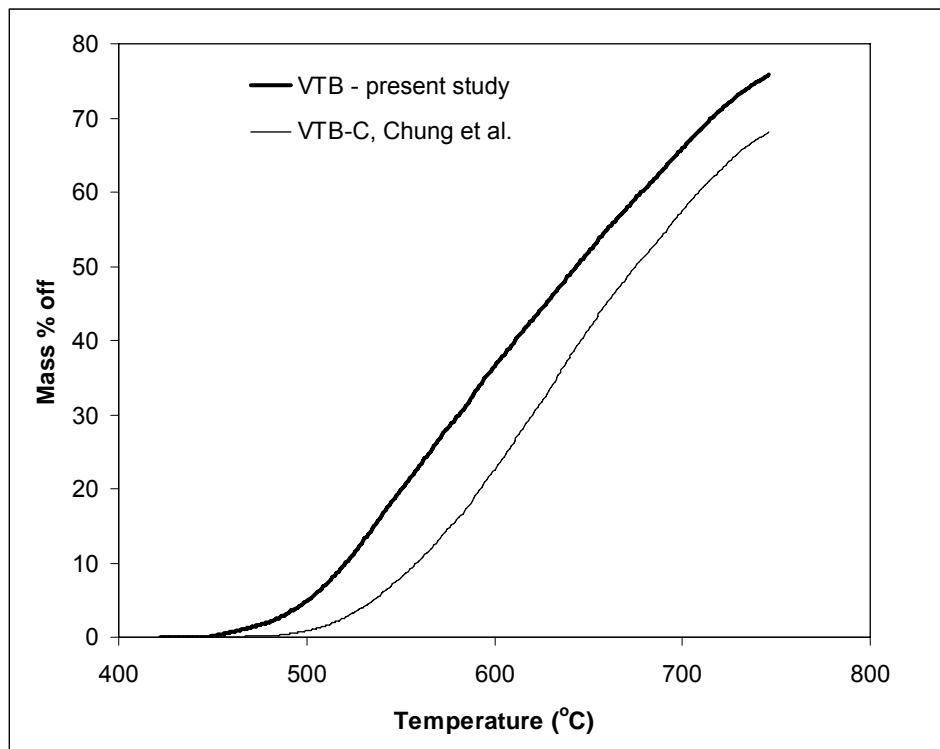


Figure 5-1 Comparison of high temperature simulated distillation curve for VTB used in the present study and that separated by supercritical extraction by Chung and coworkers.

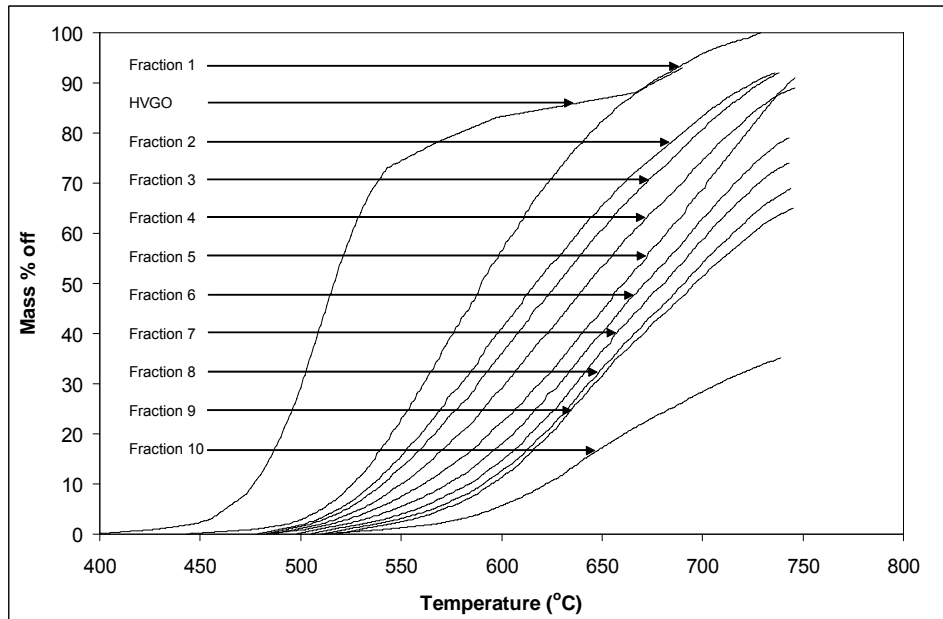


Figure 5-2 High temperature simulated distillation curves (from left to right) for narrow cut heavy vacuum gas oil (HVGO) and supercritically extracted fractions 1 through 10.

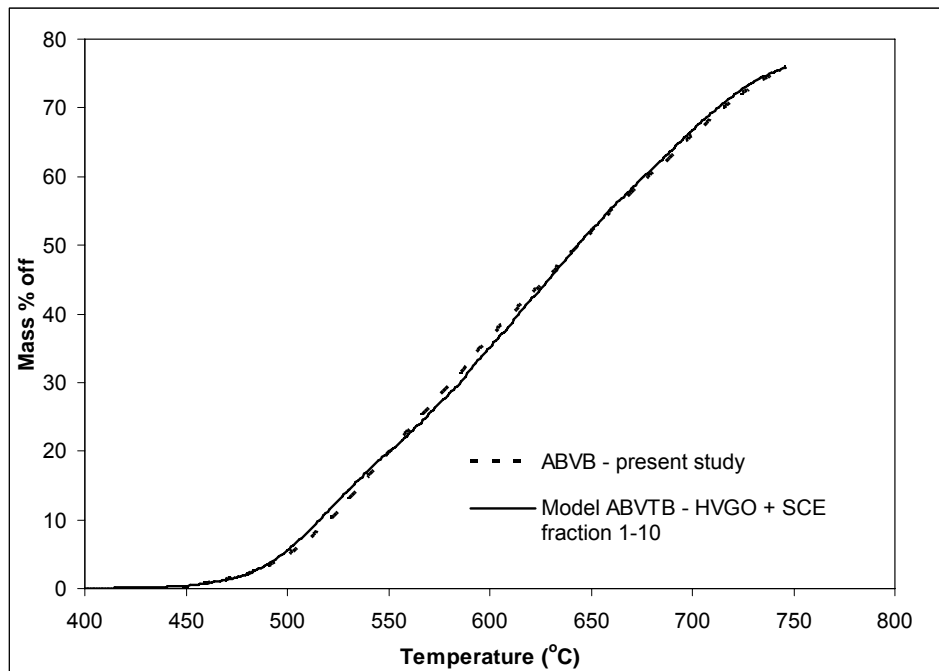


Figure 5-3 High temperature simulated distillation curves for VTB used in the present study and that for a model based on the ten supercritically extracted (SCE) fractions and a narrow cut heavy vacuum gas oil (HVGO).



**Table 5-2 Composition of VTB used in the present study in terms of mass fractions of ten supercritically extracted (SCE) fractions and a narrow cut heavy vacuum gas oil (HVGO).**

<b>Component</b>	<b>Mass Fraction</b>
HVGO	0.1592
SCE Fraction #1	0.1807
SCE Fraction #2	0.0741
SCE Fraction #3	0.0575
SCE Fraction #4	0.0801
SCE Fraction #5	0.0491
SCE Fraction #6	0.0333
SCE Fraction #7	0.0250
SCE Fraction #8	0.0197
SCE Fraction #9	0.0159
SCE Fraction #10	0.3055

With the inclusion of the narrow cut HVGO a partly inconsistent model for VTB is created. Approximately 84 wt.% of VTB can be modeled by 60 molecular representations. Critical properties for this portion of the VTB model can be estimated by an appropriate GC method such as that of Marrero and Gani. On the other hand, the remaining 16 wt.% of the VTB model is represented by a component characterized by bulk properties (average MW, boiling point, and density). For this portion of the model, critical properties can be estimated by, for example, correlations developed by Twu.

## **5.2. ESTIMATION OF CRITICAL PROPERTIES FOR VTB**

As previously discussed, the apparent superiority of the Marrero-Gani GC method over other methods is mainly due to the large number of groups considered for first, second, and third order contributions. The Marrero-Gani GC method is inherently simple but actual computation is complex due to the large number of complex groups. Fortunately, this method is commercially available in a software package called ProPred<sup>132</sup>. This software allows molecules to be imported in a variety of standard formats and then automatically calculates molecular properties using four different GC methods. The methods and primary properties calculated are summarized in Table 5-3.

**Table 5-3 GC methods and properties estimated using CAPEC's ProPred software package**

<b>GC Method</b>	<b>Properties Calculated</b>
Marrero and Gani	$T_b$ , $T_c$ , $P_c$ , $V_c$ , melting point ( $T_m$ ), Gibbs free energy of formation ( $G^\circ_f$ ), enthalpy of formation ( $H^\circ_f$ ), enthalpy of vaporization ( $H_v$ ), enthalpy of fusion ( $H^\circ_{fus}$ ), 1-octanol-water partition coefficient ( $\log(K_{ow})$ ), water solubility ( $\log(K_{ws})$ ), solubility parameter ( $\delta$ )
Constantinou, Gani and O'Connell	$T_b$ , $T_c$ , $P_c$ , $V_c$ , $\omega$ , melting point ( $T_m$ ), Gibbs free energy of formation ( $G^\circ_f$ ), enthalpy of formation ( $H^\circ_f$ ), enthalpy of vaporization ( $H_v$ ), molar volume, glass transition temperature
Joback and Reid	$T_b$ , $T_c$ (from $T_b$ ), $P_c$ , $V_c$ , melting point ( $T_m$ ), Gibbs free energy of formation ( $G^\circ_f$ ), enthalpy of formation ( $H^\circ_f$ ), enthalpy of vaporization ( $H_v$ ), enthalpy of fusion ( $H^\circ_{fus}$ )
Wilson-Jasperson	$T_c$ , $Z_c$

### 5.2.1. GC Methods for Very Large and Complex Molecules

Not all of the properties shown in Table 5-3 could be calculated for every molecular representation for VTB. Some GC methods do not have contributions for groups found in some of these molecules. For example, there was no group contribution for metalloporphyrins in any of the GC methods. It was found that estimation of acentric factor by the GC method of Constantinou *et al.* was not possible for most of the molecular representations because contributions were not known for many groups in these representations. Therefore, the correlation of Ambrose and Walton was used with critical properties and boiling points from the Marrero and Gani GC method.

The creators of ProPred suggest use with structures containing no more than 148 atoms. The molecular representations of VTB contain from 100 to as many as 668 atoms. The limits of the software were pushed so that molecules with up to 269 atoms could be analyzed and this included all molecular representation in the first nine supercritically extracted fractions. For fraction 10, which contained from 531 to 668 atoms, it was necessary to split the molecules arbitrarily into four parts. The splitting was done in the approximate midpoint of long aliphatic chains connecting large groups or cluster of groups. In these cases, ProPred was employed to identify and count the groups for the GC methods and then the properties were calculated in Microsoft Excel using the appropriate contributions and summation methods. This approach for dealing with very

large molecules may introduce an error in the GC method but this is believed to be negligible compared to the accuracy of the method for very large molecules. An additional approximation was made for one molecule in fraction 10 which contained a metalloporphyrin group. Since no group contribution was available for this part of the molecule, this group was excised and not considered in calculations of the properties of the molecule.

### 5.2.2. Critical Properties

Critical pressure, temperature, and volume were calculated by the Marrero-Gani and Joback-Reid GC methods. Only critical temperature and critical compressibility factor were calculated with the Wilson-Jasperson GC method. The results are discussed and compared in the following sections.

#### 5.2.2.1. Marrero-Gani GC Method

The critical properties estimated for representational molecules for VTB are summarized in Table 5-4. The calculated critical properties can be conveniently compared by plotting them as a function of molecular weight.

Figure 5-4 shows the expected relatively smooth trend of increasing critical temperature with increasing molecular weight. An outlier with a molecular weight of 474.89 g/mole and critical temperature of 1161K corresponds to a cycloparaffin with paraffinic substituents and no heteroatoms. It is generally expected that molecules containing heteroatoms (e.g., sulphur) and aromatic substituents should have higher critical temperatures than simple hydrocarbon of the same molecular weight. The particularly long hydrocarbon backbone of this paraffinic molecule may account for its higher critical temperature compared to other members of this fraction. The highest molecular weight molecules comprising Fraction 10 have considerably higher critical temperatures than all other molecules representing the model VTB. The molecules comprising Fraction 10 might be considered outliers even though they appear to follow the trend with increasing molecular weight because of the large gaps in molecular weights and critical temperatures between Fraction 1 through 9 and Fraction 10. However, Fraction 10 represents a much larger portion of the crude than any other fraction and, therefore, the average molecular weight might be expected to be distinctly

greater than that for the other nine fractions. Another factor to consider is the role that associative behaviour may play in the measurement of molecular weight. Nevertheless, despite this break in the trend for molecular weight between Fraction 1 and Fraction 10, the wide range of molecular weights which makes this fluid highly asymmetric.

The expected trend of decreasing critical pressure with increasing molecular weight is shown in Figure 5-5. The outliers identified in the plot of critical temperature are also outliers in the plot of critical pressure. The asymptotic approach of the GC method to the limiting critical pressure of 5.99 bar is evident in this plot. As noted in an earlier section, the limiting value of 5.99 bar inherent in the Marrero-Gani correlation is significantly higher than the value of 2.68 bar predicted on theoretical grounds for large n-paraffins by Tsonopoulos and Tan.

The critical volume increases linearly with increasing molecular weight and appears to be remarkably independent of molecular structure. Note once again the paraffinic molecule with molecular weight of 474.89 g/mole and those comprising Fraction 10 are outliers with respect to all other molecules.

The critical compressibility factors were calculated for all of the representational molecules and are plotted against molecular weight in Figure 5-7. The graph shows that  $Z_c$  increases with molecular weight. In contrast, for simple hydrocarbons (n-paraffins, aromatics and sulphur containing compounds) with molecular weights less than 500 g/mole,  $Z_c$  roughly decreases with increasing molecular weight (Appendix 4). It can be seen that most of the molecules have  $Z_c$  clustering around an average value of 0.27 which is within the range of 0.24 to 0.29 for  $Z_c$  exhibited by most hydrocarbons. It has been noted by Poling *et al.* that on theoretical grounds  $Z_c$  should be less than 0.291 for molecules with critical temperatures greater than 100K (e.g., heavier than hydrogen and helium). More than half of the molecules representing VTB have values of  $Z_c$  less than 0.291 consistent with this hypothesis. Above a molecular weight of about 1200 g/mole,  $Z_c$  exceeds the 0.291 limiting value. The group of molecules constituting Fraction 10 show very large values of  $Z_c$  around 0.6, double the value expected for typical hydrocarbons. The values of  $Z_c$  for the molecules in fraction 10 indicate that they belong to a different class than all other molecules representing VTB and make the system asymmetric. If, as noted above, the high molecular weight of Fraction 10 was due to

associative behaviour, then the molecular mass and molecular structure might be at least twice as large as it is in reality. With a molecular weight of  $\sim 2,000$  g/mole instead of  $\sim 4,000$  g/mole, due to a smaller critical volume, the critical compressibility factor would most likely be about 0.35 which would be much closer to the range of 0.24 to 0.29 typical of hydrocarbons.

Up to 88 wt.% of fraction 10 is composed of species classified as asphaltenes. As mentioned in a previous section, asphaltenes are now believed to consist of aggregates of three to six molecules of molecular weight of about 750 g/mole (e.g., Mullins *et al.*<sup>95, 98</sup> and Yarranton *et al.*). However, this molecular weight is still controversial as recent measurements by Qian *et al.* indicate an average molecular weight of 1238 g/mole. Therefore, the current model of VTB treats the asphaltenes as an associated system and the critical properties given in Table 5-4 are really pseudo-critical properties. With this approach asphaltenes only interact with the rest of the mixture as an associated lump. Alternatively, if molecular weights in this range (750 to 1238 g/mole) are accepted for asphaltenes then the representational model VTB would exhibit the discontinuous molecular weight and critical properties as shown above. Here asphaltenes interact with each other and the rest of the system as individual molecules. The challenge with this latter approach is that the CEOS would have to account for the associative behaviour of asphaltenes. The inclusion of associative behaviour in CEOS is very challenging even for relatively simple systems unless major assumptions are made as noted previously.

Table 5-5 summarizes the calculated molar average properties for the model VTB with composition given in Table 5-2. Critical properties for the SCE fractions are those given in Table 5-4. The critical properties for the narrow cut heavy vacuum gas oil were calculated using the correlations of Riazi and Daubert with the mass average boiling point and specific gravity as inputs (see Appendix 3). Compared to mass average properties, molar average properties tend to emphasize those of the molecules or fractions having the lowest molecular weight. The mass average boiling point calculated from high temperature simulated distillation data was 916.2K. Here the non-eluting fraction accounting for 23.7 wt.% of VTB was assigned a boiling of 1023K. The true mass averaged boiling point will be significantly higher. Nevertheless, as expected, this

under-estimated mass average boiling point is higher than the molar average value of 862.7K.

**Table 5-4 Results for GC method estimation of critical properties (Marrero-Gani) and acentric factors from Constantinou-Gani-O'Connell (CGO) and Ambrose and Walton (AW) for VTB representational molecules.**

ID <sup>a</sup>	MW (g/mole)	T <sub>b</sub> (K)	T <sub>c</sub> (K)	P <sub>c</sub> (bar)	V <sub>c</sub> (m <sup>3</sup> /kmole)	Acentric factor	
						MG <sup>b</sup>	AW
F1M1	474.89	924.50	1161.81	7.15	3.7380	0.4380	0.4315
F1M2	597.06	778.43	988.52	9.30	2.0497	0.5570	0.5511
F1M3	480.85	725.33	923.92	9.95	1.7608	0.5830	0.5767
F1M4	554.89	794.59	1027.58	9.93	1.8177	0.4690	0.4639
F1M5	770.18	880.58	1126.47	8.05	2.6372	0.3980	0.3929
F1M6	749.27	850.01	1080.43	8.31	2.6373	0.4670	0.4610
F2M1	687.20	824.24	1047.33	8.32	2.5033	0.4700	0.4643
F2M2	1082.76	907.77	1157.58	7.32	3.6844	0.3510	0.3461
F2M3	719.28	816.08	1031.75	8.14	2.5657	0.4910	0.4856
F2M4	512.83	775.16	1009.22	9.97	1.7569	0.4260	0.4215
F2M5	985.81	874.82	1083.84	7.13	3.6637	0.5500	0.5435
F2M6	1294.31	944.13	1162.82	6.81	4.6516	0.5630	0.5557
F3M1	629.08	751.74	1018.19	8.85	2.2302	0.1390	0.1374
F3M2	720.17	852.59	1075.96	8.89	2.4056	0.5740	0.5669
F3M3	985.81	874.70	1083.32	7.12	3.6741	0.5520	0.5452
F3M4	692.22	820.17	1023.90	8.39	2.4921	0.6190	0.6123
F3M5	1075.81	931.54	1168.01	7.27	3.7318	0.4690	0.4618
F3M6	561.04	752.19	956.65	9.11	2.0508	0.5300	0.5242
F4M1	878.43	897.03	1169.70	8.23	2.9178	0.2910	0.2876
F4M2	925.55	862.19	1116.71	7.64	3.1851	0.2820	0.2784
F4M3	701.22	826.93	1047.94	8.15	2.5776	0.4740	0.4688
F4M4	641.09	798.35	1025.14	9.23	2.1868	0.4680	0.4632
F4M5	891.51	851.71	1113.66	7.67	3.0265	0.2300	0.2270
F4M6	703.18	825.79	1050.41	8.39	2.5264	0.4680	0.4627
F5M1	800.31	872.54	1086.91	8.13	2.7628	0.6130	0.6056
F5M2	799.39	839.80	1040.29	7.81	2.8116	0.6290	0.6220
F5M3	1171.98	921.30	1164.00	6.97	4.1595	0.3780	0.3731
F5M4	951.58	903.74	1131.51	7.41	3.2997	0.4950	0.4883
F5M5	1161.88	955.90	1187.11	7.21	3.8307	0.5390	0.5326
F5M6	1021.72	914.00	1139.80	7.24	3.5471	0.5080	0.5016
F6M1	762.25	864.00	1080.08	8.41	2.5946	0.6100	0.6025
F6M2	979.64	910.17	1127.28	7.41	3.4064	0.5870	0.5788
F6M3	1061.73	924.50	1161.81	7.15	3.7380	0.4380	0.4315
F6M4	1298.15	972.74	1213.47	6.80	4.5769	0.4540	0.4478
F6M5	1217.96	917.04	1204.15	7.15	3.9738	0.1630	0.1607
F6M6	1285.09	981.95	1217.89	6.89	4.4526	0.5130	0.5054

F7M1	1347.23	962.35	1209.19	6.87	4.5808	0.4080	0.4014
F7M2	1213.95	912.05	1196.04	7.10	4.0556	0.1660	0.1629
F7M3	1151.86	950.24	1193.17	6.96	4.0648	0.4220	0.4166
F7M4	1178.93	954.01	1180.11	7.00	4.0794	0.5490	0.5413
F7M5	1298.11	974.14	1201.58	6.94	4.3880	0.5660	0.5588
F7M6	1477.41	1006.05	1241.60	6.71	4.9624	0.5330	0.5250
F8M1	1242.00	895.26	1209.97	7.03	4.1331	0.0220	0.0214
F8M2	1014.72	906.80	1122.77	7.30	3.5589	0.5760	0.5688
F8M3	1499.44	990.41	1246.67	6.66	5.1649	0.7300	0.3645
F8M4	1255.07	971.12	1202.62	7.01	4.2022	0.5400	0.5329
F8M5	1051.68	911.36	1164.28	7.30	3.6292	0.3370	0.3322
F8M6	1358.18	992.33	1228.18	6.73	4.8088	0.5100	0.5032
F9M1	1620.57	1030.50	1283.20	6.59	5.4285	0.4430	0.4364
F9M2	1172.94	952.50	1181.05	7.09	3.9781	0.5380	0.5317
F9M3	1150.85	958.93	1194.27	7.25	3.8096	0.5200	0.5134
F9M4	1066.78	924.87	1142.86	7.23	3.6748	0.5860	0.5782
F9M5	1475.31	997.98	1252.67	6.79	4.9158	0.4050	0.3998
F9M6	1280.98	975.44	1238.11	7.06	4.2536	0.3560	0.3508
F10M1	3348.24	1201.42	1494.29	6.20	10.9657		0.3958
F10M2	4131.46	1253.38	1554.36	6.15	13.1739		0.4116
F10M3	4172.54	1245.75	1549.17	6.11	14.0187		0.3846
F10M4	4137.63	1255.44	1545.39	6.13	12.9287		0.4688
F10M5	4119.39	1250.86	1548.82	6.13	13.4936		0.4205
F10M6	4033.32	1243.62	1542.03	6.13	13.2667		0.4097

- F<sub>xx</sub> refers to supercritical fraction xx and M<sub>x</sub> refers to molecule number.*
- Acentric factor calculated in ProPred using Marrero-Gani critical properties*
- Acentric factor calculated by correlation of Ambrose and Walton using Marrero-Gani critical properties.*

**Table 5-5 Calculated molar average properties for model VTB.**

<b>Property</b>	<b>Molar average value</b>
<b>MW (g/mole)</b>	888.9
<b>T<sub>b</sub> (K)</b>	864.0
<b>T<sub>c</sub> (K)</b>	1078.1
<b>P<sub>c</sub> (kPa)</b>	1066.3
<b>V<sub>c</sub> (m<sup>3</sup>/kmole)</b>	3.3031

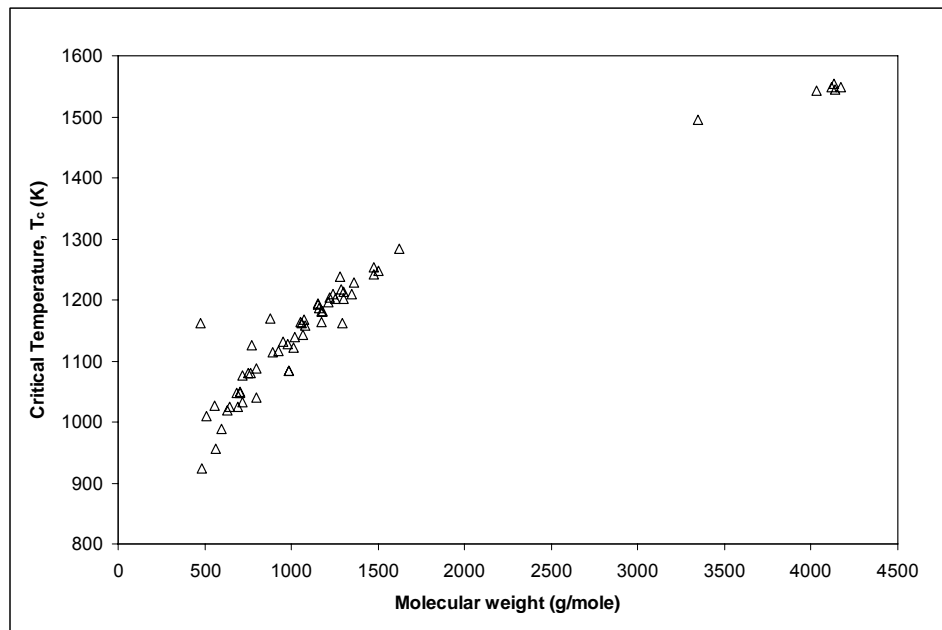


Figure 5-4 Critical temperature estimated by the Marrero-Gani GC method versus molecular weight of the representational molecules for VTB.

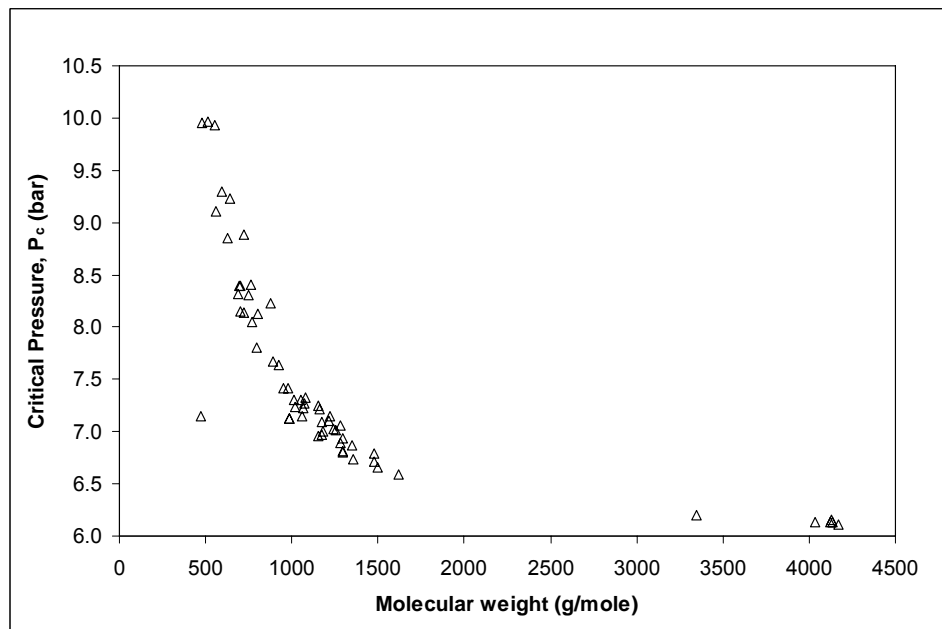


Figure 5-5 Critical pressure estimated by the Marrero-Gani GC method versus molecular weight of the representational molecules for VTB.



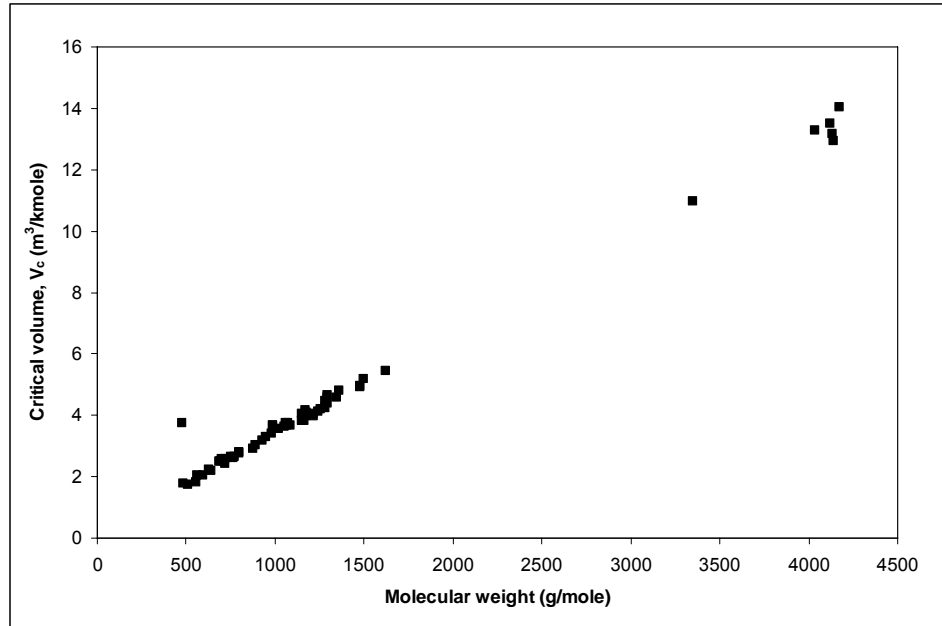


Figure 5-6 Critical volume estimated by the Marrero-Gani GC method versus molecular weight of the representational molecules for VTB.

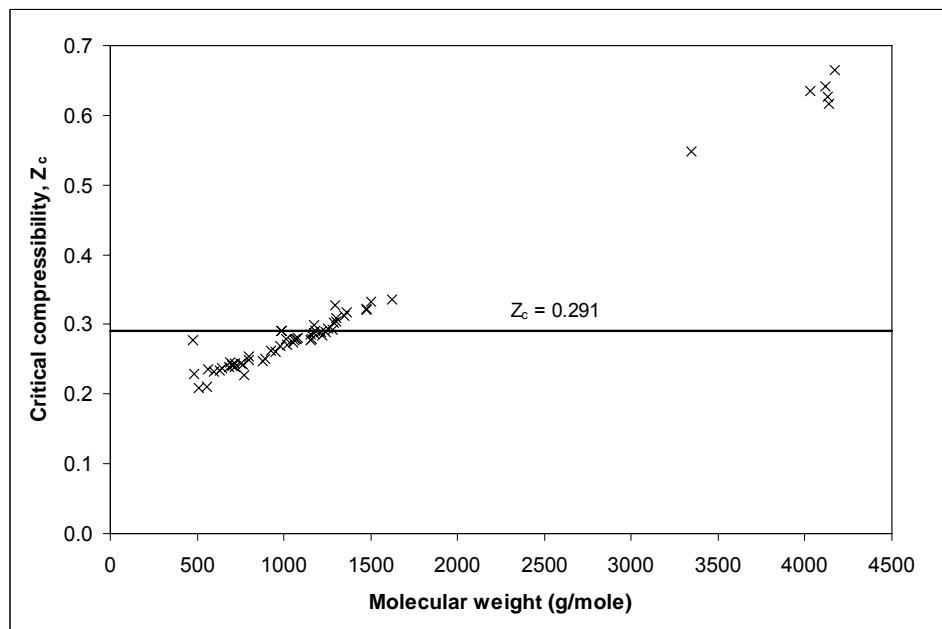


Figure 5-7 Critical compressibility factor, calculated from critical properties estimated by the Marrero-Gani GC method, versus molecular weight of the representational molecules for VTB.

#### 5.2.2.2. Comparison with Joback and Reid

The GC method of Joback and Reid led to very different predictions of critical temperatures (Figure 5-8) and pressures (Figure 5-9) compared to the method of Marrero and Gani. In contrast to the GC method of Marrero and Gani, the method of Joback and Reid does not yield critical temperatures which exhibit a smooth trend with increasing molecular weight. In some cases, the method leads to negative values for critical temperature contrary to the expectations for real fluids. It should be noted that the Joback and Reid GC method for critical temperature relies on the normal boiling point which is also estimated by the method. In contrast to critical temperatures, critical pressures from the Joback-Reid GC method exhibit only positive values and smoothly decreasing values with increasing molecular weight. Critical pressure predictions by the Joback-Reid method are consistently lower than those from the Marrero-Gani method. In the case of critical volume, the Joback-Reid and Marrero-Gani GC methods appear to give similar results (Figure 5-10)

It is likely that the data set used to develop this GC method consisted of low molecular weight compound, i.e., with low, measurable critical temperatures. Joback and Reid acknowledge that their GC method was developed from regression of critical data tabulated by Ambrose and Walton but no range was specified for critical properties or molecular weight in this data set. An examination of the data set of Ambrose and Walton shows that for n-alkane it extends to n-eicosane ( $T_c$  768K,  $P_c$  not specified) and for aromatics to p-terphenyl ( $T_c$  926K and  $P_c$  3320 kPa). The weakness of the Joback-Reid GC method become evident when the critical compressibility factor is calculated and plotted against molecular weight as shown in Figure 5-11. The Joback-Reid method led to values of  $Z_c$  which were less than 0.1 and therefore below the limiting value of 0.291 suggested by Poling *et al.*. The trend of decreasing  $Z_c$  with increasing molecular is reasonable but the values are low. The negative values of  $Z_c$  are due to the negative values of critical temperature predicted by this GC method. The values of  $Z_c$  very close to zero as well as negative values of  $Z_c$  indicate that the Joback-Reid GC method is not suitable for predicting the critical properties of heavy hydrocarbon whose boiling points are unknown.

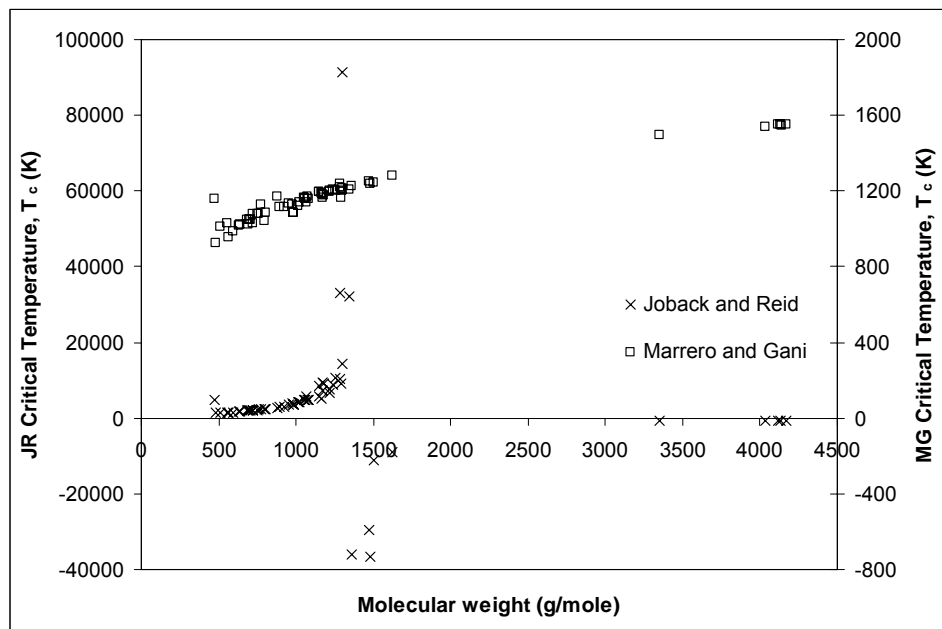


Figure 5-8 Comparison of critical temperatures estimated by the Joback-Reid and Marrero-Gani GC methods versus molecular weight of the representational molecules for VTB.

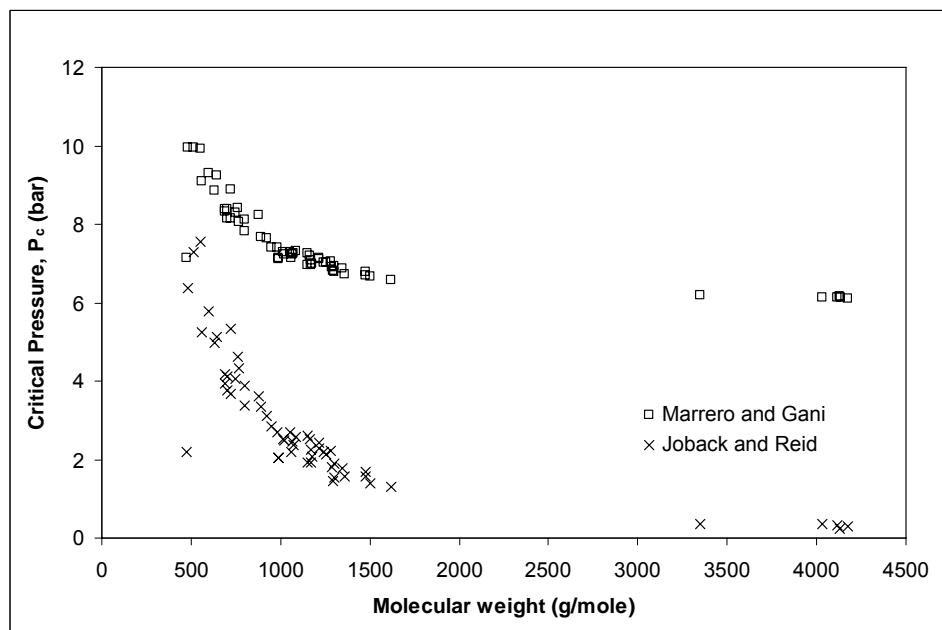


Figure 5-9 Comparison of critical pressures estimated by the Joback-Reid and Marrero-Gani GC methods versus molecular weight of the representational molecules for VTB.

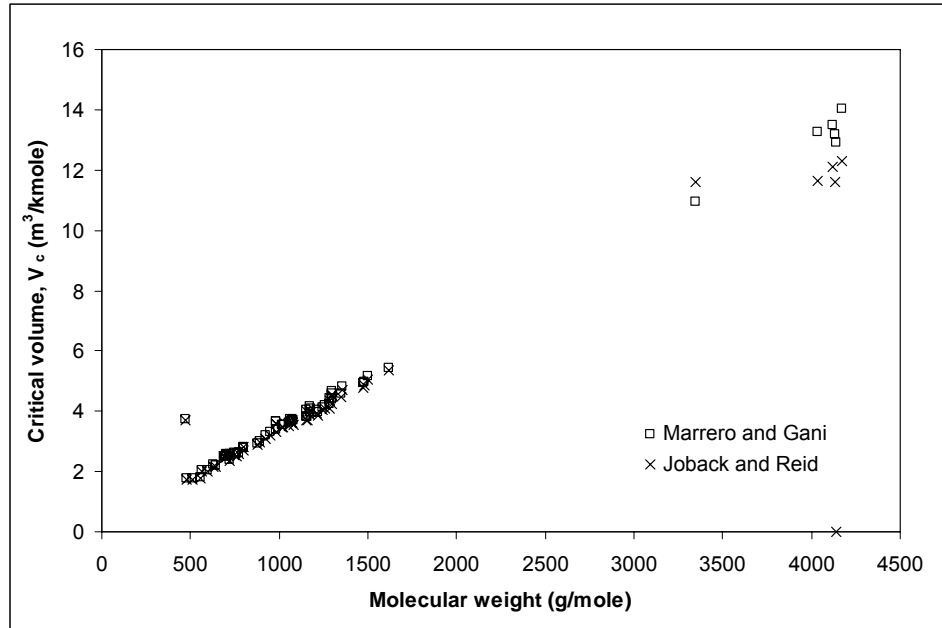


Figure 5-10 Comparison of critical volumes estimated by the Joback-Reid and Marrero-Gani GC methods versus molecular weight of the representational molecules for VTB.

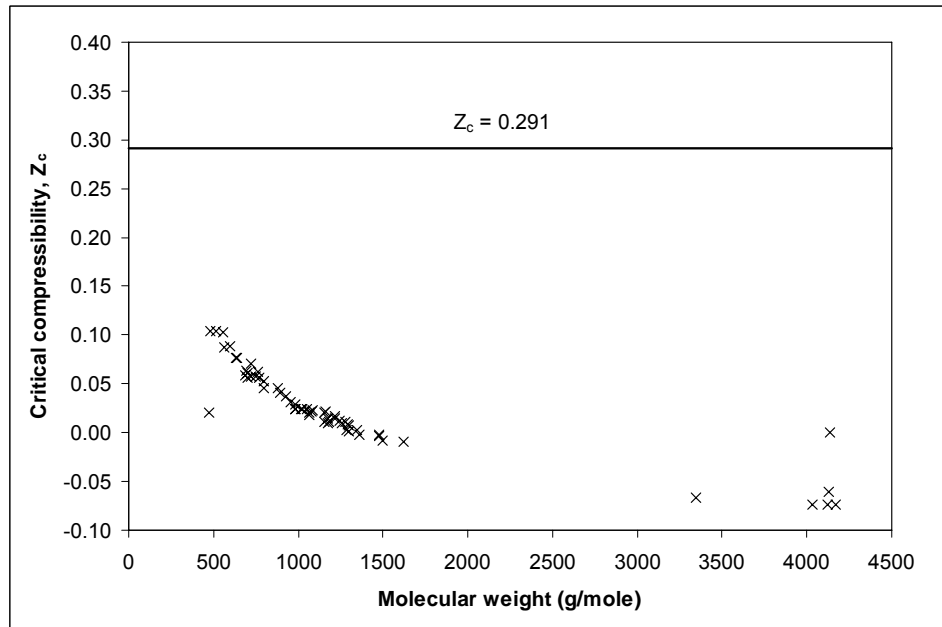


Figure 5-11 Critical compressibility factor, calculated critical properties estimated by the Joback-Reid GC method, versus molecular weight of the representational molecules for VTB.

### 5.2.2.3. Comparison with Wilson-Jasperson

The Wilson-Jasperson GC method predicts only critical temperature and compressibility factor directly if the boiling point is known or can be estimated by some other method (Marrero-Gani GC method in this case). Estimations of critical pressure and volume rely on the estimated critical temperature and are not presented. The predictions from the Wilson-Jasperson method are compared with those from the Marrero-Gani GC method in Figure 5-12 and Figure 5-13. The critical temperatures predicted by the Wilson-Jasperson GC method are significantly lower than those from the Marrero-Gani method (Figure 5-12). Unlike the the Joback-Reid GC method, critical temperatures estimated by the Wilson-Jasperson method showed only positive in values.

The critical compressibility factors for the molecules representing fractions 1 through 9 all lie between 0.1 and 0.2 and, therefore, satisfy the criteria of being less than 0.291 as hypothesized by Poling *et al.*. While values for  $Z_c$  from the Wilson-Jasperson method, like that from Joback-Reid, exhibit the expected trend of decreasing  $Z_c$  with increasing molecular weight, the values for  $Z_c$  predicted by the Wilson-Jasperson method are larger and always positive. Critical compressibility factors could not be obtained for fraction 10.

Although the Wilson-Jasperson GC method yields critical temperatures and compressibility factors which appear reasonable, it has several deficiencies compared to the Marrero-Gani GC methods. Estimation of critical temperature by the Wilson-Jasperson GC method requires that either the true boiling be known, which is not possible for heavy hydrocarbons, or that the boiling point be estimated by some other method. Another shortcoming of the Wilson-Jasperson method is that estimation of critical pressure and volume relies on the estimated critical temperature so any error in its estimation is compounded for critical pressure and volume. Additionally, the Wilson-Jasperson method is not sophisticated enough to distinguish isomers. Given the challenge in estimation of boiling point for large hydrocarbons and also that their larger size and complexity requires that the interconnectedness of groups be accounted for, the Wilson-Jasperson GC method is not recommended for large hydrocarbons with molecular weight higher than 500 g/mole or whose true boiling points are unknown.

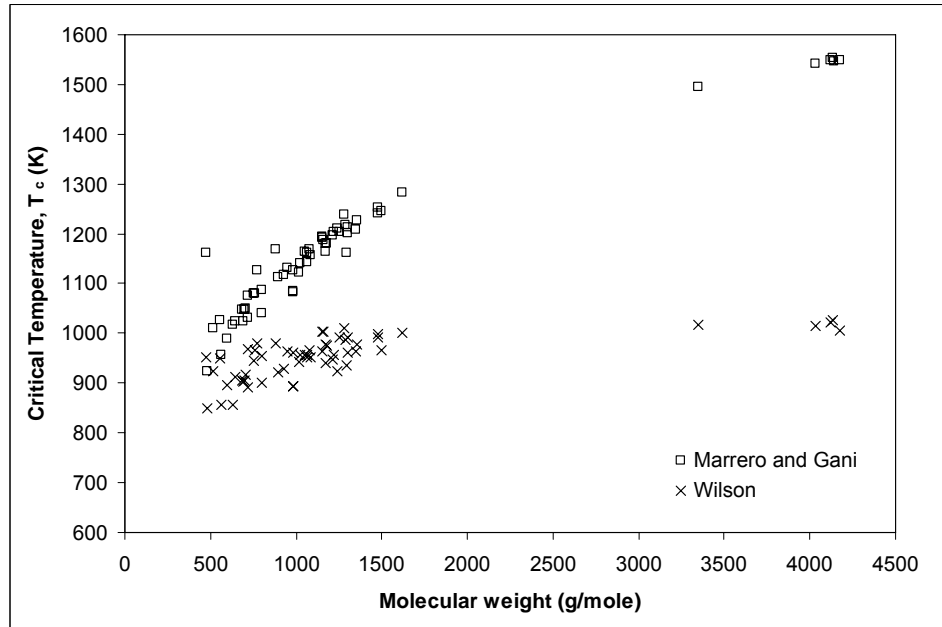


Figure 5-12 Comparison of critical temperatures estimated by the Wilson-Jasperson and Marrero-Gani GC methods versus molecular weight of the representational molecules for VTB.

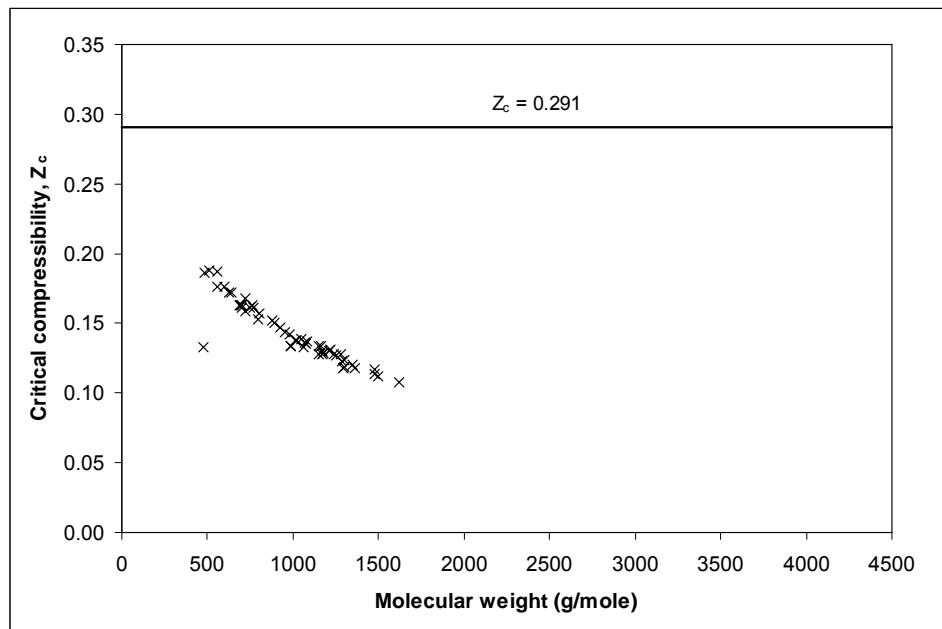


Figure 5-13 Critical compressibility factor, calculated critical properties estimated by the Wilson-Jasperson GC method, versus molecular weight of the representational molecules for VTB.

### 5.2.3. Boiling Point

#### 5.2.3.1. Marrero-Gani and Joback-Reid GC Methods

Both the Marrero-Gani and Joback-Reid GC methods can be used to predict the boiling points of the representational molecules. The results of these predictions are shown in Figure 5-14. Both sets of predictions exhibit a smooth trend of increasing boiling point with increasing molecular weight. The Joback-Reid GC method, however, predicts normal boiling points that are substantially higher than one would expect given the molecular weights and evidence from the high temperature simulated distillation presented in a previous section. Based on predictions for critical temperatures, it was concluded that the Joback-Reid GC method was not suitable for these molecules and the present predictions for normal boiling point also support the same conclusion with respect to prediction of boiling points.

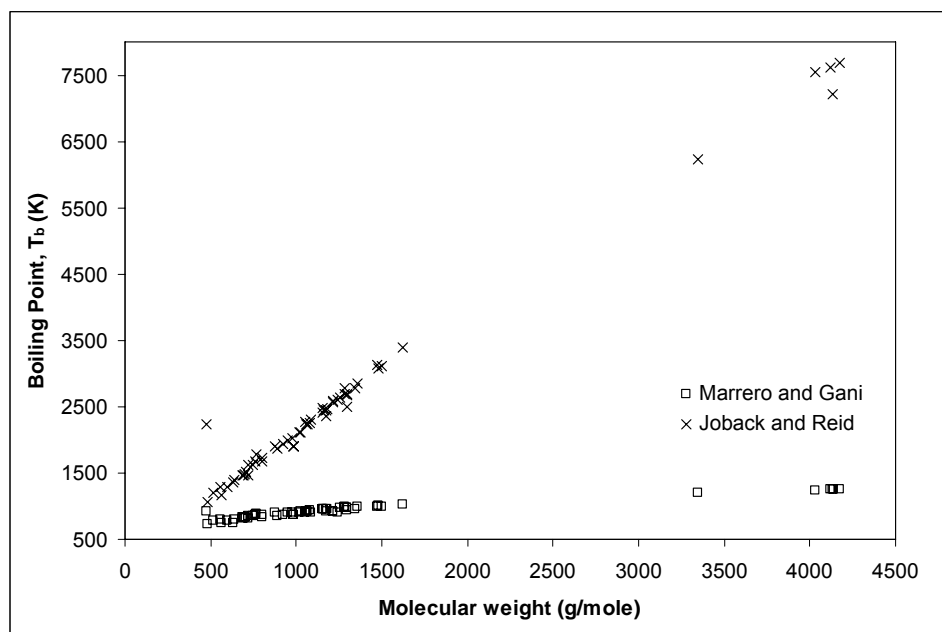


Figure 5-14 Comparison of normal boiling points estimated by the Joback-Reid and Marrero-Gani GC methods versus molecular weight of the representational molecules for VTB.

### 5.2.3.2. Predicted and Measured Distillation Curves

Given the apparently reasonable predictions for normal boiling points for the molecular representations for VTB, it is useful to compare the predicted distillation curve for the model VTB and the measured high temperature simulated distillation (HTSD) curve. For this comparison, the optimized composition of the model VTB given in Table 5-2 along with the high temperature simulated distillation curve for the narrow cut heavy vacuum gas oil and the estimated boiling points of the sixty molecular representations comprising fraction 1 through 10 are used. The result is shown in Figure 5-15. The model appears to be shifted to lower boiling point by about 60°C, however, considering the limitations of HTSD this is a fairly good match.

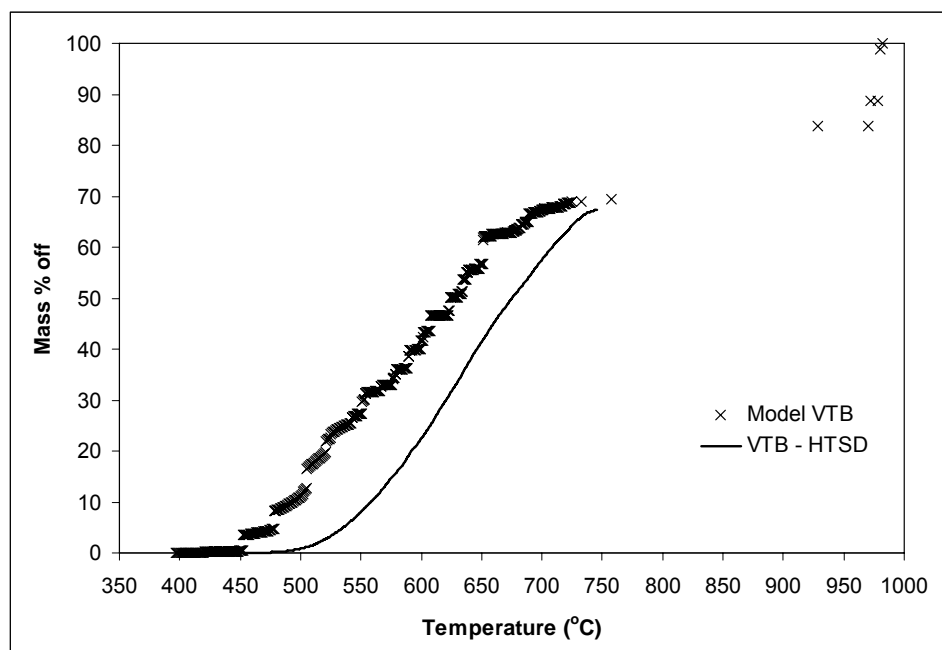


Figure 5-15 Comparison of measured high temperature simulated distillation curve for VTB and that calculated from the model comprised of molecular representations and a narrow boiling range heavy vacuum gas oil.

### 5.2.4. Acentric Factor

Acentric factors were calculated by the GC method of Marrero and Gani using ProPred and the correlation of Ambrose and Walton from critical properties and boiling points. The results of these calculations for all representational molecules are tabulated



in Table 5-4 and compared in Figure 5-16. Both methods yield very similar values for the acentric factors. ProPred could not be used to calculate acentric factors for Fraction 10 because of reasons discussed above.

In general, the calculated acentric factors are relatively small compared to values expected for high molecular weight hydrocarbon. For example, the acentric factors for n-decane and n-eicosane are 0.490 and 0.865, respectively. Figure 5-17 shows a plot of acentric factor versus molecular weight for aromatics taken from HYSYS 3.2 database. It can be seen that acentric factor increases with molecular weight and is as high as 1.0299 for n-hexadecylbenzene. It would be expected, therefore, that for molecules with significantly higher molecular weights, such as those for VTB representation, the acentric factors should be considerably higher than 1. Instead the acentric factors calculated for the molecular representations of VTB range from 0.022 to 0.730 for representations with molecular weights ranging from 474.9 to 4172.6 g/mole (Table 5-4). Nevertheless, the acentric factors for the simple aromatics presented in Figure 5-17 and VTB molecular representations in Table 5-4 are both consistent with predictions from the correlation of Ambrose and Walton. The low acentric factors calculated for the molecular representations of VTB can, therefore, be considered reasonable and consistent with the predicted critical properties and normal boiling point for these molecules. The applicability of the correlation of Ambrose and Walton to such large molecules as those for VTB is not absolutely certain.

As noted above, based on theoretical considerations, all molecules with critical temperatures ( $T_c$ ) greater than 100K should have critical compressibility factors ( $Z_c$ ) less than 0.291. Poling *et al.* have suggested a means of checking the consistency of critical properties by use of the following equation:

$$Z_c = 0.291 - 0.080\omega \quad (5.1)$$

Since  $Z_c$  must always be positive, this implies a maximum value of 3.6375 for the acentric factor. When equation (5.1) was applied by Poling *et al.* to a database of 145 compounds with  $T_c$  greater than 100K and dipole moment less than 1.0 Debye, the average absolute error was 2% and only nine compounds had an error larger than 5%.

Figure 5-18 shows a plot of  $Z_c$  from equation (5.1) versus  $Z_c$  from the critical properties determined by the Marrero-Gani GC method. The acentric factors for the highly asphaltenic fraction 10 are clear outliers as were its critical properties relative to those of all other fractions. If fraction 10 was excluded from the analysis, the average absolute error in  $Z_c$  from equation (5.1) was 11.8% and the maximum error was 32.7%. Although these errors are larger than those reported by Poling *et al.*, they indicate that there is some consistency between critical properties and acentric factor. This is expected since, as noted above, the calculated acentric factors were consistent with the correlation of Ambrose and Walton which is based on critical properties and boiling points. In considering the larger error it should also be noted that the dipole moments are not known, therefore equation (5.1) may not be applicable to all of the representational molecules.

#### 5.2.5. Density of Model VTB

As discussed in an earlier section, many correlations for critical properties are based on normal boiling point and specific gravity. Although it is an objective of this work to employ critical properties derived from molecular representation, it is nevertheless of interest to determine how well densities and boiling points might be predicted for these representational molecules. The predictions of normal boiling points were discussed above. As discussed in a previous section, Gray has proposed a correlation for density, equation (2.71), based on elemental composition. This correlation has been applied to calculate the densities of all the components of the model VTB which include the narrow cut heavy vacuum gas oil and sixty representational molecules.

The results for the representational molecules are tabulated in Appendix 4. Table 5-6 shows estimated densities for the ten SCE fractions assuming ideal mixing of the six molecules in each fraction and all sixty molecules plus HVGO for the model VTB. There was a close correspondence between the measured densities and those calculated using the correlation developed by Gray. These results along with those for boiling points indicate that the representational model VTB is a reasonable one.

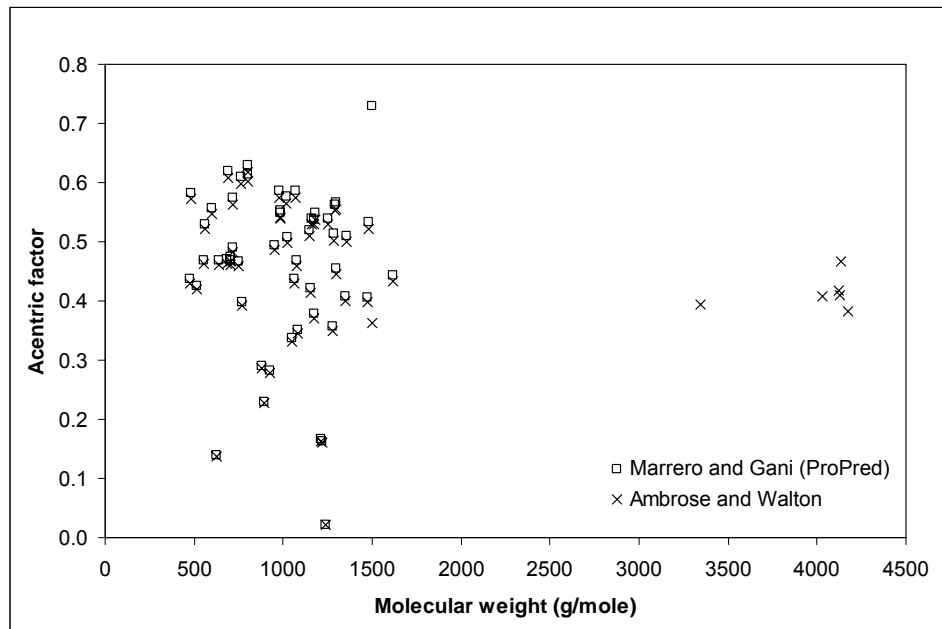


Figure 5-16 Comparison of acentric factors estimated by the Constantinou-Gani- O'Connell and the GC method and Ambrose-Walton correlation versus molecular weight of the representational molecules for VTB.

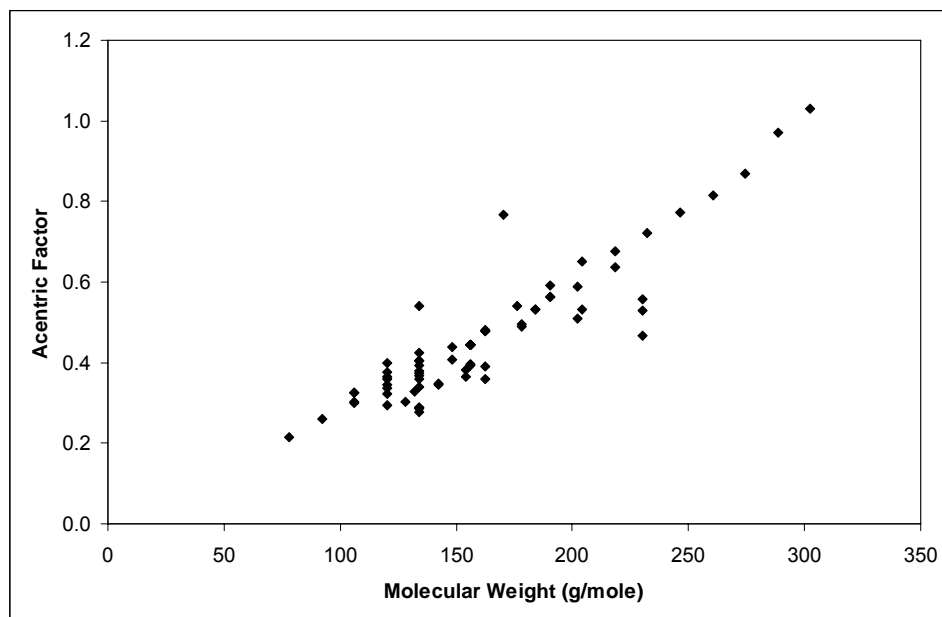


Figure 5-17 Acentric factor vs. molecular weight for simple aromatics from the HYSYS 3.2 database.

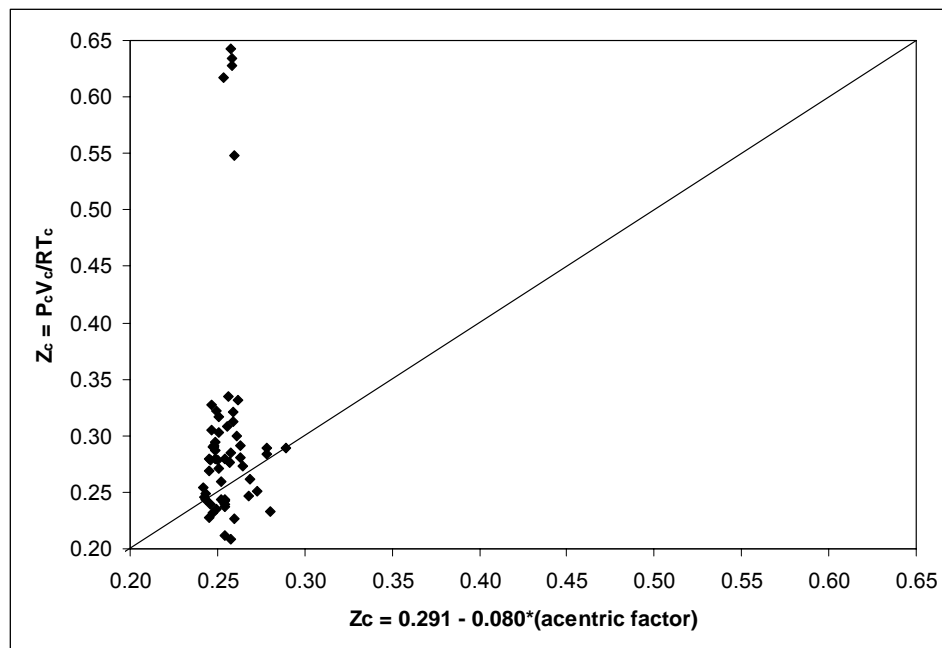


Figure 5-18 Plot of critical compressibility factor calculated from acentric factor versus that calculated from critical properties estimated from the Marrero-Gani GC method.

Table 5-6 Comparison of estimated density of model VTB fractions with measured values for SCE fractions and heavy vacuum gas oil (HVGO).

Component	Density (g/mL)		ARE <sup>3</sup>
	Calculated <sup>1</sup>	Measured <sup>2</sup>	
HVGO	1.0316	1.0204	1.1%
SCE Fraction #1	0.9558	0.9745	1.9%
SCE Fraction #2	0.9808	0.9930	1.2%
SCE Fraction #3	0.9887	1.0061	1.7%
SCE Fraction #4	1.0189	1.0228	0.4%
SCE Fraction #5	1.0423	1.0427	0.0%
SCE Fraction #6	1.0452	1.0543	0.9%
SCE Fraction #7	1.0700	1.0646	0.5%
SCE Fraction #8	1.0718	1.0678	0.4%
SCE Fraction #9	1.0814	1.0736	0.7%
SCE Fraction #10	1.1537	-	-
VTB	1.0462	1.0868	3.7%

Notes:

1. Calculated from densities of the six representational molecules in each fraction and summed assuming ideal mixing. Density of HVGO is from bulk elemental composition.
2. Measured for each SCE fraction and HVGO.
3. Absolute relative error.

### 5.3. SUMMARY

The molecular representations developed by Sheremata for VTB were combined with various group contribution methods (Marrero and Gani; Joback and Reid; Wilson-Jasperson) to predict critical properties, acentric factor, and normal boiling point. The sixty molecular representations developed by Sheremata included molecules with molecular weights as high as 4,173 g/ mole. Six of the representations had molecular weights over 3,000 g/mole and twenty-one representations had molecular weights over 1,200 g/mole. These molecular weights are significantly higher than values of 750 g/mole predicted for unassociated asphaltenes by Mullins and co-workers. The six molecular representations with molecular weights over 3,000 g/mole may, therefore, represent associated molecules. Utilization of such pseudo-critical properties for associated molecules effectively introduces association into the CEOS since the Peng-Robinson CEOS cannot by itself account for such behaviour.

The Marrero-Gani GC methods led to the most consistent and reasonable molecular properties for VTB components. In contrast, the Joback-Reid GC method could lead to physically unrealistic critical properties such as negative critical temperatures. Critical compressibility factors calculated from the critical properties derived from the Marrero-Gani GC method were within the range ( $Z_c \sim 0.29$ ) expected for heavy hydrocarbons. In contrast, the Joback-Reid derived critical properties led to critical compressibility which were close to zero or negative. Wilson-Jasperson's GC method was not practical for heavy hydrocarbons such as VTB because it required that the boiling point be known and any error in this estimate was propagated to all critical properties. Although the Marrero-Gani GC method was superior to the other two methods evaluated, for critical pressure it shows an asymptotic approach to a limiting value of 599 kPa. Theoretical considerations of n-paraffins indicate that the limiting critical pressure should be around 268 kPa. Nevertheless, based on this work, the Marrero-Gani group contribution method is recommended for heavy hydrocarbons.

Boiling points predicted by the Marrero-Gani GC method showed remarkable consistency with high temperature simulated distillation data for VTB. The distillation curve synthesized from boiling points predicted by the Marrero-Gani GC method was shifted to a lower temperature by about 60°C. On the other hand, boiling points

predicted by the Joback and Reid GC method could be several hundred to two thousand degrees higher than the values from simulated distillation.

Based on the reasonable properties predicted by the Marrero-Gani GC method, a model of VTB was developed which was suitable for phase equilibrium calculations with the Peng-Robinson cubic equation of state. The model was created by matching the high temperature simulated distillation curve for VTB used in the present work to that for the specific Athabasca vacuum residue, for which the molecular representations of Sheremata was developed, by including a heavy vacuum gas oil. Due to the synthesis of a final model for VTB based on simulated distillation data for the heavy vacuum gas oil and molecular representations of the heavier fraction, the model was not consistent but it represented the best compromise between accuracy in defining VTB composition and having a model based solely on molecular representations.

---

## 6.0 PARTIAL MOLAR VOLUMES AT INFINITE DILUTION

---

### 6.1. PARTIAL MOLAR VOLUME OF BINARY MIXTURES

Partial molar volume is one of several partial derivatives of an extensive thermodynamic property with respect to composition:

$$\bar{V}_i = \left( \frac{\partial V}{\partial n_i} \right)_{T, P, n_{j \neq i}} \quad (6.1)$$

where:

$\bar{V}_i$  - partial molar volume with respect to  $i^{\text{th}}$  component

$V$  - volume of the system, an extensive thermodynamic property

The partial molar volume ( $\bar{V}_i$ ) of the  $i^{\text{th}}$  component is the contribution from the addition of  $n_i$  moles of the  $i^{\text{th}}$  component to the system volume at constant temperature and pressure. Partial molar volumes are not equivalent to molar volumes except for ideal solutions and the change in partial molar volumes with respect to temperature, pressure, and composition reflects the thermodynamic behaviour of the system. The partial molar volume at infinite dilution of the  $i^{\text{th}}$  component,  $\bar{V}_i^\infty$ , reflects the effect of the first infinitesimal amount of solute addition. As discussed by Maham *et al.*,  $\bar{V}_i^\infty$  is sensitive to molecular interactions in a mixture and is useful for investigating and validating models for the thermodynamic behaviour of solutions. For example, the pressure dependence of Henry's constant can be determined from the integral of  $\bar{V}_i^\infty dP$ .

Specific partial volume was determined determined from the slope of the density of a VTB-solvent solution versus mass fraction of VTB as the concentration of VTB approaches zero:

$$\bar{V}_{VTB}^\infty = \frac{MW_{VTB}}{\rho_{solvent}} - \frac{MW_{VTB}}{\rho_{solvent}^2} \left( \frac{\partial \rho_{solution}}{\partial x_{VTB}} \right) \quad (6.2)$$

where:

$x_{VTB}$  - mass fraction of VTB.

Since the true molecular weight of the heavy oil was unknown, specific partial volumes (mL/g) of components were determined by Maham and co-workers rather than partial molar volume (mL/mole):

$$v_{VTB}^{-\infty} = \frac{\bar{V}_{VTB}^{-\infty}}{MW_{VTB}} = \frac{1}{\rho_{solvent}} - \frac{1}{\rho_{solvent}^2} \left( \frac{\partial \rho_{solution}}{\partial x_{VTB}} \right) \quad (6.3)$$

Specific partial volumes at infinite dilution ( $\bar{v}_i^{-\infty}$ ) for VTB in toluene, 1-methylnaphthalene, quinoline and a 50/50 (m/m) mixture of toluene and dodecane were determined by Maham *et al.* at 25, 40, 60, and 80°C at atmospheric pressure. The solutions used for these measurements were prepared at room temperature and then equilibrated at the measurement temperature. Goodkey<sup>133</sup> have subsequently shown that the thermal history of these solutions may have an impact on the specific partial volumes determined. They determined the excess volumes of mixing for VTB/n-decane mixtures as a function of VTB concentration and temperature. The excess volumes were found to be negative for solutions prepared at room temperature and then heated to measurement temperatures up to 80°C. However, if the solutions were first annealed at 160°C for 1 hour and then cooled to the measurement temperature the excess volume was positive. Goodkey concluded that VTB/n-decane mixtures exhibited irreversible mixing behaviour and that excess volume of mixing tended towards zero as temperature was increased whether the sample was annealed or not.

For simplicity of data analysis, only the three systems with pure solvents were considered. Additionally, the data for the system of toluene and VTB was not considered because it did not exhibit a smooth change of  $\bar{v}_i^{-\infty}$  with increasing temperature as did the systems with 1-methylnaphthalene and quinoline. The data for the two selected systems were regressed to determine critical properties of the solute, VTB, using the Peng-



Robinson CEOS and the proposed mixing rules. The objective was to determine if any of the mixing rules exhibited an advantage over the others.

### 6.1.1. Generalized Partial Molar Volume at Infinite Dilution

The partial molar volume at infinite dilution for a two-component system can be derived directly from the Peng-Robinson CEOS but the form of the equation will depend on the particular mixing rules used. Since several different mixing rules were being investigated, it was most convenient to develop a generalized form of the expression for  $\bar{V}_1^\infty$  which can readily be modified for the mixing rules being considered. Such an expression is the following for a binary mixture of solute (1) and solvent (2):

$$\bar{V}_1^\infty = \frac{\frac{RT}{\underline{V}_2 - n_2 b_2} + \frac{n_2 RT}{(\underline{V}_2 - n_2 b_2)^2} \left( \frac{\partial n_1 b}{\partial n_1} \right) - \frac{\frac{\partial}{\partial n_1} (a n_1^2)}{\underline{V}_2^2 + 2b_2 n_2 \underline{V}_2 - n_2^2 b_2^2} + \frac{2a n_1^2}{(\underline{V}_2^2 + 2b_2 n_2 \underline{V}_2 - n_2^2 b_2^2)^2} + \left[ \underline{V}_2 \left( \frac{\partial n_1 b}{\partial n_1} \right) - n_2 b_2 \left( \frac{\partial n_1 b}{\partial n_1} \right) \right]}{\left[ \frac{n_2 RT}{(\underline{V}_2 - n_2 b_2)^2} - \frac{2a n_2^2 (\underline{V}_2 + n_2 b_2)}{(\underline{V}_2^2 + 2b_2 n_2 \underline{V}_2 - n_2^2 b_2^2)^2} \right]} \quad (6.4)$$

where:

$n_i$  - total moles of all components

$\underline{V}_2$  - extensive volume of system at infinite dilution of the solute component 1

All other terms in equation (6.4) have the same meaning as discussed in Chapter 2.

There can be a further simplification if the mixing rules are of the form:

$$\begin{aligned} a_{mix} &= \sum_i \sum_j x_i x_j a_{ij} \\ b_{mix} &= \sum_i \sum_j x_i x_j b_{ij} \end{aligned} \quad (6.5)$$

The simplified form of equation (6.4) resulting from the above form of the mixing rule is:

$$\bar{V}_1^\infty = \frac{\frac{RT}{V_2 - b_2} + \frac{RT(2b_{12} - b_2)}{(V_2 - b_2)^2} - \frac{2a_{21}}{V_2^2 + 2b_2V_2 - b_2^2} + \frac{2a_2[V_2(2b_{12} - b_2) - b_2(2b_{12} - b_2)]}{(V_2^2 + 2b_2V_2 - b_2^2)^2}}{\left[ \frac{RT}{(V_2 - b_2)^2} - \frac{2a_2(V_2 + b_2)}{(V_2^2 + 2b_2V_2 - b_2^2)^2} \right]} \quad (6.6)$$

Note that equation (6.6) does not depend on the molar volume of the solute, only that of the solvent,  $V_2$ . The derivations for the above relationships for  $\bar{V}_1^\infty$  are given in Appendix 5. For the single mixing rules, the cross-term  $b_{12}$  is easily determined from the relationships given in equations (2.57), (2.58), (2.59), and (2.60). In the case of the composite mixing rules, the cross term  $b_{12}$  included a contribution from the vdW mixing rule combined with the contribution from the second mixing rule:

$$b_{12} = m_{12}b_{12,MR1} + (1 - m_{12})b_{12,MR2} \quad (6.7)$$

Here, MR1 and MR2 are the van der Waals and second mixing rules, respectively, and  $m_{12}$  is the binary mixing parameter previously discussed. The form of the binary mixing parameter used was that given by equation (2.93).

### 6.1.2. Calculation Methodology

The experimental data for specific partial volume at infinite dilution  $\bar{v}_i^\infty$  of VTB were used to estimate critical properties for VTB using a non-linear least squares regression. Critical properties and molecular weight were constrained, as discussed in an earlier section, by use of correlations of either Twu or Riazi and Daubert which are based on specific gravity and normal boiling point. The acentric factor was based on the estimated critical properties and normal boiling point using the correlation of Ambrose and Walton. The calculation methodology is summarized in Figure 6-1. The mixing rules for the co-volume term which were investigated included those discussed previously:

(a) van der Waals, (b) Lorentz, (c) geometric mean, and (d) Lee and Sandler. In addition to these co-volume mixing rules, the proposed composite mixing rules, which are a combination of the van der Waals mixing rule and contributions from one of the other three mixing rules, were also investigated.

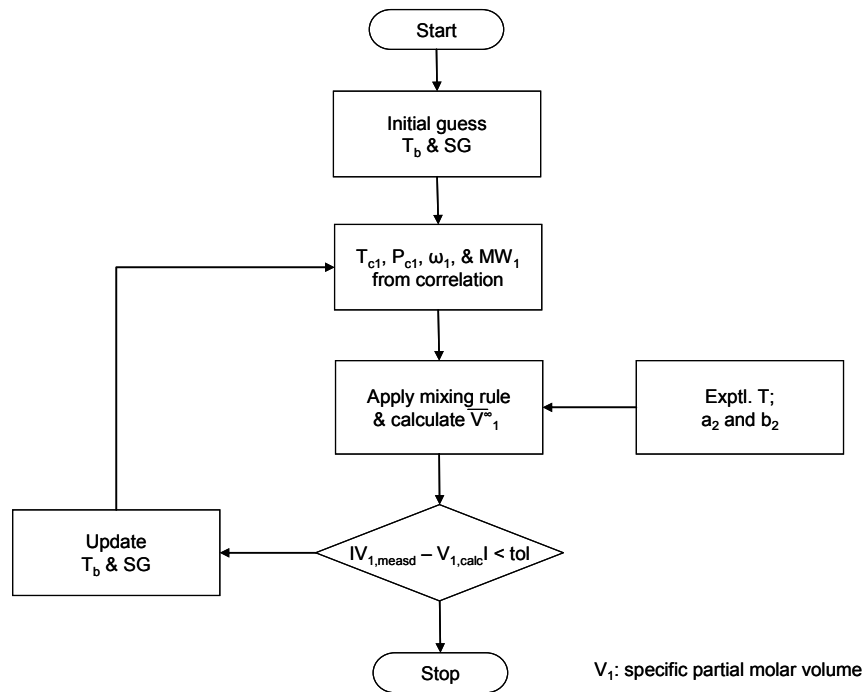


Figure 6-1 Flowchart for determining critical properties from regression of specific partial molar volume data.

## 6.2. RESULTS

The data for  $\bar{v}_i^\infty$  of VTB in 1-methylnaphthalene and quinoline were regressed together rather than separately. Data for  $\bar{v}_i^\infty$  of VTB in toluene were not used because they did not exhibit a smooth trend with increasing temperature and it could not be ascertained whether this was due to experimental accuracy of changes in phase behaviour (e.g., association) of the fluid mixture. Correlations used in regression of the

data required two adjustable parameters to predict four molecular properties ( $T_c$ ,  $P_c$ ,  $\omega$ , and MW) in order to calculate the specific partial volume at infinite dilution. Since only four data points were available for each solvent, a separate regression of data for each solvent may offer data that is too sparse for reliable interpretation. It is useful for the discussion which follows to tabulate the measured and estimated properties of VTB discussed in earlier sections. These properties and their values are tabulated in Table 6-1.

**Table 6-1 Summary of VTB properties derived from various sources**

Source Property	Measured	Regressed Vap. Press.	Regressed PVT data	Molar avg. GC method
$T_c$ (K)		-	1010.47	1078.1
$P_c$ (kPa)		-	2197.6	1066.3
MW (g/mole)	1048 <sup>a</sup>	-	289.75	888.9
$T_b$ (K)	916.2 <sup>b</sup>	738/754	761.29	864.0

*a. Vapour pressure osmometry*

*b. Mass average from HTSD data. The fraction boiling above 750°C was assigned a single boiling point of 750°C. This value represents a lower minimum average boiling point.*

#### 6.2.1. *Two Constrained Critical Properties*

The correlations based on normal boiling point and specific gravity developed by Twu were discussed earlier. These correlations provide an internally consistent basis for estimating critical properties of hydrocarbons by using n-paraffins as a reference. Molecular weight can also be estimated from these correlations. Twu's correlations were used to constrain the critical properties and molecular weight. Acentric factors were estimated from the regressed normal boiling point and Twu critical properties using the correlation developed by Ambrose and Walton.

The results from non-linear regression of all  $\bar{v}_i^\infty$  data for 1-methylnaphthalene and quinoline are summarized in Table 6-2. Figure 6-2 shows an example of the correspondence between the determined specific partial volumes and those predicted by the model using the composite vdW/Lee and Sandler mixing rule. With a single mixing rule for co-volume, the total absolute relative error was between 3.6 and 5.9% indicating good agreement with measured data. None of the single mixing rules give molecular weights close to the measured values. Both the van der Waals and Lee and Sandler mixing rules led to reasonable values for boiling points and are close to the lower limiting value determined from simulated distillation data and also to the molar average

boiling point determined from the Marrero-Gani GC method. The van der Waals and Lee and Sandler mixing rules also led to reasonable values for critical pressure. However, of these two mixing rules, only the Lee and Sandler mixing rule yielded a reasonable value for specific gravity. The Lorentz and geometric mean mixing rules led to anomalously low values for critical temperature, average molecular weight and boiling point, and correspondingly large values for critical pressure.

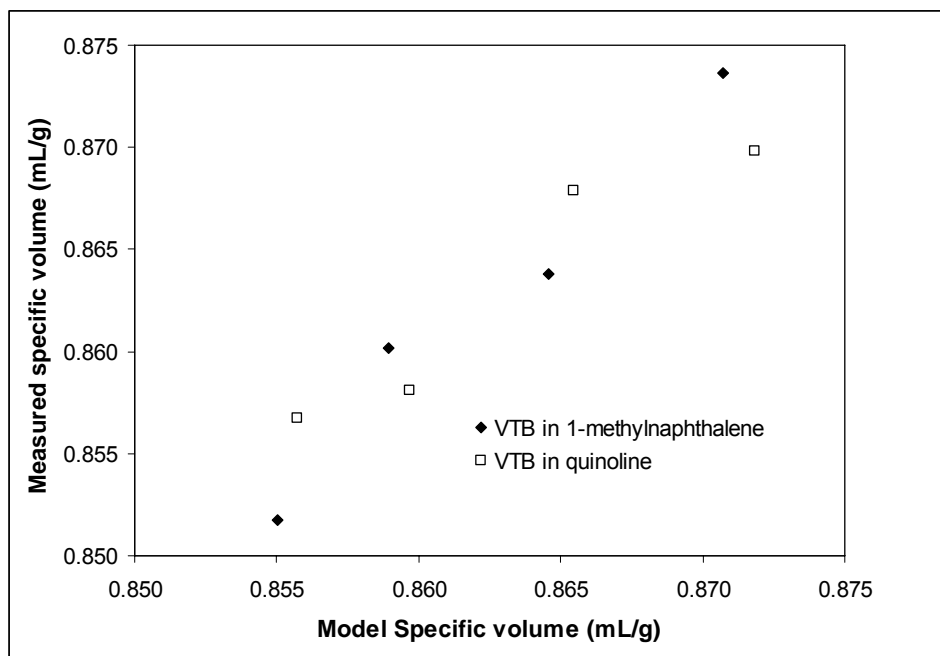


Figure 6-2 Comparison between the measured specific partial volume of VTB and that predicted by the model using the composite van der Waals and Lee and Sandler mixing rule.

The application of the composite mixing rules led to improved agreement with the measured data as indicated by lower values for total absolute relative error compared to that with the single mixing rule. All of the composite mixing rules gave similar results for all properties. While the values for critical temperature, molecular weight, and boiling point might be considered reasonable, the regressed values for critical pressure were too high and the specific gravity too low for heavy hydrocarbons. Note that despite the unreasonableness of the acentric factor, the model does fit the data quite well as shown, for example, in Figure 6-2.

Table 6-2 Regressed properties for VTB from measured specific partial volume at infinite dilution in 1-methylnaphthalene and quinoline. Critical properties are constrained by Twu's correlations.

Property	Single Mixing Rule				Composite Mixing Rule: vdW +		
	vdW	Lorentz	Geom. Mean	Lee & Sandler	Lorentz	Geom. Mean	Lee & Sandler
T <sub>c</sub> (K)	1121.1	681.0	701.7	1156.3	1281.2	1281.2	1281.1
P <sub>c</sub> (kPa)	1441.1	5294.0	4872.2	1417.8	5058.3	5005.3	5106.4
Acentric Factor	2.0077	1.3593	1.3727	1.2460	2.1514	2.1492	2.1534
MW (g/mole)	581.0	95.9	107.3	571.3	555.8	557.6	554.3
T <sub>b</sub> (K)	956.0	516.4	535.5	943.4	1032.6	1033.0	1032.3
Specific Gravity	0.6809	0.5941	0.6045	1.1669	0.6641	0.6642	0.6640
TARE*	5.9%	4.1%	3.6%	4.8%	1.8%	1.8%	1.8%

$$*TARE - Total\ absolute\ relative\ error\ \sum_i \left( \left| \frac{v_{calc,i}^{\infty} - v_{meas,i}^{\infty}}{v_{meas,i}^{\infty}} \right| \right)$$

### 6.2.2. Riazi-Daubert Constrained Critical Properties

Compared to the inter-dependent and internally consistent correlations developed by Twu for critical properties, those developed by Riazi and Daubert are completely independent of each other. The correlations of Riazi and Daubert were used to constrain the critical properties and molecular weight. Acentric factors were estimated from the regressed normal boiling point and Riazi-Daubert critical properties using the correlation developed by Ambrose and Walton.

The results from non-linear regression of all  $v_i^{\infty}$  data for VTB in 1-methylnaphthalene and quinoline are summarized in Table 6-3. When a single mixing rule for co-volume was employed, the van der Waals mixing rule for co-volume led to reasonable values for all properties with the exception of the acentric factor, which was much higher than known values for high molecular weight hydrocarbons. In comparison, the Lorentz and geometric mean mixing rules yield unreasonably low values for critical temperature, molecular weight, and boiling point. The mixing rule of Lee and Sandler provide more reasonable results than those from Lorentz and geometric mean mixing rules; however, critical temperature and molecular weight might be considered too low.

All three composite mixing rules led to reasonable, consistent and similar values for critical temperature, boiling points and molecular weight, which are comparable to

values summarized in Table 6-1. The critical pressure of about 3230 kPa was much higher than values predicted from the regression of PVT or molar averaging of values obtained from the Marrero-Gani GC method. The values obtained for critical pressure are high in comparison to the high molecular weights predicted. The predicted acentric factors are considered to be extremely large and without precedent. According to a relationship proposed by Poling *et al.* (see equation (5.1)), the maximum value for the acentric factor is 3.6375 for molecules with limiting value of 0.291 for critical compressibility.

**Table 6-3 Regressed properties for VTB from measured specific partial volume at infinite dilution in 1-methylnaphthalene and quinoline. Critical properties are constrained by Riazi and Daubert's correlations.**

Property	Single Mixing Rule				Composite Mixing Rule: vdW +		
	vdW	Lorentz	Geom. Mean	Lee & Sandler	Lorentz	Geom. Mean	Lee & Sandler
T <sub>c</sub> (K)	1049.2	811.6	777.4	938.8	1186.0	1185.6	1186.4
P <sub>c</sub> (kPa)	835.9	2465.8	2976.4	1295.4	3234.4	3237.3	3231.6
Acentric Factor	3.6665	0.9428	0.8084	1.7644	7.9590	7.9350	7.9830
MW (g/mole)	932.2	251.6	205.0	514.6	1245.6	1242.7	1248.6
T <sub>b</sub> (K)	962.3	619.1	575.2	795.9	1099.8	1099.1	1100.4
Specific Gravity	0.9993	0.9767	0.9858	0.9749	1.2022	1.2022	1.2022
TARE	5.0%	2.0%	2.0%	3.1%	2.9%	2.9%	2.9%

### 6.3. SUMMARY

Specific partial volumes of VTB in 1-methylene and quinoline were regressed using different forms of the newly proposed co-volume mixing rules as well as the conventional van der Waals mixing rules. The regressions were constrained by the property correlation of Twu and Riazi and Daubert.

The four basic mixing rules led to widely different values for the molecular properties. Significant effort was devoted to determining whether this was due to various local minima dependent on the initial guesses for T<sub>b</sub> and SG used for the least squares non-linear optimization. In each case, it was found that initial guesses either led to these solutions or resulted in complex solutions. It is believed that these widely different results from the four basic mixing rules are a consequence of the nature of these mixing rules and their derivative properties as discussed in the following chapter.

Consistent with this conclusion, was the observation that, with the composite mixing rules, the solutions were identical from the different mixing rules. One possible reason for this similarity of results with the three composite mixing rules may be the dominant contribution of the van der Waals mixing rule to the overall composite mixing rule. The second mixing rule may simply represent a perturbation of the van der Waals mixing rule.

Compared to the van der Waals and the other basic mixing rules, the proposed composite mixing rule led to improved correspondence with the measured specific partial volumes for VTB. Although individual regressed critical properties, acentric factors, and molecular weights were in some cases reasonable for the heavy, asymmetric VTB mixture, no set of regressed properties were completely internally consistent and reasonable.

The major limitation in the analysis of this data is in considering VTB as a single component. Unfortunately, given the small size of the data set (eight points), the multi-component models for VTB previously described could not be used since the simplest of these models (see later chapter) includes ten components. Additionally, as discussed in a previous chapter, EOS such as Peng-Robinson characteristically lead to poor predictions of molar volumes and this also results apparently in unreasonable properties from regression of partial molar volume data.

It is concluded that, compared to the van der Waals mixing rule, the proposed composite mixing rules result in a better fit with experimental data and may be useful for asymmetric systems such as mixtures containing bitumen. It is also concluded that, as with regressions of vapour pressure data for VTB, the property correlations of Riazi - Daubert and Twu used for conventional, low boiling, and low molecular weight hydrocarbons are not suitable for a heavy asymmetric mixture of hydrocarbons.



---

## 7.0 PREDICTION OF BUBBLE POINT PRESSURE

---

### 7.1. BUBBLE POINT PRESSURE AND DENSITY

The proposed composite mixing rules for co-volume discussed in Chapter 2 were applied and evaluated in comparison to four simple mixing rules (van der Waals, Lorentz, geometric mean, and Lee-Sandler). The proposed composite co-volume mixing rules were applied to a binary asymmetric mixture of ethane and n-tetratetracontane and then to multi-component mixtures of VTB and VTB with n-decane.

#### 7.1.1. Phase Equilibrium Calculations

Calculations of vapour liquid equilibria (VLE) are mainstays of chemical engineering and plant design. Bubble points are a class of VLE calculations in which we are concerned with the temperature and pressure conditions of a liquid at which the first bubble of vapour is formed and also the composition of this vapour. There are two types of bubble point calculations depending on which variable is being sought, temperature or pressure, given the other as input. Dew point VLE calculations are the converse of bubble point calculation in that the temperature and pressure conditions of the vapour at which the first drop of liquid is formed and also the composition of this drop are sought. Just as for bubble point VLE calculations, there are two types of dew point calculations depending on whether temperature or pressure is to be determined. Isothermal flash calculation is yet another type of VLE calculation where the composition, temperature and pressure of a feed are known and we are interested in the composition of vapour and liquid, as well as the fraction of vapour (or liquid) at these conditions.

There are three conditions that all of the above VLE, and any other phase equilibrium calculations must satisfy for a system of  $n_c$  components:

(i) Material balance condition ( $n_c$  equation):

$$(1 - \xi)x_i + \xi y_i - z_i = 0 \quad (7.1)$$

(ii) Equilibrium condition ( $n_c$  equations):

$$\mu_i^L(T, P, \bar{x}) = \mu_i^V(T, P, \bar{y}) \quad (7.2)$$

(iii) Stability condition (1 equation):

$$\Delta G > 0 \quad (7.3)$$

where:

$\xi$  : the fraction (moles/moles) of feed in the vapour phase

$\bar{x}$  : vector of mole fractions in liquid

$\bar{y}$  : vector of mole fractions in vapour phase

Typically, the first two conditions are the only criteria employed for solving VLE and other phase equilibria problems. While the first two conditions are often sufficient to solve many problems, Baker *et al.*<sup>134</sup> have illustrated that there are instances where this approach can lead to incorrect predictions of phase behaviour. In such cases, the stability condition must also be applied. The stability condition requires that the Gibbs energy of the mixture must be the global minimum for the system at the given temperature and pressure.

The stability condition forms the basis of the so-called tangent plane criterion and is expressed mathematically as:

$$D_x(T, P, \bar{y}) = RT \sum_{i=1}^{n_c} y_i \ln \left[ f_i(T, P, \bar{y}) / f_i(T, P, \bar{x}) \right] \geq 0 \quad (7.4)$$

Implicit in equation (7.4) is that, for a given temperature and pressure, the system with liquid composition  $\bar{x}$  and vapour composition  $\bar{y}$  represents the unique system having the global minimum Gibbs energy. Note that this equation also explicitly implies that the fugacities, and therefore chemical potentials, of a species must have the identical value in the gas and liquid phases.

The tangent plane criterion is briefly described in Appendix 6. All equations related to the application of the tangent plane criterion are derived and presented in their generalized forms (i.e., they include generalized derivatives of the mixing rules) ready for application to any simple or composite mixing rule for co-volume. The relevant generalized equations include those for: (a) fugacity coefficient, (b) partial molar volume, and (c) Jacobian ( $J_p = dD_x/dP$ ) for solving for bubble point pressure using a so-called quasi-Newton successive substitution method of Nghiem and co-workers<sup>135</sup>.

The calculation methodology for bubble point pressure is summarized in Figure 7-1. This methodology follows that outlined previously by Nghiem and co-workers. The example data provided by Nghiem *et al.* were used to evaluate and verify the Matlab code used to calculate the bubble point pressure.

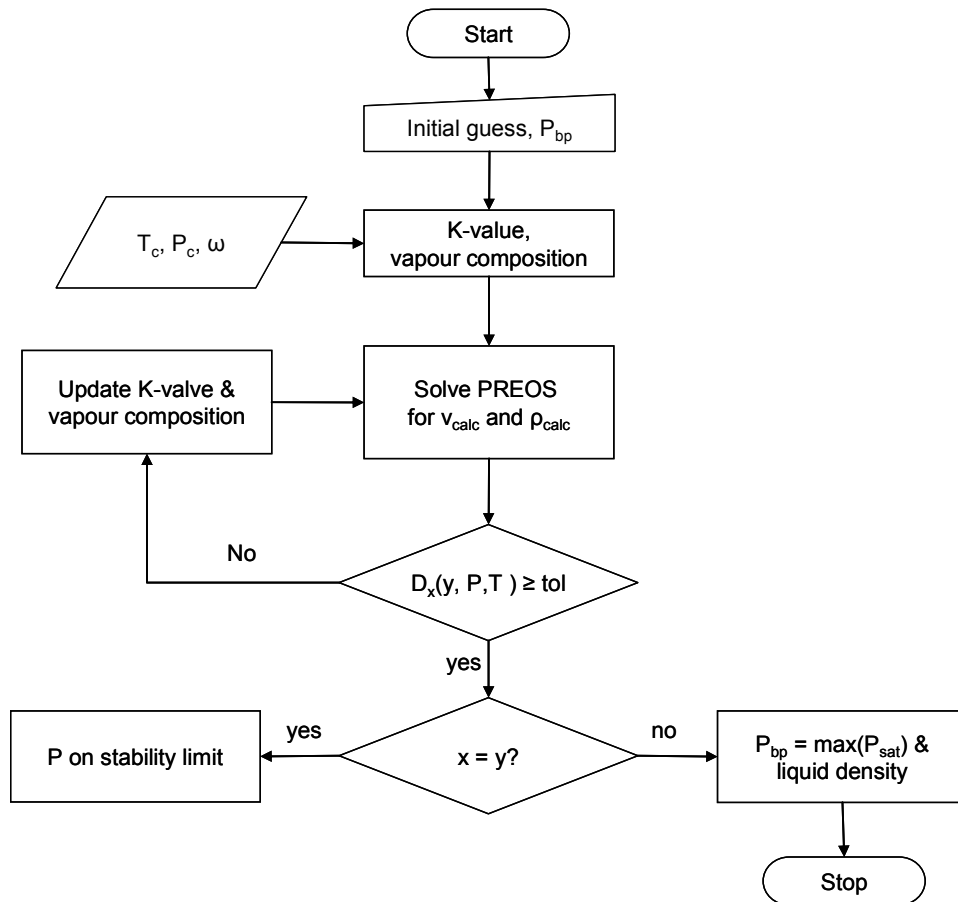


Figure 7-1 Calculation methodology for bubble point pressure.

As noted by Nghiem *et al.*, up to four solutions can be found for the bubble point pressure. Two of the four solutions are trivial in the sense that the composition in the gas phase is identical to that in the liquid phase. Such solutions lie on the stability limit. The other two solutions represent the higher and lower saturation pressure. The higher saturation pressure corresponds to the bubble point pressure. It should be further noted that the calculation procedures employed are only applicable for systems involving simple vapour-liquid phase behaviour. The method does not include any consideration for liquid-liquid phase splitting. The Matlab codes for the calculations are given in Appendix 7.

## 7.2. ETHANE/N-TETRATETRACONTANE ASYMMETRIC MIXTURE

The solubility of ethane in n-tetratetracontane was measured by Gasem and co-workers<sup>136</sup> at 100 and 150°C and pressures between 0.39 and 3.1 MPa. Unfortunately, the authors do not comment specifically on possible liquid-liquid-vapour phase behaviour at these conditions. Systems consisting of ethane and n-paraffins heavier than n-octadecane are known to exhibit liquid-liquid-vapour equilibrium at conditions close to the critical point of ethane (see for example Peters *et al.*<sup>137</sup>). Since the above measurements were made far away from the critical pressure of ethane (4.871 MPa and 305.3K), it was assumed that such liquid-liquid phase behaviour does not occur for the current system. Additionally, Shaw and Behar illustrate that, in case of binary mixtures of asymmetric n-paraffins, the LLV line will lie below the melting point of the solute, tetratetracontane (melting point 85.6°C) in this case.

Bubble point pressures were calculated using the Peng-Robinson CEOS with van der Waals mixing rules and alternate mixing rules for co-volume. In all cases, the binary interaction parameter,  $k_{ij}$ , was zero. As discussed in an earlier chapter, setting  $k_{ij} = 0$ , does not imply that the mixture is ideal and can sometimes lead to incorrect phase behaviour or non-convergence of CEOS calculation. The critical properties used for ethane and n-tetratetracontane were those given by Gasem *et al.*. Different proposed forms of the binary mixing parameter,  $m_{ij}$ , were evaluated and these are summarized in Table 7-1 along with the values for  $m_{ij}$  for a binary mixture of ethane and n-tetratetracontane. Binary mixing parameters of the Forms A, B, and C were presented earlier. Form D differs from Form A by the inclusion of a contribution from a  $2b_{ij}$  term

in the denominator. Binary mixing parameters of the form A, B, C, and D have a value of zero for molecules with identical co-volumes. In such instances the composite mixing rules reduce to the van der Waals mixing rules. A binary mixing parameter of the Form E is also introduced which has a value of one for molecules with identical co-volumes and, therefore, reduces to the non-vdW component of the composite mixing rule.

**Table 7-1 Forms of binary mixing parameters and values for a binary mixture of ethane and n-tetradecane.**

Binary mixing parameter	$m_{12} = m_{21}$	$m_{11} = m_{22}$
Form A: $m_{ij} = \frac{(b_i - b_j)^2}{(b_i^2 + b_j^2)}$	0.9590	0
Form B: $m_{ij} = 1 - \frac{2(b_i b_j)^{0.5}}{(b_i + b_j)}$	0.7194	0
Form C: $m_{ij} = \frac{abs(b_i - b_j)}{(b_i + b_j)}$	0.9598	0
Form D: $m_{ij} = \frac{(b_i - b_j)^2}{(b_i + b_j)^2}$	0.9213	0
Form E: $m_{ij} = 1 - \frac{(b_i - b_j)^2}{(b_i^2 + b_j^2)}$	0.0410	1

The results from application of the single mixing rules (van der Waals, Lorentz, geometric mean, and Lee and Sandler) as well as the composite mixing rules with the various binary mixing parameters are summarized in Table 7-2 and Table 7-3 for mixtures of at 100 and 150°C, respectively. The results of the calculations with the various mixing rules are compared in terms of the average absolute relative difference or error between the calculated values and those reported by Gasem *et al.*.

Figure 7-2 shows the reported bubble point pressure for the mixture of ethane and n-tetradecane at 100°C and predictions obtained with the van der Waals and Lee and Sandler co-volume mixing rules. The van der Waals mixing rule moderately over-predicts the bubble point pressure. On the other hand, the Lee and Sandler mixing rule severely under-predicts the bubble point pressure. The two other mixing rules yield bubble point pressures which are close to zero. When the vdW/Lee-Sandler composite

mixing rule was employed (Figure 7-3 and Table 7-2), with the binary mixing parameter of Form E, the predicted bubble point pressures were closer to the reported experimental values (AAE 13.4%) than those calculated with the van der Waals mixing rule (AAE 32.3%). The results were even better when the vdW/Lorentz composite mixing rule was used (AAE 4.6%). Similar conclusions were obtained from a consideration of measured and predicted bubble point pressures at 150°C (Table 7-3).

The results achieved with the composite mixing rules based on a binary mixing parameter of Form E were surprising. Given that this form of the binary mixing parameter results in applying non-vdW co-volume mixing to j-j pair-wise interactions but predominantly van der Waals mixing rule to i-j interactions it was expected that Form E would yield inferior performance in comparison to the Form A binary mixing parameter. This form of the binary mixing parameter also performed much better and consistently compared to any of the other proposed forms.

**Table 7-2 Average absolute error for prediction of bubble point pressure for ethane/n-tetratetracontane at 100°C by applying standard and proposed mixing rules.**

Type	vdW	Lorentz	Geom. mean	Lee-Sandler
	Average Absolute Relative Error			
Single	0.323	0.999	nc	0.944
Form of $m_{ij}$ :	Composite (vdW + 2 <sup>nd</sup> mixing rule)			
Form A	-	0.999	nc	0.937
Form B	-	0.991	nc	0.870
Form C	-	0.999	nc	0.937
Form D	-	0.999	nc	0.929
Form E	-	0.046	0.173	0.134

*nc – non-convergent result*

**Table 7-3 Average absolute error for prediction of bubble point pressure for ethane/n-tetratetracontane at 150°C by applying standard and proposed mixing rules.**

Type	vdW	Lorentz	Geom. mean	Lee-Sandler
	Average Absolute Relative Error			
Single	0.238	nc	nc	0.944
Form of $m_{ij}$ :	Composite (vdW + 2 <sup>nd</sup> mixing rule)			
Form A	-	nc	nc	0.936
Form B	-	nc	nc	0.868
Form C	-	nc	nc	0.936
Form D	-	nc	nc	0.928
Form E	-	0.083	0.196	0.076

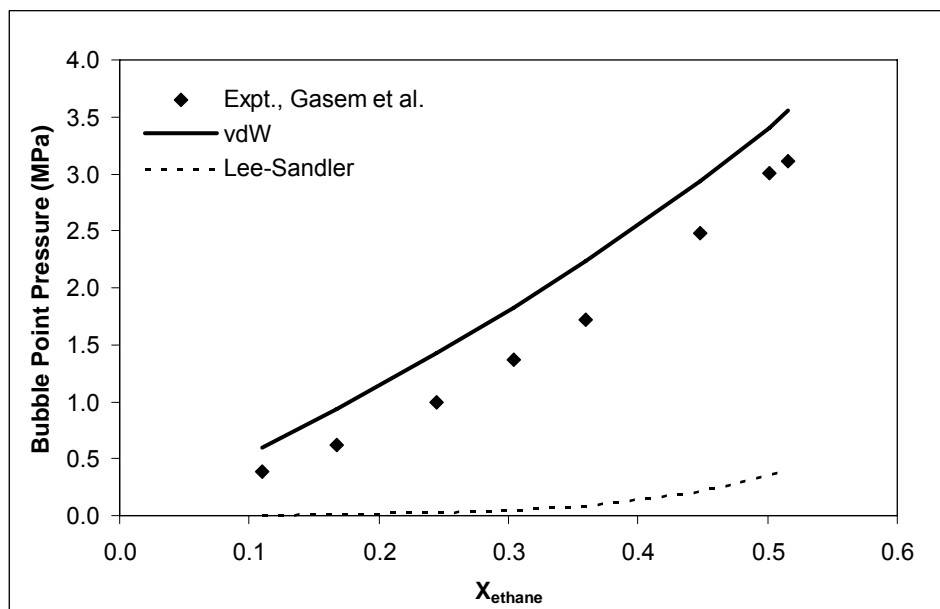


Figure 7-2 Comparison of bubble point pressure predictions and data of Gasem *et al.* with simple mixing rules for mixtures of ethane and n-tetratetracontane at 100°C.

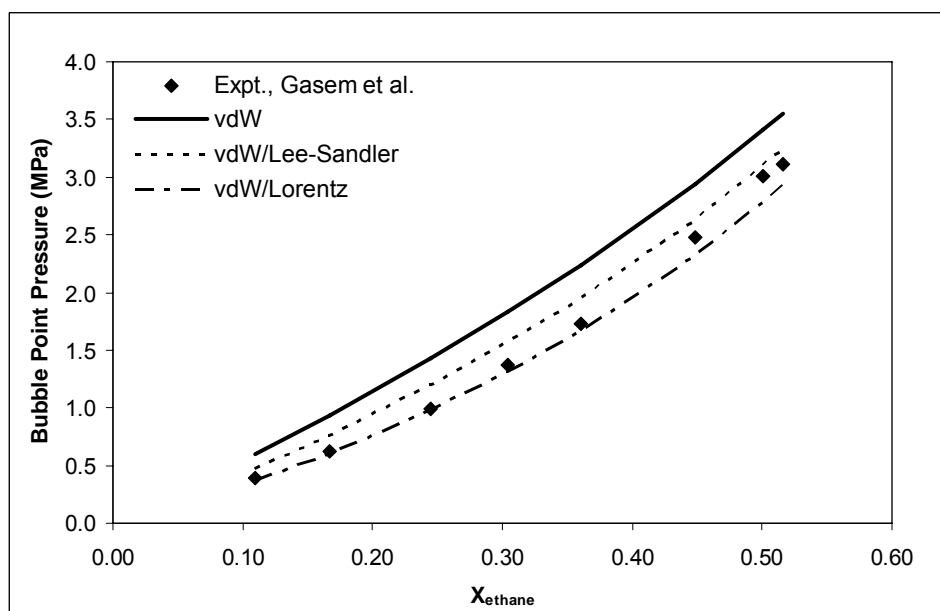


Figure 7-3 Comparison of bubble point pressure predictions and data of Gasem *et al.* with composite mixing rules for mixtures of ethane and n-tetratetracontane at 100°C.

Of the simple mixing rules for co-volume, the van der Waals (vdW) mixing rule yields the best correspondence with the data of Gasem and co-workers although the average absolute error of 32.3% and 23.8% in predictions of the bubble points of the mixture at 100°C and 150°C, respectively, might be considered high for some engineering applications. The other co-volume mixing rules (Lorentz, geometric mean, and Lee and Sandler) severely underestimate the bubble point pressure and yield unusable results. In some cases, these mixing rules do not lead to convergence and indicate a major shortcoming of the mixing rules. As mentioned above, the lack of convergence may also be partly due to setting the binary interaction parameter,  $k_{ij}$ , to zero. The Lee and Sandler mixing rule was the only alternative mixing rule which consistently converged to a real pressure.

When the binary mixing parameter of Form E was used, all of the composite mixing rules yield improvements in bubble point predictions compared to the van der Waals mixing rule. As noted earlier, the composite mixing rule composed of the Lorentz and van der Waals mixing rules surprisingly gave the best correspondence with the reported data of Gasem *et al.* With any other form of the binary mixing parameter, the correspondence with the data of Gasem *et al.* was either poor or no convergence was achieved for the calculation.

Insight into the performance of the mixing rules can be obtained by comparing the co-volumes predicted for the liquid phase. Table 7-4 summarizes the liquid phase co-volumes calculated using the van der Waals, Lee and Sandler, and composite van der Waals/Lee and Sandler mixing rules with a binary mixing parameter of Form E. The co-volumes calculated from the Lee and Sandler mixing rule were significantly lower than those from the van der Waals mixing rule. In contrast, mixture co-volumes calculated from the composite mixing rule were only slightly smaller than values calculated from the van der Waals mixing rule. It is tempting to ascribe the better performance of the composite mixing rule solely to the value of the calculated co-volumes. For a given mole fraction, a smaller co-volume leads to a lower bubble point pressure. However, generally, a lower co-volume should lead to higher bubble point pressure since smaller molecules have smaller co-volumes but higher vapour pressures. This dichotomy may



be resolved by consideration of the values of the derivatives of the co-volume mixing rules.

**Table 7-4 Co-volumes for the liquid phase ethane/n-tetratetracontane calculated using various mixing rules.**

$X_{\text{ethane}}$	Liquid co-volume (mL/g-mole)		
	vdW	Lee-Sandler	vdW/ Lee-Sandler*
0.110	1764.5	1719.5	1762.6
0.167	1654.0	1590.1	1651.4
0.245	1503.0	1417.9	1499.5
0.304	1388.7	1291.4	1384.7
0.360	1280.2	1174.3	1275.9
0.448	1109.8	996.1	1105.1
0.501	1007.1	892.2	1002.4
0.516	978.0	863.2	973.3

\* Binary mixing parameter of Form E.

Two derivatives of the co-volume mixing rule are required to solve for the bubble point pressure. The two derivatives are used in calculating the fugacity coefficient in each phase and the equality of these determines whether the two phases are in equilibrium:

$$\begin{aligned}
 \ln \varphi_i = & -\ln(1 - b\rho) - \ln Z + \frac{n}{1 - b\rho} \cdot \left( \frac{\partial b\rho}{\partial n_i} \right) \\
 & - \frac{an^2}{nbRT\sqrt{8}} \left[ \frac{(1 + \sqrt{2})}{1 + (1 + \sqrt{2})b\rho} - \frac{(1 - \sqrt{2})}{1 + (1 - \sqrt{2})b\rho} \right] \cdot \left( \frac{\partial b\rho}{\partial n_i} \right) \\
 & - \ln \left( \frac{1 + (1 + \sqrt{2})b\rho}{1 + (1 - \sqrt{2})b\rho} \right) \left[ \frac{1}{nbRT\sqrt{8}} \cdot \left( \frac{\partial an^2}{\partial n_i} \right) - \frac{an^2}{(nb)^2 RT\sqrt{8}} \cdot \left( \frac{\partial nb}{\partial n_i} \right) \right]
 \end{aligned} \tag{7.5}$$

One of the derivatives,  $\left(\frac{\partial nb}{\partial n_i}\right)$ , is also required to calculate partial molar volumes which are used to calculate the Jacobian used by the numerical method to solve for bubble point pressure (Equation (7.6)):

$$\bar{V}_i = \frac{\frac{RT}{\underline{V}_t - nb} + \frac{nRT}{(\underline{V}_t - nb)^2} \left(\frac{\partial nb}{\partial n_i}\right) - \frac{\frac{\partial}{\partial n_i}(an^2)}{\underline{V}_t^2 + 2bn\underline{V}_t - n^2b^2} + \frac{2an^2}{(\underline{V}_t^2 + 2bn\underline{V}_t - n^2b^2)^2} \left[ \underline{V}_t \left(\frac{\partial nb}{\partial n_i}\right) - nb \left(\frac{\partial nb}{\partial n_i}\right) \right]}{\left[ \frac{nRT}{(\underline{V}_t - nb)^2} - \frac{2an^2(\underline{V}_t + bn)}{(\underline{V}_t^2 + 2bn\underline{V}_t - n^2b^2)^2} \right]} \quad (7.6)$$

The values of these derivatives for the mixture of ethane/n-tetratetracontane in the liquid phase are shown in Table 7-5. It can be seen that all of the derivatives are positive for the van der Waals and composite vdW/Lee-Sandler mixing rules. However, for the Lee and Sandler mixing rule, the derivatives with respect to ethane are negative. These negative derivatives arise naturally from the analytical forms of the derivatives and the mixing rules:

$$\left(\frac{\partial b\rho}{\partial n_k}\right)_{T,\underline{V},n_{i \neq k}} = \frac{1}{\underline{V}} \left( 2 \sum_i x_i b_{ik} - b_{mix} \right) \quad (7.7)$$

$$\left(\frac{\partial nb}{\partial n_k}\right)_{T,\underline{V},n_{i \neq k}} = 2 \sum_i x_i b_{ik} - b_{mix} \quad (7.8)$$

It can be seen from equation (7.7) and (7.8) that the values of the above derivatives can become negative when the co-volume of the mixture exceeds the first term in these

equations. This is most likely to occur when the  $k^{\text{th}}$  molecule is smaller than  $i^{\text{th}}$  molecule, as in the present case with the Lee and Sandler mixing rule. These negative derivatives were also observed with the geometric mean and Lorentz co-volume mixing rules. Like the Lee and Sandler co-volume mixing rule, when combined with the van der Waals mixing rule, the geometric mean and Lorentz mixing rules yielded positive values for these derivatives.

**Table 7-5 Values of the derivatives of mixing rules for ethane/n-tetratetracontane in the liquid phase.**

Mixing Rule	$X_{\text{ethane}}$	$\left(\frac{\partial b\rho}{\partial n_i}\right)$ (mole <sup>-1</sup> )		$\left(\frac{\partial nb}{\partial n_i}\right)$ (mL/mole)	
		C <sub>2</sub>	n-C <sub>44</sub>	C <sub>2</sub>	n-C <sub>44</sub>
van der Waals	0.110	0.021891	1.0678	40.542	1977.5
	0.167	0.023276	1.1353	40.542	1977.5
	0.245	0.025479	1.2428	40.542	1977.5
	0.304	0.027444	1.3386	40.542	1977.5
	0.360	0.029609	1.4442	40.542	1977.5
	0.448	0.033793	1.6484	40.542	1977.5
	0.501	0.036932	1.8015	40.542	1977.5
	0.516	0.037928	1.8500	40.542	1977.5
Lee & Sandler	0.110	-0.17954	1.0941	-323.61	1972.0
	0.167	-0.16664	1.1758	-278.46	1964.7
	0.245	-0.14807	1.3034	-221.51	1949.9
	0.304	-0.13320	1.4150	-182.16	1935.0
	0.360	-0.11835	1.5362	-147.76	1917.9
	0.448	-0.09324	1.7660	-99.538	1885.3
	0.501	-0.07684	1.9355	-73.930	1862.1
	0.516	-0.07200	1.9889	-67.151	1855.1
vdW/Lee-Sandler	0.110	0.01385	1.0689	25.617	1977.3
	0.167	0.01580	1.1369	27.467	1977.0
	0.245	0.01878	1.2452	29.801	1976.4
	0.304	0.02133	1.3416	31.414	1975.8
	0.360	0.02406	1.4477	32.824	1975.1
	0.448	0.02914	1.6527	34.800	1973.7
	0.501	0.03283	1.8064	35.850	1972.8
	0.516	0.03398	1.8551	36.128	1972.5

These negative derivatives will have a significant impact on equilibrium calculations since they change the sign of three out of five terms in the expression for the fugacity coefficient (Equation (7.5)). The impact of the change in sign of the derivatives on the

partial molar volume will be manifested also in the Jacobian and the convergence or lack thereof for bubble point calculations. The partial molar volume (Equation (7.6)) of the smaller component in a binary mixture may also become negative as a consequence of the change in sign of these derivatives and lead to physically incorrect predictions of volumetric behaviour. Indeed, such negative partial molar volumes for ethane are obtained in the present case with the Lee and Sandler mixing rule whereas they are positive with the van der Waals and composite mixing rules. These results point to a serious pitfall in altering the mixing rule for the co-volume term. It is not only the absolute value of the mixture co-volume which is important but also the derivatives of these mixing rules.

The results shown above indicate that composite mixing rules comprised of the van der Waals mixing rule and a second mixing rule have the potential to provide improved predictions of bubble point pressure for an asymmetric binary mixture of hydrocarbons. This represents the first demonstration of a new approach to an improved mixing rule for co-volume. Although the form of the binary mixing parameter is important for good predictions of bubble point pressure, attention should also be given to the values of the various derivatives of the mixing rules.

### **7.3. BUBBLE POINT PRESSURE AND DENSITY OF VTB/N-DECANE MIXTURES**

The Lee and Sandler co-volume mixing rule, whether alone or in combination with the van der Waals, always converged to a physically meaningful result for the mixtures of ethane and n-tetradecane investigated above. In contrast, the geometric mean and Lorentz mixing did not always converge to real pressures. Additionally, the Form E of the binary mixing parameter led to the best agreement with reported measurements. The purely Lee and Sandler mixing rule and its combination with the van der Waals mixing rules, using the Form E binary mixing parameter, along with the purely van der Waals mixing rule were further investigated for their predictive accuracy for VTB mixtures.

Critical properties derived from the regression of VTB vapour pressure data as well as from the Marrero-Gani GC method applied to the sixty molecular representations for VTB were used in the investigation of the above mixing rules. For the heavy gas oil

fraction of the model VTB, Aspen HYSYS was used to create a set of pseudo-components and to calculate pseudo-critical properties from high temperature simulated distillation, density, and average molecular weight using recommended correlations built into HYSYS. Aspen HYSYS 3.2 was also used to create a model of VTB using measured high temperature simulated distillation, density, and average molecular weight of VTB. The version of HYSYS used employed the van der Waals mixing rule and a similar version of the Peng-Robinson CEOS to that employed in this study. The results from these predictive approaches were compared to measured data.

A model VTB was previously described in terms of sixty molecular representations and a percentage of heavy gas oil. The heavy gas oil fraction accounted for 15.92 wt.% of the model VTB and should ideally be proportionally represented by up to ten molecular representations or pseudo-components. The overall representation of VTB should, therefore, include seventy components. Initializing the bubble point calculation requires good estimates of bubble point pressure and K-values. For heavy oils such as VTB, the shortcut method for estimating K-values is no longer adequate and so these need to be manually input as trial guesses. For the model with seventy molecular representations for VTB this would be an extremely tedious process. It was therefore decided to reduce the total number of components representing the model VTB to twenty: ten representing the heavy gas oil fraction and ten representing the rest of the heavier fractions. Ten components representing the heavy gas oil fraction were used since this lighter fraction would contribute proportionately more to the vapour pressure of the mixture. The suitability of this representation was subsequently checked by a limited number of calculations with seventy components representing the model VTB.

The initial sixty-component representation of the heaviest fraction of VTB were reduced to ten using Kay's rule. It can be shown that, where the ratio of critical pressure is exactly unity, critical pressure and temperature derived from Kay's rule lead to the identical energy term ( $a_{\text{mix}}$ ) and co-volume term ( $b_{\text{mix}}$ ) for the mixture as those calculated using the van der Waals mixing rules. The properties of the reduced representations for the model VTB are given in Table 7-6. While Kay's rule, which yield molar average properties, was applied to critical temperature, pressure, volume, normal boiling point

and molecular weight, the correlation of Ambrose and Walton was used to calculate acentric factors from these properties.

**Table 7-6 Properties for a reduced component representation for VTB.**

Fraction*	P <sub>c</sub> (kPa)	T <sub>c</sub> (K)	V <sub>c</sub> (m <sup>3</sup> /mole)	Acentric Factor	T <sub>b</sub> (K)	MW (g/mole)	Mole Fraction
HVGO-1	1206.64	910.21	0.001326	1.0306	737.52	344.32	0.004160
HVGO-2	1082.17	948.50	0.001506	1.1161	780.98	393.15	0.010612
HVGO-3	994.63	978.34	0.001662	1.1804	815.10	433.04	0.121116
HVGO-4	946.08	993.92	0.001759	1.2165	833.59	452.79	0.105501
HVGO-5	846.10	1026.81	0.001992	1.2939	873.38	495.94	0.024389
HVGO-6	751.19	1057.81	0.002267	1.3715	912.44	533.30	0.009859
HVGO-7	684.39	1087.73	0.002520	1.4325	948.13	578.79	0.009515
HVGO-8	618.88	1120.12	0.002826	1.4959	986.85	628.68	0.013558
HVGO-9	570.04	1143.32	0.003095	1.5446	1015.61	660.03	0.010072
HVGO-10	507.16	1173.25	0.003515	1.6104	1053.77	695.72	0.005641
F1-M1-6	865.04	1054.87	0.002579	0.4959	830.50	560.39	0.176877
F2-M1-6	810.79	1070.26	0.002836	0.4473	842.52	798.96	0.095732
F3-M1-6	860.26	1038.59	0.002465	0.2664	789.59	696.84	0.085122
F4-M1-6	815.62	1104.69	0.002819	0.3379	855.10	820.22	0.100864
F5-M1-6	770.46	1103.60	0.003153	0.5509	884.83	910.05	0.055745
F6-M1-6	778.76	1115.92	0.003153	0.5596	894.71	912.78	0.037622
F7-M1-6	692.99	1203.68	0.004400	0.3589	951.36	1292.56	0.019926
F8-M1-6	704.47	1187.59	0.004156	0.2690	923.96	1218.28	0.016657
F9-M1-6	697.52	1214.37	0.004401	0.4879	975.82	1309.27	0.012518
F10-M1-6	617.30	1522.12	0.012142	0.4014	1225.35	3730.88	0.084514

\* HVGO-X indicates a heavy gas oil pseudo-component defined by Aspen HYSYS  
 FX-M1-6 indicates the Kay's rule molar average component for the six molecular representations of the X<sup>th</sup> VTB fraction described in a previous chapter.

There are two apparent inconsistencies for the properties shown in Table 7-6. The acentric factors for the heavy gas oil components are twice as large as those for the original VTB representations as well as the above reduced representations. It should be noted however that all of the acentric factors shown in the above table are consistent through the correlations of Ambrose and Walton with the critical temperature, critical pressure, and normal boiling point for each component. It can also be noted that the heaviest HVGO fractions have critical pressures lower than that for the heaviest model VTB fractions such as those in fractions F9 and F10. These apparent inconsistencies are due to the construction of the model VTB from two different approaches: (a) correlations for critical properties based on boiling point, and (b) molecular representation based on

a wide range of compositional data combined with GC methods to predict critical properties. This model represented a compromise since correlations based on boiling could not be applied to the substantial portion of VTB which was non-distillable.

### 7.3.1. 100 wt.% VTB

The vapour pressure and liquid phase densities of VTB measured as a function of temperature, from approximately 150 to 300°C, were reported in an earlier chapter. Although the volume of vapour produced during these measurements is quite low, the measured pressure is expected to be slightly lower than the true bubble point pressure, i.e., the point where the first bubble of vapor is formed. Bubble point pressures and liquid phase densities of VTB were calculated using the component properties given in Table 7-6. The predicted vapour pressures and liquid densities of VTB calculated using the various mixing rules are shown in Figure 7-4 and Figure 7-5, respectively.

None of the selected co-volume mixing rules led to bubble point pressure predictions having good correspondence with measured values. The measured bubble point pressure at 297.0°C was 15.3 kPa compared to the predicted value 0.58 kPa using the three selected co-volume mixing rules. The predicted bubble point pressure from HYSYS was even lower, being 0.01 kPa.

The predicted liquid densities from calculations with the three selected mixing rules also show poor correspondence and are about 12% higher than the measured densities. Unexpectedly, the predicted liquid densities from HYSYS show fairly good agreement with measured values and are only about 5% higher. It should be recalled that measured density of VTB was an input to HYSYS whereas only critical properties and acentric factor are required inputs for bubble point calculation routines developed here. Also, HYSYS calculations included binary interaction parameters whereas all such parameters are set equal to zero in the calculation routines developed for this study. There was no evidence that volume translation was applied to the implementation of the Peng-Robinson CEOS in HYSYS 3.2 used for these calculations.

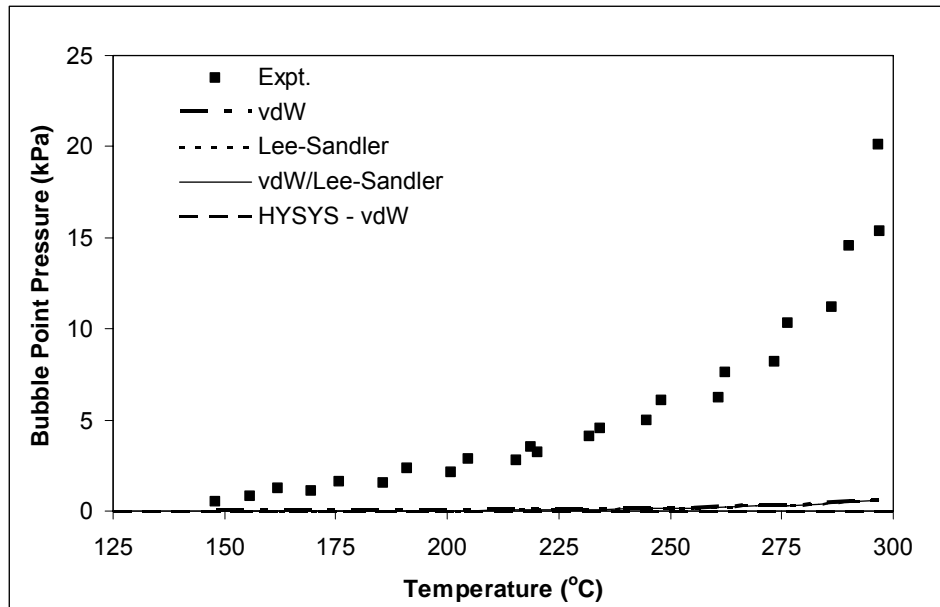


Figure 7-4 Comparison of vapour pressures for VTB measured to those predicted from the selected mixing rules.

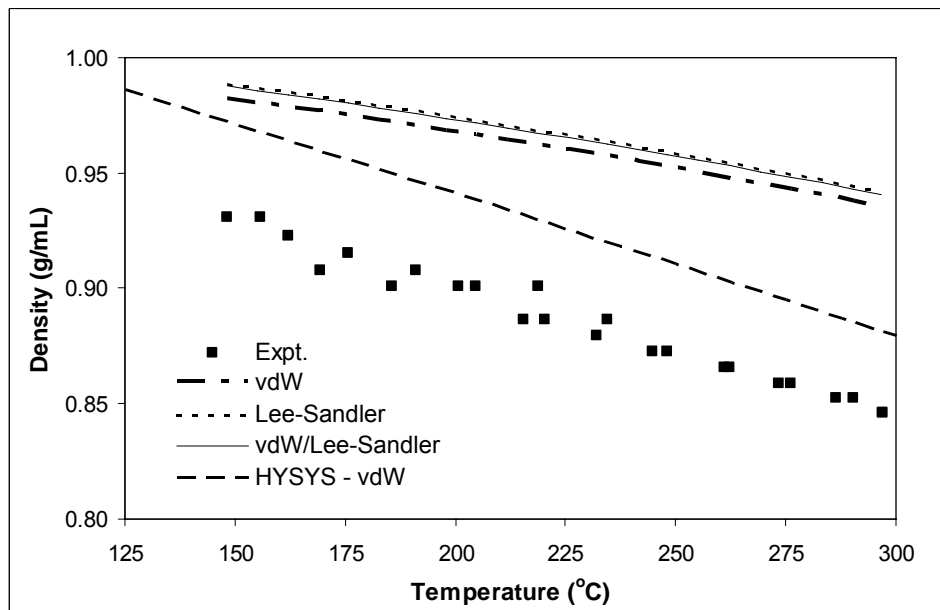


Figure 7-5 Comparison of liquid phase densities for VTB measured to those predicted from the selected mixing rules.



### 7.3.2. 90 wt.% VTB – 10 wt.% N-Decane

The model for VTB given in Table 7-6 was employed to calculate the bubble point pressure and liquid densities for a mixture of 89.95 wt.% VTB and 10.05 wt.% n-decane. Critical properties for n-decane were taken from the DIPPR database. The predictions were compared to data measured and reported by Zhang. Although Zhang did not directly measure the bubble point pressures, these were estimated by extrapolation to zero vapour volume of vapour pressure versus vapour volume data at constant temperature. Liquid phase densities were determined in a similar manner to that used in the present work and reported in an earlier chapter. Zhang reported that the above mixture exhibited simple VLE with no observed second liquid phase over the range of temperatures investigated.

Of the three mixing rules investigated, the van der Waals mixing rule yields the best agreement with the estimated bubble point pressures (Figure 7-6). The composite mixing rule composed of van der Waals and Lee-Sandler mixing rules leads to intermediate values of bubble point pressure between those predicted by the purely van der Waals and purely Lee-Sandler mixing rules. All three mixing rules underestimate the bubble point pressure particularly below 225°C. In comparison to the three evaluated mixing rules, the prediction bubble point pressures from HYSYS show fairly good agreement with the measured data especially above 175°C.

The bubble point pressures determined from the data of Zhang show a deviation in the expected trend with increasing temperature. There are a number of possible explanation for this deviation including: (i) experimental error in measurement of low pressures, (ii) evolution of dissolved gas in the mixture, (iii) change in the state of the mixture such as solid phase present at low temperature being dissolved at high temperature, and (iv) errors due to extrapolation of pressure versus vapour volume at constant temperature to obtained bubble point pressures. Insight into this deviation can be obtained by comparing the bubble point pressures from Zhang's data and that calculated for the model VTB with van der Waals mixing rules to the vapour pressure of n-decane (Figure 7-7). It can be seen that the bubble point pressure determined from measured data is higher than the vapour pressure for n-decane; however, this does not

necessarily prove or imply an experimental error. Further investigation is required to resolve the origin of the observed trends in bubble point pressure.

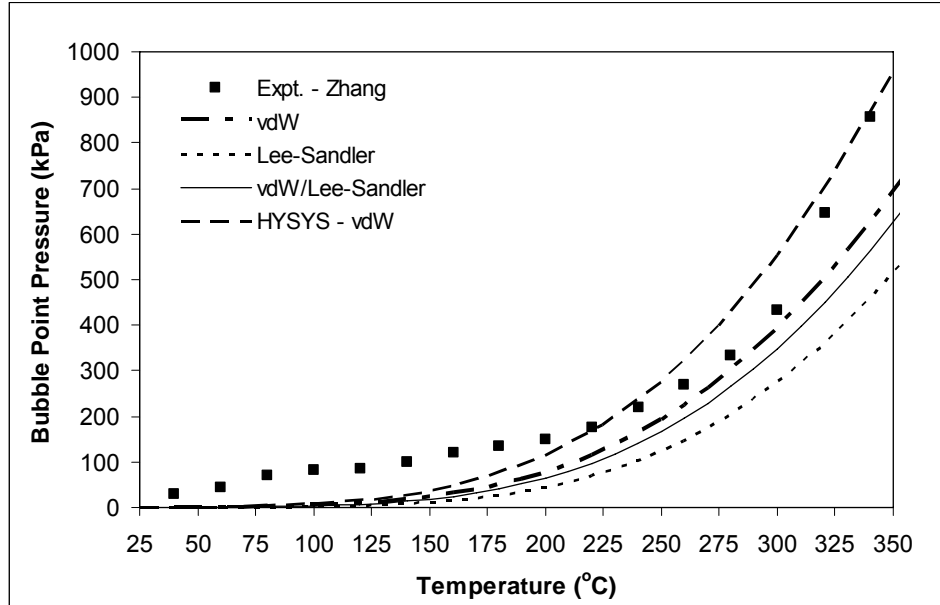


Figure 7-6 Comparison of measured bubble point pressures for 89.95 wt.% VTB mixture with n-decane (data of Zhang) to prediction from the selected mixing rules.

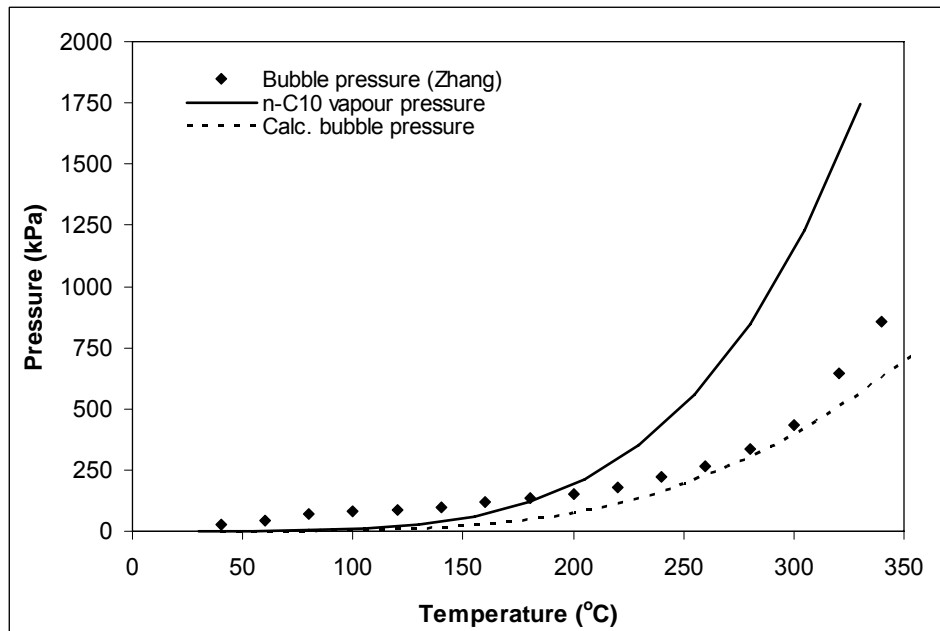


Figure 7-7 Comparison of measured bubble point pressure or 89.95 wt.% VTB mixture with n-decane (data of Zhang) to prediction from the van der Waals mixing rules and vapour pressure of pure n-decane

For prediction of liquid densities (Figure 7-8), the van der Waals mixing rule leads to excellent agreement with the measured values. The composite mixing rule also yields fairly good agreement. The Lee-Sandler mixing rule gives the right trend in liquid density although densities are slightly over-estimated over the entire temperature range. In contrast, HYSYS significantly over-predicts densities below 250°C and under-predicts densities above 250°C. HYSYS gives an almost constant slope for  $d\rho/dT$  whereas the three mixing rules give nearly identical slopes which better reflect the temperature dependence of the experimental data.

The critical properties from regression of measured vapour pressure for VTB were also used to calculate the bubble point pressure and density for the above mixture. This approach effectively treats VTB as a single-component system. The results are summarized in Figure 7-9 and Figure 7-10. It can be seen that the results obtained from treating VTB as a single component led to poorer agreement with the measured data for the three mixing rules than the above twenty-component representation. Interestingly, the results from the three mixing rules for the single-component VTB representation show almost identical results for bubble point pressure and density where as for the twenty-component VTB representation each mixing rule leads to slightly different results.

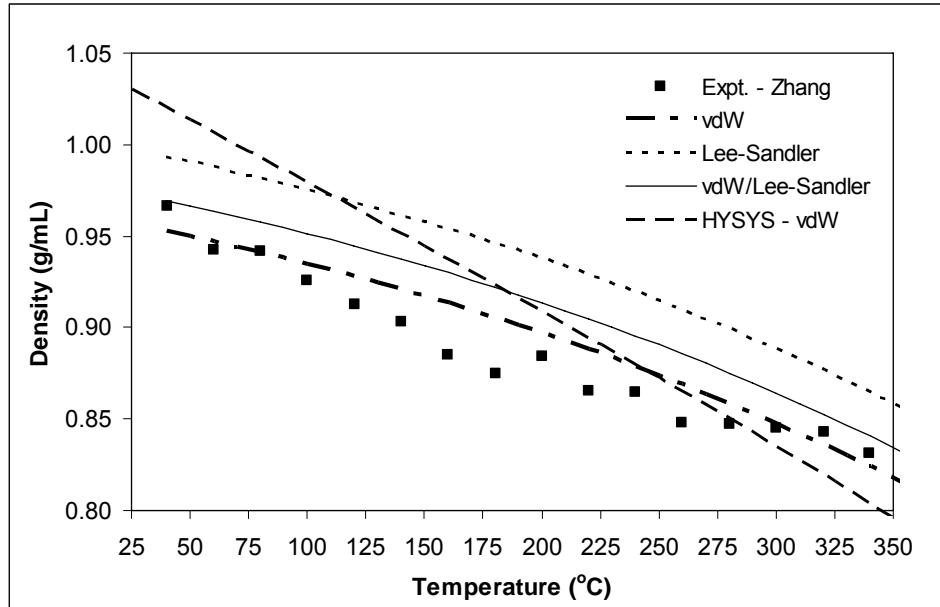


Figure 7-8 Comparison of measured liquid densities for 89.95 wt.% VTB mixture (data of Zhang) with n-decane to prediction from the selected mixing rules.

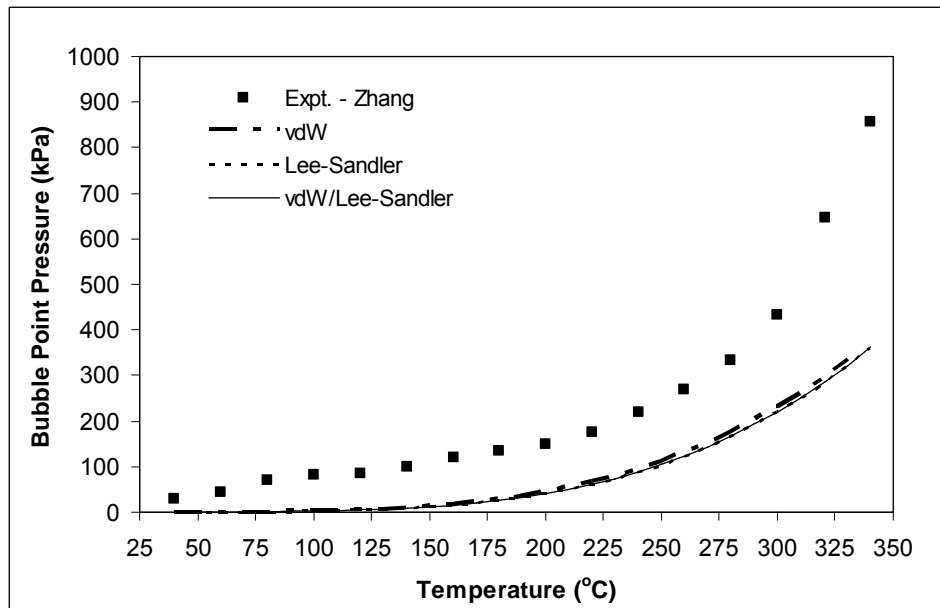


Figure 7-9 Comparison of measured bubble point pressures for 89.95 wt.% VTB mixture with n-decane (data of Zhang) to prediction from the selected mixing rules and a single-component representation for VTB.

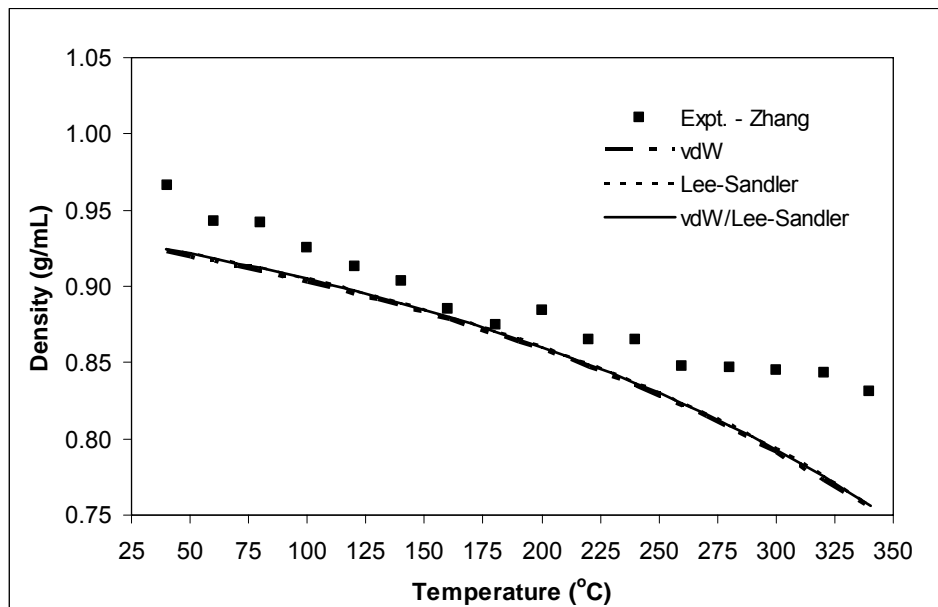


Figure 7-10 Comparison of measured liquid densities for 89.95 wt.% VTB mixture with n-decane (data of Zhang) to prediction from the selected mixing rules and a single-component representation for VTB.

### 7.3.3. 10 wt.% VTB – 90 wt.% N-Decane

In contrast to the previous mixture with 90 wt.% VTB, the present mixture exhibited LLV phase behaviour for temperatures above 100°C. The data of Zhang shows that the second liquid phase could account for as much as 3.2% of the total liquid volume. Since the present methodology employed for bubble point pressure prediction does not account for liquid-liquid phase splitting, it is not suitable for predictions of this mixture. Additionally, since the mixture was very rich in n-decane, the bubble point pressure and liquid phase densities will be dominated by n-decane. Nevertheless, bubble point pressure and liquid density calculations were made in an attempt to contrast the present approach VLE of highly asymmetric mixtures with the approach taken by Van Waeyenberghe.

Similar calculations to those carried out for the 89.95 wt.% VTB mixture with n-decane were also carried out for a 10.03 wt.% VTB mixture. The results are summarized in Figure 7-11 and Figure 7-12. The predictions from calculations using the three selected mixing rules and HYSYS were compared to the data reported by Zhang. The three

selected mixing rules give excellent agreement with measured data and almost identical bubble point pressures and liquid densities. The GC contribution based Peng-Robinson CEOS used by Van Waeyenberghe underestimated the bubble point pressure and the agreement with experimental data was not as good as that achieved here. For liquid densities, Van Waeyenberghe obtained slightly better agreement with experimental results than that achieved in the present work. It is necessary to point out, however, that the GC contribution based Peng-Robinson CEOS employed by Van Waeyenberghe included volume translation. In comparison to the above approaches, HYSYS under-predicts the bubble point pressure and over-predicts liquid density and results in large deviations from the measured data.

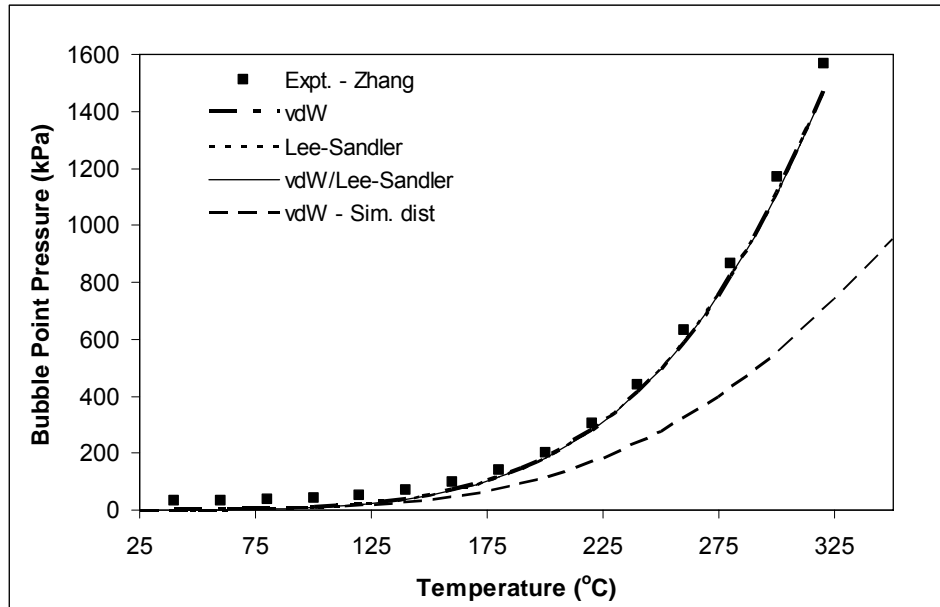


Figure 7-11 Comparison of measured bubble point pressures for 10.03 wt.% VTB mixture with n-decane (data of Zhang) to prediction from the selected mixing rules.

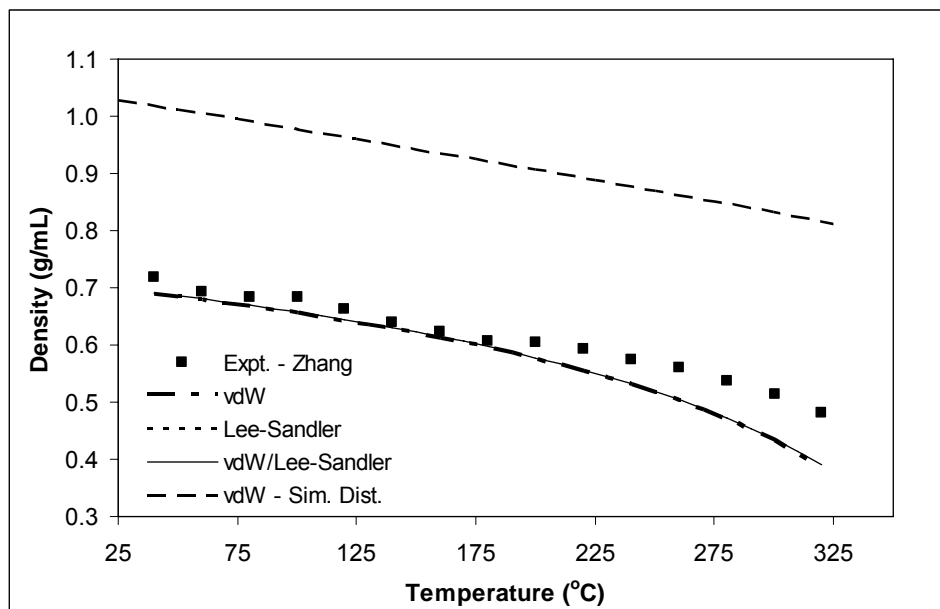


Figure 7-12 Comparison of measured liquid densities for 10.03 wt.% VTB mixture with n-decane (data of Zhang) to prediction from the selected mixing rules.

#### 7.3.4. Sensitivity Analysis

As noted earlier, the representation of VTB was reduced from seventy components to twenty components. It was also shown that a single-component representation yielded a worse prediction than the twenty-component representation. Additionally, while the twenty-component representation could lead to significantly different results for each of the three mixing rules, the single-component representation leads to almost identical results from these mixing rules. Calculations have been carried out with the seventy-component representation of VTB for the VTB/n-decane mixture containing 89.95 wt.% VTB. The results are summarized in Figure 7-13 and Figure 7-13. For bubble point pressure predictions, the seventy-component representation yields almost identical results to the twenty-component representation. The average absolute relative difference in bubble point pressure between both sets of predictions was 0.45%. The predicted liquid phase densities were also different for the two representations. The average absolute relative difference in liquid phase density between both sets of predictions was 0.73%.

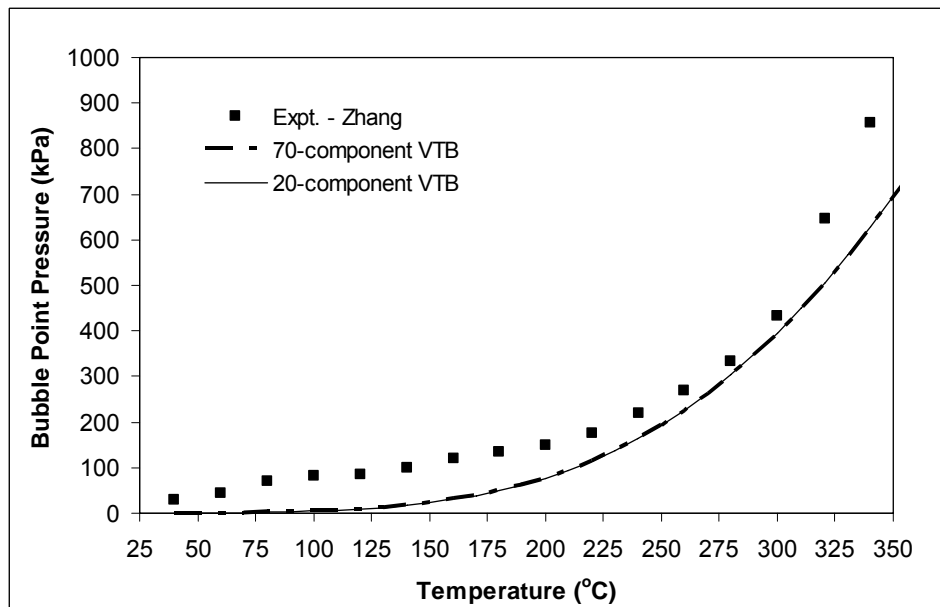


Figure 7-13 Comparison of the seventy and twenty-component representations for VTB for prediction of bubble point pressure with van der Waals mixing rules for 89.95 wt.% VTB mixture with n-decane (data of Zhang).

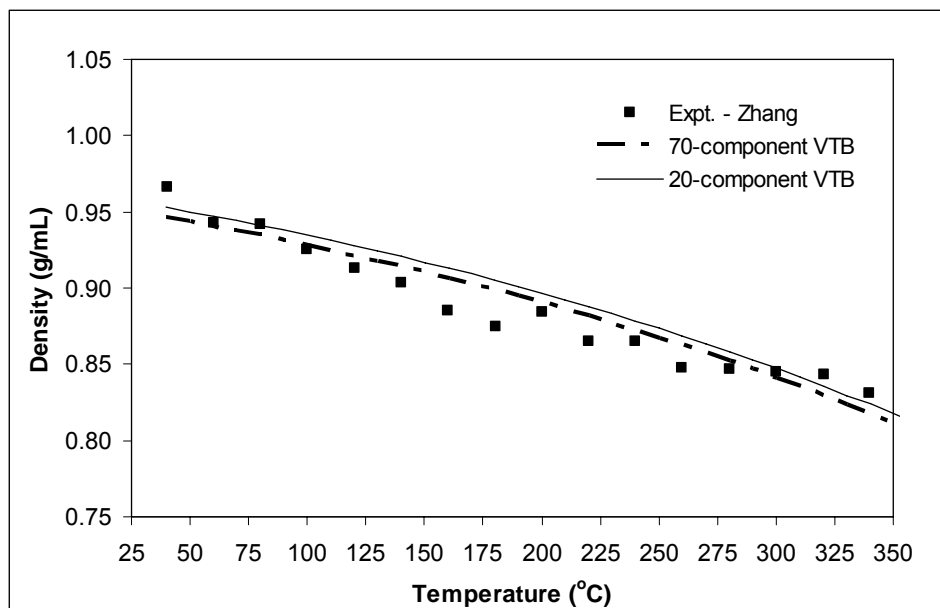


Figure 7-14 Comparison of the seventy and twenty-component representations for VTB for prediction of liquid phase density with van der Waals mixing rules for 89.95 wt.% VTB mixture with n-decane (data of Zhang).



## 7.4. SUMMARY

### 7.4.1. Ethane/n-Tetratetracontane

The proposed composite mixing rules and their basic counterparts were evaluated for the prediction of the bubble point pressure for an asymmetric mixture of ethane and n-tetratetracontane. All calculations, except those done with HYSYS, were carried out with the binary interaction parameters set equal to zero. Of the four basic mixing rules investigated, the van der Waals mixing rule led to the best agreement with experimental bubble point pressure data. Indeed, the other three mixing rules either did not converge or showed greater than 99% deviation from experimental data. It was found that the Lorentz, geometric mean, and Lee-Sandler co-volume mixing rules showed unreasonable negative values for the derivatives of these co-volume mixing rules with the consequence of incorrect predictions for phase behaviour. For example, negative partial molar volumes were predicted for ethane whereas these should be positive. It is important when modifying the mixing rules for co-volume that attention be given to the impact of the derivatives of the mixing rules on all thermodynamic properties functions not simply those being sought.

Incorrect negative derivatives of co-volume mixing rule and negative partial molar volumes for ethane were not obtained, when the basic mixing rules were combined to form the proposed composite mixing rule. Five forms of the binary mixing parameter, required for composite mixing rules, were evaluated. When the binary mixing parameter of Form E was used, significantly improved predictions of bubble point pressure were obtained compared to those from the van der Waals mixing rule.

Of the three single mixing rules investigated, only the Lee-Sandler mixing rule consistently converged to real and positive bubble point pressures. When the Lee-Sandler rule was combined with the van der Waals rule to form the new composite mixing rule, the average absolute deviation from experimental data was reduced by a factor of three compared to the van der Waals mixing rule.

### 7.4.2. VTB and VTB/n-decane

Based on the results obtained for ethane and n-tetratetracontane, only the van der Waals and Lee-Sandler mixing rules in their basic and composite forms were applied to

mixtures of VTB. The models for VTB used were those based on the molecular representations of Sheremata. All calculations, except those done with HYSYS, were carried out with the binary interaction parameters set equal to zero.

#### 100% VTB

Independent of which model was used, the three mixing rules significantly under-predicted the bubble point pressures of pure VTB. One possible explanation for this is that the measured bubble point pressures were increased by the presence of lighter hydrocarbons produced from thermal reactions of VTB. Also, despite changes to the mixing rules for co-volume, the Peng-Robinson CEOS may not be applicable to heavy asymmetric mixtures of VTB. Liquid densities were over-predicted with these co-volume mixing rules by only 5 to 10% which is within the expected accuracy for the Peng-Robinson CEOS. It was expected that pressure predictions should show better correspondence with measurements than density predictions with this CEOS and this points to a possibility of error in bubble point pressure measurement due to thermal reaction of VTB.

#### 90% VTB/10% n-decane

For a 90 wt.% mixture of VTB with n-decane, the van der Waals mixing rule with the model VTB based on Sheremata's molecular representations provided the best correspondence with measured bubble point pressures and measured liquid densities. The basic Lee-Sandler mixing rule yielded the poorer correspondence with measured data. The composite mixing rule gave predictions intermediate between van der Waals and Lee-Sandler mixing rules for pressure and density. Predictions using the van der Waals mixing rule and a model VTB based on simulated distillation data gave reasonable correspondence with bubble point pressure but poor correspondence with liquid density. Thermal reaction of VTB likely contributed to poorer agreement with predicted bubble point pressures at lower temperatures.

#### 10% VTB/90% n-decane

With the model VTB based on Sheremata's molecular representations, all three co-volume mixing rules gave excellent correspondence with measure bubble point pressures and liquid densities. This mixture was reported by Zhang to exhibit LLV behaviour. The presence of LLV behaviour was problematic for the present bubble point

calculation methodology which does not account for such behaviour. The good agreement in the present case might imply that the small fraction of molecules forming the second liquid phase (~3.2% of total liquid volume) was not significant enough to affect the bubble point pressure dominated by the large mole fraction of n-decane. The impact of thermal reactions of the VTB on the measured data would be overshadowed by the larger molefraction of n-decane.

It is significant that predictions using commercially available process simulation software, with VTB described by simulated distillation, molecular weight, and density data, yielded poor correspondence with the measured data for 90 wt.% and 10 wt.% VTB mixtures. This poor correspondence was achieved despite using the same Peng-Robinson CEOS and van der Waals mixing rule with binary interaction parameters which were non-zero. This indicates the VTB model, based on molecular representations developed by Sheremata and properties derived from the Marrero-Gani GC method, was superior to the simpler model based on boiling point and density correlations to predict critical properties.

#### Model Complexity

It was found that a representation of VTB which included only twenty components gave very similar results to that containing seventy components. A one-component model was found to be substantially inferior to a twenty-component model. These results imply that if representations could be developed with, for example, six molecules to describe each saturate, aromatic, resin, and asphaltene fractions for VTB such a model might be sufficient to provide useful phase equilibrium calculations.

---

## 8.0 SUMMARY, CONCLUSIONS AND RECOMMENDATIONS

---

### 8.1. SUMMARY AND CONCLUSIONS

#### 8.1.1. Introduction

Much effort has been expended towards improving the so-called alpha function and mixing rule for the energy term in the Peng-Robinson and other cubic equations of state (CEOS). Much less attention has been devoted to the co-volume term. However, these efforts have not led to significantly better predictions for high boiling, high molecular weight, and asymmetric crude oil mixtures. A new approach was developed and demonstrated for improving predictions of phase behaviour of heavy, asymmetric mixtures such as bitumen. The approach hinges on a new type of mixing rule for the co-volume term called a composite mixing rule.

Four basic and three composite co-volume mixing rules were evaluated for predicting properties of heavy and asymmetric crude oil mixtures typified by Athabasca bitumen vacuum tower bottoms (VTB). The four basic co-volume mixing rules are: (i) van der Waals (vdW), (ii) Lorentz, (iii) geometric mean, and (iv) Lee-Sandler. The composite mixing rules were formed from a linear combination of the vdW mixing rule with one of the other three mixing rules. The combination of mixing rules was mediated by a so-called binary mixing parameter which considers the differences in the co-volume of two interacting molecules. Several forms of this binary mixing parameter were evaluated by application to an asymmetric mixture of ethane and n-tetratetracontane.

Solving the Peng-Robinson CEOS requires critical properties and acentric factor for each VTB component. Two well established (Joback-Reid and Wilson-Jasperson) and one newer (Marrero-Gani) group contribution (GC) methods were applied and evaluated for estimation of critical properties from molecular representations for VTB developed by Sheremata. Predictions using the above mixing rules and critical properties, determined from GC methods, were compared to measured data for VTB (this work) and reported bubble point pressure and density data for mixtures of VTB with n-decane (data of Zhang).

A detailed summary was presented at the end of each chapter. The main findings and conclusions are summarized below.

### 8.1.2. *Main Findings and Conclusions*

Critical properties from vapour pressure of VTB and specific volume of VTB in pure solvents:

- Vapour pressure measurements of VTB even below 300°C are subject to errors due to thermal reactions which alter the composition and produce light hydrocarbons that increase the apparent vapour pressure.
- Regression of vapour pressure or specific volume data to extract critical properties must be constrained with a property relationship (e.g., Twu or Riazi-Daubert) otherwise a unique solution could not be obtained.
- Regressions employing the composite mixing rules led to significantly improved correspondence with specific volume data compared to regressions employing the vdW mixing rule.
- The property correlations of Riazi-Daubert and Twu are not applicable to VTB since they predict unreasonable properties, even though these properties led to good correspondence with measured data.

Group contribution methods for model VTB based on the molecular representations of Sheremata:

- Marrero-Gani GC methods led to the most consistent and reasonable critical properties for a model VTB based on the molecular representations of Sheremata.
- Boiling points predicted by the Marrero-Gani GC method showed remarkably good consistency with high temperature simulated distillation data for VTB. Boiling points predicted by the Joback and Reid GC method could be several hundred to two thousand degrees higher than the values from simulated distillation.

- Joback-Reid GC method could lead to physically unrealistic critical properties such as negative critical temperatures.
- Critical compressibility factors calculated from the critical properties derived from the Marrero-Gani GC method were within the range ( $Z_c \sim 0.29$ ) expected for heavy hydrocarbons. In contrast, the Joback-Reid derived critical properties led to values which were close to zero or negative.
- Wilson-Jasperson's GC method was not practical for heavy hydrocarbons such as VTB because it required that the boiling point be known.

#### Bubble point pressures $C_2/n-C_{44}$

- Of the four basic mixing rules investigated, the vdW mixing rule led to the best agreement with experimental data for  $C_2/n-C_{44}$  mixtures.
- The Lorentz, geometric mean and Lee-Sandler co-volume mixing rule showed unreasonable negative values for the derivatives of these mixing rules with the consequence of incorrect predictions for phase behaviour.
- It is important when modifying the mixing rules for co-volume that attention be given to the impact of the derivatives of the mixing rules on all thermodynamic properties functions not simply those being sought.
- The specific form of the binary mixing parameter is a key factor in the performance of the composite mixing rules.
- The composite rule composed of the Lee-Sandler and vdW mixing rules and Form E binary mixing parameter reduced the average absolute deviation from experimental data by a factor of three compared to the vdW mixing rule.
- The proposed composite mixing rules have the potential to provide superior phase behaviour predictions when applied to asymmetric binary mixtures.

#### VTB and VTB/n-decane:

- vdW, Lee-Sandler, and the composite mixing rules significantly under-predicted the bubble point pressure of pure VTB.

- Liquid densities of pure VTB were over-predicted by only 5 to 10% which is in the range of expected error for the Peng Robinson CEOS
- Compared to predicted density, vapour pressure predictions showed poorer correspondence with data indicates errors in bubble point pressure due to thermal reactions of VTB.
- Model VTB based on molecular representation with properties derived from Marrero-Gani GC methods can provide significantly better bubble point pressures and liquid density for VTB/n-decane mixtures using the Peng-Robinson CEOS and vdW mixing rule than a model based on boiling point and specific gravity.
- For a 90 wt.% mixture of VTB with n-decane, the vdW mixing rule provided the best correspondence with measured bubble point pressures and liquid densities. The composite vdW/Lee-Sandler mixing rule gave predictions intermediate between vdW and Lee-Sandler mixing rules for pressure and density.
- For a 10 wt.% VTB with n-decane, the vdW, Lee-Sandler and composite mixing rules gave excellent correspondence with measured bubble point pressures and liquid densities.
- Predictions from commercial process simulation software, with VTB described by simulated distillation, yielded poor overall correspondence with the measured bubble pressure and liquid density for 90 wt.% and 10 wt.% VTB mixtures.
- A VTB model developed from molecular representations which included only twenty components gave very similar results to that containing seventy components. A one-component model was found to be substantially inferior to a twenty-component model.

## 8.2. RECOMMENDATIONS

The group contribution methods of Marrero and Gani should be further evaluated for predictions of the critical properties of heavy crude mixtures such as VTB. In concert with this, further efforts should be made to improve the molecular representation of

VTB. It might be possible to simplify and yet improve the model by using few molecular representations.

Use of a composite mixing rule for co-volume is a new approach to phase behaviour of heavy asymmetric hydrocarbon mixtures that should be further evaluated. Other combinations of mixing rules and binary mixing parameters may yet provide better predictions than those used in the present work. The binary mixing parameter of the form used in this work may not be generally applicable to other systems because it reduces to the non-vdW mixing rule for molecules of similar co-volumes but to the vdW mixing rule for molecules of very dissimilar co-volumes. Other superior forms of the binary mixing parameter may also be possible which are not based simply on relative co-volumes.



---

## 9.0 REFERENCES

---

1. Agarwal, R.; Li, Y.-K.; Santollani, O.; Satyro, M.A.; Vieler, A. Uncovering the Realities of Simulations Part 1. *Chem. Eng. Prog.* May 2001, 42 -52.
2. van der Waals, J.D. Over de Continuïteit van den Gas- en Vloeistoftoestand (on the continuity of the gas and liquid state), Ph.D. thesis, Leiden (1873).
3. Sengers, J.V.; Kayser, R.F.; Peters, C.J.; White, Jnr, H.J. Equations of State for Fluids and Fluid Mixtures, *Experimental Thermodynamics, Volume V, Part 1 & 2*, Elsevier: The Netherlands, 2005.
4. Gray, M.R. *Upgrading Petroleum Residues and Heavy Oils*; M. Dekker: New York, 1994.
5. Speight, J.G. *The Chemistry and Technology of Petroleum*, Marcel Dekker, New York, 1999.
6. *Canada's Oil Sands, Opportunities and Challenges to 2015: An Update*. National Energy Board of Canada. June 2006.
7. King, R.W.; Zhao, L.; Huang, H.; McFarlane, R.A.; Gao, J. Steam and Solvent Coinjection Test: Fluid Property Characterization, Society of Petroleum Engineers, Petroleum of Society of the Canadian Institute of Mining, Metallurgy and Petroleum and Canadian Heavy Oil Association Joint Meeting, International Thermal Operations and Heavy Oil Symposium, Nov. 1-3/2005, SPE 97842.
8. Sharma, A.; Dandekar, A.Y.; Chukwu, G.A.; Khataniar, S.; Patil, S.L.; Haslebacher, W.F.; Chaddock, J. Phase Behavior Measurement and Modeling of Gas-to-Liquids and Alaska North Slope Crude Oil Blends. *Energy Sources*. 27 (2005) 709 - 718.
9. Zhang, X.H.; Chodakowski, M.; Shaw, J.M. The Impact of Multiphase Behaviour on Coke Deposition in Commercial Hydrotreating Catalyst under Sedimentation Conditions. *Energy & Fuels* 19 (2005) 1405 - 1411.
10. Gray, M.R. New Technique Defines the Limits of Upgrading Heavy Oils, Bitumens. *Oil & Gas Journal*, January 7, 2002.
11. Shaw, J.M.; Behar, E. SLLV Phase Behaviour and Phase Diagram Transitions in Asymmetric Hydrocarbon Fluids, *Fluid Phase Equilibria* 209 (2003) 185 - 206.

12. Chung, K.H.; Xu, C.; Hu, Y.; Wang, R. Supercritical Fluid Extraction Reveals Resid Properties, *Oil and Gas Journal*, January 20, 1997, 66-69.
13. Gray, M.R.; Qian, X.-F.; Chung, K. Thermal and Catalytic Hydrocracking of Supercritical Fluid-Extracted Vacuum Residue, *Proceedings of 213th National Meeting, American Chemical Society, Division of Petroleum Chemistry, International Symposium on Advances in Catalysis and Processes for Heavy Oil Conversion*, San Francisco, CA, April 13-17, 1997, 359-363.
14. Zhao, Z.; Kotlyar, L.S.; Woods, J.R.; Sparks, B.D.; Gao, J.; Chung, K. H. The Chemical Composition of Solubility Classes from Athabasca Bitumen Pitch Fractions, *Petroleum Science and Technology* 21(1&2) (2003) 183-199.
15. Sheremata J. M., Doctoral Thesis, University of Alberta. 2006.
16. Sheremata, J.M.; Gray, M.R.; Dettman, H.D.; McCaffrey, W.C.; Quantitative Molecular Representation and Sequential Optimization of Athabasca Asphaltenes, *Energy and Fuels* 18 (2004) 1377 - 1384.
17. Marrero, J.; Gani, R. Group-Contribution Based Estimation of Pure Component Properties. *Fluid Phase Equilibria* 183-184 (2001) 183 - 208.
18. Peng, D.-Y.; Robinson, D.B. A new Two-Constant Equation of State. *Industrial & Engineering Chemistry Fundamentals* 15 (1976) 59 - 64.
19. Agarwal, R.; Li, Y.-K.; Santollani, O.; Satyro, M.A.; Vieler, A.; Uncovering the Realities of Simulations Part 2. *Chem. Eng. Prog.* June 2001, 64 -72.
20. de Hemptinne, J.-C.; Ungerere, P. Accuracy of the Volumetric Predictions of Some Important Equations of State for Hydrocarbons, Including a Modified version of the Lee\_Kesler method, *Fluid Phase Equilibria* 106 (1995) 81-109.
21. Mohammad-Reza, R.; Mansoori, G.A. Simple Equation of State Accurately Predicts Hydrocarbon Densities. *Oil & Gas J.* July 12, 1993 108 - 111.
22. Poling, B.E.; Prausnitz, J.M.; O'Connell, J.P. *The Properties of Gases and Liquids*, 5th Edition; McGraw-Hill: New York, 2000.
23. Trebble, M.A. A Four-Parameter Cubic Equation of State. Ph.D. Thesis (1986) University of Calgary.

24. Sandler, S.I. Models for Thermodynamic and Phase Equilibria Calculation. Marcel Dekker: New York. 1994, p. 96.
25. Deiters, U.K. Calculation of Densities from Cubic Equations of State. AIChE Journal 48(4) (2002) 882-886.
26. Thiesen, M. Untersuchungen über die Zustandsgleichung. Annalen der Physik und Chemie. 24 (1885) 467 - 492.
27. Redlich, O.; Kwong, J.N.S. On the Thermodynamics of Solutions. Chemical Reviews 44 (1949) 233 -244.
28. (a) Wilson, G.M. Vapor-Liquid Equilibria Correlated by Means of a Modified Redlich-Kwong Equation of State. Advances in Cryogenic Engineering 9 (1964) 168 - 176; (b) Wilson, G.M. Calculation of Enthalpy Data from a Modified Redlich-Kwong Equation of State. Advances in Cryogenic Engineering 11 (1966) 392 -400.
29. (a) Pitzer, K.S. The Volumetric and Thermodynamic Properties of Fluids. I. Theoretical Basis and Virial Coefficients. Journal of the American Chemical Society. 77(13) (1955) 3427 - 3433; (b) Pitzer, K.S.; Lippmann, D.Z.; Curl Jr., R.F.; Huggins, C.M.; Petersen, D.E. The Volumetric and Thermodynamic Properties of Fluids. II. Compressibility Factor, Vapour Pressure and Entropy of Vaporization. Journal of the American Chemical Society. 77(13) (1955) 3433 - 3440.
30. Soave, G. Equilibrium Constants from a Modified Redlich-Kwong Equation of State. Chemical Engineering Science. 27 (1972) 1197 - 1203.
31. (a) Twu, C.H.; Sim, W.D.; Tassone, V. An Extension of CEOS/AE Zero-Pressure Mixing Rules for an Optimum Two-Parameter Cubic Equation of State. Industrial and Chemical Engineering Research. 41 (2002) 931 - 937. (b) *ibid.* A Versatile Liquid Activity Model for SRK, PR and a New Cubic Equation-of-State TST. Fluid Phase Equilibria 194-197 (2002) 385 - 399.
32. Lee, B.I.; Kesler, M.G. A Generalized Thermodynamic Correlation Based on Three-Parameter Corresponding States. American Institute of Chemical Engineers Journal. 21 (1975) 510 - 527.
33. Schmidt, G.; Wenzel, H. A Modified van der Waals Type Equation of State. Chemical Engineering Science. 35 (1980) 1503 - 1512.

34. Trebble, M.A.; Bishnoi, P.R. Accuracy and Consistency Comparisons of Ten Cubic Equations of State for Polar and Non-polar Compounds. *Fluid Phase Equilibria* 29 (1986) 465 - 474.
35. Salim, P.H.; Trebble, M.A. A Modified Trebble-Bishnoi equation of state: Thermodynamic Consistency Revisited. *Fluid Phase Equilibria*. 65 (1991) 59 - 71.
36. (a) Robinson, D.B.; Peng, D.-Y. The Characterization of the Heptanes and Heavier Fraction for the GPA Programs. Gas Processors Association. Report RR-28 1978. (b) Robinson, D.B.; Peng, D.-Y. and Chung, S.Y.-K. The development of the Peng-Robinson Equation and its Application to Phase Equilibrium in a System Containing Methanol. *Fluid Phase Equilibria*. 24 (1985) 25 - 41.
37. Stryjek, R.; Vera, J.H. An Improved Peng-Robinson Equation of State for Pure Compounds and Mixtures. *Canadian Journal of Chemical Engineering*. 64 (1986) 323-333.
38. Soave, G. Improvement of the van der Waals Equation of State. *Chemical Engineering Science* 39 (1984) 357 - 369.
39. Androulakis, I.P.; Kalospiros, N.S.; Tassios, D.P. Thermophysical Properties of Pure Polar and Nonpolar Compounds with a Modified VdW-711 Equation of State. *Fluid Phase Equilibrium* 45 (1989) 135 - 163.
40. Twu, C.H.; Coon, J.E.; Cunningham, J.R. A New Generalized Alpha Function for a Cubic Equation of State. Part 1. Peng-Robinson Equation. *Fluid Phase Equilibria* 105 (1995) 49 - 59.
41. Matahias, P.M.; Klotz, H.C. Take a Closer Look at Thermodynamic Property Models. *Chemical Engineering Progress*. June 1994, 67 -75
42. Cismondi, M.; Mollerup, J. Development and Application of a Three-parameter RK-PR Equation of State. *Fluid Phase Equilibrium*. 232 (2005) 74 - 89.
43. Salim, P.H.; Trebble, M.A. Thermodynamic Property Predictions from the Trebble-Bishnoi-Salim Equation of State. *Fluid Phase Equilibria*. 65 (1991) 41 - 57.
44. Satyro, M.A. An Equation of State Based on Significant Structure Theory. Ph.D. Thesis. (1997) University of Calgary.

45. Mathias, P.M.; Copeman, T.W. Extension of the Peng-Robinson Equation of State to Complex Mixtures: Evaluation of the Various Forms of the Local Composition Concept. *Fluid Phase Equilibria* 13 (1983) 91 - 108.
46. Design Institute for Physical Properties, Sponsored by AIChE DIPPR Project 801 - Full Version. Design Institute for Physical Property Data/AIChE.
47. Carnahan, N.F.; Starling, K.E. Intermolecular Repulsion and the Equation of State for Fluids. *American Institute of Chemical Engineers Journal* 18 (1972) 1184 - 1189.
48. Kubic, W.L. A Quartic Hard Chain Equation of State for Normal Fluids, *Fluid Phase Equilibria*. 31 (1986) 35 - 56.
49. Soave, G. A Non-cubic Equation of State for PVT and Phase Equilibrium Calculations (Pure Compounds). *Fluid Phase Equilibria*. 56 (1990) 39 - 57.
50. Scott, R.L. *Physical Chemistry, An Advanced Treatise*. Vol. 8A, Chapter 1. Academic Press: New York 1971.
51. Shah, V.M.; Bienkowski, P.R.; Cochran, H.D. Generalized Quartic Equation of State for Pure Nonpolar Fluids. *American Institute of Chemical Engineers Journal*. 40 (1994) 152 - 159.
52. Heideman, R.A.; Prausnitz, J.M. A van der Waals-type Equation of State for Fluids with Associating Molecules. *Proceedings of the National Academy of Science*. 73 (1976) 1773 - 1776.
53. Chapman, W. G.; Gubbins, K. E.; Jackson, G.; Radosz, M. SAFT: Equation-of-State Solution Model for Associating Fluids. *Fluid Phase Equilibria* 52 (1989) 31 - 38.
54. Chapman, W. G.; Gubbins, K. E.; Jackson, G.; Radosz, M. New Reference Equation of State for Associating Liquids. *Industrial and Engineering Chemistry Research*. 29 (1990) 1709 - 1721.
55. Huang, S.H.; Radosz, M.. Equation of State for Small, Large, Polydisperse, and Associating Molecules. *Industrial and Engineering Chemistry Research*. 29 (1990) 2284 - 2294.
56. Ting, P.D.; Joyce, P.C.; Prasanna, K.J.; Chapman, W.G.; Thies, M.C. Phase Equilibrium Modeling of Mixtures of Long-chain Alkanes Using Peng-Robinson and SAFT. *Fluid Phase Equilibria*. 206 (2003) 267 - 286.

57. Voulgaris, M.; Stamatakis, S.; Magoulas, K.; Tassios, D. Prediction of Physical Properties for Non-Polar Compounds, Petroleum and Coal Tar Fractions. *Fluid Phase Equilibria*. 64 (1991) 73 - 106.
58. Ambrose, D.; Young, C.L. Vapor-Liquid Critical Properties of Elements and Compounds. 1. An Introductory Survey. *Journal of Chemical & Engineering Data*. 40 (1995) 345 - 357.
59. Teja, A.S.; Gude, M.; Rosenthal, D.J. Novel Methods for Measurement of the Critical Properties of Thermally Unstable Fluids. *Fluid Phase Equilibria*. 52 (1989) 193 - 200.
60. Ribeiro, N.; Casimiro, T.; Duarte, C.; da Ponte, M.N.; Aguiar-Ricardo, A. Vapor-Liquid Equilibrium and Critical Line of the CO<sub>2</sub> + Xe System. Critical Behavior of CO<sub>2</sub> + Xe versus CO<sub>2</sub> + n-Alkanes. *Journal of Physical Chemistry B*. 104 (2000) 791 - 795.
61. TRC Thermodynamic Tables, Hydrocarbons, Thermodynamics Research Center: College Station, Texas, 1985.
62. Riazi, M.R. Characterization and Properties of Petroleum Fractions. American Society for Testing and Materials: Pennsylvania, 2005.
63. Tsonopoulos, C.; Tan, Z. The Critical Constants of Normal Alkanes from Methane to Polyethylene II. Application of Flory Theory. *Fluid Phase Equilibria*. 83 (1993) 127 - 138.
64. Kesler, M.G.; Lee, B.I. Improve Predictions of Enthalpy of Fractions. *Hydrocarbon Processing*. (March 1976) 153 - 158.
65. Riazi, M.R.; Daubert, T.E. Simplifying Property Predictions. 59 (1980) 115 - 116
66. Twu, C.H. An Internally Consistent Correlation for Predicting the Critical Properties and Molecular Weights of Petroleum and Coal-Tar Liquids. *Fluid Phase Equilibria*. 16 (1984) 137 - 150.
67. Riazi, M.R.; Daubert, T.E. Characterization Parameters for Petroleum Fractions. *Industrial and Engineering Chemistry Research*. 26 (1987) 755 - 759.
68. HYSYY Version 3.2 from Aspen Technology Inc. Cambridge, Massachusetts.

69. Maxwell, J.B.; Bonnell, L.S. Derivation and Precision of a New Vapour Pressure Correlation for Petroleum Hydrocarbons. *Industrial and Engineering Chemistry*. 49 (1957) 1187 - 1196.
70. Gray, R.D.; Heidman, J.L.; Springer, R.D.; Tsionopoulos, C. Characterization and Property Prediction for Heavy Petroleum and Synthetic Liquids. *Fluid Phase Equilibria*. 53 (1989) 355 - 376.
71. Ambrose, D.; Walton, J. Vapour Pressures up to Their Critical Temperatures of Normal Alkanes and 1-alkanols. *Pure & Applied Chemistry*. 61 (1989) 1395 - 1403.
72. Joback, K.G.; Reid, R.C. Estimation of Pure-Component Properties from Group-Contributions. *Chemical Engineering Communication*. 57 (1987) 233 - 243.
73. Wilson, G.M.; Jaspersen, L.V. Critical Constants  $T_c$ ,  $P_c$  Estimation Based on Zero, First and Second Order Methods. AIChE Spring Meeting, New Orleans, LA, 1996.
74. Computer Aided Process-Product Engineering Center (CAPEC) Database, Department of Chemical Engineering, Technical University of Denmark, Lyngby, Denmark, 2000.
75. Han, B.; Peng, D.-Y. A Group-Contribution Correlation for Predicting the Acentric Factors of Organic Compounds. *Canadian Journal of Chemical Engineering*. 71 (1993) 332 -334.
76. Constantinou, L.; Gani, R.; O'Connell, J.P. Estimation of the Acentric Factor and the Liquid Molar Volume at 298K using a New Group Contribution Method. *Fluid Phase Equilibria*. 104 (1995) 11 - 22.
77. Coniglio, L.; Trassy, L.; Rauzy, E. Estimation of Thermophysical Properties of Heavy Hydrocarbons through a Group Contribution Based Equation of State. *Industrial and Engineering Chemistry Research*. 39 (2000) 5037 - 5048.
78. Crampon, C.; Trassy, L.; Avauillé, L.; Neau, E.; Coniglio, L. Simplification and Extension of a Predictive Group Contribution Method for Estimating Heavy Organic Pure Compound Vapor Pressures. I. Hydrocarbons. *Fluid Phase Equilibria*. 216 (2004) 95 - 109.

79. Coniglio, L.; Nopuviaire, A. A Method for Estimating the Normal Boiling Point of Heavy Hydrocarbons Suitable for a Group-Contribution-Based Equation of State. *Industrial and Engineering Chemistry Research*. 40 (2001) 1781 – 1790.
80. (a) Ambrose, D. Correlation and Estimation of Vapor-Liquid Critical Properties. I. Critical Temperatures of Organic Compounds, National Physical Laboratory, Teddington, UK, NPL Report Chemistry 92, 1978. (b) Ambrose, D. Correlation and Estimation of Vapor-Liquid Critical Properties. II. Critical Pressures and Volumes of Organic Compounds, National Physical Laboratory, Teddington, UK, NPL Report Chemistry 98, 1979.
81. Van Waeyenberghe, A. Estimation of Thermophysical Properties Of Athabasca Vacuum Residue Using a Group Contribution Based Equation of State. M.Sc. Thesis (2006). University of Alberta.
82. Radosz, M.; Lin, H.-M.; Chao, K.-C. High-Pressure Vapor-Liquid Equilibria in Asymmetric Mixtures Using New Mixing Rules. *Industrial & Engineering Chemistry Process Design and Development*. 21 (1982) 653 – 658.
83. Good, R.J.; Hope, C.J. New Combining Rule for Intermolecular Distances in Intermolecular Potential Functions. *Journal of Chemical Physics*. 53 (1970) 540 -543.
84. Lee, K.-H.; Sandler, S.I. The Generalized van der Waals Partition Function - IV. Local Composition Models for Mixtures of Unequal-Size Molecules. *Fluid Phase Equilibria*. 34 (1987) 113 – 147.
85. Kontogeorgis, G.M.; Coutsikos, P.; Harismiadis, V.I.; Fredenslund, A.; Tassios, D.P. A Novel Method for Investigating the Repulsive and Attractive Parts of Cubic Equations of State and the Combining Rules used with the vdW-1f Theory. *Chemical Engineering Science*. 53 (1997) 541 – 552.
86. Hall, K.R.; Iglesias-Silve, G.A.; Mansoori, G.A. Quadratic Mixing Rules for Equation of State. Origins and Relationships to the Virial Expansion. *Fluid Phase Equilibria*. 91 (1993) 67 – 76.
87. McGregor, D.R.; Holste, J.C.; Eubank, P.T.; Marsh, K.N.; Hall, K.R.; Schouten, J. An Interaction Model for Third Virial Coefficients Which Provides Simplified Equations for Mixtures. *Fluid Phase Equilibria*. 35 (1987) 153 – 164.



88. Orbey, H; Sandler, S.I. On the Combination of Equation of State and Excess Free Energy Models. *Fluid Phase Equilibria*. 111 (1995) 53 - 70.
89. Harismiadis, V.I.; Koutras, N.K.; Tassios, D.P.; Panagiotopoulos, A.Z. How Good is Conformal Solution Theory fo Phase Equilibrium Predictions? *Fluid Phase Equilibria*. 65 1991) 1 - 18.
90. Bird, R.B.; Stewart, W.E.; Lightfoot, E.N. *Transport Phenomena*; Wiley: New York. 2002.
91. Rodgers, R.P.; Schaub, T.M.; Marshall, A.G. *Petroleomics: MS Returns to its Roots*. *Analytical Chemistry*. January 1, 2005. 21A - 27A.
92. Strausz, O.P. *The Chemistry of Alberta Oil Sands, Bitumens and Heavy Oils*. Alberta Energy Research Institute: Calgary. 2003.
93. Standard Test Method for Boiling Range Distribution of Petroleum Distillates in Boiling Range from 174 to 700°C by Gas Chromatography. American Society for Testing and Materials International, Method D 6352-02.
94. Zhao, S.; Kotlyar, L.S.; Woods, J.R.; Sparks, B.D.; Gao, J.; Chung, K.H. The Chemical Composition of Solubility Classes from Athabasca Bitumen Pitch Fractions. *Petroleum Science and Technology*. 21 (2003) 183 - 199.
95. Mullins, O.C.; Sheu, E. Y.; Hammami, A.; Marshall, A.G. *Asphaltenes, Heavy Oils, and Petroleomics*. Springer: New York. 2006.
96. Yarranton, H.W. Asphaltene Self-Association. *Journal of Dispersion Science and Technology*. 26 (2005) 5 - 8.
97. Sheremata, J.M.; Gray, M.R.; Dettman, H.D.; McCaffrey, W.C. Quatitative Molecular Representation and Sequential Optimization of Athabasca Bitumen. *Energy & Fuels*. 18 (2004) 1377 - 1384.
98. Mullins, O.C.; Sheu, E.Y., Hammami, A.; Marshall, A.G. *Asphaltenes, Heavy Oils and, Petroleomics*. Springer: New York, 2007.
99. Qian, K.; Edwards, K.E.; Siskin, M.; Olmstead, W.N.; Mennito, A.S., Dechert, G.J.; Hoosain, N.E. Desorption and Ionization of Heavy Petroleum Molecules and Measurement of Molecular Weight Distributions. *Energy & Fules*. 21 (2007) 1042 - 1047.

100. Shaw, J.M.; Behar, E. SLLV Phase Behaviour and Phase Diagram Transitions in Asymmetric Hydrocarbon Fluids. *Fluid Phase Equilibria*. 209 (2003) 185 – 206.
101. Diedrichs, A.; Rarery, J.; Gmehling, J. Prediction of Liquid Heat Capacities by the Group Contribution Equation of State VTPR. *Fluid Phase Equilibria*. 248 (2006) 56 – 69.
102. Panagiotopoulos, A.Z.; Reid, R.C. Multiphase High Pressure Equilibria in ternary Aqueous Systems. *Fluid Phase Equilibria*. 29 (1986) 525 – 534.
103. Sandoval, R.; Wilczek-Vera, G.; Vera, J.H. Prediction of Vapor-Liquid Equilibria with the PRSV Equation of State. *Fluid Phase Equilibria*. 52 (1989) 119 – 126.
104. Michelsen, M.L.; Kistenmacher, H. On Composition-Dependent Interaction Coefficients. *Fluid Phase Equilibria*. 58 (1990) 229 – 230.
105. Mathias, P.M.; Klotz, H.C.; Prausnitz, J.M. Equation-of-State Mixing Rules for Multicomponent Mixtures: The Problem of Invariance. *Fluid Phase Equilibria*. 67 (1991) 31 – 44.
106. Anderko. Equation-of-State Methods for the Modelling of Phase Equilibria. *Fluid Phase Equilibria*. 61 (1990) 145 – 225.
107. Orbey, H.; Sandler, S.I. Modeling Vapor-Liquid Equilibria: Cubic Equations of State and Their Mixing Rules. Cambridge University Press: New York. 1998.
108. Stryjek, R. Correlation and Prediction of VLE Data for n-alkane Mixtures. *Fluid Phase Equilibria*. 56 (1990) 141 – 151.
109. Voros, N.G.; Tassios, D.P. Vapor-Liquid Equilibria in Nonpolar/Weakly Polar Systems with Different Types of Mixing Rules. *Fluid Phase Equilibria*. 91 (1993) 1 – 29.
110. Nishiumi, H.; Arai, T.; Takeuchi, K. Generalization of the Binary Interaction Parameters of the Peng Robinson Equation of State by Component Family. *Fluid Phase Equilibria*. 42 (1988) 43 – 62.
111. Gao, G.; Daridon, J.L.; Saint-Guirons, H.; Zans, P.; Montel, F. A Simple Correlation to Evaluate Binary Interaction Parameters of the Peng-Robinson Equation of State: Binary Light Hydrocarbon Systems. *Fluid Phase Equilibria*. 74 (1992) 85 – 93.

112. Kordas, A.; Magoulas, K.; Stamataki, S.; Tassios, D. Methane-Hydrogen Interaction Parameters Correlations for the Pen-Robinson and the t-mPR Equation of State. *Fluid Phase Equilibria*. 112 (1995) 33 - 44.
113. Chueh, P.L.; Prausnitz, J.M. Vapor-Liquid Equilibria at High Pressures, Calculation of Partial Molar Volume in Non-Polar Liquid Mixtures. *American Institute of Chemical Engineers Journal*. 13 (1967) 1099 - 1113.
114. Pedersen, K.S.; Thomassen, P.; Fredenslund, A. On the Dangers of "Tuning" Equation of State Parameters. *Chemical Engineering Science* 43 (1988) 269 - 278.
115. Katz, D.L.; Firoozabadi, A. Predicting Phase Behavior of Condensate/Crude Oil Systems Using Methane Interaction Coefficients. *Journal of Petroleum Technology, Transaction of the American Institute of Mining and Metallurgical Engineers, Petroleum Branch*. 265 (1978) 1649 - 1655.
116. Martin, J.J. Cubic Equation of State - Which? *Industrial Engineering Chemistry Fundamentals*. 18 (1979) 81 - 97.
117. Peneloux, A.; Rauzy, E.; Freze, R. A consistent Correction for Redlich-Kwong-Soave Volumes. *Fluid Phase Equilibria*. 8 (1982) 7 - 23.
118. Leibovici, C.F. Variant and Invariant Properties from Cubic Equations of State. *Fluid Phase Equilibria*. 84 (1993) 1 - 8.
119. Chou, G.F.; Prausnitz, J.M. A Phenomenological Correction to an Equation of State for the Critical Region. *American Institute of Chemical Engineers Journal*. 35 (1989) 1487 - 1496.
120. (a) Jaubert, J.-N.; Mutelet, F. VLE Predictions with Peng-Robinson Equation of State and Temperature Dependent  $k_{ij}$  Calculated Through a Group Contribution Method. *Fluid Phase Equilibria*. 224 (2004) 285 - 304. (b) Jaubert, J.-N.; Vitu, S.; Mutelet, F.; Corriou, J.-P. Extension of the PPR78 Model (Prediction 1978 Peng-Robinson EOS with Temperature Dependent  $k_{ij}$  Calculated Through a Group Contribution Method) to Systems Containing Aromatic Compounds. *Fluid Phase Equilibria* 237 (2005) 193 - 211. (c) Vitu, S.; Jaubert, J.-N.; Mutelet, F. Extension of the PPR78 Model (Prediction 1978 Peng-Robinson EOS with Temperature

- Dependent  $k_{ij}$  Calculated Through a Group Contribution Method) to Systems Containing Naphthenic Compounds. *Fluid Phase Equilibria* 243 (2006) 9 – 28.
121. Solorzano\_Zavala, M.; Barragan-Aroche, F.; Bazua, E.R. Comparative Study of Mixing Rules for Cubic Equations of State in the Prediction of Multicomponent Vapor-Liquid Equilibria. *Fluid Phase Equilibria*. 122 (1996) 99 – 116.
  122. (a) Maham, Y.; Zhang, X.; Zabeti, P.; Goodkey, J.; Allain, M.; Shaw, J. M., Specific Partial Molar Volumes at Infinite Dilution and Volumes of Mixing for Athabasca Bitumen and Bitumen Vacuum Residue + Solvent Mixtures, 7th International Conference on Petroleum Phase Behaviour & Fouling, Asheville, North Carolina, June 25-29, 2006, (b) Unpublished results.
  123. Zhang, X. The Impact of Multiphase Behaviour on Coke Deposition in Heavy Oil Hydroprocessing Catalysts. Ph.D. Thesis (2006). University of Alberta.
  124. Abedi, S.J.; Cai, H.-Y.; Seyfaie, S.; Shaw, J.M. Simultaneous phase Behaviour, Elemental Composition and Density Measurement Using X-ray Imaging. *Fluid Phase Equilibria* 158-160 (1999) 775-781.
  125. Zou, X.Y. Selective Removal of Inorganic Fine Solids, Heavy Metals and Sulfur from Bitumen/Heavy Oils. Doctoral thesis, University of Toronto, 2003.
  126. Stephan, K.; Hildwein, H. Recommended Data of Selected Compounds and Binary Mixtures. DECHEMA Chemistry Data Series Vol. 4 Parts 1-2. Institut für Technische Thermodynamik und Verfahrenstechnik, Universität Stuttgart: Stuttgart, 1987.
  127. (a) Oonk, H.A.J.; van der Linde, P.R.; Huinink, J.; Blok, J.G. Representation and Assessment of Vapour Pressure Data; a novel approach applied to crystalline 1-bromo-4-chlorobenzene, 1-chloro-4-iodobenzene and 1-bromo-4-iodobenzene. *Journal of Chemical Thermodynamics*. 30 (1998) 897 – 907. (b) van der Linde, P.R.; Blok, J.G. ; Oonk, H.A.J. Naphthalene as a Reference Substance for Vapour Pressure Measurements Looked Upon from an Unconventional Point of View. *Journal of Chemical Thermodynamics*. 30 (1998) 909 - 917.

128. Dejoz, A.; Gonzalez-Alfaro, V.; Miguel, P.J.; Vazquez, M.A. Isobaric Vapor-Liquid Equilibria for Binary Systems Composed of Octane, Decane, and Dodecane at 20 kPa. *Journal of Chemical and Engineering Data*. 41 (1996) 93 – 96.
129. Schwarz, B.J.; Wilhelm, J. A.; Prausnitz, J.M. Vapor Pressures and Saturated-Liquid Densities of Heavy Fossil-Fuel Fractions. *Industrial Engineering and Chemistry Research*. 26 (1987) 2353 – 2360.
130. Rahimi, P.; Gentzis T.; Dawson, W.H.; Fairbridge, C.; Khulbe, C.; Chung, K.; Nowlan, V.; Del Bianco, A. Investigation of Coking Propensity of Narrow Cut Fractions from Athabasca Bitumen Using Hot-Stage Microscopy. *Energy and Fuels* 12 (1998) 1020-10-30.
131. Gray, M.R Personal communication.
132. ProPred Version 3.6, May 15, 2003 provided by Computer Aided Process-Product Engineering Center (CAPEC), Department of Chemical Engineering, Technical University of Denmark.
133. Goodkey, J. Irreversible Phase Behaviors for Heavy Oil/Bitumen + solvent Mixtures at Low Temperature: a) Impact of Thermal History on the Volume of Mixing. NSERC Industrial Research Chair in Petroleum Thermodynamics, Advisory Committee Meeting, November 2005.
134. Baker, L.E.; Pierce, A.C.; Liks, K.D. Gibbs Energy Analysis of Phase Equilibria. *Society of Petroleum Engineering Journal* 22 (1982) 731 - 742.
135. Nghiem, L.X.; Li, Y.-K.; Heidemann, R.A. Application of the Tangent Plane Criteria to Saturation Pressure and Temperature Computations. *Fluid Phase Equilibria* 21 (1985) 39 – 60.
136. Gasem, K.A.; Bufkin, B.A.; Raff, A.M.; Robinson Jr., R.L. Solubilities of Ethane in Heavy Normal Paraffins at Pressures to 7.8 MPa and Temperatures from 348 to 423 K. *Journal of Chemical and Engineering Data* 34 (1989) 187 – 191.
137. Peters, C.J.; De Roo, J.L.; Lichtenthaler, R.N. Measurements and Calculations of Phase Equilibria of Binary Mixtures of Ethane + Eicosane. Part I: Vapour + Liquid Equilibria. *Fluid Phase Equilibria* 34 (1987) 287 – 308.

---

## APPENDIX 1

---

***Warning: Safety glasses and nitrile gloves required for handling solvents and beryllium cell!***

**SAFE OPERATING PROCEDURES FOR X-RAY VIEW CELL**

**Prepared by: Richard McFarlane**

**Telephone: ----- (office)  
----- (home)**

**Email: -----**

**Date: June 24, 2005**  
Revised March 8, 2006

**Version 1.2**

**NOTE**

You should carefully review and understand the operations and associated MSDS before operating this equipment.

***Warning: Safety glasses and nitrile gloves required for handling solvents and beryllium cell!***

## TABLE OF CONTENTS

<b>1.0</b>	<b>DESIGN SPECIFICATIONS SUMMARY TABLE.....</b>	<b>206</b>
<b>2.0</b>	<b>SYSTEM SCHEMATICS .....</b>	<b>207</b>
<b>3.0</b>	<b>SAFE OPERATING PROCEDURES.....</b>	<b>208</b>
3.1	INTRODUCTION.....	208
3.2	DESIGN CRITERIA .....	209
3.2.1	<i>For Pressure Components .....</i>	<i>209</i>
3.3	LOADING AND PRESSURE TESTING.....	210
3.3.1	<i>Assembly of View Cell .....</i>	<i>210</i>
3.3.2	<i>Installation in Shielded Enclosure.....</i>	<i>212</i>
3.3.3	<i>Pressure testing with x-ray source on .....</i>	<i>212</i>
3.4	LOADING LIQUID SAMPLE .....	213
3.5	SAMPLE CONDITIONING .....	214
3.5.1	<i>Low Viscosity Liquid.....</i>	<i>214</i>
3.5.2	<i>High Viscosity Liquid .....</i>	<i>214</i>
3.6	PRESSURE MEASUREMENT.....	215
3.7	EMERGENCY RESPONSE AND SHUT DOWN PROCEDURE .....	218
	<b>APPENDIX I: MSDS .....</b>	<b>219</b>



***Warning: Safety glasses and nitrile gloves required for handling solvents and beryllium cell!***

## 1.0 DESIGN SPECIFICATIONS SUMMARY TABLE

Tag Number	Description	Maximum Allowable Working Pressure
V100	100 mL beryllium cell	4000 psig @ 450°C
HV-1	Whitey, SS-41S1	2500 psig @ 38°C
HV-2	Whitey, SS-41S1	2500 psig @ 38°C
HV-3	Swagelok, SS-SS1	2000 psig @ 38°C
HV-4	Whitey, SS-41S1	2500 psig @ 38°C
HV-5	Whitey, SS-41S1	2500 psig @ 38°C
HV-6	Whitey, SS-41S1	2500 psig @ 38°C
HV-7	Swagelok, SS-SS1	2000 psig @ 38°C
HV-8	Whitey, SS-41S1	2500 psig @ 38°C
HV-9	Whitey, SS-41XS1	2500 psig @ 38°C
HV-10	Whitey, SS-43XS4	2500 psig @ 38°C
HV-11	Whitey, SS-0RS2	5000 psig @ 38°C
HV-12	Swagelok, SS-41S2-A	2500 psig @ 38°C
HV-13	Whitey, SS-0RS2	5000 psig @ 38°C
HV-14	Swagelok, SS-41S2	2500 psig @ 38°C
HV-15	Swagelok, SS-41S2	2500 psig @ 38°C
PT101	Patriot, SP200-5kg-8-1	7500 psig @ 38°C
PT102	Patriot, SP200-5kg-8-1	7500 psig @ 38°C
PT103	Omega, PX5500L1-015-AI	15 psig @ -40 to 85°C
MCV-1	Concoa, 535203310	3000 psig @ 38°C
MCV-2	Concoa, 535203310	3000 psig @ 38°C
TE101	External control thermocouple	-
TIC101	Controller loop	-
TE102	Internal thermocouple	-
TE103	External control thermocouple	-
TIC103	Controller loop	-
MP1	Rotary vane vacuum pump	-



***Warning: Safety glasses and nitrile gloves required for handling solvents and beryllium cell!***

### 3.0 SAFE OPERATING PROCEDURES

#### 3.1 INTRODUCTION

A beryllium pressure vessel installed in an x-ray chamber is used to measure the vapor pressure of heavy oil. For a typical run, the cell is loaded with the heavy oil in a fumehood and then transferred to the shielded x-ray chamber. The cell is tested for leaks under high pressure and vacuum conditions. Finally, the cell is evacuated to 0 psia and heated to the desired temperature while continuously stirring. Once equilibrium has been achieved the vapor pressure is recorded and a x-ray image of the liquid in the cell is recorded for later analysis to determine the density of the liquid.

This work involves the use of a powerful x-ray source and high voltage. Typically, the x-ray source operates at 50 kilovolts and 30 mA. When the x-ray source is first turned on and conditioned, x-rays with much higher energies and intensity are generated. The system is well shielded and the access to the chamber is interlocked with the x-ray source to prevent accidental entry while x-rays are being generated.

The view cell is constructed from beryllium which is relatively unreactive. It is not expected that beryllium metal will be oxidized under the conditions used in this work, however, beryllium oxide is highly toxic and proper procedures should be followed to avoid any potential ingestion. Disposable gloves should be worn when handling the beryllium cell and the gloves should be removed and properly disposed of after use.

**Material Safety Data Sheets (MSDS) for beryllium, reagents and products are provided in the Appendix. Please review all appropriate MSDS before beginning your work.**

**The maximum amount of material charged to the view cell should occupy no more than 60 mL over the range of condition to be studied.**

## 3.2 DESIGN CRITERIA

### 3.2.1 For Pressure Components

#### 3.2.1.1 Header (Nitrogen)

The x-ray view cell is supplied by high-pressure nitrogen by 2,500 psig cylinder with a manual control valve.

#### 3.2.1.2 Header (Hydrogen)

The x-ray view cell is presently supplied with high-pressure hydrogen by a 2,300 psig cylinder with a manual control valve.

#### 3.2.1.3 Beryllium Cell

Serial Number	Cell-0100-040-450-BER/316
Volume	100 mL
Maximum Allowable Working Pressure	4000 psig
Temperature	450°C
Material	
Body	beryllium
Covers	beryllium
Closure Gasket	graphite spiral wound in 316 SS
Closure Screws	SA-193 Gr B16
Hex nuts	SA-193 Gr B16
Washers	alloy steel
Stirrer	carbon steel
Relief valve	none

### 3.3 LOADING AND PRESSURE TESTING

#### 3.3.1 Assembly of View Cell

- (1) Wear personal protective equipment (nitrile gloves, safety glasses).
- (2) All cell parts that would come in contact with the test sample should be thoroughly cleaned and dried.
- (3) Eight bolts should be sitting in the holes of the base plate. The cell mount (attached to base plate of the cell) should be securely mounted onto the assembly scaffold by three screws. It should have been left in this position after it was last disassembled.
- (4) Assemble the view cell in the sequence shown in Figure 3.1.
  - a. The channel plate has a notch which matches a pin in the lower base plate. Ensure that the pin is in the notch.
  - b. Gaskets: Two types are used: (a) Single piece integral nickel gasket and (b) Kalrez gaskets with inner and outer retaining rings. **Upper and lower gasket should be of the same type.**
  - c. The perforated stirrer support plate has a pair of tongues which must be fitted in the groove of the channel plate.
  - d. When installing the body of the view cell in step 6, the valve and thermocouple connectors should be facing you, roughly located between positions 1 and 3 as marked on the assembly scaffold (Figure 3.2).
  - e. Before installing the upper gasket and base plate, add a known mass of solid or semi-solid sample. If a liquid sample will be used, complete the cell assembly without sample addition. The liquid sample can be added at a later stage.

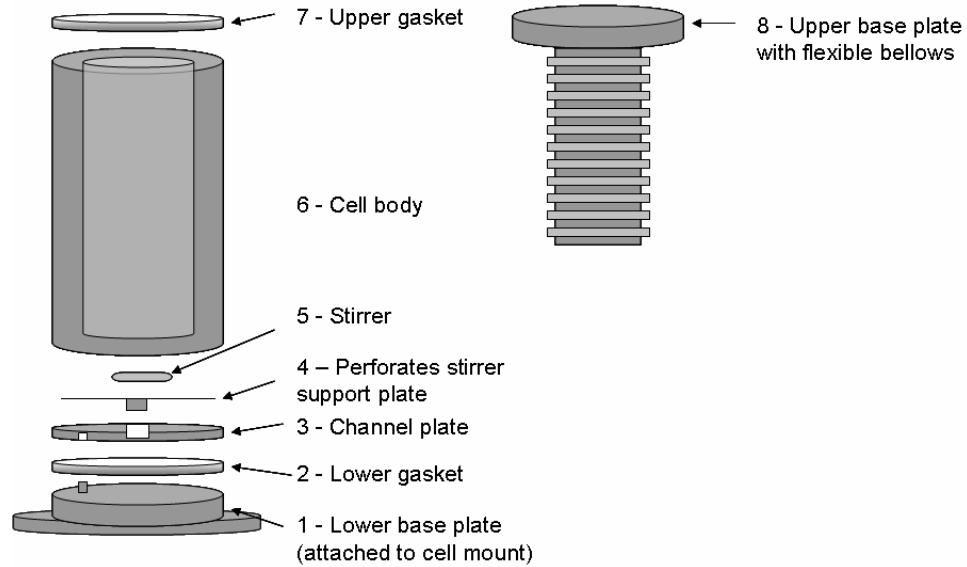


Figure 3.1 View cell assembly

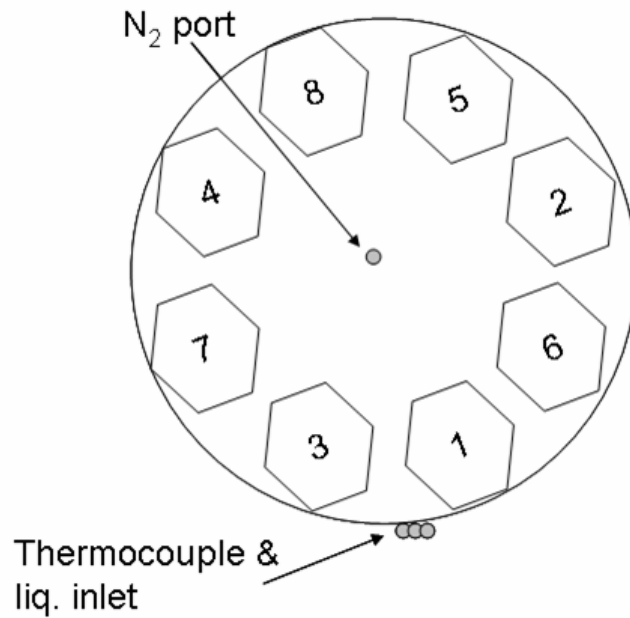


Figure 3.2 Position numbering for bolts, nuts and torque closure.

- (5) Lightly coat the bolts with molybdenum sulphide grease.
- (6) Add and finger-tighten the eight numbered sets of nuts and washers to the eight numbered bolts.
- (7) Torque each bolt in sequence, 1 to 8.

- a. For integral nickel gasket begin with a torque setting of 20 ft-lb and increase after each round by 5 ft-lb up to 55 ft-lb.
- b. For Kalrez gasket begin at 10 ft-lb and increase torque in steps of 5 ft-lb to 30 ft-lb

**Amount of solid or liquid added to view cell should occupy no more than 60 mL at room temperature and measurement conditions. The density of the material at measurement conditions should be estimated to ensure that the sample volume will not increase beyond this limit.**

### 3.3.2 Installation in Shielded Enclosure

- (1) Ensure that the magnetic stir block is installed on cell support block in the chamber.
- (2) Unscrew the cell mount from the assembly scaffold.
- (3) Transport the cell to the chamber and position over the three holes for the locking screws. The inlet ports for the cell determine the position of the view cell in the chamber. The valve and thermocouple connector should roughly face the door of the enclosure.
- (4) Secure the view cell to the cell support block.
- (5) Attach inlet lines for sample-side and bellows-side of the cells
- (6) Attach the marked thermocouple leads.
- (7) Close access door to chamber. Do not install heater furnace sections until system is tested for leaks.

### 3.3.3 Pressure testing with x-ray source on

- (1) Close valves HV1 to HV13. Leave HV14 and HV15 open.
- (2) Turn on mechanical pump
- (3) Check level of recirculating cold water in reservoir. Top up with deionized water if required. (Note: This unit sits on the shelf behind the shielded chamber).
- (4) Turn on cold water supply to wall-mounted heat exchanger. Use a modest flow rate so hose does not pop out of drain.
- (5) Turn x-ray control key (Xylon) to standby (~). Ensure access door to chamber is closed.
  - a. The x-ray source will need to be conditioned if it is being turned on for the first time today. Accept this by making the appropriate entry using the key pad.
  - b. Use key pad on control unit to enter the number of days since last use of x-ray source
  - c. Turn control key to the on position (↗)
  - d. **If the green safety circuit light is not illuminated check that the**

**access door to the chamber is closed.**

- e. Press  $\square$  1 to turn on x-ray source for conditioning. Countdown of conditioning time remaining begins
- (6) Once conditioning of the x-ray source is complete, press  $\square$  1 to turn on x-ray source. Press kV or mA to select that adjustment and use dial to set the desired value then press kV or mA to lock-in that value. Typically a value of 50 kV and 30 mA is suitable.
- (7) View x-ray image:
  - a. Turn on TV monitor
  - b. Turn on frame grabber
  - c. Turn on computer
  - d. Double-click on FS64Pro icon. Under <Acquisition> select <Live Grab> then select <Live Histogram>.
  - e. Turn on intensifier.
  - f. Use remote control to zoom and position the image within the grid pasted on the monitor.
- (8) Open HV8, HV9 and, HV10 to evacuate bellows.
- (9) Open HV4 to evacuate view cell.
- (10) Once pressure has fallen to best vacuum, close HV4 and HV8. Observe the leak rate into the view cell for 1 hour. If leak rate of view cell is acceptable, close HV9 and open HV4 and HV8 to check leak rate into bellow. If acceptable, measurements can proceed.
- (11) Turn x-ray source off by pressing  $\square$  0. **Turn the control key to standby (~), leaving cooling water on for at least 5 minutes.**

### 3.4 LOADING LIQUID SAMPLE

While the view cell system is under vacuum, a liquid sample can be loaded. This can be facilitated by use of a syringe or dip tube attached to a reservoir of the liquid.

**The x-ray source will be off for this procedure, therefore, it is important that liquid be added slowly and the pressure difference across the bellows be carefully monitored.**

- (1) HV4 and HV8 should be open and all other valves should be closed (including HV14).
- (2) Connect the pre-weighed syringe containing the liquid (or dip tube in liquid reservoir) to the inlet of HV12.
- (3) Open HV12 then open HV13 slowly so that liquid is drawn into the view cell. Close HV13 before the system begins to draw air.
- (4) Close HV12.
- (5) Detach syringe (or dip tube) and reload with liquid if required.
- (6) Repeat steps 2 to 4 as required.



- (7) Finally close HV12 and HV13.
- (8) Open HV14 slowly.
- (9) Turn off mechanical pump. Open HV11 to atmosphere then close.

### 3.5 SAMPLE CONDITIONING

Sample conditioning is required to remove air and to ensure that the sample is well mixed before the start of measurements.

**The x-ray source should be turned on for these steps.**

#### 3.5.1 Low Viscosity Liquid

- (1) HV4, HV8, HV14 and HV15 should be open and all other valves should be closed.
- (2) Turn on stirrer and set to about 600 rpm.
- (3) Turn on mechanical pump.
- (4) Turn HV10 to the “vacuum” position.
- (5) Slowly turn HV9 to the vacuum position so that pressure decreases slowly.
- (6) Evacuate the system until pressure is to equilibrium pressure for 20-30 minutes. For highly volatile samples a short period may be sufficient. Monitor the level of liquid in the view cell.
- (7) Close HV9 and HV10.
- (8) Turn off mechanical pump. Open HV11 to atmosphere then close.

#### 3.5.2 High Viscosity Liquid

- (1) HV4, HV8, HV14 and HV15 should be open and all other valves should be closed.
- (2) The sample must be heated to a sufficiently high temperature so that it can be stirred.
- (3) Start stirrer and provide suitable agitation.
- (4) Turn on mechanical pump.
- (5) Turn HV10 to the “vacuum” position.
- (6) Slowly turn HV9 to the vacuum position so that the pressure decreases slowly. Evacuate the system until pressure is at equilibrium for 20-30 minutes.

**For multi-component mixtures such as crude oils the temperature should be kept well below the initial boiling point of the sample otherwise its composition will be altered and this will affect your measurements.**

**Alternatively, the sample could be cooled to ambient before HV9 is opened to evacuate the view cell**

- (7) Evacuate the system until pressure is to equilibrium pressure for 20-30 minutes. Monitor the level of liquid in the view cell
- (8) Close HV9 and HV10.
- (9) **Homogenizing a multi-component heavy oil mixture:** It may be desirable to homogenize viscous, multi-component heavy oil mixture at the temperature at which measurements will be made.
  - a. Evacuated the view cell as outlined in the steps above.
  - b. Isolate the view cell from the vacuum pump by closing HV9 and HV10.
  - c. Heat the view cell to the maximum temperature (<340°C) while mixing and then mix at high speed for about 30 minutes.
  - d. Cool to a suitable temperature and evacuate cell and discussed above.

#### **CAUTION: KALREZ O-RINGS**

**The upper operating temperature limit for Kalrez o-rings is 300°C. Momentary excursions above this temperature are allowed but temperature should not exceed 320°C**

**Thermal cracking of crude oil become significant at 340°C and above. A significant degree of thermal cracking will alter the composition of the system and the vapour pressure curve.**

- (10) Turn off mechanical pump. Open HV11 to atmosphere then close.

### **3.6 PRESSURE MEASUREMENT**

The view cell will have been loaded with the sample and tested for leaks on high pressure and vacuum conditions. Vapor pressure and density measurements will be made at specific temperature after allowing the liquid to equilibrate at constant temperature for some time.

A good suggested strategy would be to conduct measurements as the liquid is heated from room temperature to the maximum temperature and again while it is cooling back to room temperature. This strategy may not always be convenient since the rate of cooling of the cell may be too slow. There can be a problem in cooling the cell back to room temperature for another round of measurements. For multi-component mixtures there could be hang-up of high boiling components in crevasses on the bellows and other part of the cell such that the mixture in the bottom of the cell does not have the same composition as when the first round of measurements were made. This may be a minor problem however. **The problem of liquid hang-up may be exacerbated by rapid cooling of the view cell by, for example, removing the heater sections.**

**The x-ray source should be turned on for these steps. See procedures given above.**

**The view cell should be evacuated so that the pressure in the cell is the vapour pressure of the liquid at ambient conditions.**

- (1) The view cell side and bellows side should be at vacuum conditions.
- (2) Close all valves except HV14.
- (3) Slowly bring the temperature of the view cell to the first set-point for the measurement. It is highly desirable not to overshoot the set point since cooling back to the set-point may take some time. The mixture should be continuously stirred.
- (4) As the cell is heating up, set the temperature of the pressure transducer 5°C above the set point of the view cell.
- (5) When the set-point of the view cell has been reached, monitor the temperature and pressure for 30 minutes.
- (6) Take at least two sets of vapor pressure and x-ray images (for density) spaced about 1 minute apart.
- (7) Go to the next set-point and repeat steps 3, 4 and 5.
- (8) After the highest measurement temperature has been reached take the second set of measurements either as the cell is cooled or by cooling the cell and re-heating.
- (9) After all measurements have been completed, turn off both heaters.
- (10) After cell has cooled:
  - a. Equalize pressure on both sides of the view cell by opening HV4 and HV8.
  - b. Vent cell to atmosphere.
  - c. Turn x-ray source off by pressing  $\square$  0. **Turn control key to standby (~), leaving cooling water on for at least 5 minutes.** After 5 minutes, turn control key to off position.
  - d. Turn off image intensifier.
  - e. Turn off cooling water.

- (11) **Make backup copy and transfer all saved x-ray images to computer for processing to extract density data.**
- (12) Turn off computer and frame grabber.
- (13) Remove furnace sections from view cell and disconnect cell from the manifold.
- (14) Remove cell from enclosure and bolt to assembly scaffold in the fumehood.
- (15) Disassemble cell in reverse order to the way it was assembled.
  - a. Be sure to loose the bolts in the proper order
  - b. Return nut and washers to their proper holders
  - c. Wash cell parts with toluene and allow to dry in fumehood.

### **3.7 EMERGENCY RESPONSE AND SHUT DOWN PROCEDURE**

If there is an explosion or fire, during the run and it is safe to do so:

- (1) Turn off power to furnace, if safe to do so.
- (2) Turn x-ray control key (Xylon) to standby (~)
- (3) Vacate the area and the building via the nearest exit and pull the nearest fire alarm.
- (4) Proceed to the evacuation assembly area.
- (5) Notify your supervisor.
- (6) Inform Occupational Health and Safety.

## APPENDIX I: MSDS

---

## APPENDIX 2

---

### Calibration Curve for Thermocouple

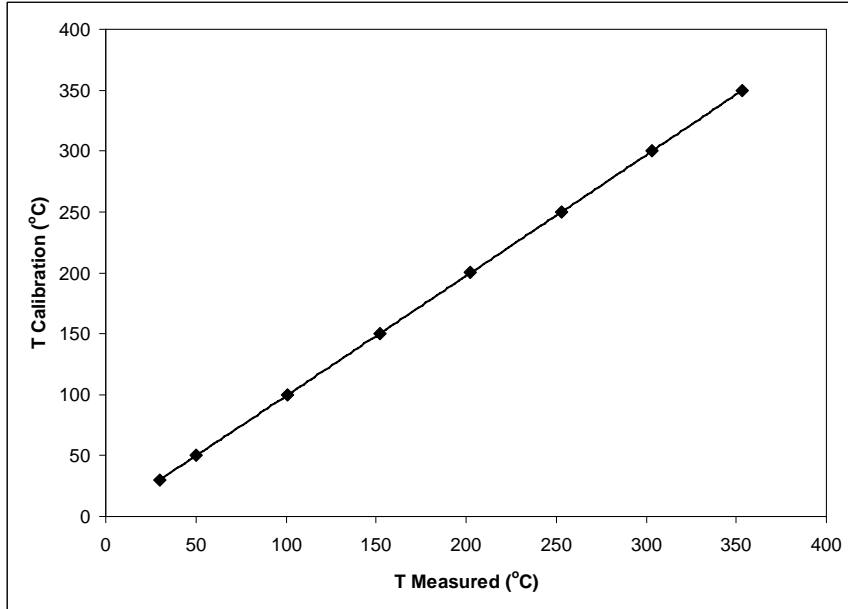


Figure A2 - 1 Calibration curve for thermocouple in the view cell.

### Calibration Curves for Pressure Transducer

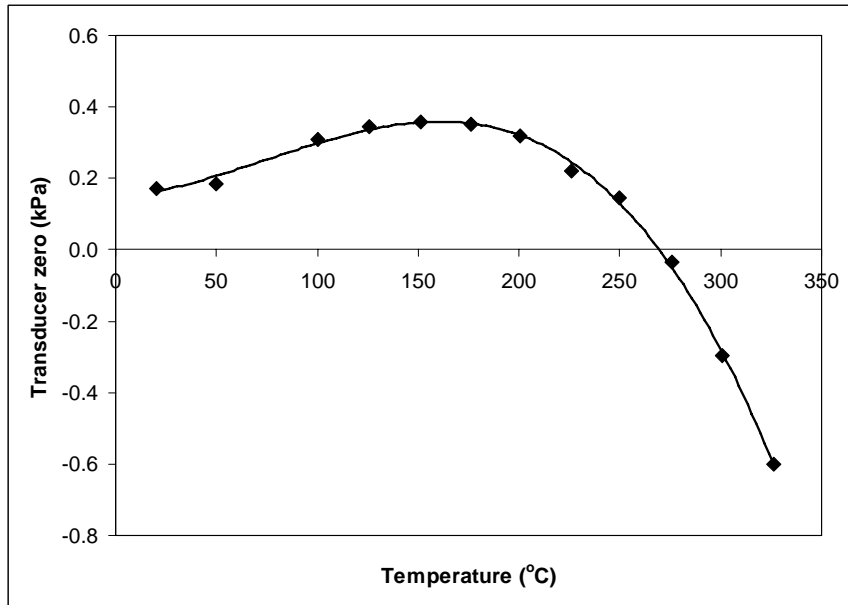


Figure A2 - 2 Zero offset of pressure transducer vs. temperature.



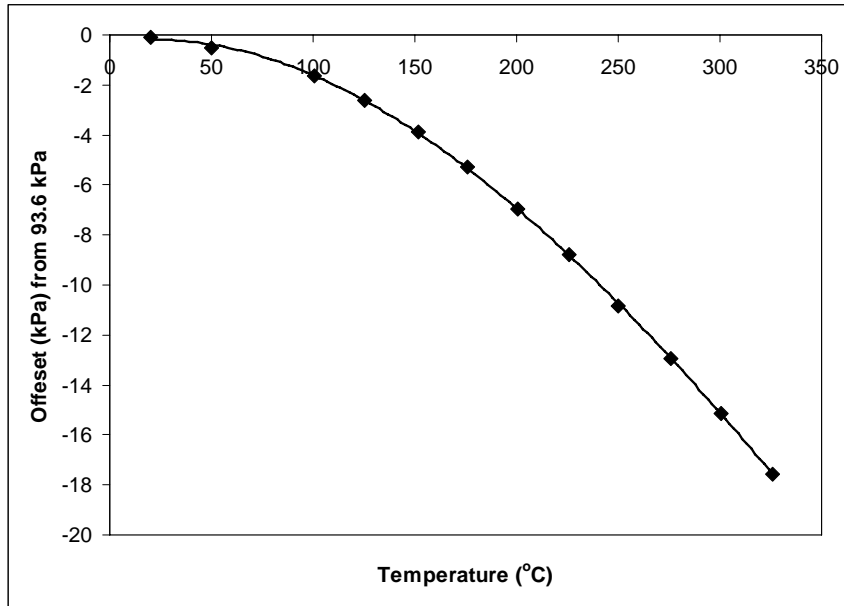


Figure A2 - 3 Offset of pressure transducer at ambient pressure vs. temperature.

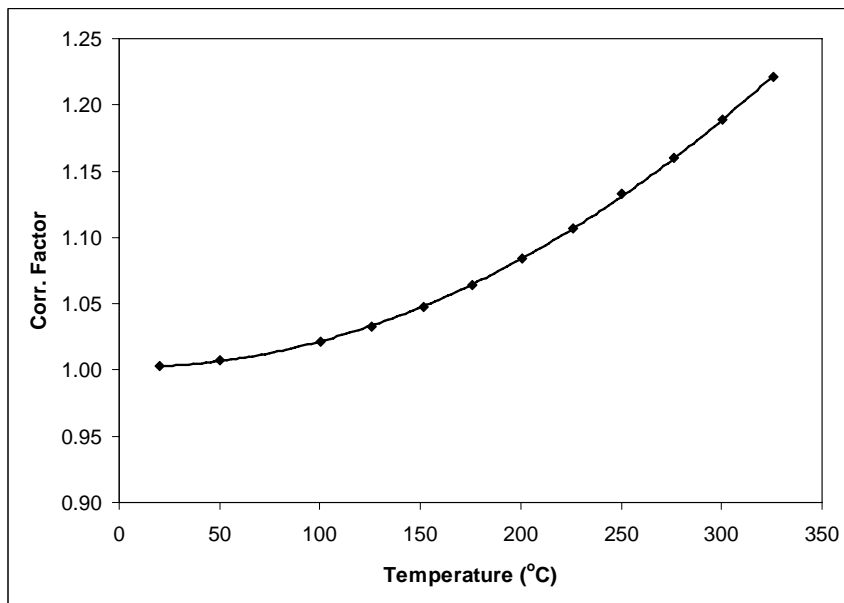


Figure A2 - 4 Correction factor for measured pressure as a function of transducer temperature.

## Volume Calibration

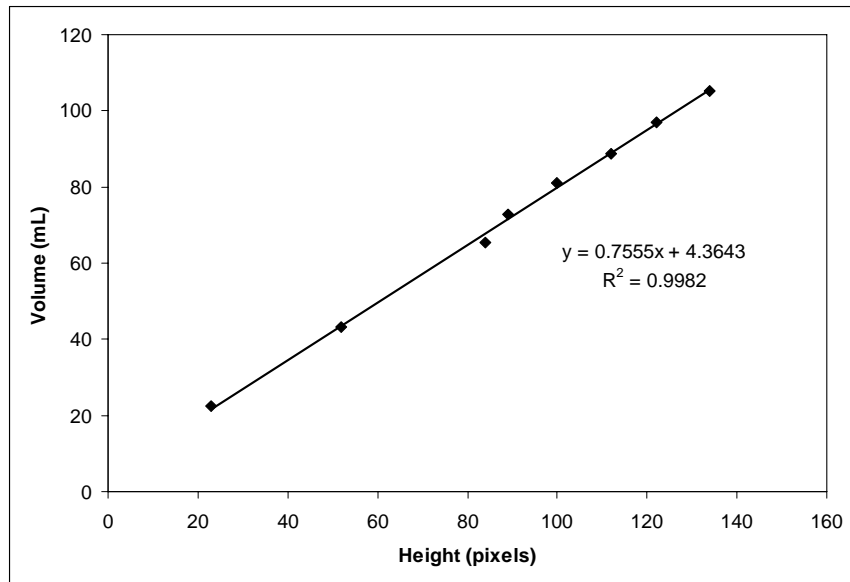


Figure A2 - 5 Volume calibration curve for x-ray view cell from 20 to 105 mL.

---

## APPENDIX 3

---

**Table A3 - 1 Coefficients for Riazi's correlations for estimating critical properties and molecular weight.**

Property	$\theta_1$	$\theta_2$	a	b	c	d	e	f
$T_c$ (K)	$T_b$ (K)	SG	35.9413	$-6.9 \times 10^{-4}$	-1.4442	$4.91 \times 10^{-4}$	0.7293	1.2771
$P_c$ (bar)	$T_b$ (K)	SG	6.9575	-0.0135	-0.3129	$9.174 \times 10^{-3}$	0.6791	-0.6807
MW (g/mole)	$T_b$ (K)	SG	42.965	$2.097 \times 10^{-4}$	-7.8712	$2.08476 \times 10^{-3}$	1/26007	4.98308

**Table A3 - 2 Programs for regression of experimental PVT data with constrained critical properties derived from Riazi-Daubert correlations.**

Matlab Program	Description
PRRD_Execute.m	Script file for PT and mass density data, initial guess for $T_b$ and SG and invoking the regression and outputting the optimized values. Values of $T_b$ and SG and PT data are passed to PR_RD.m during regression and values of liquid density are returned.
PR_RD.m	Accepts current values of $T_b$ and SG and PT data. $T_b$ and SG are used to calculate current critical properties and parameters for PR CEOS. These parameters along with PT data are in turn passed to PREOS.m which returns the current value of liquid molar density. Using the current value of molecular weight, mass density are calculated and returned to PRRD_Execute.m
PREOS.m	Accepts parameters for PR CEOS and PT data and then solves for and returns molar volume of liquid phase to PR_RD.m
rdcritical.m	Accepts $T_b$ and SG and returns critical properties and acentric factor

**Table A3 - 3 Programs for regression of experimental PVT data with constrained critical properties derived from Twu correlations.**

Matlab Program	Description
PRTwu_Execute.m	Script file for PT and mass density data, initial guess for $T_b$ and SG and invoking the regression and outputting the optimized values. Values of $T_b$ and SG and PT data are passed to PR_Twu.m during regression and values of liquid density are returned.
PR_Twu.m	Accepts current values of $T_b$ and SG and PT data. $T_b$ and SG are used to calculate current critical properties and parameters for PR CEOS. These parameters along with PT data are in turn passed to PREOS.m which returns the current value of liquid molar density. Using the current value of molecular weight, mass density are calculated and returned to PRTwu_Execute.m
PREOS.m	Accepts parameters for PR CEOS and PT data and then solves for and returns molar volume of liquid phase to PR_Twu.m
twucritical.m	Accepts $T_b$ and SG and returns critical properties and acentric factor
Twutheta.m	Returns a function to twucritical.m and PR_Twu.m that must be solved in order to calculate critical properties

### PRRD Execute.m

```
% Script file to regress PVT data to estimate critical properties.  
% Riazi-Daubert's correlation is used to constrain Tc,Pc, MW.  
% Acentric factor is constrained by the correlation of Ambrose.  
% An initial guess for Tb and SG are required
```

```
% Clear all variables from workspace  
clear
```

```
% Measured density (g/mL):  
% Yin is a Nx1 matrix of responses
```

```
% ABVB data
```

```
Y = [0.9307;
```

```
0.9230;
```

```
0.9154;
```

```
0.9080;
```

```
0.9007;
```

```
0.9007;
```

```
0.8863;
```

```
0.8725;
```

```
0.8657;
```

```
0.8590;
```

```
0.8525;
```

```
0.8460;
```

```
0.9307;
```

```
0.9080;
```

```
0.9007;
```

```
0.9007;
```

```
0.8863;
```

```
0.8863;
```

```
0.8794;
```

```
0.8725;
```

```
0.8657;
```

```
0.8590;
```

```
0.8525;
```

```
0.8460
```

```
];
```

```
% Independent variables (experimental data) for calculating density are  
% are vapour pressure (kPa) (first column) and temperature in C (second  
% column).
```

```
% ABVB data
```

```
Xin = [0.52203 148.11
```

```
1.20670 162.05;
```

```

1.63390 175.70;
2.34531 191.06;
2.88615 204.75;
3.51665 218.81;
4.50847 234.45;
6.03616 248.17;
7.58394 262.37;
10.33700 276.26;
14.52598 290.23;
20.11171 296.83;
0.80405 155.78;
1.11919 169.48;
1.52992 185.69;
2.09031 200.82;
2.74722 215.61;
3.20012 220.31;
4.08018 231.99;
4.97212 244.76;
6.23190 260.99;
8.17774 273.51;
11.16956 286.36;
15.33125 297.01
];

```

```

% Convert pressure in kPa to Pa

```

```

X(:,1) = 1000*Xin(:,1);

```

```

% Convert temperature from C to K

```

```

X(:,2) = (Xin(:,2) + 273.15);

```

```

% Initial guesses for fluid parameters B(Tb(C); SG:

```

```

% B is a 2x1 matrix of parameters to fit

```

```

Bin = [250.0; 0.85];

```

```

B(1) = (Bin(1) + 273.15); % Temperature in Kelvin

```

```

B(2) = 1000*Bin(2);

```

```

% Options for nlinfit

```

```

options = statset('MaxIter', 100000, 'TolFun', 1e-12, 'ToIX', 1e-12);

```

```

% Run least squares parameter fit:

```

```

[Bfit,Residual,Jacobian] = nlinfit(X,Y,@PR_RD,B, options);

```

```

% Estimate 95% confidence interval for fit:

```

```

CI = nlparci(Bfit,Residual,Jacobian);

```

```

% Plot data with 95% confidence limits:

```

```

%nlintool(X,Y,@PR2_Press,B)

% Model predictions
Ymod = PR_RD(Bfit,X);
Y;

% Sum residuals of absolute relative error
Tare = sum(abs(Y - Ymod)./Y);

%Gas constant
Rg = 8.314472; % Gas constant 8.31447 (m3_Pa/mole_K) from NIST
(http://physics.nist.gov/cuu/Constants/index.html)

% Plotting the results
% V from model for plotting
Ymod = PR_RD(Bfit,X);

%Maximum and minimum for plot
xmini = min(Ymod);
xmaxi = max(Ymod);
ymini = min(Y);
ymaxi = max(Y);

maxi = [xmaxi ymaxi];
mini = [xmini ymini];

smaxi = max(maxi);
smini = min(mini);

% Bold axes
axes('FontWeight','bold','FontSize', 14);

% Plot data and calculations
% Ranges for individual curves:
k = plot(Ymod,Y,'bo','MarkerFaceColor','auto');

set(k, 'Markersize', 10);

% Ranges for axes so that plot is square:
axis([smini smaxi smini smaxi]);

% Label for axes:
L = xlabel('Density - Model (g/mL)');
m = ylabel('Density - Measd. (g/mL)');
set(L,'FontWeight','bold','FontSize', 16);
set(m,'FontWeight','bold','FontSize', 16);

```

```
q = title('Regression of ABVB Density Constrained by Riazi Critical Properties');
set (q,'FontWeight', 'bold','FontSize', 15);
```

```
% Optimum Tb (K) and SG
```

```
Bfit = abs(Bfit);
```

```
Tb = Bfit(1);
```

```
SG = Bfit(2)/1000;
```

```
%Calculate critical properties from optimized Tb and SG
```

```
crit = rdcritical(Tb,SG);
```

```
Tc = crit(1);
```

```
Pc = crit(2)/1000; % Pc in kPa
```

```
omega = crit(3);
```

```
MW = crit(4);
```

```
Vc = crit(5);
```

```
% Calculated ac and b from optimized Tb and SG :
```

```
ac = 0.45723553*Rg^2*Tc^2/(Pc*1000);
```

```
b = 0.07779607*Rg*Tc/(Pc*1000);
```

```
% Optimum properties
```

```
Op = [Tc;Pc;Vc;omega;MW;ac;b;Tb;SG];
```

```
% Calculate critical properties from 95% confidence limits Tb and SG
```

```
CI = abs(CI);
```

```
Tb1 = CI(1,1);
```

```
Tb2 = CI(1,2); % Tb must be in R
```

```
SG1 = CI(2,1)/1000; % Correction for scaling
```

```
SG2 = CI(2,2)/1000; % Correction for scaling
```

```
% Tb must be in Kelvin
```

```
crit1 = rdcritical(Tb1,SG1); %95% limits for Tc (K), Pc (Pa), omega and MW
```

```
crit2 = rdcritical(Tb2,SG2);
```

```
crit1(2) = crit1(2)/1000; %Pc in kPa
```

```
crit2(2) = crit2(2)/1000; %Pc in kPa
```

```
CIcrit = [crit1 crit2]; % concatenate 95% limits for Tc, Pc (Pa), omega and MW
```

```
ac1 = 0.45723553*Rg^2*crit1(1)^2/(crit1(2)*1000); % Note that Pc is in Pa for these equations
```

```
b1 = 0.07779607*Rg*crit1(1)/(crit1(2)*1000);
```

```
ac2 = 0.45723553*Rg^2*crit2(1)^2/(crit2(2)*1000);
```

```
b2 = 0.07779607*Rg*crit2(1)/(crit2(2)*1000);
```

```
CIab = [ac1 ac2; b1 b2]; % 95% limits for ac and b
```



CI(1,1:2) = CI(1,1:2); % 95% limits for Tb in K

CI(2,1:2) = CI(2,1:2)/1000; % Correction for scaling

CIprop = [CIcrit; CIab; CI]; % Concatenate 95% confidence limit Tb and SG with those for critical properties

% Format output

format long e

'Calculated values for Tc(K), Pc(kPa), Vc (m3/mole), omega and MW(g/mole), ac(J/m3/mole2) and b(m3/mole) and optimum Tb(K) and SG'

Op

'95% confidence interval for calculated Tc(K), Pc(kPa), omega and MW(g/mole), Vc(m3/mole), ac (J/m3/mole2), b (m3/mole), Tb(K) and SG'

CIprop

'Sum absolute relative error'

Tare

Y

Ymod

---

### **PR\_RD.m**

function YY = PR\_RD(B,X)

% This function provides the equation to which parameters for ABVB will be fitted using PR EOS.

% The function is generic in that different mixing rules can be employed.

% Riazi-Daubert's correlation is used to limit Tc,Pc, MW and omega when Tb and SG are specified.

%

% X is a matrix containing the following parameters:

% d - liquid phase density (kg/m3)

% T - Temperature (K)

%

% B is a matrix of the parameters to be fitted:

% Tb - Boiling point in Kelvin

% S.G. - Specific gravity \* 1000 at 15.6C

%

% Correlations developed by Riazi and Daubert are used to compute critical properties from Tb and S.G.:

% b - Co-volume of oil (m3/mole)

% a - Attractive parameter for oil (J-m3/mole2)

% MW - Molar mass of oil (g/mole)

```

%    omega - acentric factor for oil

% Gas constant (J/mole-K)
Rg = 8.314472; % Gas constant 8.31447 (m3_Pa/mole_K) from NIST
(http://physics.nist.gov/cuu/Constants/index.html)

% Oil parameters
Tb = abs(B(1));
SG = abs(B(2)/1000);

% Experimental data:
P = X(:,1);
T = X(:,2);

% Tc, Pc and MW from Riazi and Daubert
Tc = 35.9413*(exp(-6.9e-4*Tb - 1.4442*SG + 4.91e-4*Tb*SG))*Tb^0.7293*SG^1.2771; % T in
Kelvin
Pc = 6.9575*(exp(-1.35e-2*Tb - 0.3129*SG + 9.174e-3*Tb*SG))*Tb^0.6791*SG^-0.6807; % Pc
in bars
MW = 42.965*(exp(2.097e-4*Tb - 7.78712*SG + 2.08476e-
3*Tb*SG))*Tb^1.26007*SG^4.98308;
% MW = 170.335; % True MW for n-dodecane

% Compute omega from Tc, Pc and Tb using method of Ambrose
omega = -(log(Pc) + ((-5.97616*(1-Tb/Tc)+1.29874*(1-Tb/Tc)^1.5 -0.60394*(1-Tb/Tc)^2.5-
1.06841*(1-Tb/Tc)^5)/((Tb/Tc))))/((-5.03365*(1-Tb/Tc)+1.11505*(1-Tb/Tc)^1.5 -
5.41217*(1-Tb/Tc)^2.5-7.46628*(1-Tb/Tc)^5)/((Tb/Tc)));

Pc = 1e5*Pc; % Pc in Pa

% Oil parameters
b = 0.07779607*Rg*Tc/Pc;
ac = 0.45723553*Rg^2*Tc^2/Pc;

if omega < 0.491;
    m = 0.37464 + 1.54226*omega - 0.26992*omega^2;
else
    m = 0.379642 + 1.48503*omega - 0.164423*omega^2 + 0.016666*omega^3;
end

alpha = (1 + m*(1-(T./Tc).^0.5)).^2;
a = ac*alpha;

% No mixing rules required for single component

% PR EOS for density
% From measured P and T compute molar volumes

```

```

V = [];
for j = 1:length(P)
    Pj = P(j);
    Tj = T(j);
    aj = a(j);
    V(j,1) = PREOS(aj,b,Pj,Tj);
end
YY = (MW./V)*1e-6;

end

```

---

### **PREOS.m**

```

function Vj = PREOS(aj,b,Pj,Tj)

% Solve PR EOS for a pure fluid.

% Gas constant 8.31447(J/mole/K):
R = 8.3143;

% Solution for a PR-EOS
A = aj*Pj/(R^2*Tj^2);
B = b*Pj/(R*Tj);

c(1) = 1; % coeff for Z^3
c(2) = -(1-B); % a2, coeff for Z^2
c(3) = A-3*B^2-2*B; %a1, coeff for Z^1
c(4) = -(A*B-B^2-B^3); % a0, coeff for Z^0

% Solution method 1
Z = roots(c); % Solve for roots of CEOS

% Find real roots for case where R>0
Zss = [];
m = length(Z);

    for w = 1:m
        v(w,1) = isreal(Z(w,1));
        if v(w,1) == 1
            Zss = [Zss;Z(w,1)];
        end
    end

Zs = [];
m = length(Zss);

```

```

for w = 1:m
    if Zss(w,1) > 0
        Zs= [Zs;Zss(w,1)];
    end
end

% Select smallest Z as liquid root
Zliq = min(Zs);
Vj = Zliq*R*Tj/Pj; % Molar volume of liquid phase

end

```

---

### **rdcritical.m**

```

function f = rdcritical(Tb,SG)

% Tc and Pc from Riazi; MW by API method
Tc = 35.9413*(exp(-6.9e-4*Tb - 1.4442*SG + 4.91e-4*Tb*SG))*Tb^0.7293*SG^1.2771; % T in Kelvin
Pc = 6.9575*(exp(-1.35e-2*Tb - 0.3129*SG + 9.174e-3*Tb*SG))*Tb^0.6791*SG^-0.6807; % Pc in bars
Vc = 6.1677e4*(exp(-7.583e-3*Tb - 28.5524*SG + 0.01172*Tb*SG))*Tb^1.20493*SG^17.2074; % Vc in m3/mol
MW = 42.965*(exp(2.097e-4*Tb - 7.78712*SG + 2.08476e-3*Tb*SG))*Tb^1.26007*SG^4.98308;
% MW = 170.335; % True MW for n-dodecane

% Compute omega from Tc, Pc and Tb using method of Ambrose
omega = -(log(Pc) + ((-5.97616*(1-Tb/Tc)+1.29874*(1-Tb/Tc)^1.5 -0.60394*(1-Tb/Tc)^2.5-1.06841*(1-Tb/Tc)^5)/((Tb/Tc))))/((-5.03365*(1-Tb/Tc)+1.11505*(1-Tb/Tc)^1.5 -5.41217*(1-Tb/Tc)^2.5-7.46628*(1-Tb/Tc)^5)/((Tb/Tc)));

Pc = 1e5*Pc; % Pc in Pa

f = [Tc;
Pc;
omega;
MW;
Vc];

```

---

### PRTwu\_ Execute.m

```
% Script file to regress PVT data to estimate critical properties.
% Twu's correlation is used to constrain Tc,Pc, MW.
% Acentric factor is constrained by the correlation of Ambrose.
% An initial guess for Tb and SG are required

% Clear all variables from workspace
clear

% Measured density (g/mL):
% Yin is a Nx1 matrix of responses

% ABVB data
Y = [0.9307;
0.9230;
0.9154;
0.9080;
0.9007;
0.9007;
0.8863;
0.8725;
0.8657;
0.8590;
0.8525;
0.8460;
0.9307;
0.9080;
0.9007;
0.9007;
0.8863;
0.8863;
0.8794;
0.8725;
0.8657;
0.8590;
0.8525;
0.8460
];

% Independent variables (experimental data) for calculating density are
% are vapour pressure (kPa) (first column) and temperature in C (second
% column).

% ABVB data
Xin = [0.52203 148.11
1.20670 162.05;
```

```

1.63390 175.70;
2.34531 191.06;
2.88615 204.75;
3.51665 218.81;
4.50847 234.45;
6.03616 248.17;
7.58394 262.37;
10.33700 276.26;
14.52598 290.23;
20.11171 296.83;
0.80405 155.78;
1.11919 169.48;
1.52992 185.69;
2.09031 200.82;
2.74722 215.61;
3.20012 220.31;
4.08018 231.99;
4.97212 244.76;
6.23190 260.99;
8.17774 273.51;
11.16956 286.36;
15.33125 297.01
];

```

```

% Convert pressure in kPa to Pa

```

```

X(:,1) = 1000*Xin(:,1);

```

```

% Convert temperature from C to K

```

```

X(:,2) = (Xin(:,2) + 273.15);

```

```

% Initial guesses for fluid parameters B(Tb(C); SG):

```

```

% B is a 2x1 matrix of parameters to fit

```

```

Bin = [250.0; 0.85];

```

```

B(1) = 1.8*(Bin(1) + 273.15); % Temperature in Rankin

```

```

B(2) = 1000*Bin(2);

```

```

% Options for nlinfit

```

```

options = statset('MaxIter', 100000, 'TolFun', 1e-12, 'TolX', 1e-12);

```

```

% Run least squares parameter fit:

```

```

[Bfit,Residual,Jacobian] = nlinfit(X,Y,@PR_Twu,B, options);

```

```

% Estimate 95% confidence interval for fit:

```

```

CI = nlparci(Bfit,Residual,Jacobian);

```

```

% Plot data with 95% confidence limits:
%nlintool(X,Y,@PR2_Press,B)

% Model predictions
Ymod = PR_Twu(Bfit,X);
Y;

% Sum residuals of absolute relative error
Tare = sum(abs(Y - Ymod)./Y);

%Gas constant
Rg = 8.314472; % Gas constant 8.31447 (m3_Pa/mole_K) from NIST
(http://physics.nist.gov/cuu/Constants/index.html)

% Plotting the results
%V from model for plotting
Ymod = PR_Twu(Bfit,X);

%Maximum and minimum for plot
xmini = min(Ymod);
xmaxi = max(Ymod);
ymini = min(Y);
ymaxi = max(Y);

maxi = [xmaxi ymaxi];
mini = [xmini ymini];

smaxi = max(maxi);
smini = min(mini);

% Bold axes
axes('FontWeight','bold','FontSize', 14);

% Plot data and calculations
% Ranges for individual curves:
k = plot(Ymod,Y,'bo','MarkerFaceColor','auto');

set(k, 'Markersize', 10);

% Ranges for axes so that plot is square:
axis([smini smaxi smini smaxi]);

% Label for axes:
L = xlabel('Density - Model (g/mL)');
m = ylabel('Density - Measd. (g/mL)');
set(L,'FontWeight','bold','FontSize', 16);

```

```

set (m,'FontWeight', 'bold','FontSize', 16);

q = title('Regression of ABVB Density Constrained by Twu Critical Properties');
set (q,'FontWeight', 'bold','FontSize', 15);

% Optimum Tb (R) and SG
Bfit = abs(Bfit);
Tb = Bfit(1);
SG = Bfit(2)/1000;

%Calculate critical properties from optimized Tb and SG
crit = twucritical(Tb,SG);
Tc = crit(1);
Pc = crit(2)/1000; % Pc in kPa
omega = crit(3);
MW = crit(4);
Vc = crit(5);

% Calculated ac and b from optimized Tb and SG :
ac = 0.45723553*Rg^2*Tc^2/(Pc*1000);
b = 0.07779607*Rg*Tc/(Pc*1000);

% Optimized Tb output in K
Tb = Tb/1.8;

% Optimum properties
Op = [Tc;Pc;Vc;omega;MW;ac;b;Tb;SG];

% Calculate critical properties from 95% confidence limits Tb and SG
CI = abs(CI);
Tb1 = CI(1,1);
Tb2 = CI(1,2); % Tb must be in R
SG1 = CI(2,1)/1000; % Correction for scaling
SG2 = CI(2,2)/1000; % Correction for scaling

% Tb must be in R
crit1 = twucritical(Tb1,SG1); %95% limits for Tc (K), Pc (Pa), omega and MW
crit2 = twucritical(Tb2,SG2);

crit1(2) = crit1(2)/1000; %Pc in kPa
crit2(2) = crit2(2)/1000; %Pc in kPa

CIcrit = [crit1 crit2]; % concatenate 95% limits for Tc, Pc (Pa), omega and MW

ac1 = 0.45723553*Rg^2*crit1(1)^2/(crit1(2)*1000); % Note that Pc is in Pa for these
equations
b1 = 0.07779607*Rg*crit1(1)/(crit1(2)*1000);

```



```
ac2 = 0.45723553*Rg^2*crit2(1)^2/(crit2(2)*1000);
b2 = 0.07779607*Rg*crit2(1)/(crit2(2)*1000);
```

```
CIab = [ac1 ac2; b1 b2]; % 95% limits for ac abd b
```

```
CI(1,1:2) = CI(1,1:2)/1.8; % 95% limits for Tb in K
CI(2,1:2) = CI(2,1:2)/1000; % Correction for scaling
```

```
CIprop = [CIcrit; CIab; CI]; %Concatenate 95% confidence limit Tb and SG with those for
critical properties
```

```
% Format output
format long e
```

```
'Calculated values for Tc(K), Pc(kPa), Vc (m3/mole), omega and MW(g/mole),
ac(J/m3/mole2) and b(m3/mole) and optimum Tb(K) and SG'
Op
```

```
'95% confidence interval for calculated Tc(K), Pc(kPa), omega and MW(g/mole),
Vc(m3/mole), ac (J/m3/mole2), b (m3/mole), Tb(K) and SG'
CIprop
```

```
'Sum absolute relative error'
Tare
```

```
Y
Ymod
```

---

### PR\_Twu.m

```
function YY = PR_Twu(B,X)
% This function provides the equation to which parameters for ABVB will be fitted
using PR EOS.
% The function is generic in that different mixing rules can be employed.
% Twu's correlation is used to limit Tc,Pc, MW and omega when Tb and SG are
specified.
%
% X is a matrix containing the following parameters:
%   d - liquid phase density (kg/m3)
%   T - Temperature (K)
%
% B is a matrix of the parameters to be fitted:
%   Tb - Boiling point in Rankin
%   S.G. - Specific gravity * 1000 at 15.6C
%
% Correlations developed by Twu are used to compute critical properties
```

```

% from Tb and S.G.:
%   b - Co-volume of oil (m3/mole)
%   a - Attractive parameter for oil (J-m3/mole2)
%   MW - Molar mass of oil (g/mole)
%   omega - acentric factor for oil

% Gas constant (J/mole-K)
Rg = 8.314472; % Gas constant 8.31447 (m3_Pa/mole_K) from NIST
(http://physics.nist.gov/cuu/Constants/index.html)

% Oil parameters
Tb = abs(B(1));
SG = abs(B(2)/1000);

% Experimental data:
P = X(:,1);
T = X(:,2);

% First compute reference properties for n-alkane with Tb and S.G.
Tco = Tb*(0.533272 + 0.191017*1e-3*Tb + 0.779681*1e-7*Tb^2 - 0.284376*1e-10*Tb^3 +
0.959468*1e28/Tb^13)^-1;
alpha = 1-(Tb/Tco);
Vco = (1-(0.419869 - 0.505839*alpha - 1.56436*alpha^3 - 9481.70*alpha^14))^-8;
SGo = 0.843593 - 0.128624*alpha - 3.36159*alpha^3 - 13749.5*alpha^12;

% Need to iterate for MWo
MW0 = Tb/(10.44 - 0.0052*Tb);
theta0 = log(MW0);
options=optimset('Display','off');
[theta,fval] = fsolve(@(theta) Twutheta(theta,Tb),theta0,options);
MWo = exp(theta);

Pco = (3.83354 + 1.19629*alpha^0.5 + 34.8888*alpha + 36.1952*alpha^2 +
104.193*alpha^4)^2;

% Use reference values for n-alkane to compute properties for fluid
dSGT = exp(5*(SGo - SG))-1;
fT = dSGT*(-0.362456/Tb^0.5 + (0.0398285 - 0.948125/Tb^0.5)*dSGT);
Tcr = Tco*((1 + 2*fT)/(1-2*fT))^2; % Tc in Rankin
Tc = Tcr/1.8;

dSGV = exp(4*(SGo^2 - SG^2))-1;
fV = dSGV*(0.466590/Tb^0.5 +(-0.182421 + 3.01721/Tb^0.5)*dSGV);
Vcf = Vco*((1 + 2*fV)/(1-2*fV))^2; % Vc in ft3/lb/mole
Vc = Vcf/(35.314666721*453.592370000) ;

dSGP = exp(0.5*(SGo - SG))-1;

```

```

fP = dSGP*((2.53262 - 46.1955/Tb^0.5 - 0.00127885*Tb) +(-11.4277 + 252.140/Tb^0.5 +
0.00230535*Tb)*dSGP);
Pcp = Pco*(Tcr/Tco)*(Vco/Vcf)*((1 + 2*fP)/(1 - 2*fP))^2; % Pc in psia
Pc = Pcp*6894.757293168;

dSGM = dSGT;
x = abs(0.0123420 - 0.328086/Tb^0.5);
fM = dSGM*(x +(-0.0175691 + 0.193168/Tb^0.5)*dSGM);
MW = exp(log(MWo)*((1 + 2*fM)/(1-2*fM))^2); % MW in lb/lb-mol = g/g-mol
% MW = 170.335; % True MW for n-dodecane

% Compute omega from Tc, Pc and Vc using method of Ambrose
omega =-(log(Pc*0.986923266716E-05) +((-5.97616*(1-(Tb/1.8)/Tc)+1.29874*(1-
(Tb/1.8)/Tc)^1.5 -0.60394*(1-(Tb/1.8)/Tc)^2.5-1.06841*(1-
(Tb/1.8)/Tc)^5)/((Tb/1.8)/Tc)))/((-5.03365*(1-(Tb/1.8)/Tc)+1.11505*(1-
(Tb/1.8)/Tc)^1.5 -5.41217*(1-(Tb/1.8)/Tc)^2.5-7.46628*(1-
(Tb/1.8)/Tc)^5)/((Tb/1.8)/Tc));

% Oil parameters
b = 0.07779607*Rg*Tc/Pc;
ac = 0.45723553*Rg^2*Tc^2/Pc;

if omega < 0.491;
    m = 0.37464 + 1.54226*omega - 0.26992*omega^2;
else
    m = 0.379642 + 1.48503*omega - 0.164423*omega^2 + 0.016666*omega^3;
end

alpha = (1 + m*(1-(T./Tc).^0.5)).^2;
a = ac*alpha;

% No mixing rules required for single component

% PR EOS for density
% From measured P and T compute molar volumes
V = [];
for j = 1:length(P)
    Pj = P(j);
    Tj = T(j);
    aj = a(j);
    V(j,1) = PREOS(aj,b,Pj,Tj);
end
YY = (MW./V)*1e-6;
YY;
end

```

## twucritical.m

function f = twucritical(Tb,SG)

% First compute reference properties for n-alkane with Tb and S.G.

Tco = Tb\*(0.533272 + 0.191017\*1e-3\*Tb + 0.779681\*1e-7\*Tb^2 - 0.284376\*1e-10\*Tb^3 + 0.959468\*1e28/Tb^13)^-1;

alpha = 1-(Tb/Tco);

Vco = (1-(0.419869 - 0.505839\*alpha - 1.56436\*alpha^3 - 9481.70\*alpha^14))^-8;

SGo = 0.843593 - 0.128624\*alpha - 3.36159\*alpha^3 - 13749.5\*alpha^12;

% Need to iterate for MWo

MW0 = Tb/(10.44 - 0.0052\*Tb);

theta0 = log(MW0);

options=optimset('Display','off');

[theta,fval] = fsolve(@(theta) Twutheta(theta,Tb),theta0,options);

MWo = exp(theta);

Pco = (3.83354 + 1.19629\*alpha^0.5 + 34.8888\*alpha + 36.1952\*alpha^2 + 104.193\*alpha^4)^2;

% Use reference values for n-alkane to compute properties for fluid

dSGT = exp(5\*(SGo - SG))-1;

fT = dSGT\*(-0.362456/Tb^0.5 + (0.0398285 - 0.948125/Tb^0.5)\*dSGT);

Tcr = Tco\*((1 + 2\*fT)/(1-2\*fT))^2; % Tc in Rankin

Tc = Tcr/1.8; % Tc in K

dSGV = exp(4\*(SGo^2 - SG^2))-1;

fV = dSGV\*(0.466590/Tb^0.5 + (-0.182421 + 3.01721/Tb^0.5)\*dSGV);

Vcf = Vco\*((1 + 2\*fV)/(1-2\*fV))^2; % Vc in ft<sup>3</sup>/lb/mole

Vc = Vcf/(35.314666721\*453.592370000); % Vc in m<sup>3</sup>/mole

dSGP = exp(0.5\*(SGo - SG))-1;

fP = dSGP\*((2.53262 - 46.1955/Tb^0.5 - 0.00127885\*Tb) + (-11.4277 + 252.140/Tb^0.5 + 0.00230535\*Tb)\*dSGP);

Pcp = Pco\*(Tcr/Tco)\*(Vco/Vcf)\*((1 + 2\*fP)/(1 - 2\*fP))^2; % Pc in psia

Pc = Pcp\*6894.757293168; % Pc in Pa

dSGM = dSGT;

x = abs(0.0123420 - 0.328086/Tb^0.5);

fM = dSGM\*(x + (-0.0175691 + 0.193168/Tb^0.5)\*dSGM);

MW = exp(log(MWo)\*((1 + 2\*fM)/(1-2\*fM))^2); % MW in lb/lb-mol = g/g-mol

% MW = 170.335; % True MW for n-dodecane

% Compute omega from Tc, Pc and Vc using method of Ambrose

```

omega =-(log(Pc*0.986923266716E-05) +((-5.97616*(1-(Tb/1.8)/Tc)+1.29874*(1-
(Tb/1.8)/Tc)^1.5 -0.60394*(1-(Tb/1.8)/Tc)^2.5-1.06841*(1-
(Tb/1.8)/Tc)^5)/(((Tb/1.8)/Tc)))/((-5.03365*(1-(Tb/1.8)/Tc)+1.11505*(1-
(Tb/1.8)/Tc)^1.5 -5.41217*(1-(Tb/1.8)/Tc)^2.5-7.46628*(1-
(Tb/1.8)/Tc)^5)/(((Tb/1.8)/Tc)));

```

```

f = [Tc;
Pc;
omega;
MW;
Vc];
end

```

---

### **Twutheta.m**

```

function f = Twutheta(theta,Tb)
% Function to solve for theta in Twu's correlation for MW of heavy hydrocarbons
% Called within PR_Twu and twucritical

f = (exp(5.71419 + 2.71579*theta - 0.286590*theta^2 - 39.8544/theta - 0.122488/theta^2) -
24.7522*theta + 35.3155*theta^2) - Tb;

end

```

---

## APPENDIX 4

---

**Table A4 - 1 Compositions of molecules representing fractions 1 to 6 from Shermata and coworkers.**

Fraction #	Molecule #	Mole fraction %	MW (g/mol)	# of atoms					Density (g/mL)
				C	H	N	S	O	
fraction 1	1	30.44	474.89	34	66	0	0	0	0.8412
	2	20.03	597.06	39	64	0	2	0	1.0339
	3	19.80	480.85	35	60	0	0	0	0.8608
	4	12.51	554.89	37	46	0	2	0	1.0787
	5	12.34	770.18	57	71	1	0	0	1.1162
	6	4.88	749.27	53	80	0	1	0	0.9449
fraction 2	1	37.10	687.20	48	78	0	1	0	0.9410
	2	23.42	1082.76	75	103	1	2	0	1.1334
	3	17.18	719.28	50	86	0	1	0	0.9298
	4	11.22	512.83	36	48	0	1	0	0.9904
	5	11.10	985.81	71	132	0	0	0	0.8482
	6	0.01	1294.31	94	164	0	0	0	0.8582
fraction 3	1	64.80	629.08	44	68	0	1	0	0.9544
	2	13.71	720.17	48	65	1	2	0	1.2568
	3	8.40	985.81	71	132	0	0	0	0.8482
	4	7.69	692.22	47	81	1	1	0	1.1698
	5	4.70	1075.81	75	110	0	2	0	0.9745
	6	0.75	561.04	38	72	0	1	0	0.9351
fraction 4	1	29.70	878.43	62	87	1	1	0	1.1314
	2	24.99	925.55	64	92	0	2	0	0.9918
	3	16.92	701.22	49	80	0	1	0	0.9389
	4	13.12	641.09	45	68	0	1	0	0.9559
	5	9.49	891.51	59	86	0	3	0	1.0493
	6	5.77	703.18	52	78	0	0	0	0.8799
fraction 5	1	40.03	800.31	56	81	1	1	0	1.1513
	2	22.40	799.39	54	86	0	2	0	0.9957
	3	14.20	1171.98	82	122	0	2	0	0.9651
	4	12.99	951.58	66	94	0	2	0	0.9900
	5	10.37	1161.88	80	104	0	3	0	1.0242
	6	0.01	1021.72	71	104	0	2	0	0.9795
fraction 6	1	44.15	762.25	51	71	1	2	0	1.2336
	2	38.00	979.64	68	98	0	2	0	0.9856
	3	11.16	1061.73	79	112	0	0	0	0.8874
	4	4.81	1298.15	94	136	0	1	0	0.9226
	5	1.59	1217.96	82	104	0	4	0	1.0610
	6	0.29	1285.09	90	125	1	2	0	1.0940

**Table A4 - 2 Compositions of molecules representing fractions 7 to 10 Shermata and coworkers.**

Fraction #	Molecule #	Mole fraction %	MW (g/mol)	# of atoms					Density (g/mL)
				C	H	N	S	O	
fraction 7	1	63.77	1347.23	92	131	1	3	0	1.1180
	2	19.08	1213.95	84	108	0	3	0	1.0200
	3	11.33	1151.86	86	118	0	0	0	0.8916
	4	3.97	1178.93	82	115	1	2	0	1.1112
	5	1.58	1298.11	90	120	0	3	0	1.0081
	6	0.27	1477.41	102	141	1	3	0	1.1012
fraction 8	1	38.09	1242.00	86	112	0	3	0	1.0158
	2	33.09	1014.72	69	107	1	2	0	1.1347
	3	20.88	1499.44	106	147	1	2	0	1.0650
	4	5.74	1255.07	83	115	1	4	0	1.1772
	5	1.82	1051.68	74	102	2	1	0	1.2496
	6	0.38	1358.18	99	140	2	0	0	1.1294
fraction 9	1	26.09	1620.57	117	150	0	2	0	0.9601
	2	21.11	1172.94	79	113	1	3	0	1.1518
	3	19.78	1150.85	78	103	1	3	0	1.1661
	4	17.56	1066.78	71	103	1	3	0	1.1766
	5	13.29	1475.31	103	127	1	3	0	1.1144
	6	2.17	1280.98	91	109	1	2	0	1.1114
fraction 10	1	51.93	3348.24	231	289	3	7	1	1.1519
	2	30.28	4131.46	273	339	1	13	5	1.0987
	3	14.54	4172.54	287	366	6	8	1	1.2301
	4*	3.22	4137.63	276	310	12	4	7	1.4529
	5	0.01	4119.39	286	351	3	8	2	1.1197
	6	0.01	4033.32	275	349	3	9	3	1.1332

\* Also includes two vanadium atoms



**Table A4 - 3 Properties provided by Syncrude for narrow cut heavy vacuum gas oil**

Density (g/mL) @ 20°C	MW (g/mole)	S (ppm)	N (ppm)	C (wt.%)	H (wt.%)
1.0204	470	44860	5739	85.1	9.49

**Table A4 - 4 Properties of Syncrude for narrow cut heavy vacuum gas oil calculated from Riazi-Daubert and Twu correlations using a mass average boiling point of 812.1K and specific gravity of 1.0305\*.**

Property	Molar average value	
	Riazi-Daubert	Twu
MW (g/mole)	514.1	417.9
T <sub>b</sub> (K)	812.1	812.1
T <sub>c</sub> (K)	961.6	1006.4
P <sub>c</sub> (kPa)	1747.4	1357.9
V <sub>c</sub> (m <sup>3</sup> /kmole)	2.1248	1.2686
ω	2.0216	1.0749

\* From equivalent density at 4°C estimated using ASTM D1250 tables

**Table A4 - 5 Comparison of properties predicted by three GC methods.**

ID	MW (g/mol)	Ambrose	Marerro & Gani					Joback and Reid				Wilson		
		omega	T <sub>b</sub> (K)	T <sub>c</sub> (K)	P <sub>c</sub> (bar)	V <sub>c</sub> (cm <sup>3</sup> /mole)	omega	Z <sub>c</sub>	T <sub>b</sub> (K)	T <sub>c</sub> (K)	P <sub>c</sub> (bar)	V <sub>c</sub> (cm <sup>3</sup> /mole)	T <sub>c</sub> (K)	Z <sub>c</sub>
F1M1	474.89	0.431	924.50	1161.81	7.15	3737.95	0.438	0.277	2228.21	4744.41	2.20	3692.5	952.35	0.133
F1M2	597.06	0.551	778.43	988.52	9.30	2049.72	0.557	0.232	1285.40	1591.95	5.77	2017.5	896.01	0.176
F1M3	480.85	0.577	725.33	923.92	9.95	1760.76	0.583	0.228	1056.74	1294.18	6.38	1749.5	849.07	0.186
F1M4	554.89	0.464	794.59	1027.58	9.93	1817.74	0.469	0.211	1289.44	1584.70	7.57	1787.5	950.75	0.187
F1M5	770.18	0.393	880.58	1126.47	8.05	2637.20	0.398	0.227	1771.03	2417.85	4.33	2589.5	978.82	0.161
F1M6	749.27	0.461	850.01	1080.43	8.31	2637.34	0.467	0.244	1613.03	2149.42	4.05	2558.5	943.90	0.161
F2M1	687.20	0.464	824.24	1047.33	8.32	2503.28	0.470	0.239	1459.18	1989.14	3.93	2489.5	905.95	0.163
F2M2	1082.76	0.346	907.77	1157.58	7.32	3684.44	0.351	0.280	2302.73	4792.14	2.59	3559.5	952.25	0.137
F2M3	719.28	0.486	816.08	1031.75	8.14	2565.66	0.491	0.243	1471.08	1960.27	3.68	2549.5	891.45	0.159
F2M4	512.83	0.422	775.16	1009.22	9.97	1756.93	0.426	0.209	1198.20	1470.47	7.30	1741.5	923.18	0.188
F2M5	985.81	0.543	874.82	1083.84	7.13	3663.67	0.550	0.290	1902.42	3600.82	2.03	3589.5	892.73	0.134
F2M6	1294.31	0.556	944.13	1162.82	6.81	4651.55	0.563	0.328	2491.44	9239.53	1.46	4499.5	934.90	0.118
F3M1	629.08	0.137	751.74	1018.19	8.85	2230.19	0.139	0.233	1350.98	1707.91	4.97	2175.5	856.24	0.172
F3M2	720.17	0.567	852.59	1075.96	8.89	2405.55	0.574	0.239	1622.11	2100.52	5.32	2333.5	967.97	0.168
F3M3	985.81	0.545	874.70	1083.32	7.12	3674.13	0.552	0.290	1902.86	3656.29	2.03	3595.5	892.60	0.134
F3M4	692.22	0.612	820.17	1023.90	8.39	2492.10	0.619	0.246	1468.72	1949.45	4.18	2450.5	902.87	0.163
F3M5	1075.81	0.462	931.54	1168.01	7.27	3731.80	0.469	0.279	2259.29	4790.18	2.37	3642.5	966.60	0.135
F3M6	561.04	0.524	752.19	956.65	9.11	2050.79	0.530	0.235	1172.84	1451.66	5.24	2017.5	856.86	0.176
F4M1	878.43	0.288	897.03	1169.70	8.23	2917.80	0.291	0.247	1906.32	2780.74	3.62	2898.5	979.48	0.152
F4M2	925.55	0.278	862.19	1116.71	7.64	3185.13	0.282	0.262	1931.37	3048.55	3.11	3080.5	929.36	0.147
F4M3	701.22	0.469	826.93	1047.94	8.15	2577.63	0.474	0.241	1482.50	2065.42	3.77	2551.5	904.84	0.161
F4M4	641.09	0.463	798.35	1025.14	9.23	2186.84	0.468	0.237	1395.54	1744.35	5.13	2173.5	913.32	0.172
F4M5	891.51	0.227	851.71	1113.66	7.67	3026.48	0.230	0.251	1868.84	2890.40	3.35	2963.5	921.44	0.150
F4M6	703.18	0.463	825.79	1050.41	8.39	2526.35	0.468	0.243	1522.73	2001.42	4.12	2470.5	917.48	0.163
F5M1	800.31	0.606	872.54	1086.91	8.13	2762.84	0.613	0.249	1729.63	2420.86	3.89	2703.5	955.25	0.157
F5M2	799.39	0.622	839.80	1040.29	7.81	2811.58	0.629	0.254	1681.08	2495.31	3.38	2825.5	900.82	0.153
F5M3	1171.98	0.373	921.30	1164.00	6.97	4159.49	0.378	0.300	2363.38	9277.03	1.92	4021.5	939.93	0.128
F5M4	951.58	0.488	903.74	1131.51	7.41	3299.71	0.495	0.260	1988.72	3486.58	2.85	3217.5	962.53	0.144
F5M5	1161.88	0.533	955.90	1187.11	7.21	3830.67	0.539	0.280	2445.73	5197.14	2.52	3708.5	1003.29	0.134
F5M6	1021.72	0.502	914.00	1139.80	7.24	3547.10	0.508	0.271	2111.22	4250.69	2.48	3475.5	955.64	0.138
F6M1	762.25	0.602	864.00	1080.08	8.41	2594.63	0.610	0.243	1681.54	2262.39	4.63	2506.5	966.03	0.163
F6M2	979.64	0.579	910.17	1127.28	7.41	3406.35	0.587	0.269	2029.06	3753.69	2.69	3323.5	962.05	0.142
F6M3	1061.73	0.431	924.50	1161.81	7.15	3737.95	0.438	0.277	2228.21	4744.41	2.20	3692.5	952.35	0.133
F6M4	1298.15	0.448	972.74	1213.47	6.80	4576.87	0.454	0.308	2666.11	91461.75	1.55	4536.5	961.69	0.119
F6M5	1217.96	0.161	917.04	1204.15	7.15	3973.84	0.163	0.284	2583.77	6813.31	2.43	3864.5	956.64	0.131
F6M6	1285.09	0.505	981.95	1217.89	6.89	4452.58	0.513	0.303	2692.30	32964.99	1.80	4350.5	986.59	0.123
F7M1	1347.23	0.401	962.35	1209.19	6.87	4580.84	0.408	0.313	2782.36	32179.00	1.77	4464.5	962.75	0.120
F7M2	1213.95	0.163	912.05	1196.04	7.10	4055.62	0.166	0.290	2565.94	7497.86	2.27	3923.5	946.59	0.130
F7M3	1151.86	0.417	950.24	1193.17	6.96	4064.83	0.422	0.285	2418.77	8559.25	1.92	4028.5	963.51	0.128
F7M4	1178.93	0.541	954.01	1180.11	7.00	4079.43	0.549	0.291	2469.50	9244.48	2.08	3976.5	974.26	0.129
F7M5	1298.11	0.559	974.14	1201.58	6.94	4388.02	0.566	0.305	2698.11	14282.63	1.91	4252.5	991.58	0.124
F7M6	1477.41	0.525	1006.05	1241.60	6.71	4962.44	0.533	0.323	3077.52	- 36478.96	1.57	4850.5	992.25	0.114
F8M1	1242.00	0.021	895.26	1209.97	7.03	4133.11	0.022	0.289	2610.74	8770.11	2.18	4029.5	922.97	0.128
F8M2	1014.72	0.569	906.80	1122.77	7.30	3558.90	0.576	0.278	2105.58	4310.20	2.51	3480.5	942.00	0.138
F8M3	1499.44	0.364	990.41	1246.67	6.66	5164.91	0.730	0.332	3113.90	- 11037.24	1.40	5060.5	965.65	0.112

F8M4	1255.07	0.533	971.12	1202.62	7.01	4202.24	0.540	0.295	2640.95	10734.43	2.14	4089.5	991.02	0.127
F8M5	1051.68	0.332	911.36	1164.28	7.30	3629.22	0.337	0.274	2276.03	4716.12	2.71	3500.5	956.85	0.139
F8M6	1358.18	0.503	992.33	1228.18	6.73	4808.75	0.510	0.317	2842.34	- 36039.79	1.56	4687.5	977.87	0.118
F9M1	1620.57	0.436	1030.50	1283.20	6.59	5428.45	0.443	0.335	3384.47	-9120.70	1.29	5352.5	999.94	0.108
F9M2	1172.94	0.532	952.50	1181.05	7.09	3978.11	0.538	0.287	2451.27	7194.67	2.25	3883.5	977.96	0.130
F9M3	1150.85	0.513	958.93	1194.27	7.25	3809.56	0.520	0.278	2473.01	5651.35	2.62	3699.5	1002.63	0.134
F9M4	1066.78	0.578	924.87	1142.86	7.23	3674.78	0.586	0.280	2236.44	5765.32	2.47	3612.5	957.74	0.136
F9M5	1475.31	0.400	997.98	1252.67	6.79	4915.78	0.405	0.320	3134.04	- 29421.37	1.69	4762.5	997.74	0.117
F9M6	1280.98	0.351	975.44	1238.11	7.06	4253.61	0.356	0.292	2781.08	10324.99	2.23	4098.5	1009.74	0.128
F10M1	3348.24	0.396	1201.42	1494.29	6.20	10965.66			6222.90	-747.08	0.35	11615.5	1017.29	
F10M2	4131.46	0.412	1253.38	1554.36	6.15	13173.93			7203.48	-575.71	0.25	11615.5	1026.60	
F10M3	4172.54	0.385	1245.75	1549.17	6.11	14018.74			7684.36	-596.24	0.30	12298.5	1006.53	
F10M4	4137.63	0.469	1255.44	1545.39	6.13	12928.70								
F10M5	4119.39	0.421	1250.86	1548.82	6.13	13493.62			7607.30	-621.45	0.31	12120.5	1021.51	
F10M6	4033.32	0.410	1243.62	1542.03	6.13	13266.74			7544.88	-655.01	0.34	11633.5	1014.98	

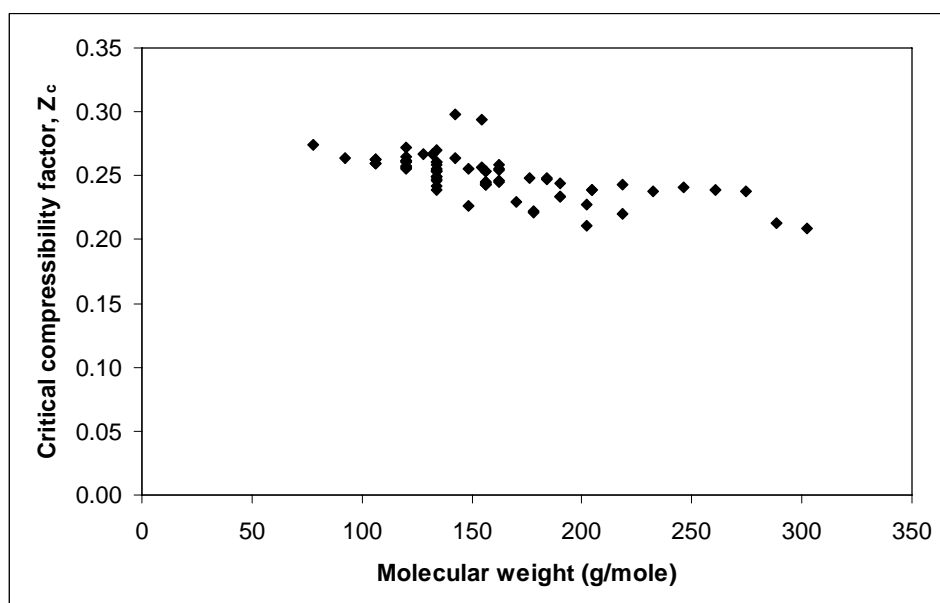


Figure A4 - 1 Critical compressibility factor for aromatics versus molecular weight.

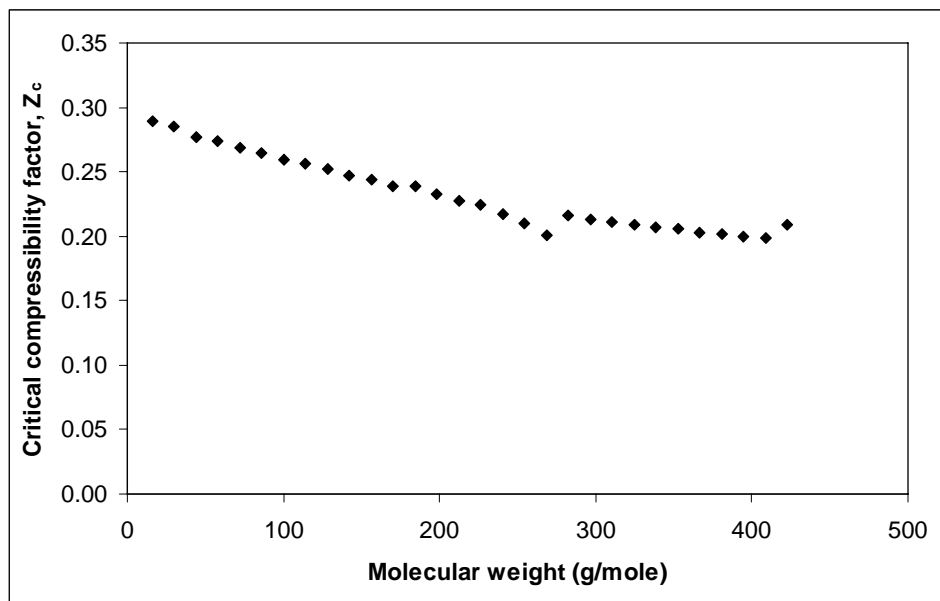


Figure A4 - 2 Critical compressibility factor for n-paraffins versus molecular weight.

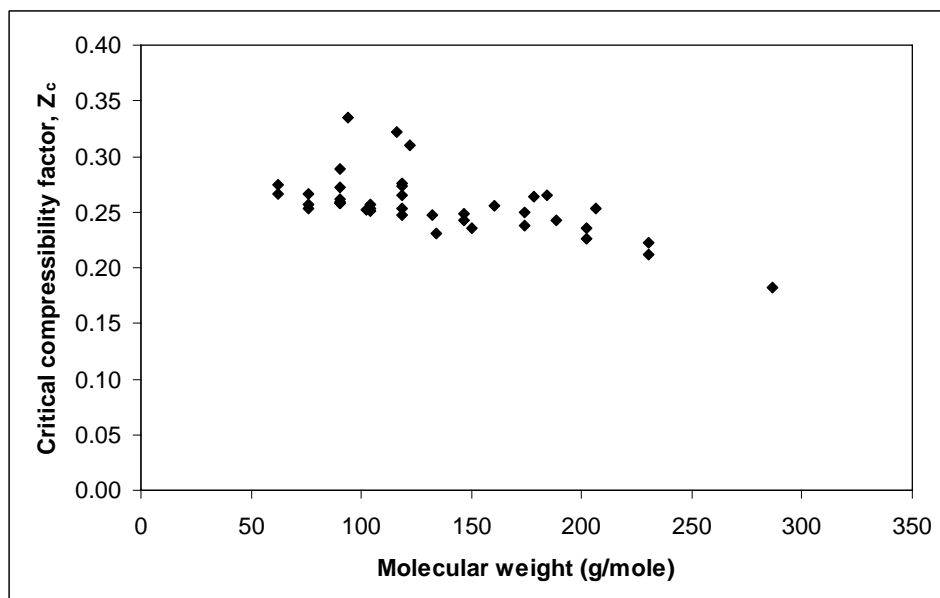
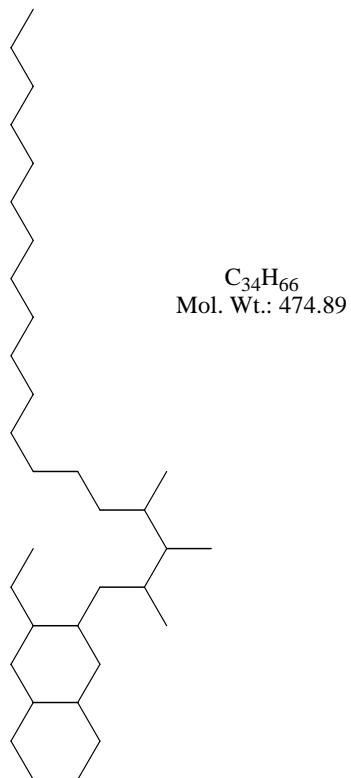


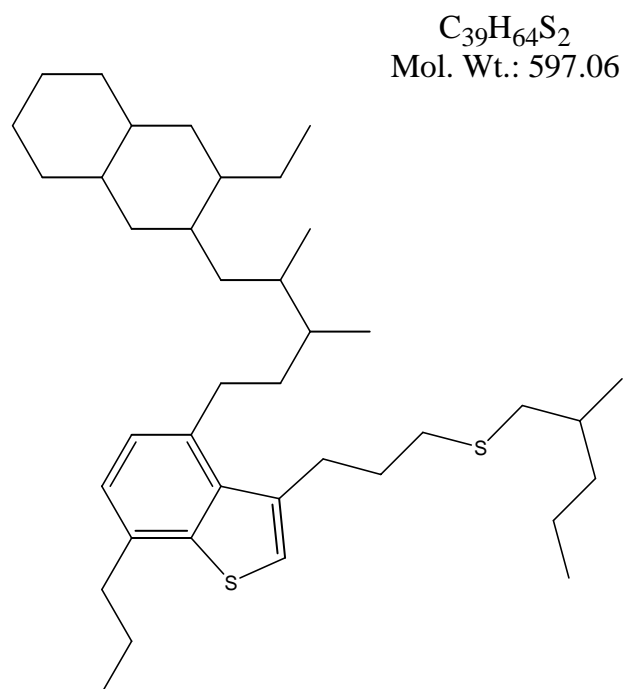
Figure A4 - 3 Critical compressibility factor for thiols, thioethers and thiophenes versus molecular weight.

**Shermata's FRACTION 1**

Molecule # 1

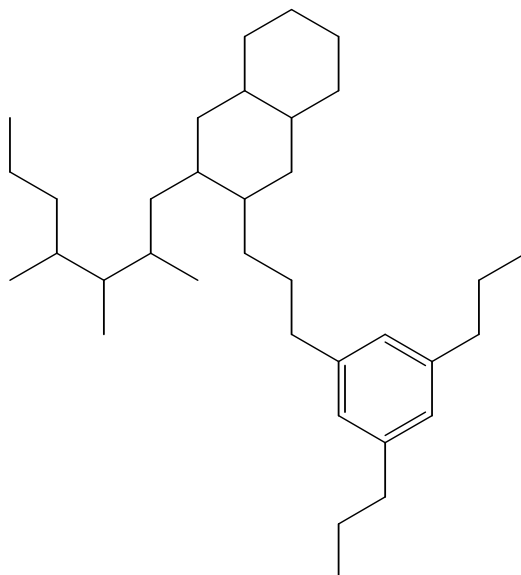


Molecule # 2



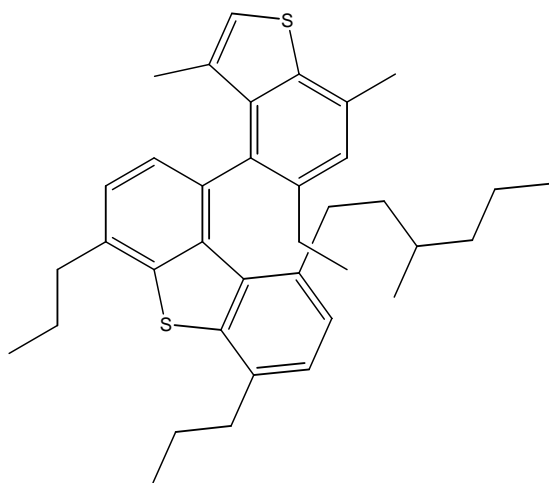
Molecule # 3

$C_{35}H_{60}$   
Mol. Wt.: 480.85

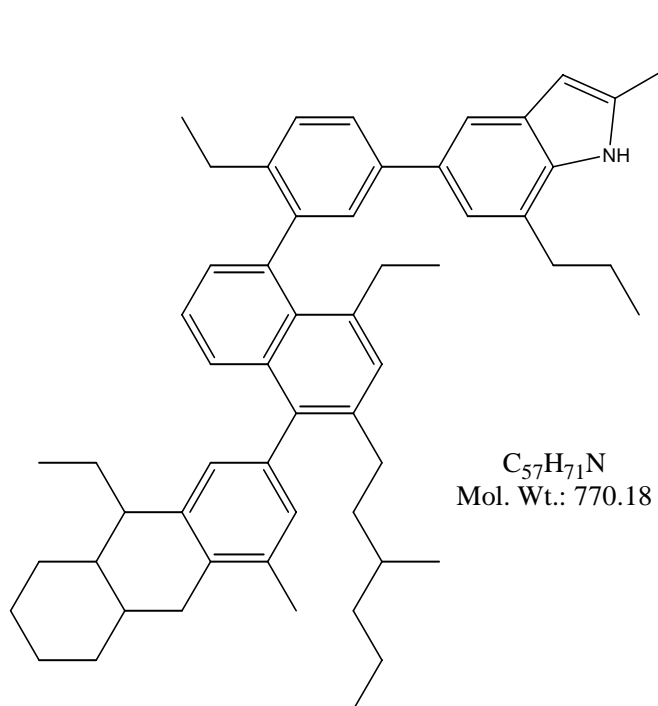


Molecule # 4

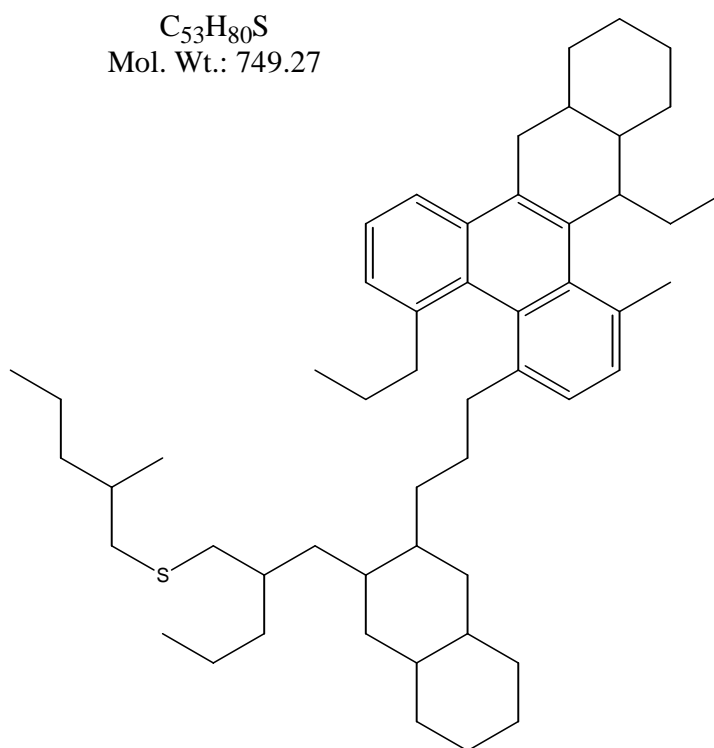
$C_{37}H_{46}S_2$   
Mol. Wt.: 554.89



Molecule # 5

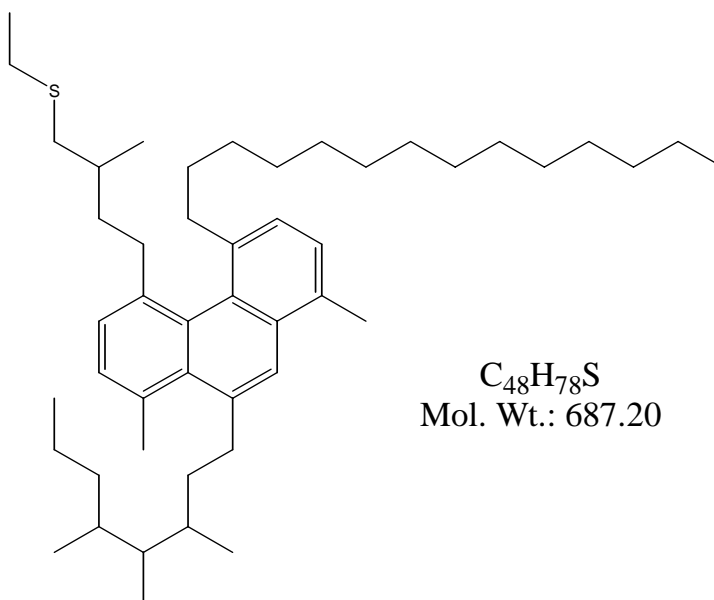


Molecule # 6



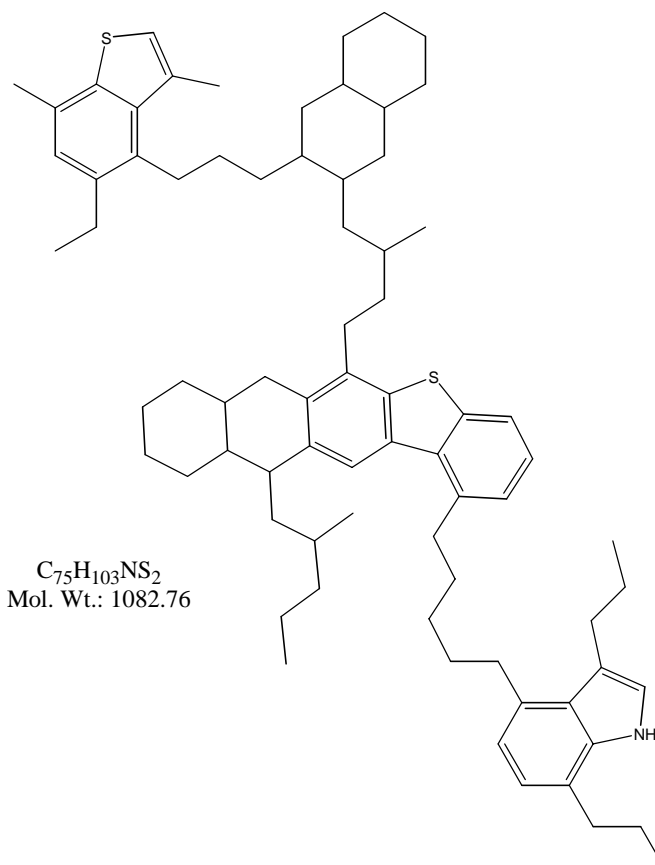
**Shermata's FRACTION 2**

Molecule # 1



$C_{48}H_{78}S$   
Mol. Wt.: 687.20

Molecule # 2

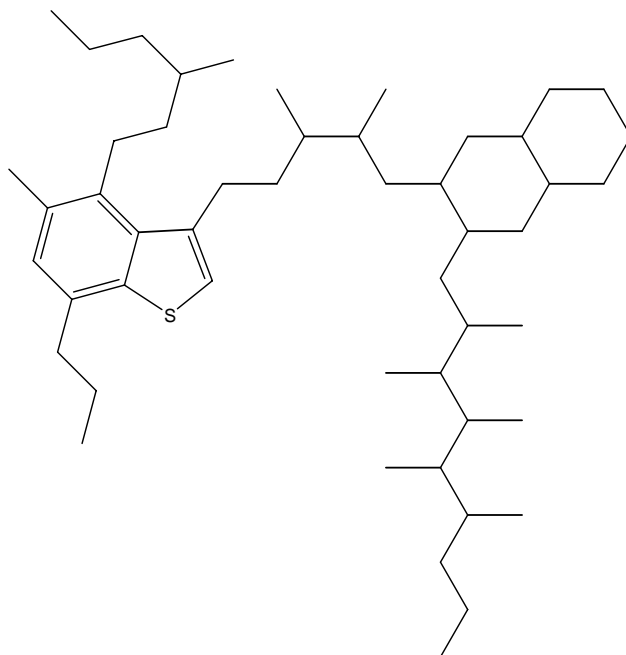


$C_{75}H_{103}NS_2$   
Mol. Wt.: 1082.76



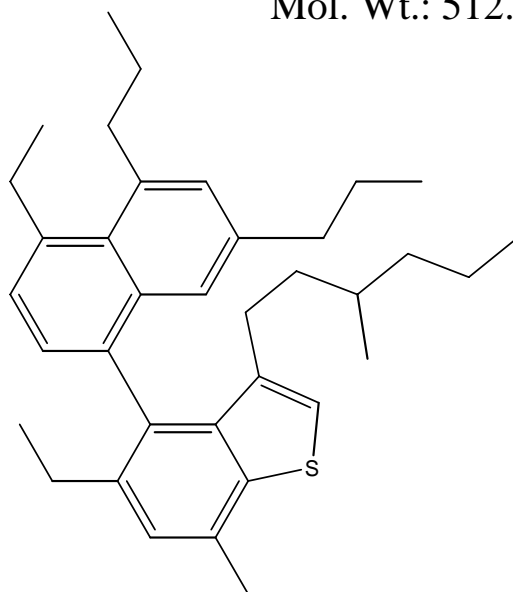
Molecule # 3

$C_{50}H_{86}S$   
Mol. Wt.: 719.28



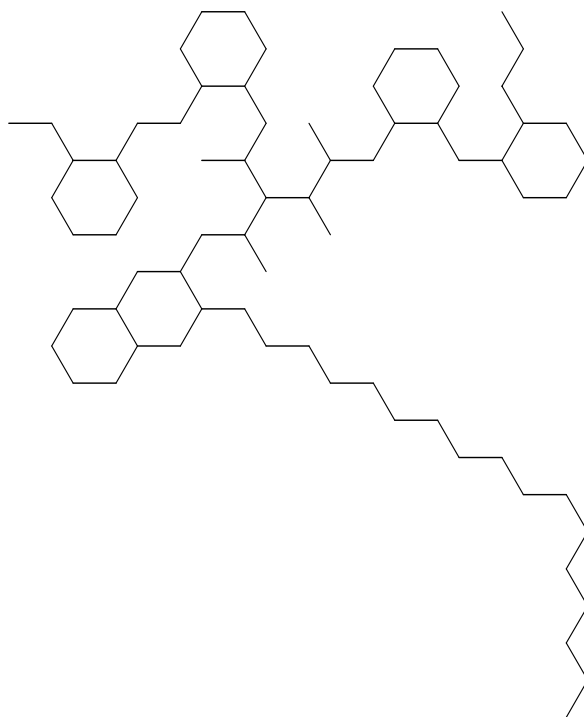
Molecule # 4

$C_{36}H_{48}S$   
Mol. Wt.: 512.83



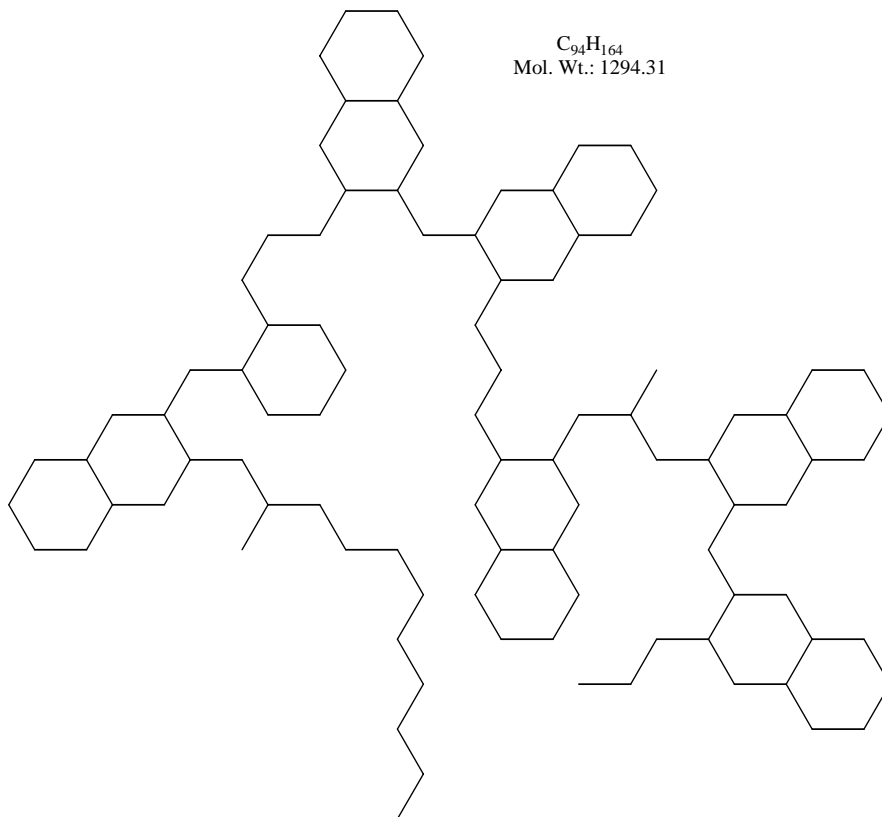
Molecule # 5

$C_{71}H_{132}$   
Mol. Wt.: 985.81



Molecule # 6

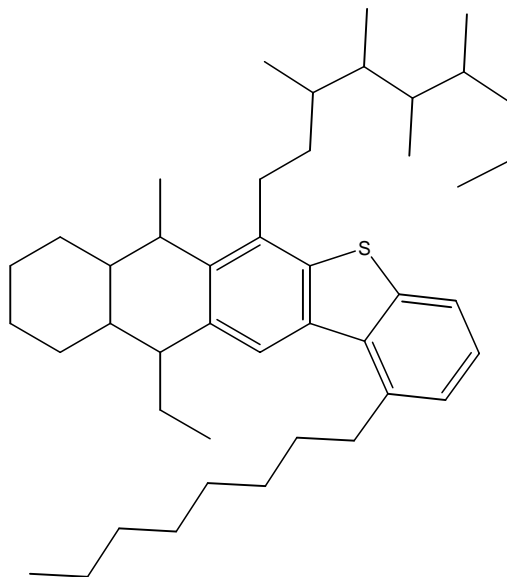
$C_{94}H_{164}$   
Mol. Wt.: 1294.31



**Shermata's FRACTION 3**

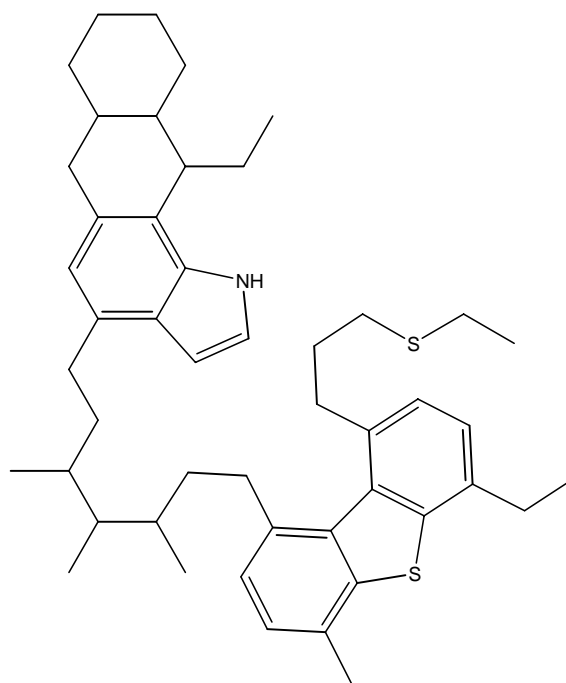
Molecule #1

$C_{44}H_{68}S$   
Mol. Wt.: 629.08

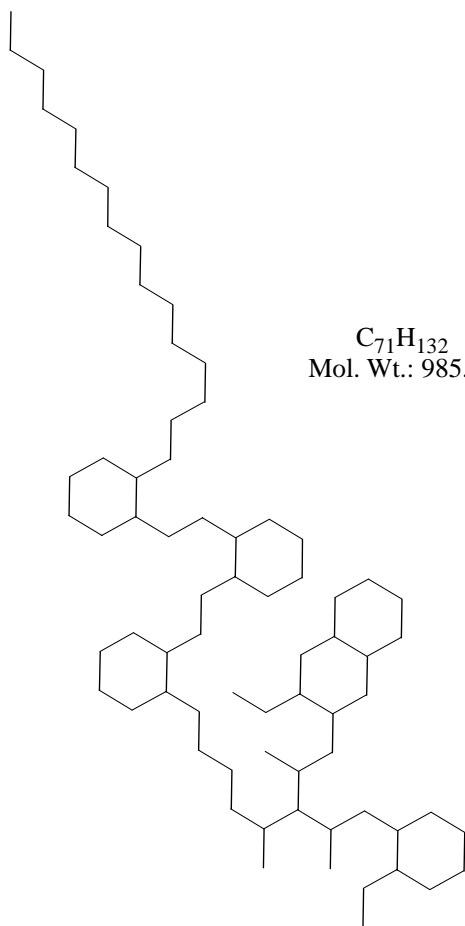


Molecule # 2

$C_{48}H_{65}NS_2$   
Mol. Wt.: 720.17

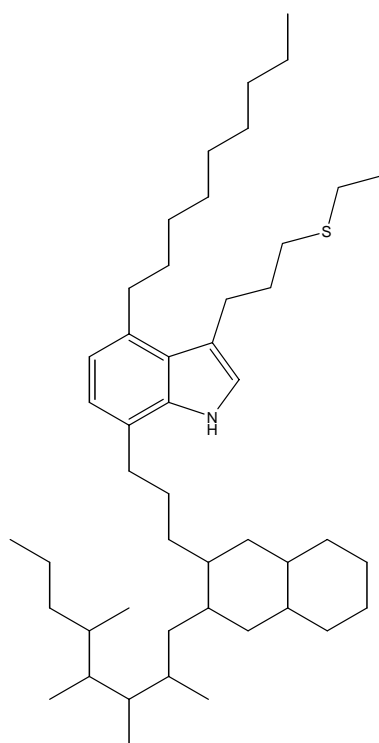


Molecule #3



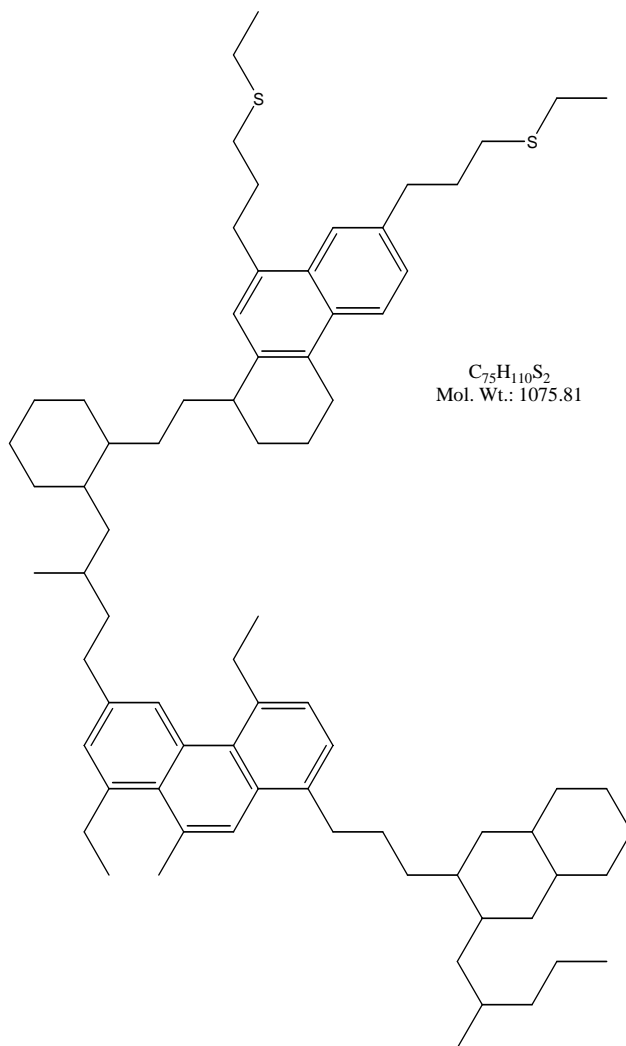
$C_{71}H_{132}$   
Mol. Wt.: 985.81

Molecule #4

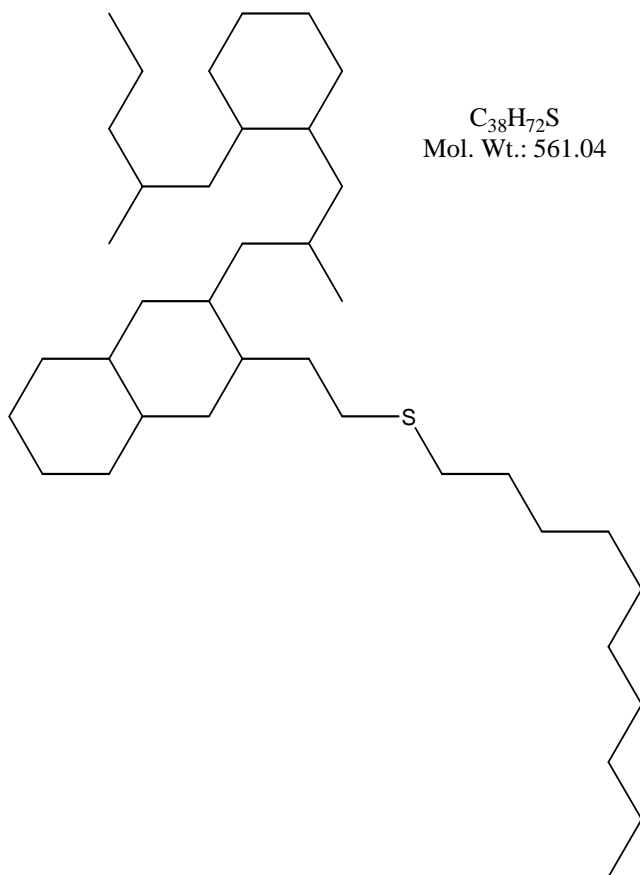


$C_{47}H_{81}NS$   
Mol. Wt.: 692.22

Molecule #5

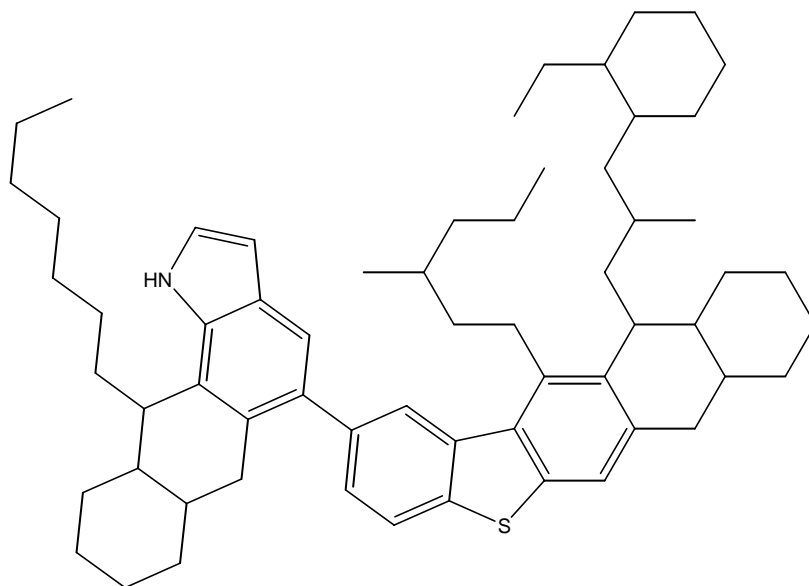


Molecule # 6



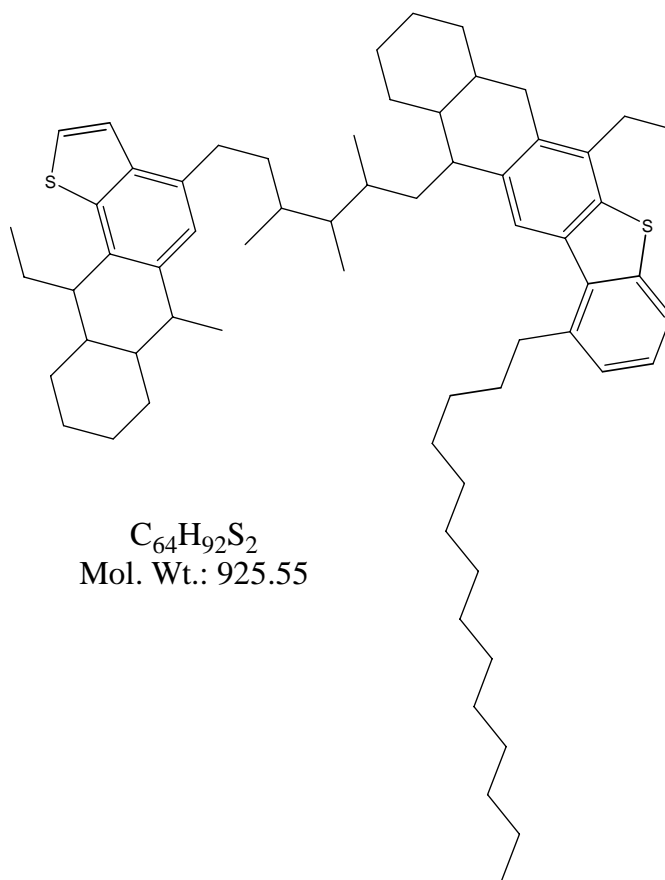
**Shermata's FRACTION 4**

Molecule #1



$C_{62}H_{87}NS$   
Mol. Wt.: 878.43

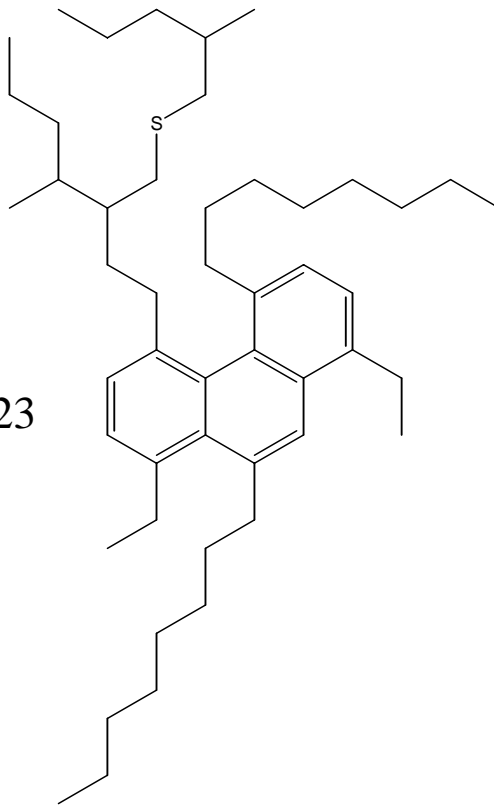
Molecule # 2



$C_{64}H_{92}S_2$   
Mol. Wt.: 925.55

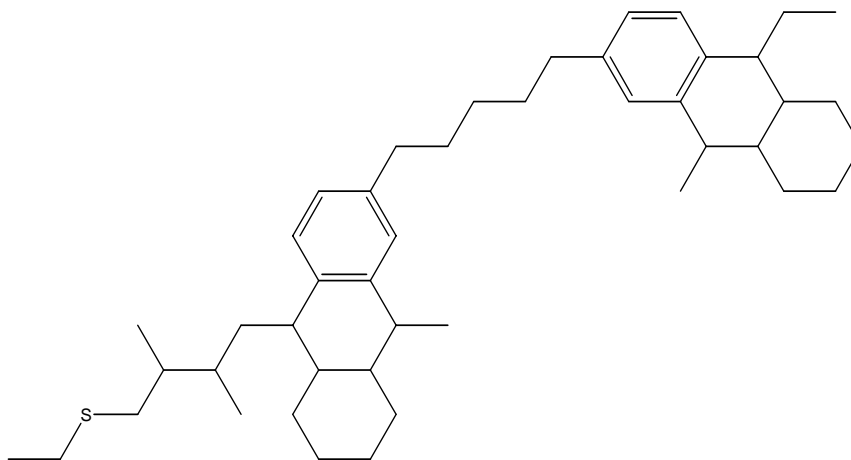
Molecule # 3

$C_{49}H_{80}S$   
Mol. Wt.: 701.23



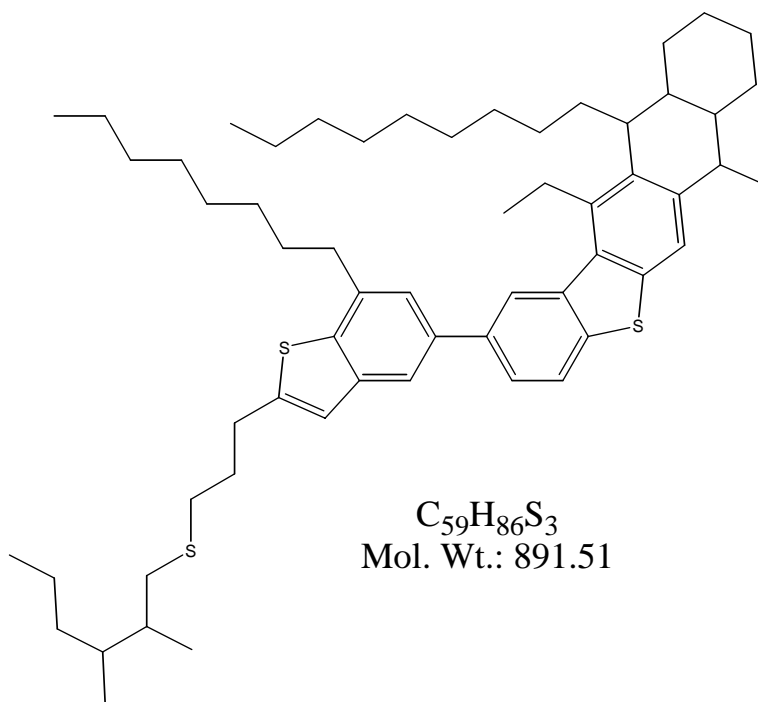
Molecule #4

$C_{45}H_{68}S$   
Mol. Wt.: 641.09

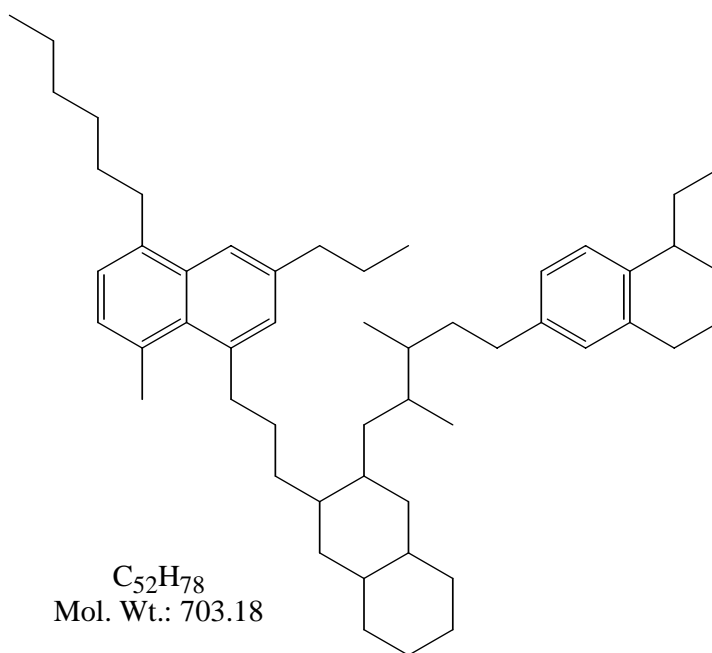




Molecule #5

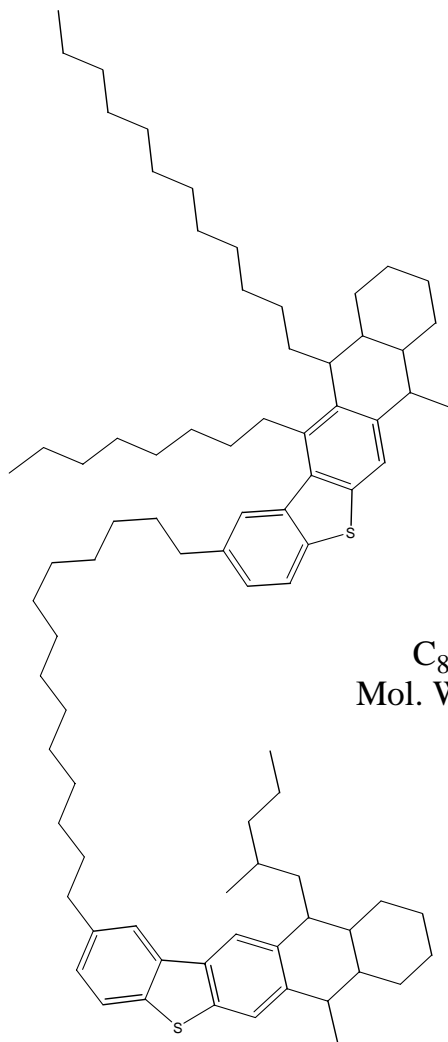


Molecule #6



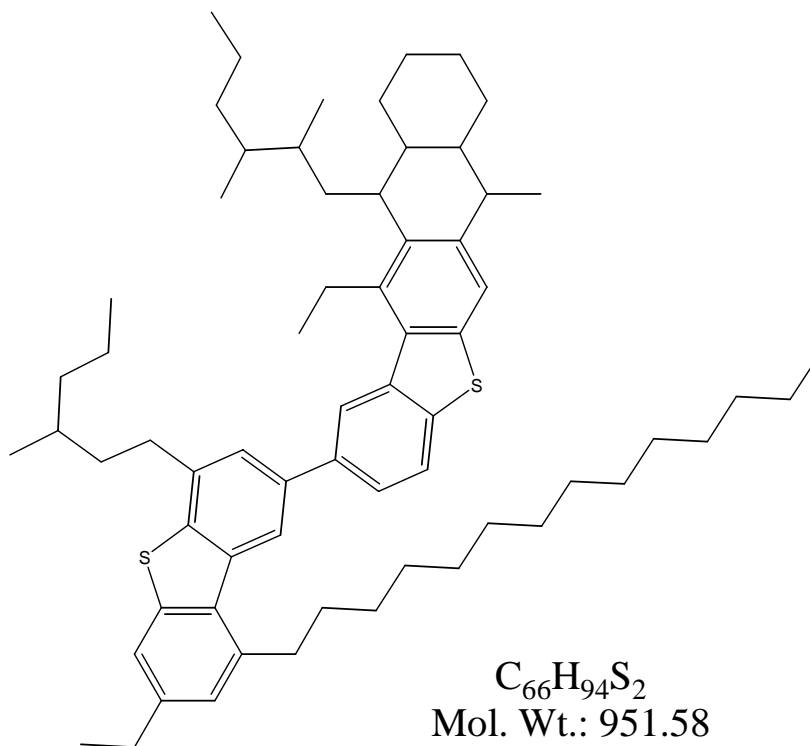


Molecule #3

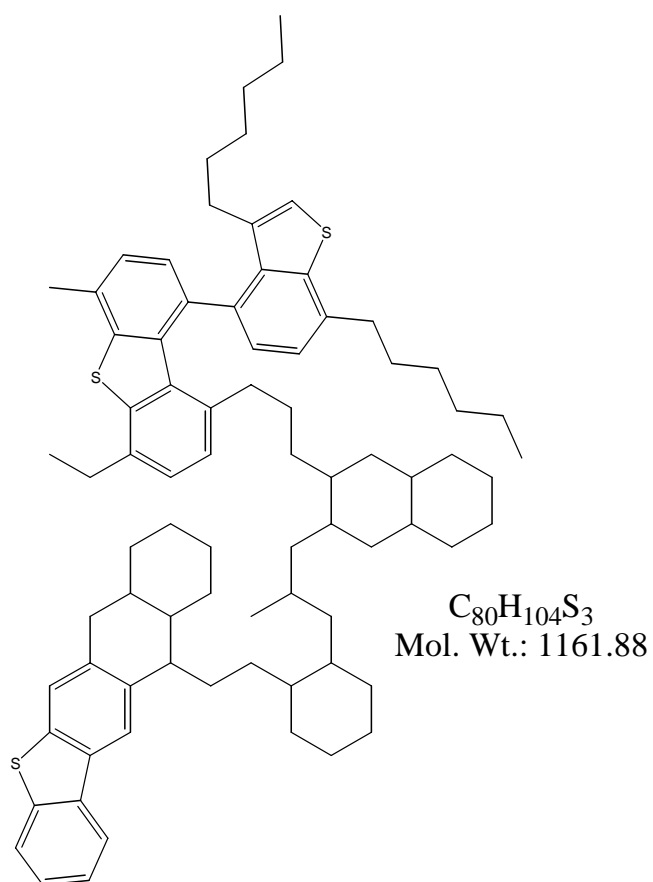


$C_{82}H_{122}S_2$   
Mol. Wt.: 1171.98

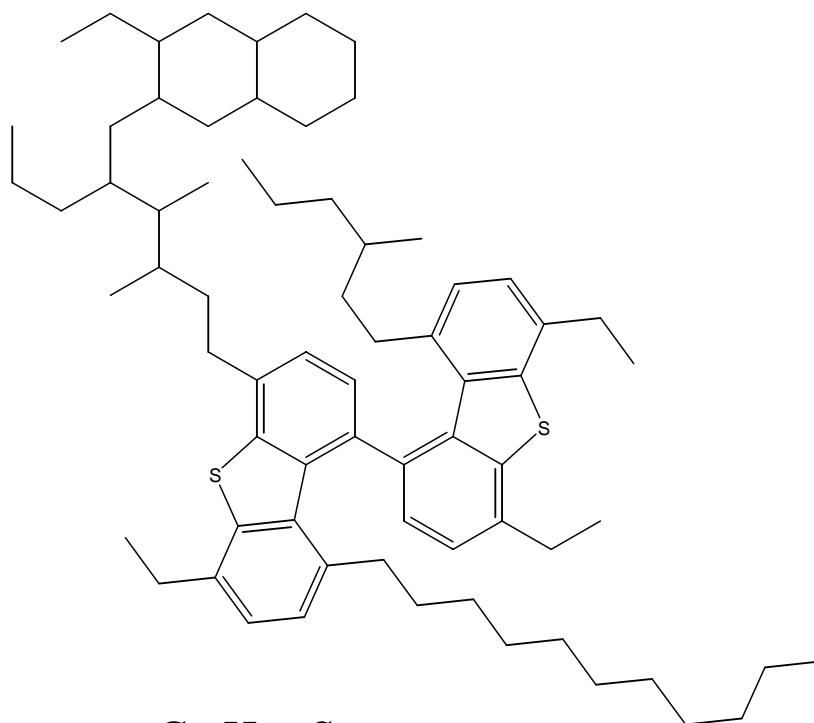
Molecule # 4



Molecule # 5



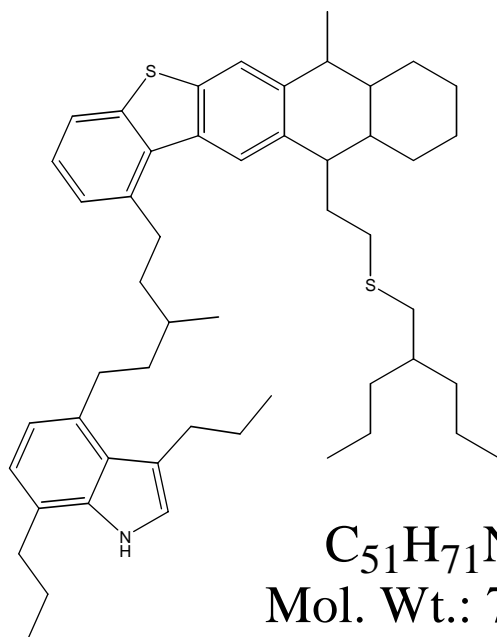
Molecule # 6



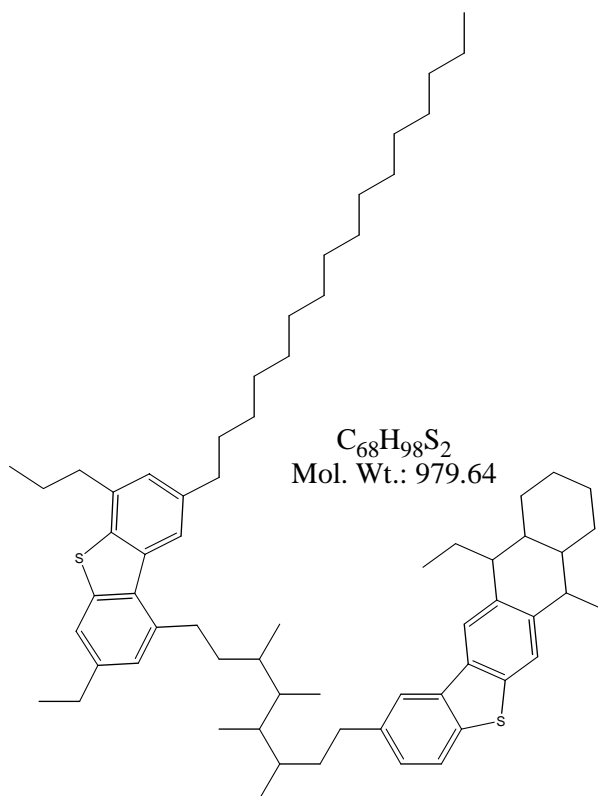
$C_{71}H_{104}S_2$   
Mol. Wt.: 1021.72

**Shermata's FRACTION 6**

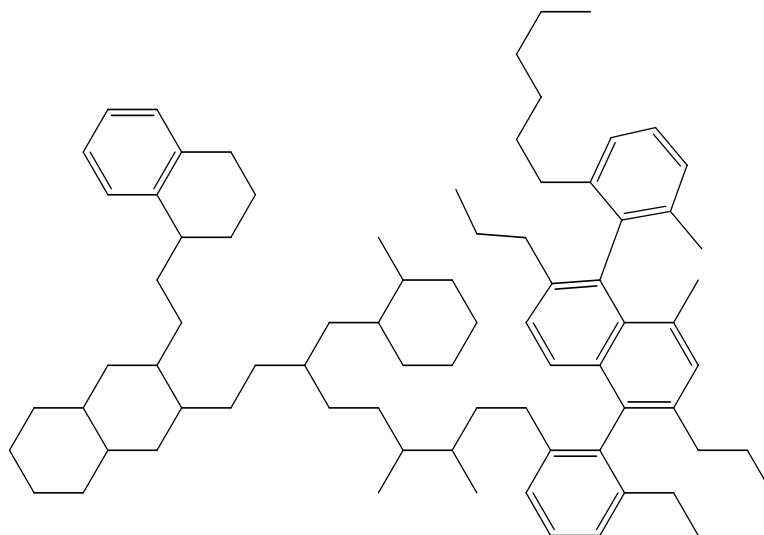
Molecule # 1



Molecule # 2

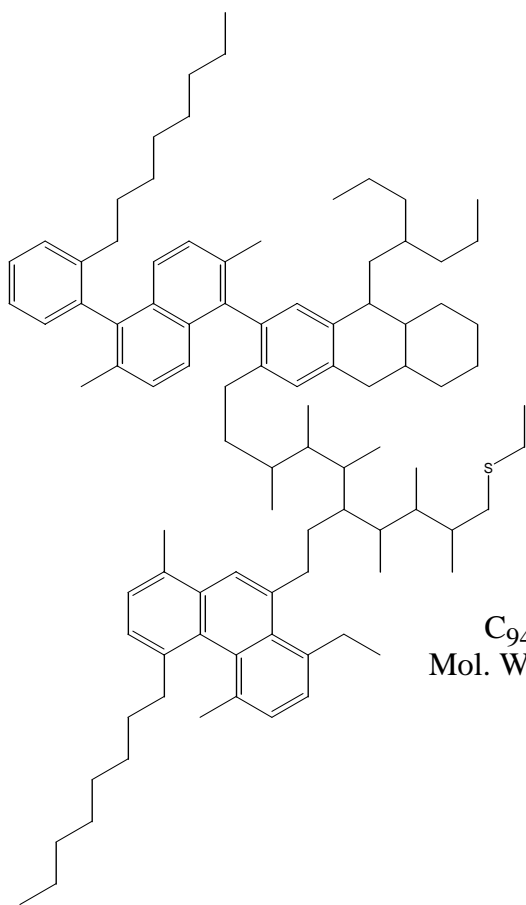


Molecule # 3



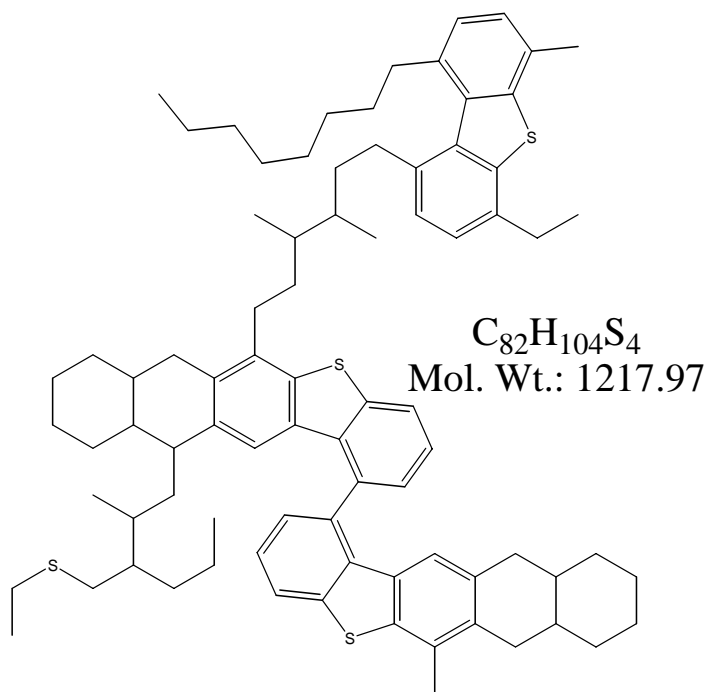
$C_{79}H_{114}$   
Mol. Wt.: 1063.75

Molecule # 4

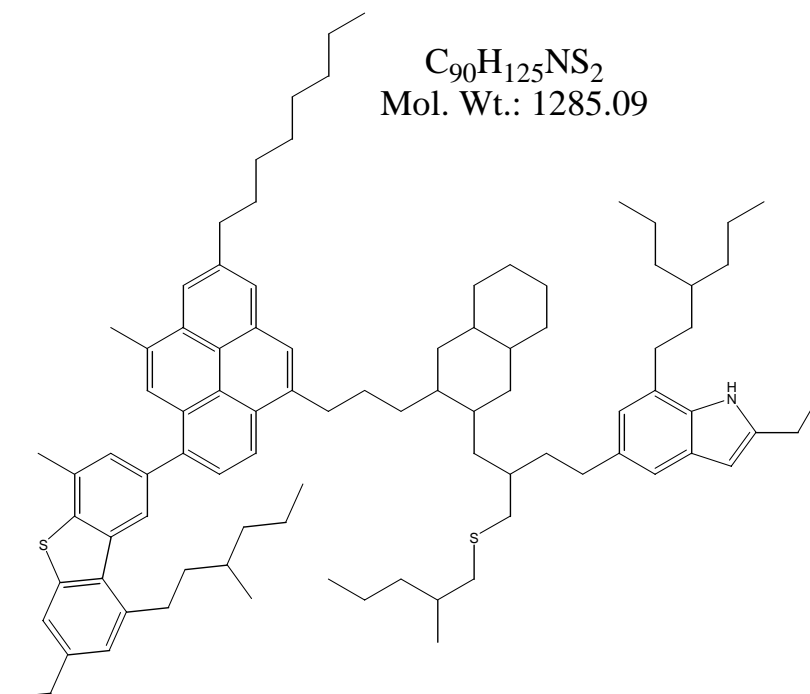


$C_{94}H_{136}S$   
Mol. Wt.: 1298.15

Molecule # 5



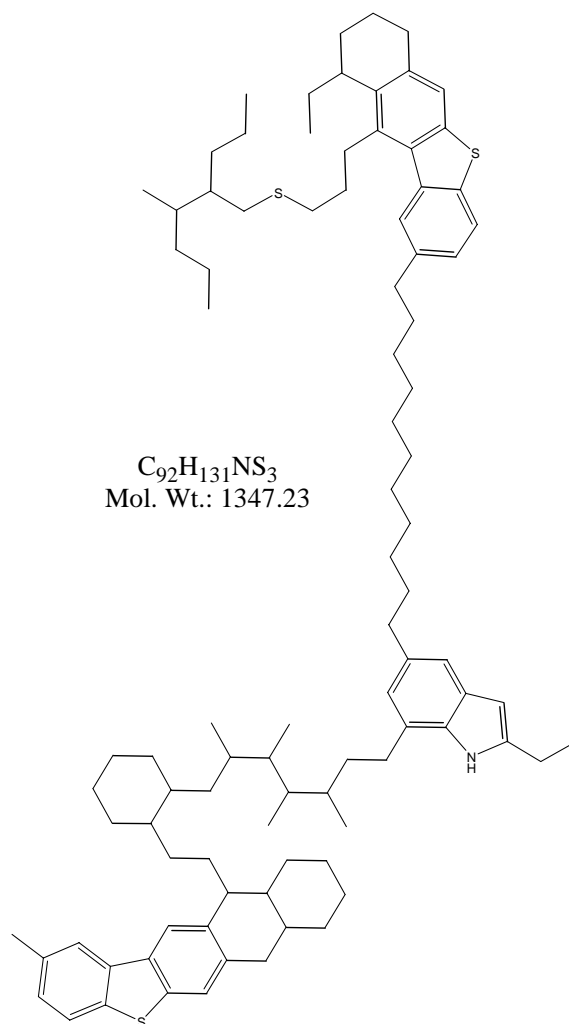
Molecule # 6



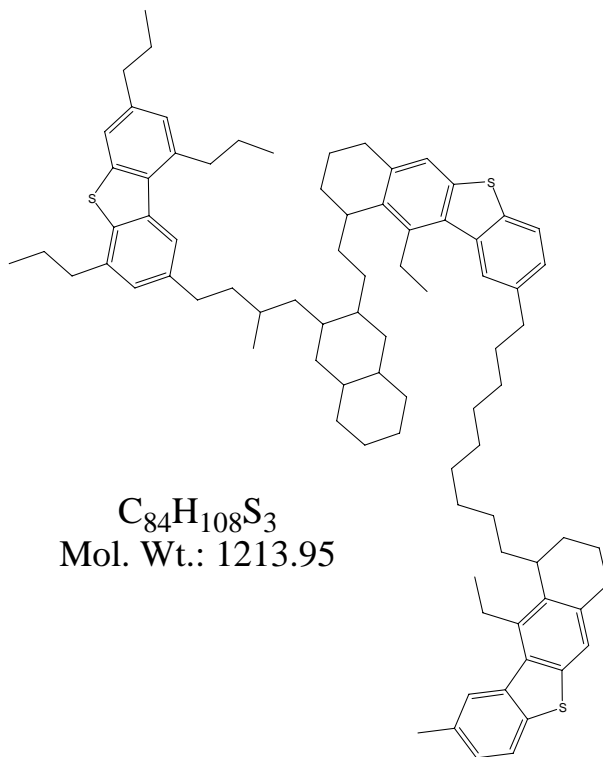


# Shermata's FRACTION 7

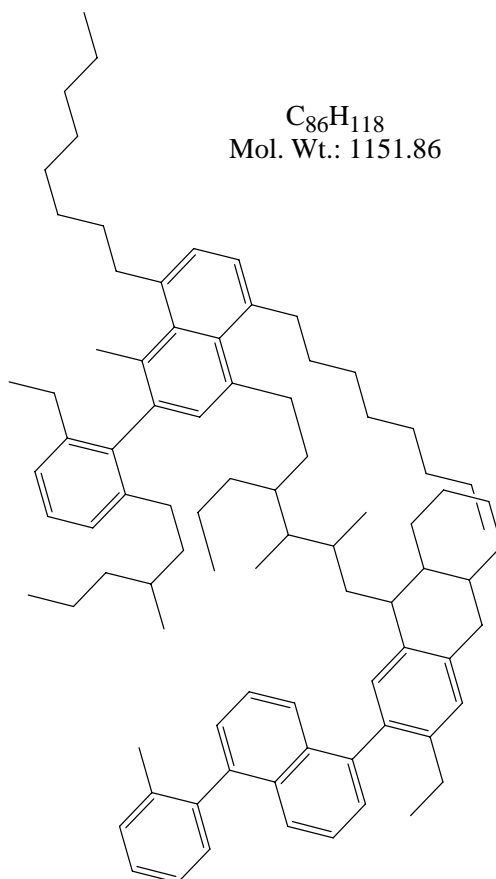
Molecule #1



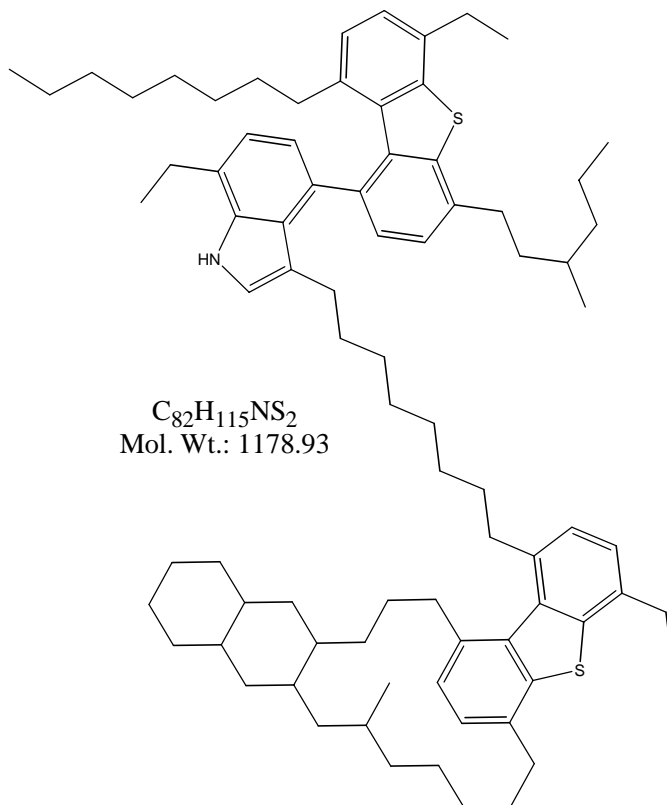
Molecule # 2



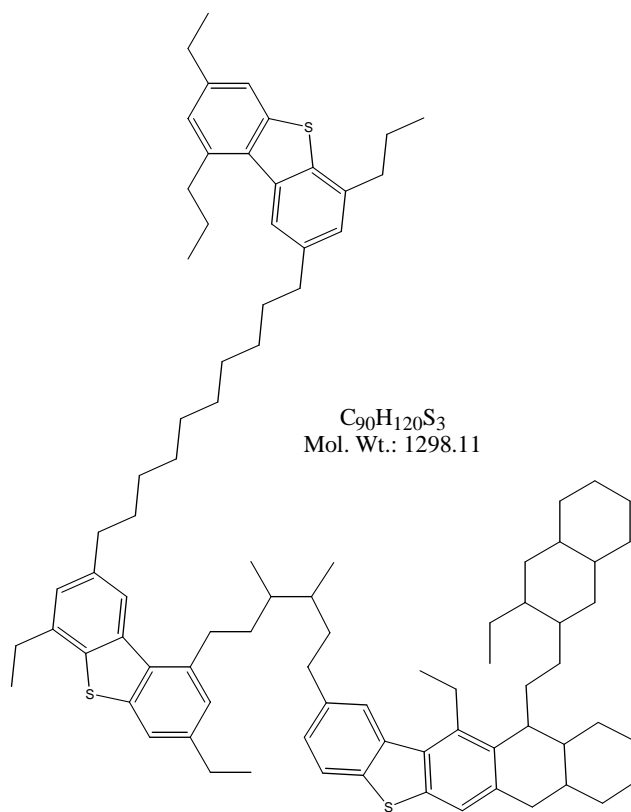
Molecule #3



Molecule # 4



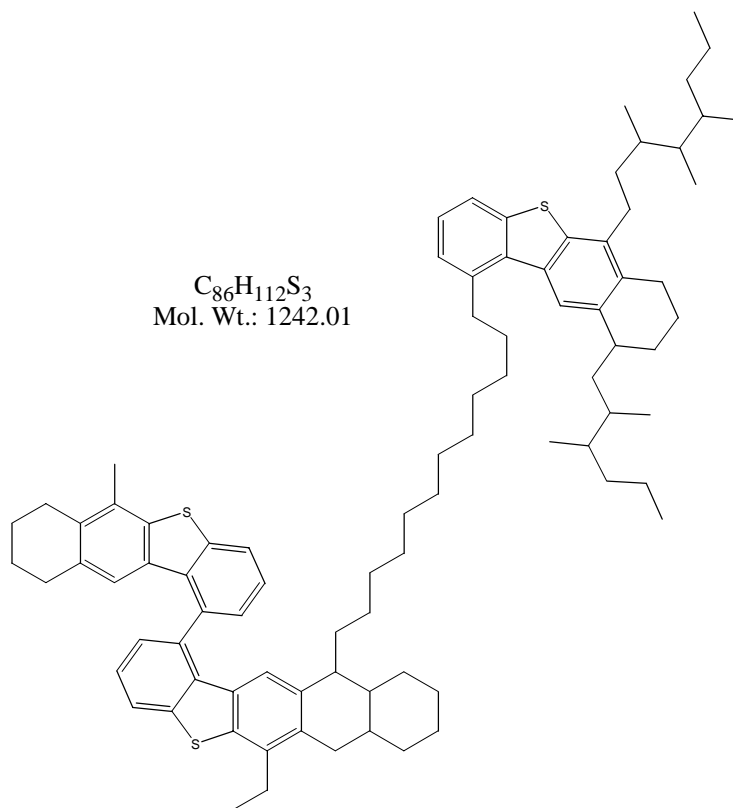
Molecule # 5



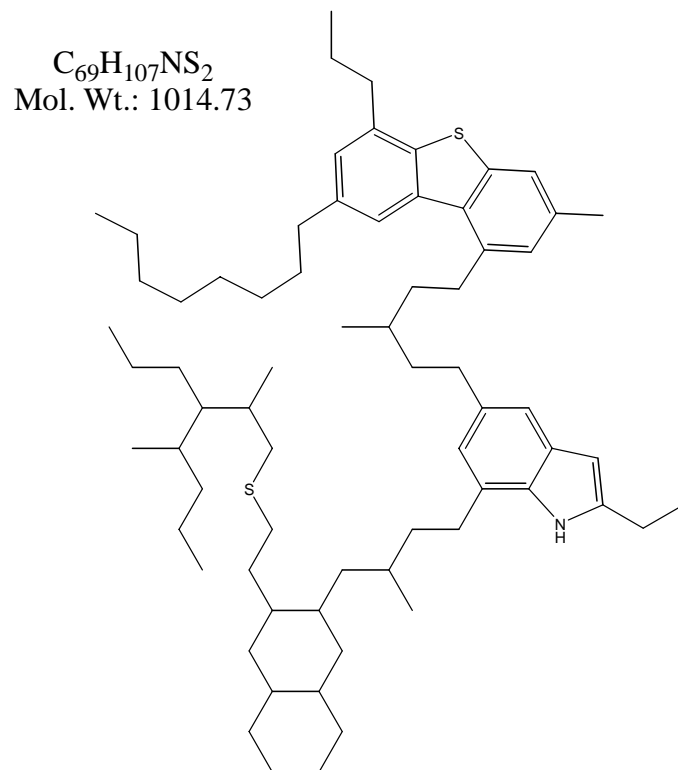


## Shermata's FRACTION 8

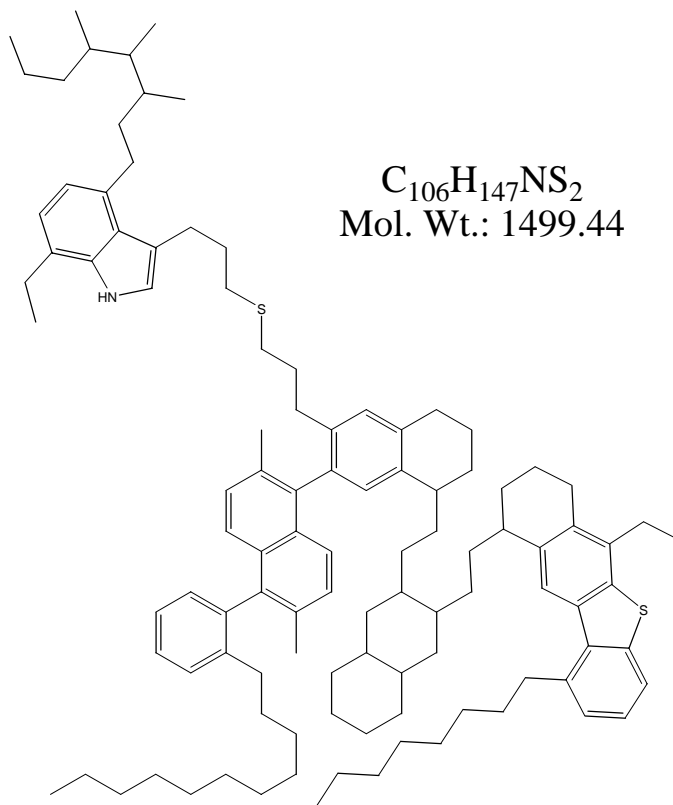
Molecule #1



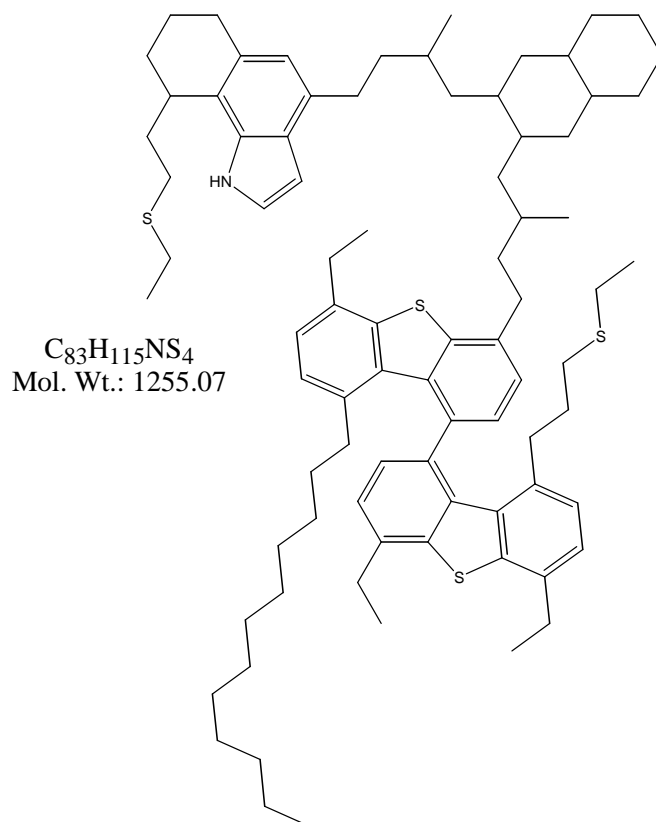
Molecule #2



Molecule # 3



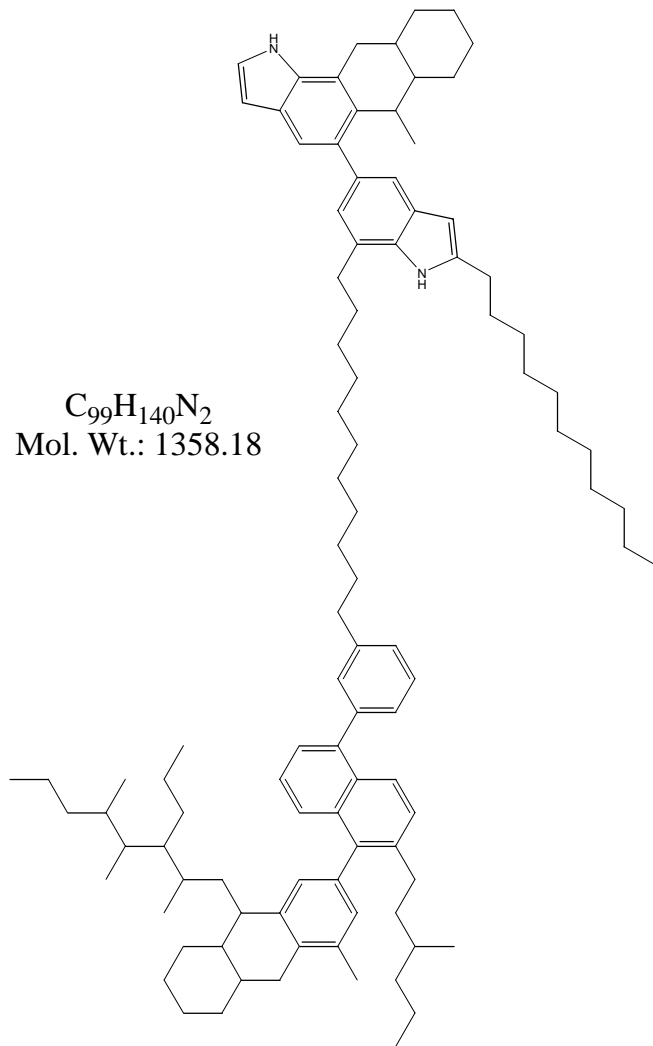
Molecule # 4





Molecule # 6

$C_{99}H_{140}N_2$   
Mol. Wt.: 1358.18

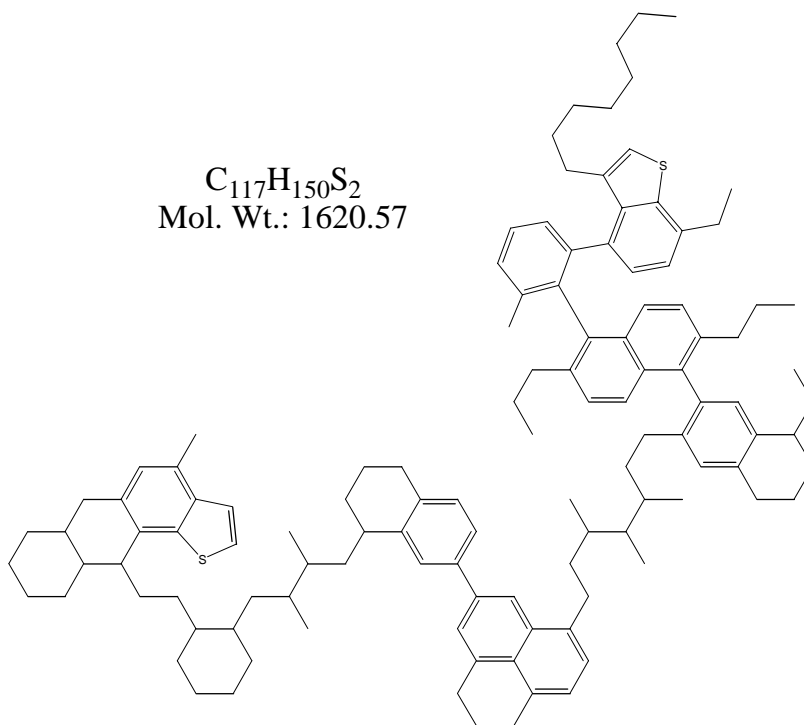




**Shermata's FRACTION 9**

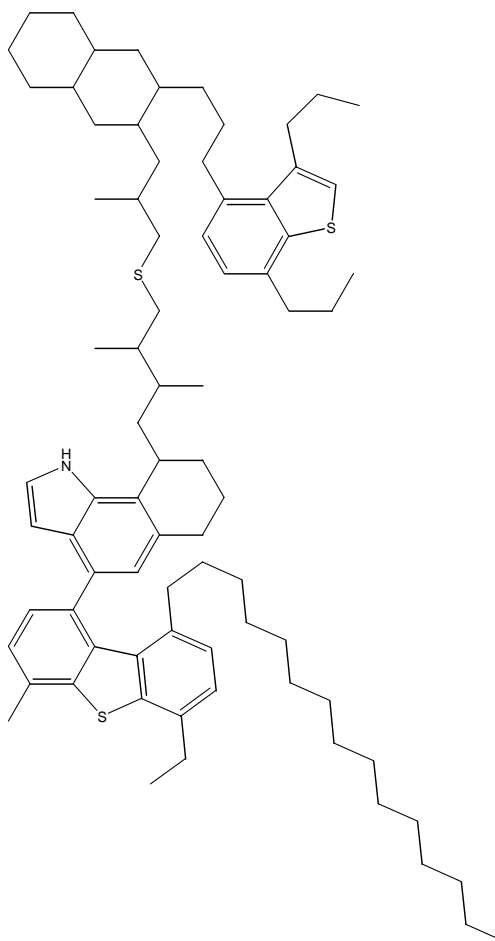
Molecule #1

$C_{117}H_{150}S_2$   
Mol. Wt.: 1620.57



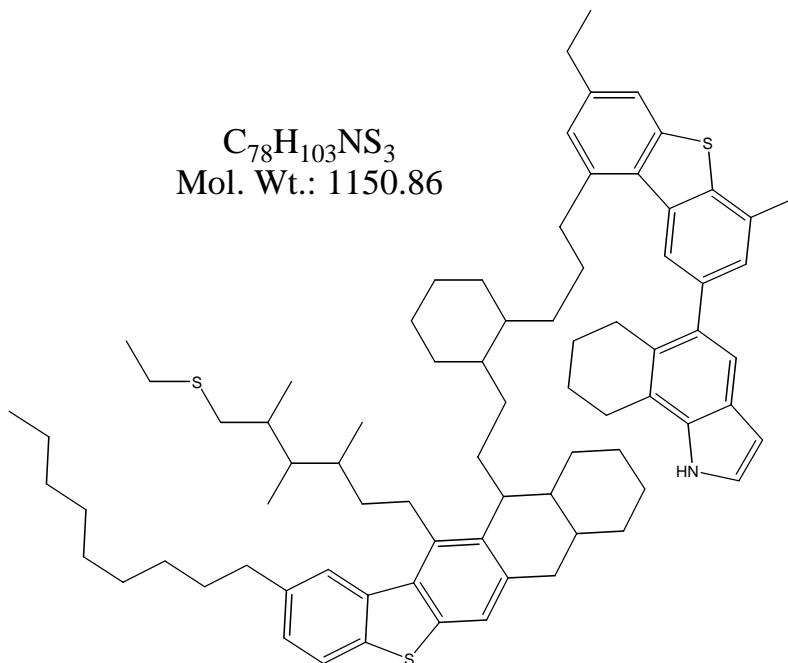
Molecule #2

$C_{79}H_{113}NS_3$   
Mol. Wt.: 1172.95

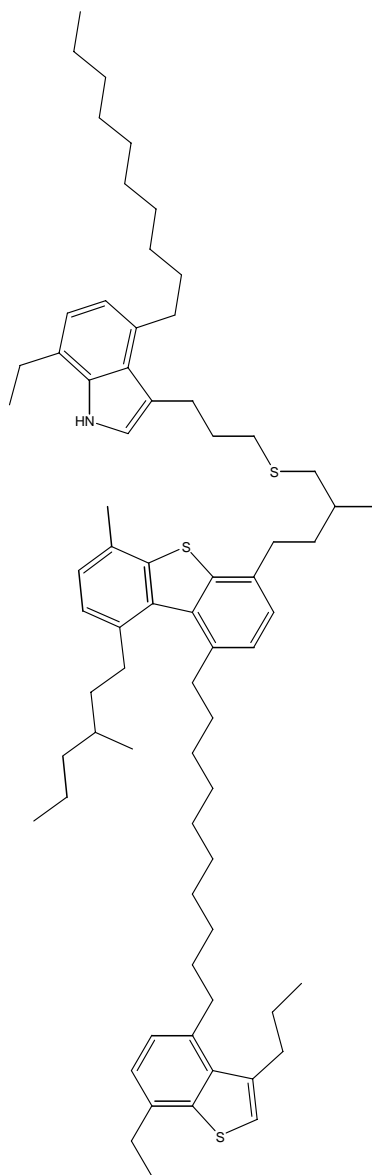


Molecule #3

$C_{78}H_{103}NS_3$   
Mol. Wt.: 1150.86

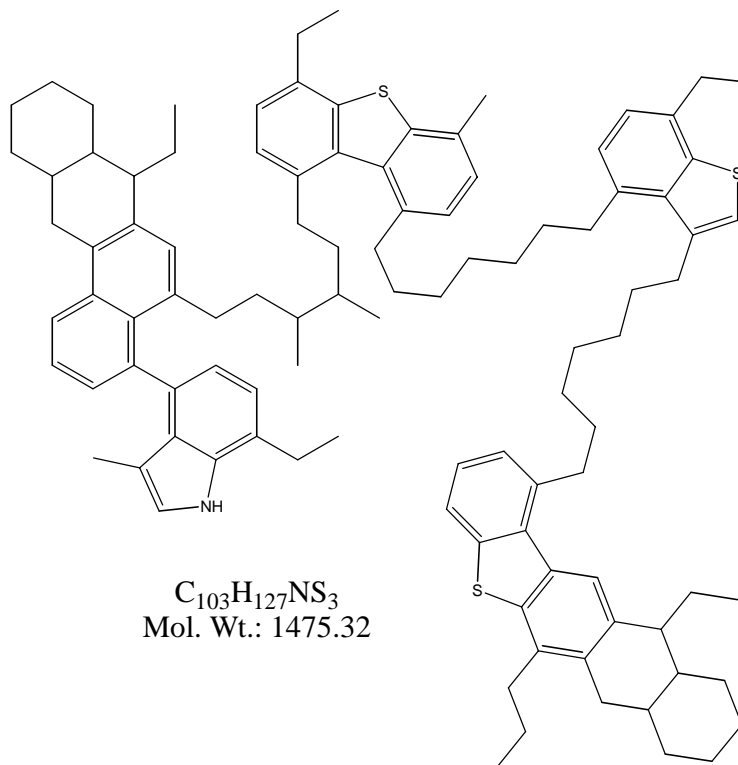


Molecule #4

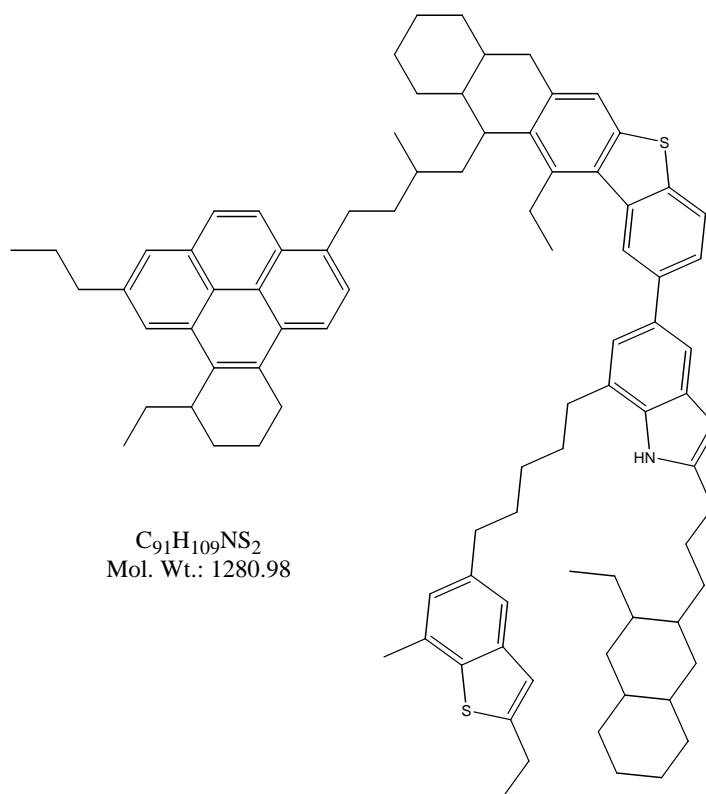


$C_{71}H_{103}NS_3$   
Mol. Wt.: 1066.78

Molecule #5

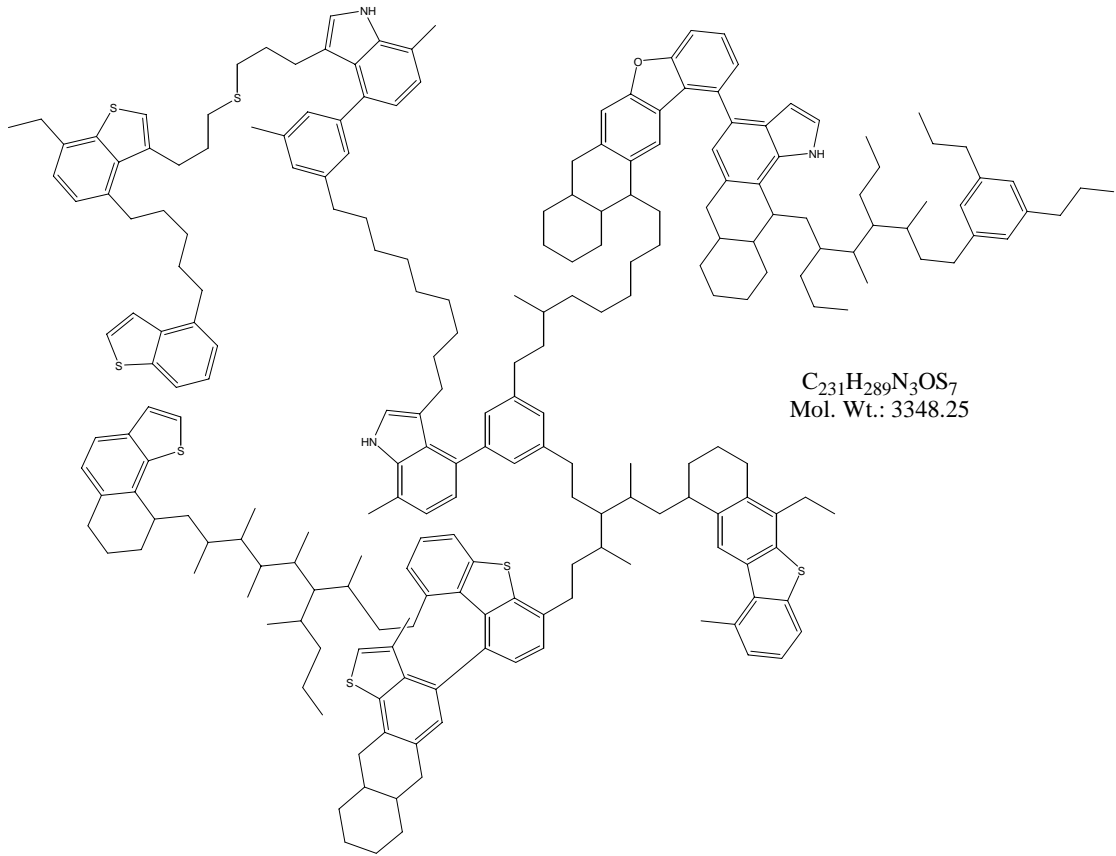


Molecule #6

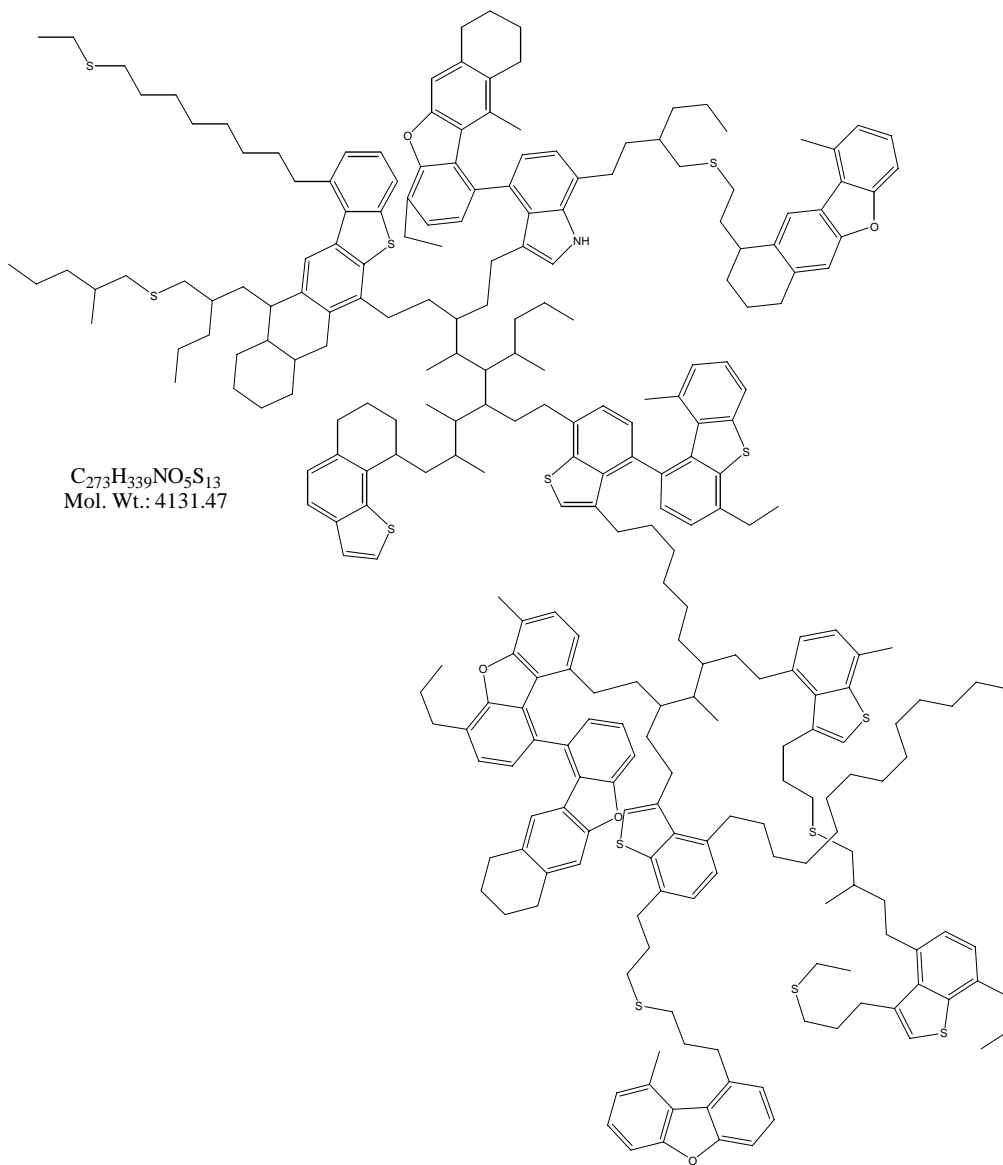


**Shermata's FRACTION 10**

Molecule #1

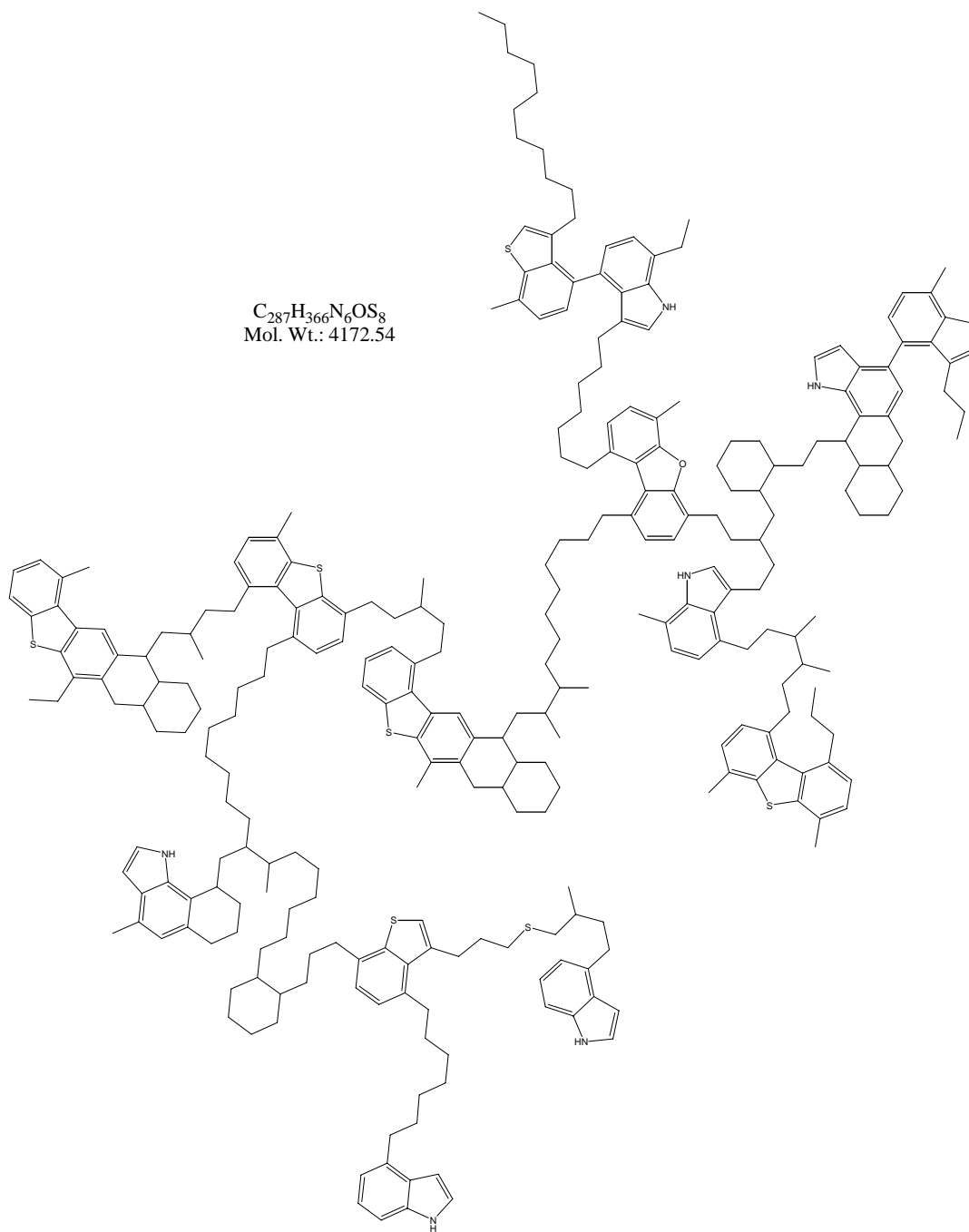


Molecule # 2

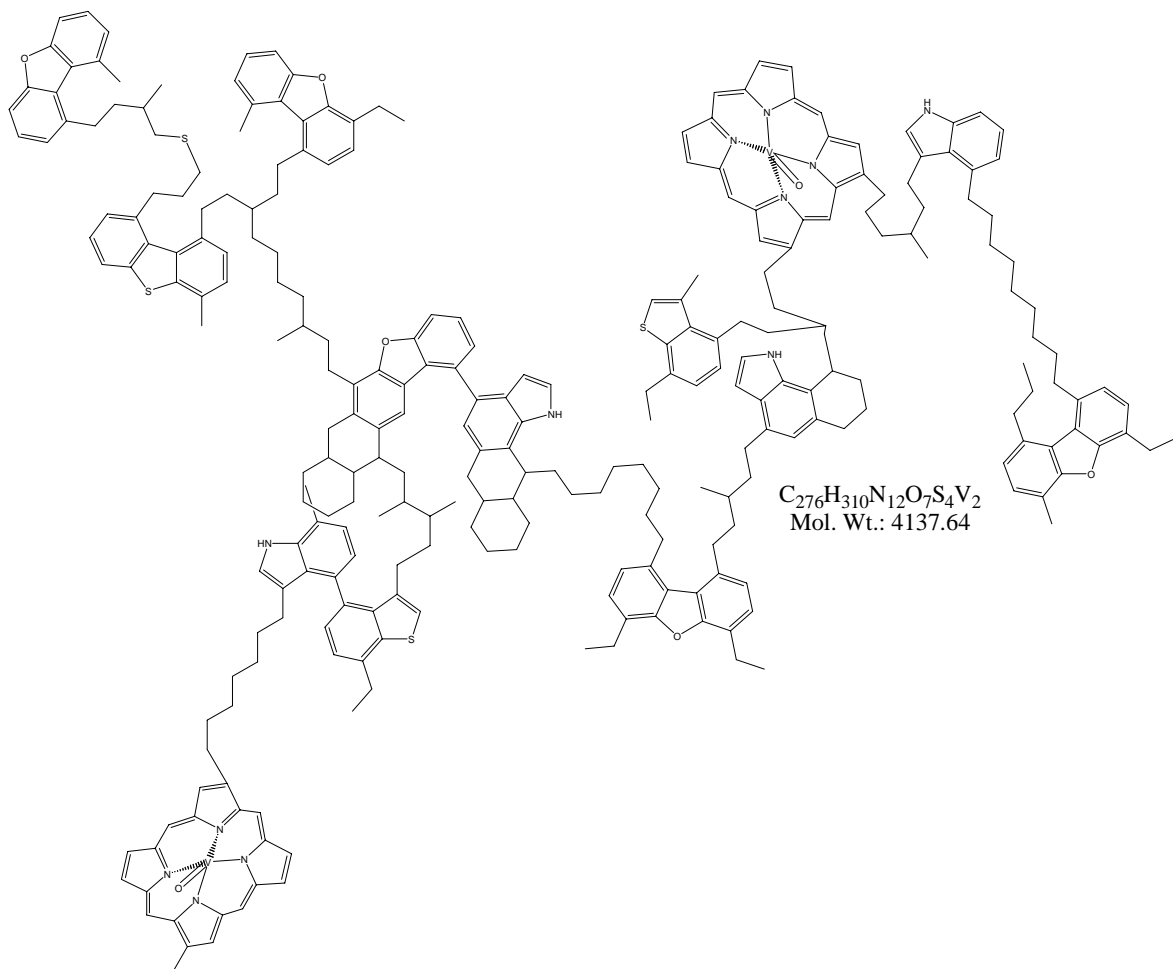


Molecule #3

$C_{287}H_{366}N_6OS_8$   
Mol. Wt.: 4172.54



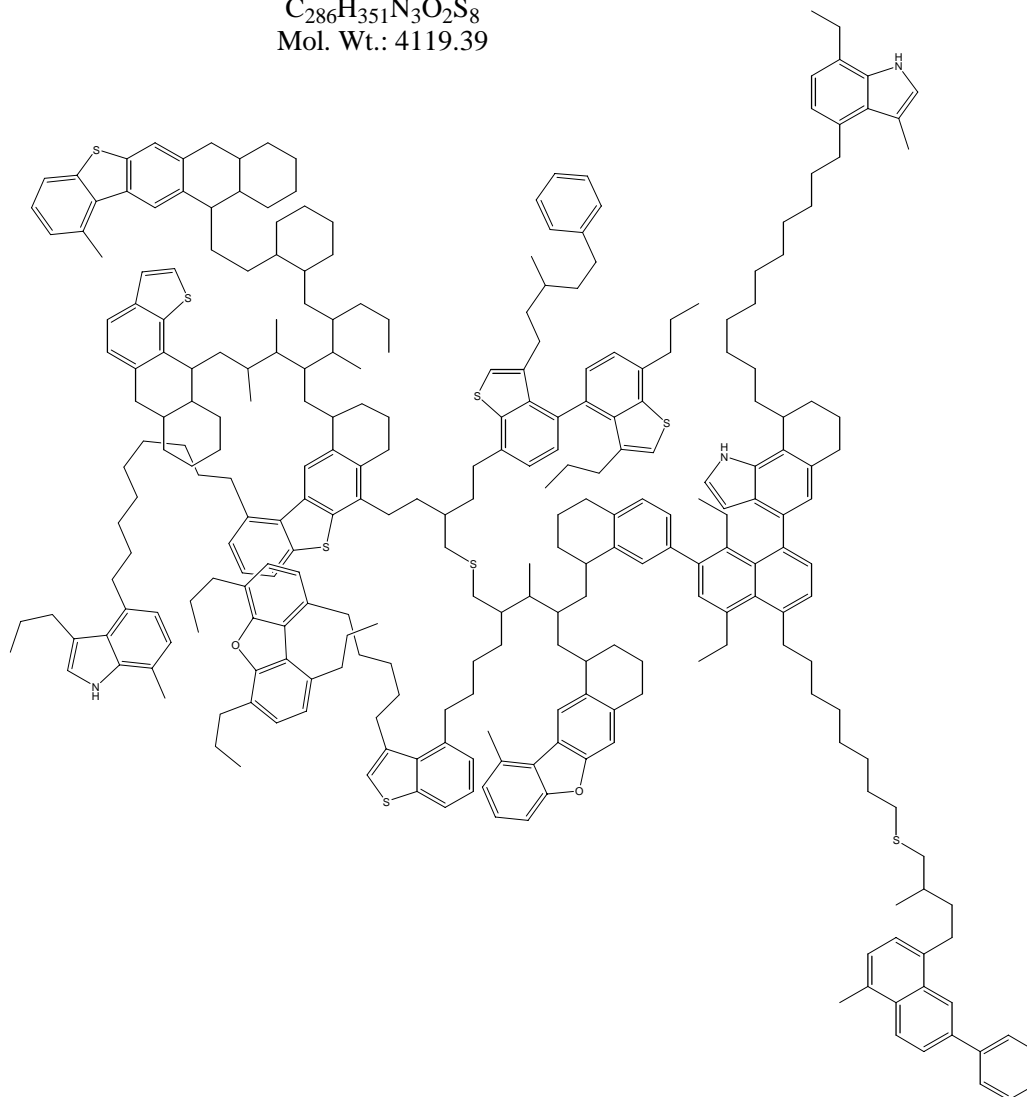
Molecule # 4



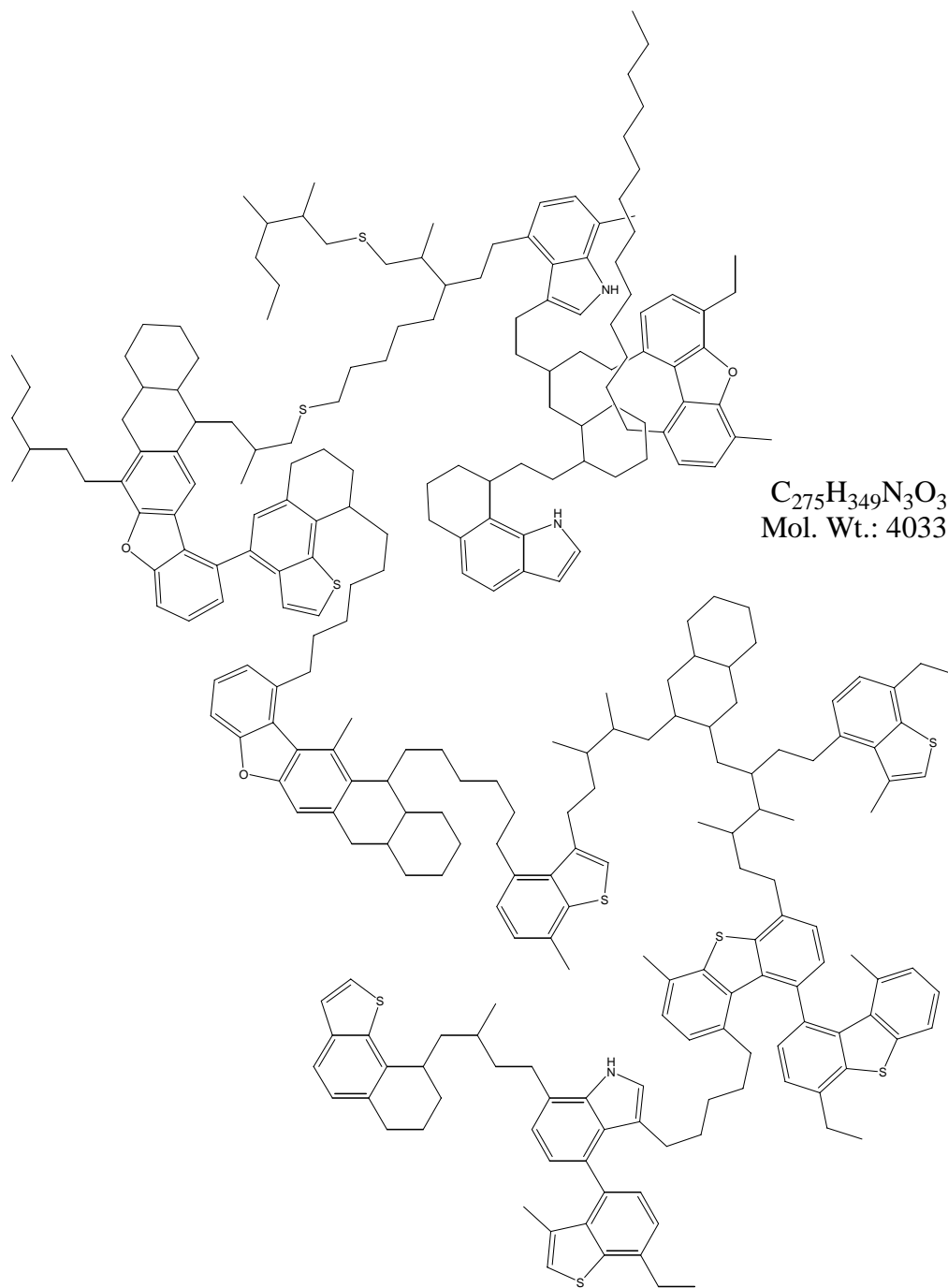


Molecule # 5

$C_{286}H_{351}N_3O_2S_8$   
Mol. Wt.: 4119.39



Molecule #6



$C_{275}H_{349}N_3O_3S_9$   
Mol. Wt.: 4033.33

---

## APPENDIX 5

---

**Partial Molar Volume from PREOS with General Mixing Rule**

$$P = \frac{RT}{V-b} - \frac{a}{V^2 + 2bV - b^2}$$

$$V = \frac{V_i}{n_i}$$

$$\therefore P = \frac{RT}{\frac{V_i}{n_i} - b} - \frac{a}{\left(\frac{V_i}{n_i}\right)^2 + 2b\frac{V_i}{n_i} - b^2} = \frac{n_i RT}{V_i - n_i b} - \frac{n_i^2 a}{V_i^2 + 2bn_i V_i - n_i^2 b^2}$$

Differentiating wrt  $n_i$

$$0 = \frac{RT}{V_i - n_i b} \cdot (1) - \frac{n_i RT}{(V_i - n_i b)^2} \cdot \left[ \frac{\partial V_i}{\partial n_i} - \left( \frac{\partial n_i b}{\partial n_i} \right) \right] - \frac{\frac{\partial}{\partial n_i} (an_i^2)}{V_i^2 + 2bn_i V_i - n_i^2 b^2} + an_i^2 \frac{\frac{\partial}{\partial n_i} (V_i^2 + 2bn_i V_i - n_i^2 b^2)}{(V_i^2 + 2bn_i V_i - n_i^2 b^2)^2}$$

$$0 = \frac{RT}{V_i - n_i b} - \frac{n_i RT}{(V_i - n_i b)^2} \cdot \left[ \frac{\partial V_i}{\partial n_i} - \left( \frac{\partial n_i b}{\partial n_i} \right) \right] - \frac{\frac{\partial}{\partial n_i} (an_i^2)}{V_i^2 + 2bn_i V_i - n_i^2 b^2} + \frac{2an_i^2}{(V_i^2 + 2bn_i V_i - n_i^2 b^2)^2} \left[ V_i \frac{\partial V_i}{\partial n_i} + V_i \left( \frac{\partial n_i b}{\partial n_i} \right) + bn_i \frac{\partial V_i}{\partial n_i} - n_i b \left( \frac{\partial n_i b}{\partial n_i} \right) \right]$$

$$\frac{\partial V_i}{\partial n_i} = \bar{V}_i$$

$$\bar{V}_i \left[ \frac{n_i RT}{(V_i - n_i b)^2} - \frac{2an_i^2 (V_i + bn_i)}{(V_i^2 + 2bn_i V_i - n_i^2 b^2)^2} \right] = \frac{RT}{V_i - n_i b} + \frac{n_i RT}{(V_i - n_i b)^2} \left( \frac{\partial n_i b}{\partial n_i} \right) - \frac{\frac{\partial}{\partial n_i} (an_i^2)}{V_i^2 + 2bn_i V_i - n_i^2 b^2} + \frac{2an_i^2}{(V_i^2 + 2bn_i V_i - n_i^2 b^2)^2} \left[ V_i \left( \frac{\partial n_i b}{\partial n_i} \right) - n_i b \left( \frac{\partial n_i b}{\partial n_i} \right) \right]$$

$$\frac{RT}{V_i - n_i b} + \frac{n_i RT}{(V_i - n_i b)^2} \left( \frac{\partial n_i b}{\partial n_i} \right) - \frac{\frac{\partial}{\partial n_i} (an_i^2)}{V_i^2 + 2bn_i V_i - n_i^2 b^2} +$$

$$\therefore \bar{V}_i = \frac{\frac{2an_i^2}{(V_i^2 + 2bn_i V_i - n_i^2 b^2)^2} \left[ V_i \left( \frac{\partial n_i b}{\partial n_i} \right) - n_i b \left( \frac{\partial n_i b}{\partial n_i} \right) \right]}{\left[ \frac{n_i RT}{(V_i - n_i b)^2} - \frac{2an_i^2 (V_i + bn_i)}{(V_i^2 + 2bn_i V_i - n_i^2 b^2)^2} \right]}$$

Partial molar volume at infinite dilution for a 2-component system:

$$\lim_{n_1 \rightarrow 0} \bar{V}_i = \bar{V}_1^\infty$$

$$\bar{V}_1^\infty = \frac{\frac{RT}{V_2 - n_2 b_2} + \frac{n_2 RT}{(V_2 - n_2 b_2)^2} \left( \frac{\partial n_1 b}{\partial n_1} \right) - \frac{\frac{\partial}{\partial n_1} (a n_1^2)}{V_2^2 + 2b_2 n_2 V_2 - n_2^2 b_2^2} + \frac{2a n_1^2}{(V_2^2 + 2b_2 n_2 V_2 - n_2^2 b_2^2)^2} + \left[ \frac{V_2}{V_2 - n_2 b_2} \left( \frac{\partial n_1 b}{\partial n_1} \right) - n_2 b_2 \left( \frac{\partial n_1 b}{\partial n_1} \right) \right]}{\left[ \frac{n_2 RT}{(V_2 - n_2 b_2)^2} - \frac{2a n_2^2 (V_2 + n_2 b_2)}{(V_2^2 + 2b_2 n_2 V_2 - n_2^2 b_2^2)^2} \right]}$$

$$\frac{\partial}{\partial n_k} (a n_1^2) = \frac{\partial}{\partial n_k} \left( n_1^2 \sum_i \sum_j x_i x_j a_{ij} \right) = \frac{\partial}{\partial n_k} \left( \sum_i \sum_j n_i n_j a_{ij} \right) = 2 \sum_{i \neq k} n_i a_{ik}$$

$$\frac{\partial (n_1 b)}{\partial n_i} = \frac{\partial}{\partial n_i} \left( n_1 \sum_i \sum_j x_i x_j b_{ij} \right) = \frac{\partial}{\partial n_i} \left( \frac{1}{n_1} \sum_i \sum_j n_i n_j b_{ij} \right) = \frac{2}{n_1} \sum_{i \neq k} n_i b_{ik} - \frac{1}{n_1^2} \sum_i \sum_j n_i n_j b_{ij} = \frac{2}{n_1} \sum_{i \neq k} n_i b_{ik} - b$$

For 2 – component mixture :

$$\frac{\partial}{\partial n_k} (a n_1^2) = 2 \sum_{i \neq k} n_i a_{ik} = 2 n_2 a_{21}$$

$$\frac{\partial (n_1 b)}{\partial n_i} = \frac{2}{n_1} \sum_{i \neq k} n_i b_{ik} - b = 2 b_{12} - b_2$$

$$\bar{V}_1^\infty = \frac{\frac{RT}{V_2 - n_2 b_2} + \frac{n_2 RT (2b_{12} - b_2)}{(V_2 - n_2 b_2)^2} - \frac{2n_2 a_{21}}{V_2^2 + 2b_2 n_2 V_2 - n_2^2 b_2^2} + \frac{2a_2 n_1^2}{(V_2^2 + 2b_2 n_2 V_2 - n_2^2 b_2^2)^2} + \left[ \frac{V_2 (2b_{12} - b_2) - n_2 b_2 (2b_{12} - b_2)}{V_2 - n_2 b_2} \right]}{\left[ \frac{n_2 RT}{(V_2 - n_2 b_2)^2} - \frac{2a_2 n_2^2 (V_2 + n_2 b_2)}{(V_2^2 + 2b_2 n_2 V_2 - n_2^2 b_2^2)^2} \right]}$$

$$\bar{V}_1^\infty = \frac{\frac{RT}{V_2 - b_2} + \frac{RT (2b_{12} - b_2)}{(V_2 - b_2)^2} - \frac{2a_{21}}{V_2^2 + 2b_2 V_2 - b_2^2} + \frac{2a_2 [V_2 (2b_{12} - b_2) - b_2 (2b_{12} - b_2)]}{(V_2^2 + 2b_2 V_2 - b_2^2)^2}}{\left[ \frac{RT}{(V_2 - b_2)^2} - \frac{2a_2 (V_2 + b_2)}{(V_2^2 + 2b_2 V_2 - b_2^2)^2} \right]}$$

**Table A5 - 1 Programs for regression of experimental partial molar volume at infinite dilution data with constrained critical properties derived from Riazi-Daubert correlations.**

<b>Matlab Program</b>	<b>Description</b>
PRGRD_Execute.m	Script file for specific molar volume, temperature and solvent data, initial guess for $T_b$ and SG and invoking the regression and outputting the optimized values. Values of $T_b$ and SG and the above data are passed to PR_RD.m during regression and values of specific molar volume are returned.
PRGRD_PMV.m	Accepts current values of $T_b$ and SG and specific molar volume, temperature and solvent data. $T_b$ and SG are used to calculate current critical properties and acentric factor. These parameters along with above data are used to calculate the specific partial molar volume at infinite dilute for the oil which is then returned to PRGRD_Execute.m
RiaziD.m	Accepts $T_b$ and SG and returns critical properties and acentric factor

**Table A5 - 2 Programs for regression of experimental partial molar volume at infinite dilution data with constrained critical properties derived from Twu correlations.**

<b>Matlab Program</b>	<b>Description</b>
PRGTwu_Execute.m	Script file for specific molar volume, temperature and solvent data, initial guess for $T_b$ and SG and invoking the regression and outputting the optimized values. Values of $T_b$ and SG and the above data are passed to PR_Twu.m during regression and values of specific molar volume are returned.
PRGTwu_PMV.m	Accepts current values of $T_b$ and SG and specific molar volume, temperature and solvent data. $T_b$ and SG are used to calculate current critical properties and acentric factor. These parameters along with above data are used to calculate the specific partial molar volume at infinite dilute for the oil which is then returned to PRGTwu_Execute.m
twucritical.m	Accepts $T_b$ and SG and returns critical properties and acentric factor
Twutheta.m	Returns a function to twucritical.m and PRGTwu.m that must be solved in order to calculate critical properties

### PRGRD Execute.m

```
% Script file to invoke NLINFIT and load function to fit from PRGRD_PMV.m
% We are solving for partial molar volume at infinite dilution using PR EOS and any
desired
% (G for general) mixing rules for "a" and "b".
% Riazi-Daubert correlation is used to limit Tc,Pc, MW and omega when Tb and SG are
specified.
```

```
% Clear all variables from workspace
clear
```

```
% Gas constant (J/mole-K)
Rg = 8.314472;
```

```
% Measured specific partial molar volumes at infinite dilution (m3/g):
% Y is a Nx1 matrix of responses
```

```
Y = [
8.55716E-07;
8.67772E-07;
8.52896E-07;
8.60775E-07;
```

```
8.51745E-07;
8.60142E-07;
8.63773E-07;
8.73665E-07;
```

```
8.56751E-07;
8.58103E-07;
8.6788E-07;
8.69806E-07
];
```

```
% Measured T (K) and molar volume (V2 (m3/mole)) for each solvent
```

```
% Toluene
Xs1 = [298.15 1.075013E-04;
313.15 1.089227E-04;
333.15 1.110201E-04;
353.15 1.133883E-04;
];
```

```
T = Xs1(:,1);
```

```

% Critical properties from DIPPR database
Tc = 591.75;
Pc = 41.08*1e5;
omega = 0.264012;
b = 0.07779607390389232*Rg*Tc/Pc;
[i,j]=size(Xs1);
b = b*ones(i,1);

ac = 0.4572355289213894*Tc^2*Rg^2/Pc;

m = 0.37464 + 1.54266*omega - 0.26992*omega^2;
alpha = (1 + m*(1 - (T./Tc).^0.5)).^2;
a = ac*alpha;

```

```

Xs1 = [Xs1,b,a];

```

```

% 1-methylnaphthalene
Xs2 = [298.15 1.483321E-04;
313.15 1.493593E-04;
333.15 1.508260E-04;
353.15 1.524145E-04;
];

```

```

T = Xs2(:,1);

```

```

% Critical properties from DIPPR database
Tc = 772.00;
Pc = 36.00*1e5;
omega = 0.341609;
b = 0.07779607390389232*Rg*Tc/Pc;
[i,j]=size(Xs2);
b = b*ones(i,1);

```

```

ac = 0.4572355289213894*Tc^2*Rg^2/Pc;

```

```

m = 0.37464 + 1.54266*omega - 0.26992*omega^2;
alpha = (1 + m*(1 - (T./Tc).^0.5)).^2;
a = ac*alpha;

```

```

Xs2 = [Xs2,b,a];

```

```

% quinoline
Xs3 = [298.15 1.179892E-04;
313.15 1.187947E-04;
333.15 1.199431E-04;
353.15 1.211846E-04];

```



```

T = Xs3(:,1);
% Critical properties from DIPPR database
Tc = 782.15;
Pc = 48.6*1e5;
omega = 0.346481;
b = 0.07779607390389232*Rg*Tc/Pc;
[i,j]=size(Xs3);
b = b*ones(i,1);

ac = 0.4572355289213894*Tc^2*Rg^2/Pc;

m = 0.37464 + 1.54266*omega - 0.26992*omega^2;
alpha = (1 + m*(1 - (T./Tc).^0.5)).^2;
a = ac*alpha;

Xs3 = [Xs3,b,a];

% Independent variables for calculaing specific partial molar volumes - T, V2, b2 and a2:
% X is Nx4 matrix of independent variables

% ABVB, toluene, 1-methylnaphthalene, quinoline
X= [Xs1;Xs2;Xs3];
% X= [Xs2;Xs3];
% X= [Xs3];

% Initial guesses for oil parameter B(Tb(R); 1000*SG):
% B is a 2x1 matrix of parameters to fit
B = [2000; 1100];

% Options for nlinfit
options = statset('MaxIter', 1000, 'TolFun', 1e-12, 'TolX', 1e-12);

% Run least squares parameter fit:
[Bfit,Residual,Jacobian] = nlinfit(X,Y,@PRGRD_PMV,B, options);

% Estimate 95% confidence interval for fit:
CI = nlparci(Bfit,Residual,Jacobian);

% Plot data with 95% confidence limits:
%nlintool(X,Y,@PRG2_PMV,B)

% Model predictions
Ymod = PRGRD_PMV(Bfit,X);

```

```

% Sum residuals of absolute relative error
Tare = sum(abs(Y - Ymod)./Y);

%Gas constant
Rg = 8.314472;

% Plotting the results
% V from model for plotting
Ymod = PRGRD_PMV(Bfit,X);

%Maximum and minimum for plot
xmini = min(Ymod);
xmaxi = max(Ymod);
ymini = min(Y);
ymaxi = max(Y);

maxi = [xmaxi ymaxi];
mini = [xmini ymini];

smaxi = max(maxi);
smini = min(mini);

% Bold axes
axes('FontWeight','bold','FontSize', 14);

% Plot data and calculations
% Ranges for individual curves:
k =
plot(Y(1:4),Ymod(1:4),'bo',Y(5:8),Ymod(5:8),'gd',Y(9:12),Ymod(9:12),'ks','MarkerFaceColor',
'r','auto');
% k = plot(Y(1:4),Ymod(1:4),'bo',Y(5:8),Ymod(5:8),'gd','MarkerFaceColor','auto');
% k = plot(Y(1:4),Ymod(1:4),'bo','MarkerFaceColor','auto');

set (k, 'Markersize', 10);

% Ranges for axes so that plot is square:
axis([smini smaxi smini smaxi]);

% Label for axes:
L = xlabel('V^\infty_m_e_a_s_d_ (m^3/mole)');
m = ylabel('V^\infty_m_o_d_e_l (m^3/mole)');
set (L,'FontWeight','bold','FontSize', 16);
set (m,'FontWeight', 'bold','FontSize', 16);
%

n = legend('toluene','1-methylnaphthalene','quinoline');
set (n,'FontWeight', 'bold','FontSize', 14);

```

```

legend boxoff;

% q = title('Oil with Riazi-Daubert Critical Properties');
q = title('ABVB with Twu Critical Properties');
set (q,'FontWeight', 'bold','FontSize', 15);
% Optimum Tb (R) and SG
Tb = Bfit(1);
SG = Bfit(2)/1000;

%Calculate critical properties from optimized Tb and SG
crit = RiaziD(Tb,SG);
Tc = crit(1);
Pc = crit(2)/1000; % Pc in kPa
omega = crit(3);
MW = crit(4);

% Calculated ac and b from optimized Tb and SG :
ac = 0.45723553*Rg^2*Tc^2/(Pc*1000);
b = 0.07779607*Rg*Tc/(Pc*1000);

% Optimized Tb output in K
Tb = Tb/1.8;

% Optimum properties
Op = [Tc;Pc;omega;MW;ac;b;Tb;SG];

% Calculate critical properties from 95% confidence limits Tb and SG
Tb1 = CI(1,1);
Tb2 = CI(1,2); % Tb must be in R
SG1 = CI(2,1)/1000; % Correction for scaling
SG2 = CI(2,2)/1000; % Correction for scaling

% Tb must be in R
crit1 = RiaziD(Tb1,SG1); %95% limits for Tc (K), Pc (Pa), omega and MW
crit2 = RiaziD(Tb2,SG2);

crit1(2) = crit1(2)/1000; %Pc in kPa
crit2(2) = crit2(2)/1000; %Pc in kPa

CIcrit = [crit1 crit2]; % concatenate 95% limits for Tc, Pc (Pa), omega and MW

ac1 = 0.45723553*Rg^2*crit1(1)^2/(crit1(2)*1000); % Note that Pc is in Pa for these
equations
b1 = 0.07779607*Rg*crit1(1)/(crit1(2)*1000);
ac2 = 0.45723553*Rg^2*crit2(1)^2/(crit2(2)*1000);
b2 = 0.07779607*Rg*crit2(1)/(crit2(2)*1000);

```

CIab = [ac1 ac2; b1 b2]; % 95% limits for ac abd b

CI(1,1:2) = CI(1,1:2)/1.8; % 95% limits for Tb in K

CI(2,1:2) = CI(2,1:2)/1000; % Correction for scaling

CIprop = [CIcrit; CIab; CI]; %Concatenate 95% confidence limit Tb and SG with those for critical properties

% Format output

format long e

'Calculated values for Tc(K), Pc(kPa), omega, MW(g/ mole), ac (J/m3/mole2), b (m3/mole) and optimum Tb (K) and SG'

Op

'95% confidence interval for calculated Tc(K), Pc(kPa), omega, MW(g/ mole), ac (J/m3/mole2), b (m3/mole), Tb (K) and SG'

CIprop

'Sum absolute relative error'

Tare

Y

Ymod

---

### PRGRD\_PMV.m

function Y = PRGRD\_PMV(B,X)

% This function provides the equation to which parameters for an oil will be fitted using PR CEOS.

% The function is generic in that different mixing rules can be employed.

% Riazi-Daubert correlation is used to limit Tc,Pc, MW and omega when Tb and SG are specified.

%

% X is a matrix containing the following parameters:

% T - Temperature (K)

% V2 - Molar volume of solvent (m3/mole)

% b2 - Co-volume of solvent (m3/mole)

% a2- Attractive parameter for solvent (J-m3/mole2)

%

% B is a matrix of the parameters to be fitted:

% Tb - Boiling point in Rankin

% S.G. - specific gravity at 15.6C

%

% Correltaions developed by Riazi-Daubert are used to compute critical properties

% from Tb and S.G.:

```

% b1 - Co-volume of oil (m3/mole)
% a1 - Attractive parameter for oil (J-m3/mole2)
% MW - Molar mass of oil (g/mole)
% omega - acentric factor for oil

% Gas constant (J/mole-K)
Rg = 8.314472;

% Oil parameters
Tb = B(1);
SG = B(2)/1000;

% Solvent parameters:
T = X(:,1);
V2 = X(:,2);
b2 = X(:,3);
a2 = X(:,4);

% Compute Tc, Pc
% Tb must be in Kelvin
Tb = Tb/1.8;

% Tc and Pc from Riazi and Daubert; MW by API method
Tc = 35.9413*(exp(-6.9e-4*Tb - 1.4442*SG + 4.91e-4*Tb*SG))*Tb^0.7293*SG^1.2771; % T in Kelvin
Pc = 6.9575*(exp(-1.35e-2*Tb - 0.3129*SG + 9.174e-3*Tb*SG))*Tb^0.6791*SG^-0.6807; % Pc in bars
Vc = 6.1677e4*(exp(-7.583e-3*Tb - 28.5524*SG + 0.01172*Tb*SG))*Tb^1.20493*SG^17.2074; % Vc in m3/mol
MW = 42.965*(exp(2.097e-4*Tb - 7.78712*SG + 2.08476e-3*Tb*SG))*Tb^1.26007*SG^4.98308;

Pc = 1e5*Pc; % Pc in Pa

% Compute omega from Tc, Pc and Vc using method of Ambrose
% Tb in Kelvin
omega = -(log(Pc*0.986923266716E-05) +((-5.97616*(1-(Tb)/Tc)+1.29874*(1-(Tb)/Tc)^1.5 - 0.60394*(1-(Tb)/Tc)^2.5-1.06841*(1-(Tb)/Tc)^5)/(((Tb)/Tc)))/((-5.03365*(1-(Tb)/Tc)+1.11505*(1-(Tb)/Tc)^1.5 -5.41217*(1-(Tb)/Tc)^2.5-7.46628*(1-(Tb)/Tc)^5)/(((Tb)/Tc)));

% Oil parameters
b1 =0.077796076*Rg*Tc/Pc;
ac =0.457235532*Tc^2*Rg^2/Pc;

if omega < 0.491;

```

```

    m = 0.37464 + 1.54226*omega - 0.26992*omega.^2;
else
    m = 0.379642 + 1.48503*omega - 0.164423*omega.^2 + 0.016666*omega.^3;
end

alpha = (1 + m*(1 - (T./Tc).^0.5)).^2;
a1 = ac*alpha;

% Differentiation of mixing rules:
% Differentiation of a (ad); do not include the n2 term in the denominator:

% vdW mixing rule, energy term:
a12 = (a1.*a2).^0.5;
ad = 2*a12 - 2*a2;

% vdW linear mixing rule
% b12 = 0.5*(b1 + b2);
b12vdw = 0.5*(b1 + b2);

% Lorentz mixing rule
% b12 = 0.125*(b1.^(1/3) + b2.^(1/3)).^3;

% Geometric mean rule
% b12 = (b1.*b2).^0.5;

% Lee and Sandler mixing rule
b12 = ((b1.^(2/3) + b2.^(2/3))./2).^3/2;

% Binary interaction term for co-volumes
lij = ((b1 - b2).^2/(b1^2 + b2.^2));
% lij = 1 - ((b1 - b2).^2/(b1^2 + b2.^2));
% lij = 1 - 2*(b1*b2).^0.5/(b1 + b2);
% lij = 0; % Single vdW mixing rule
% lij = 1; % non-vdW mixing rule

% Differentiation of co-volume term:
bd = (1-lij)*(2*b12vdw - 2*b2) + lij*(2*b12 - 2*b2);

% Numerator for Y
yn = (Rg*T./(V2-b2)+ Rg*(bd + b2).*T./(V2-b2).^2 -(ad + 2*a2)./(V2.^2 + 2*b2.*V2 -
b2.^2)+ a2.*(2*V2.*bd + 2*b2.*V2 - 2*b2.^2 - 2*b2.*bd)./(V2.^2 + 2*b2.*V2 - b2.^2).^2);

% Numerator for Y
yd = (Rg*T./(V2-b2).^2 - 2*a2.*(V2 + b2)./(V2.^2 + 2*b2.*V2 - b2.^2).^2);

% Function to be fitted:
Y = (yn./yd)./MW;

```

---

### RiaziD.m

function f = RiaziD(Tb,SG)

% Function to calculate Tc, Pc and omega from Tb in R and SG

% Tb must be in Kelvin

Tb = Tb/1.8;

% SG is unscaled

% Tc and Pc from Riazi and Daubert; MW by API method

Tc = 35.9413\*(exp(-6.9e-4\*Tb - 1.4442\*SG + 4.91e-4\*Tb\*SG))\*Tb^0.7293\*SG^1.2771; % T in Kelvin

Pc = 6.9575\*(exp(-1.35e-2\*Tb - 0.3129\*SG + 9.174e-3\*Tb\*SG))\*Tb^0.6791\*SG^-0.6807; % Pc in bars

Vc = 6.1677e4\*(exp(-7.583e-3\*Tb - 28.5524\*SG + 0.01172\*Tb\*SG))\*Tb^1.20493\*SG^17.2074; % Vc in m3/mol

MW = 42.965\*(exp(2.097e-4\*Tb - 7.78712\*SG + 2.08476e-3\*Tb\*SG))\*Tb^1.26007\*SG^4.98308;

% Compute omega from Tc, Pc and Tb using method of Ambrose

omega = -(log(Pc/1.01325) + ((-5.97616\*(1-Tb/Tc)+1.29874\*(1-Tb/Tc)^1.5 -0.60394\*(1-Tb/Tc)^2.5-1.06841\*(1-Tb/Tc)^5)/((Tb/Tc))))/((-5.03365\*(1-Tb/Tc)+1.11505\*(1-Tb/Tc)^1.5 -5.41217\*(1-Tb/Tc)^2.5-7.46628\*(1-Tb/Tc)^5)/((Tb/Tc)));

Pc = 1e5\*Pc; % Pc in Pa

f = [Tc;

Pc;

omega;

MW];

---

### PRGTWu\_Execute.m

% Script file to invoke NLINFIT and load function to fit from PRGTWu\_PMV.m

% We are solving for partial molar volume at infinite dilution using PR EOS and any desired

% (G for general) mixing rules for "a" and "b".

% Twu's correlation is used to limit Tc,Pc, MW and omega when Tb and SG are specified.

```

% Clear all variables from workspace
clear

% Gas constant (J/mole-K)
Rg = 8.314472;

% Measured specific partial molar volumes at infinite dilution (m3/g):
% Y is a Nx1 matrix of responses

Y = [
% 8.55716E-07;
% 8.67772E-07;
% 8.52896E-07;
% 8.60775E-07;

8.51745E-07;
8.60142E-07;
8.63773E-07;
8.73665E-07;

8.56751E-07;
8.58103E-07;
8.6788E-07;
8.69806E-07
];

% Measured T (K) and molar volume (V2 (m3/mole)) for each solvent

% % Toluene
% Xs1 = [298.15 1.075013E-04;
% 313.15 1.089227E-04;
% 333.15 1.110201E-04;
% 353.15 1.133883E-04;
% ];
%
% T = Xs1(:,1);
%
% % Critical properties from DIPPR database
% Tc = 591.75;
% Pc = 41.08*1e5;
% omega = 0.264012;
% b = 0.07779607390389232*Rg*Tc/Pc;
% [i,j]=size(Xs1);
% b = b*ones(i,1);

```



```

%
% ac =0.4572355289213894*Tc^2*Rg^2/Pc;
%
% m = 0.37464 + 1.54266*omega - 0.26992*omega^2;
% alpha = (1 + m*(1 - (T./Tc).^0.5)).^2;
% a = ac*alpha;
%
% Xs1 = [Xs1,b,a];

```

```

% 1-methylnaphthalene
Xs2 = [298.15 1.483321E-04;
313.15 1.493593E-04;
333.15 1.508260E-04;
353.15 1.524145E-04;
];

```

```

T = Xs2(:,1);

```

```

% Critical properties from DIPPR database
Tc = 772.00;
Pc = 36.00*1e5;
omega = 0.341609;
b =0.07779607390389232*Rg*Tc/Pc;
[i,j]=size(Xs2);
b = b*ones(i,1);

```

```

ac =0.4572355289213894*Tc^2*Rg^2/Pc;

```

```

m = 0.37464 + 1.54266*omega - 0.26992*omega^2;
alpha = (1 + m*(1 - (T./Tc).^0.5)).^2;
a = ac*alpha;

```

```

Xs2 = [Xs2,b,a];

```

```

% quinoline
Xs3 = [298.15 1.179892E-04;
313.15 1.187947E-04;
333.15 1.199431E-04;
353.15 1.211846E-04
];

```

```

T = Xs3(:,1);

```

```

% Critical properties from DIPPR database
Tc = 782.15;
Pc = 48.6*1e5;
omega = 0.346481;
b =0.07779607390389232*Rg*Tc/Pc;

```

```

[i,j]=size(Xs3);
b = b*ones(i,1);

ac =0.4572355289213894*Tc^2*Rg^2/Pc;

m = 0.37464 + 1.54266*omega - 0.26992*omega^2;
alpha = (1 + m*(1 - (T./Tc).^0.5)).^2;
a = ac*alpha;

Xs3 = [Xs3,b,a];

% Independent variables for calculaing specific partial molar volumes - T, V2, b2 and a2:
% X is Nx4 matrix of independent variables

% ABVB, toluene, 1-methylnaphthalene, quinoline
% X= [Xs1;Xs2;Xs3];
X= [Xs2;Xs3];
% X= [Xs3];

% Initial guesses for asphaltenes parameter B(Tb(R); 1000*SG):
% B is a 2x1 matrix of parameters to fit
B = [1600; 600];

% Options for nlinfit
options = statset('MaxIter', 2000, 'TolFun', 1e-12, 'TolX', 1e-12);

% Run least squares parameter fit:
[Bfit,Residual,Jacobian] = nlinfit(X,Y,@PRGTwu_PMV,B, options);

% Estimate 95% confidence interval for fit:
CI = nlparci(Bfit,Residual,Jacobian);

% Plot data with 95% confidence limits:
%nlintool(X,Y,@PRG2_PMV,B)

% Model predictions
Ymod = PRGTwu_PMV(Bfit,X)
Y

% Sum residuals of absolute relative error
Tare = sum(abs(Y - Ymod)./Y);

%Gas constant
Rg = 8.314472;

% Plotting the results

```

```

%V from model for plotting
Ymod = PRGTwu_PMV(Bfit,X);

%Maximum and minimum for plot
xmini = min(Ymod);
xmaxi = max(Ymod);
ymini = min(Y);
ymaxi = max(Y);

maxi = [xmaxi ymaxi];
mini = [xmini ymini];

smaxi = max(maxi);
smini = min(mini);

% Bold axes
axes('FontWeight','bold','FontSize', 14);

% Plot data and calculations
% Ranges for individual curves:
% k =
plot(Y(1:4),Ymod(1:4),'bo',Y(5:8),Ymod(5:8),'gd',Y(9:12),Ymod(9:12),'ks','MarkerFaceColor','auto');
k = plot(Y(1:4),Ymod(1:4),'bo',Y(5:8),Ymod(5:8),'gd','MarkerFaceColor','auto');
% k = plot(Y(1:4),Ymod(1:4),'bo','MarkerFaceColor','auto');

set (k, 'Markersize', 10);

% Ranges for axes so that plot is square:
axis([smini smaxi smini smaxi]);

% Label for axes:
L = xlabel('V^\infty_{m_e_a_s_d} (m^3/mole)');
m = ylabel('V^\infty_{m_o_d_e_l} (m^3/mole)');
set (L,'FontWeight','bold','FontSize', 16);
set (m,'FontWeight', 'bold','FontSize', 16);
%

n = legend('toluene','1-methylnaphthalene', 'quinoline');
set (n,'FontWeight', 'bold','FontSize', 14);
legend boxoff;

% q = title('Oil with Twu Critical Properties');
q = title('ABVB with Twu Critical Properties');
set (q,'FontWeight', 'bold','FontSize', 15);

% Optimum Tb (R) and SG

```

```

Tb = Bfit(1);
SG = Bfit(2)/1000;

%Calculate critical properties from optimized Tb and SG
crit = twucritical(Tb,SG);
Tc = crit(1);
Pc = crit(2)/1000; % Pc in kPa
omega = crit(3);
MW = crit(4);

% Calculated ac and b from optimized Tb and SG :
ac = 0.45723553*Rg^2*Tc^2/(Pc*1000);
b = 0.07779607*Rg*Tc/(Pc*1000);

% Optimized Tb output in K
Tb = Tb/1.8;

% Optimum properties
Op = [Tc;Pc;omega;MW;ac;b;Tb;SG];

% Calculate critical properties from 95% confidence limits Tb and SG
Tb1 = CI(1,1);
Tb2 = CI(1,2); % Tb must be in R
SG1 = CI(2,1)/1000; % Correction for scaling
SG2 = CI(2,2)/1000; % Correction for scaling

% Tb must be in R
crit1 = twucritical(Tb1,SG1); %95% limits for Tc (K), Pc (Pa), omega and MW
crit2 = twucritical(Tb2,SG2);

crit1(2) = crit1(2)/1000; %Pc in kPa
crit2(2) = crit2(2)/1000; %Pc in kPa

CIcrit = [crit1 crit2]; % concatenate 95% limits for Tc, Pc (Pa), omega and MW

ac1 = 0.45723553*Rg^2*crit1(1)^2/(crit1(2)*1000); % Note that Pc is in Pa for these
equations
b1 = 0.07779607*Rg*crit1(1)/(crit1(2)*1000);
ac2 = 0.45723553*Rg^2*crit2(1)^2/(crit2(2)*1000);
b2 = 0.07779607*Rg*crit2(1)/(crit2(2)*1000);

CIab = [ac1 ac2; b1 b2]; % 95% limits for ac abd b

CI(1,1:2) = CI(1,1:2)/1.8; % 95% limits for Tb in K
CI(2,1:2) = CI(2,1:2)/1000; % Correction for scaling

```

Clprop = [Clcrit; Clab; CI]; %Concatenate 95% confidence limit Tb and SG with those for critical properties

% Format output  
format long e

'Calculated values for Tc(K), Pc(kPa), omega, MW(g/mole), ac (J/m<sup>3</sup>/mole<sup>2</sup>), b (m<sup>3</sup>/mole) and optimum Tb (K) and SG'  
Op

'95% confidence interval for calculated Tc(K), Pc(kPa), omega, MW(g/mole), ac (J/m<sup>3</sup>/mole<sup>2</sup>), b (m<sup>3</sup>/mole),Tb (K) and SG'  
Clprop

'Sum absolute relative error'  
Tare

Y  
Ymod

---

### PRGTwu\_PMV.m

function Y = PRGTwu\_PMV(B,X)

% This function provides the equation to which parameters for asphaltenes or oil will be fitted using PR EOS.

% The function is generic in that different mixing rules can be employed.

% Twu's correlation is used to limit Tc,Pc, MW and omega when Tb and SG are specified.

%

% X is a matrix containing the following parameters:

% T - Temperature (K)

% V2 - Molar volume of solvent (m<sup>3</sup>/mole)

% b2 - Co-volume of solvent (m<sup>3</sup>/mole)

% a2- Attractive parameter for solvent (J-m<sup>3</sup>/mole<sup>2</sup>)

%

% B is a matrix of the parameters to be fitted:

% Tb - Boiling point in Rankin

% S.G. - specific gravity at 15.6C

%

% Correltaions developed by Twu are used to compute critical properties

% from Tb and S.G.:

% b1 - Co-volume of asphaltenes (m<sup>3</sup>/mole)

% a1 - Attractive parameter for asphaltenes (J-m<sup>3</sup>/mole<sup>2</sup>)

% MW - Molar mass of asphaltenes (g/mole)

% omega - acentric factor for asphaltenes

% Gas constant (J/mole-K)

```

Rg = 8.314472;

% Oil parameters
Tb = B(1);
SG = B(2)/1000;

% Solvent parameters:
T = X(:,1);
V2 = X(:,2);
b2 = X(:,3);
a2 = X(:,4);

% First compute reference properties for n-alkane with Tb and S.G.
Tco = Tb*(0.533272 + 0.191017*1e-3*Tb + 0.779681*1e-7*Tb^2 - 0.284376*1e-10*Tb^3 +
0.959468*1e28/Tb^13)^-1;
alpha = 1-(Tb/Tco);
Vco = (1-(0.419869 - 0.505839*alpha - 1.56436*alpha^3 - 9481.70*alpha^14))^-8;
SGo = 0.843593 - 0.128624*alpha - 3.36159*alpha^3 - 13749.5*alpha^12;

% Need to iterate for MWo
MW0 = Tb/(10.44 - 0.0052*Tb);
theta0 = log(MW0);
options=optimset('Display','off');
[theta,fval] = fsolve(@(theta) Twutheta(theta,Tb),theta0,options);
MWo = exp(theta);

Pco = (3.83354 + 1.19629*alpha^0.5 + 34.8888*alpha + 36.1952*alpha^2 +
104.193*alpha^4)^2;

% Use reference values for n-alkane to compute properties for fluid
dSGT = exp(5*(SGo - SG))-1;
fT = dSGT*(-0.362456/Tb^0.5 + (0.0398285 - 0.948125/Tb^0.5)*dSGT);
Tcr = Tco*((1 + 2*fT)/(1-2*fT))^2; % Tc in Rankin
Tc = Tcr/1.8;

dSGV = exp(4*(SGo^2 - SG^2))-1;
fV = dSGV*(0.466590/Tb^0.5 + (-0.182421 + 3.01721/Tb^0.5)*dSGV);
Vcf = Vco*((1 + 2*fV)/(1-2*fV))^2; % Vc in ft3/lb/ mole
Vc = Vcf/(35.314666721*453.592370000) ;

dSGP = exp(0.5*(SGo - SG))-1;
fP = dSGP*((2.53262 - 46.1955/Tb^0.5 - 0.00127885*Tb) + (-11.4277 + 252.140/Tb^0.5 +
0.00230535*Tb)*dSGP);
Pcp = Pco*(Tcr/Tco)*(Vco/Vcf)*((1 + 2*fP)/(1 - 2*fP))^2; % Pc in psia
Pc = Pcp*6894.757293168;

dSGM = dSGT;

```

```

x = abs(0.0123420 - 0.328086/Tb^0.5);
fM = dSGM*(x + (-0.0175691 + 0.193168/Tb^0.5)*dSGM);
MW = exp(log(MWo)*((1 + 2*fM)/(1-2*fM))^2); % MW in lb/lb-mol = g/g-mol

% Compute omega from Tc, Pc and Vc using method of Ambrose
omega = -(log(Pc*0.986923266716E-05) + ((-5.97616*(1-(Tb/1.8)/Tc)+1.29874*(1-
(Tb/1.8)/Tc)^1.5 - 0.60394*(1-(Tb/1.8)/Tc)^2.5 - 1.06841*(1-
(Tb/1.8)/Tc)^5)/(((Tb/1.8)/Tc)))/((-5.03365*(1-(Tb/1.8)/Tc)+1.11505*(1-
(Tb/1.8)/Tc)^1.5 - 5.41217*(1-(Tb/1.8)/Tc)^2.5 - 7.46628*(1-
(Tb/1.8)/Tc)^5)/(((Tb/1.8)/Tc)));

% Oil parameters
b1 = 0.077796076*Rg*Tc/Pc;
ac = 0.457235532*Tc^2*Rg^2/Pc;

if omega < 0.491;
    m = 0.37464 + 1.54226*omega - 0.26992*omega.^2;
else
    m = 0.379642 + 1.48503*omega - 0.164423*omega.^2 + 0.016666*omega.^3;
end

alpha = (1 + m*(1 - (T./Tc).^0.5)).^2;
a1 = ac*alpha;

% Differentiation of mixing rules:
% Differentiation of a (ad); do not include the n2 term in the denominator:

% vdW mixing rule, energy term:
a12 = (a1.*a2).^0.5;
ad = 2*a12 - 2*a2;

% vdW linear mixing rule
b12 = 0.5*(b1 + b2);
b12vdw = 0.5*(b1 + b2);

% Lorentz mixing rule
% b12 = 0.125*(b1.^(1/3) + b2.^(1/3)).^3;

% Geometric mean rule
% b12 = (b1.*b2).^0.5;

% Lee and Sandler mixing rule
% b12 = ((b1.^(2/3) + b2.^(2/3))./2).^3/2;

% Binary interaction term for co-volumes
% lij = ((b1 - b2).^2/(b1^2 + b2.^2));

```

```

% lij = 1 - ((b1 - b2).^2/(b1^2 + b2.^2));
% lij = 1 - 2*(b1*b2).^0.5/(b1 + b2);
% lij = 0; % Single vdW mixing rule
lij = 1; % non-vdW mixing rule

% Differentiation of co-volume term:
bd = (1-lij)*(2*b12vdw - 2*b2) + lij*(2*b12 - 2*b2);

% Numerator for Y
yn = (Rg*T./(V2-b2)+ Rg*(bd + b2).*T./(V2-b2).^2 -(ad + 2*a2)./(V2.^2 + 2*b2.*V2 -
b2.^2)+ a2.*(2*V2.*bd + 2*b2.*V2 - 2*b2.^2 - 2*b2.*bd)./(V2.^2 + 2*b2.*V2 - b2.^2).^2);

% Numerator for Y
yd = (Rg*T./(V2-b2).^2 - 2*a2.*(V2 + b2)./(V2.^2 + 2*b2.*V2 - b2.^2).^2);

% Function to be fitted:
Y = (yn./yd)./MW;

```

---

### **twucritical.m**

```
function f = twucritical(Tb,SG)
```

```

% First compute reference properties for n-alkane with Tb and S.G.
Tco = Tb*(0.533272 + 0.191017*1e-3*Tb + 0.779681*1e-7*Tb^2 - 0.284376*1e-10*Tb^3 +
0.959468*1e28/Tb^13)^-1;
alpha = 1-(Tb/Tco);
Vco = (1-(0.419869 - 0.505839*alpha - 1.56436*alpha^3 - 9481.70*alpha^14))^^-8;
SGo = 0.843593 - 0.128624*alpha - 3.36159*alpha^3 - 13749.5*alpha^12;

```

```

% Need to iterate for MWo
MW0 = Tb/(10.44 - 0.0052*Tb);
theta0 = log(MW0);
options=optimset('Display','off');
[theta,fval] = fsolve(@(theta) Twutheta(theta,Tb),theta0,options);
MWo = exp(theta);

```

```

Pco = (3.83354 + 1.19629*alpha^0.5 + 34.8888*alpha + 36.1952*alpha^2 +
104.193*alpha^4)^2;

```

```

% Use reference values for n-alkane to compute properties for fluid
dSGT = exp(5*(SGo - SG))-1;
fT = dSGT*(-0.362456/Tb^0.5 + (0.0398285 - 0.948125/Tb^0.5)*dSGT);
Tcr = Tco*((1 + 2*fT)/(1-2*fT))^2; % Tc in Rankin

```



Tc = Tcr/1.8; % Tc in K

dSGV = exp(4\*(SGo^2 - SG^2))-1;

fV = dSGV\*(0.466590/Tb^0.5 + (-0.182421 + 3.01721/Tb^0.5)\*dSGV);

Vcf = Vco\*((1 + 2\*fV)/(1-2\*fV))^2; % Vc in ft3/lb/mole

Vc = Vcf/(35.314666721\*453.592370000) ; % Vc in m3/mole

dSGP = exp(0.5\*(SGo - SG))-1;

fP = dSGP\*((2.53262 - 46.1955/Tb^0.5 - 0.00127885\*Tb) + (-11.4277 + 252.140/Tb^0.5 + 0.00230535\*Tb)\*dSGP);

Pcp = Pco\*(Tcr/Tco)\*(Vco/Vcf)\*((1 + 2\*fP)/(1 - 2\*fP))^2; % Pc in psia

Pc = Pcp\*6894.757293168; % Pc in Pa

dSGM = dSGT;

x = abs(0.0123420 - 0.328086/Tb^0.5);

fM = dSGM\*(x + (-0.0175691 + 0.193168/Tb^0.5)\*dSGM);

MW = exp(log(MWo)\*((1 + 2\*fM)/(1-2\*fM))^2); % MW in lb/lb-mol = g/g-mol

% Compute omega from Tc, Pc and Vc using method of Ambrose

omega = -(log(Pc\*0.986923266716E-05) + ((-5.97616\*(1-(Tb/1.8)/Tc)+1.29874\*(1-(Tb/1.8)/Tc)^1.5 - 0.60394\*(1-(Tb/1.8)/Tc)^2.5 - 1.06841\*(1-(Tb/1.8)/Tc)^5)/(((Tb/1.8)/Tc)))/((-5.03365\*(1-(Tb/1.8)/Tc)+1.11505\*(1-(Tb/1.8)/Tc)^1.5 - 5.41217\*(1-(Tb/1.8)/Tc)^2.5 - 7.46628\*(1-(Tb/1.8)/Tc)^5)/(((Tb/1.8)/Tc)));

f = [Tc;

Pc;

omega;

MW];

---

### **Twutheta.m**

function f = Twutheta(theta,Tb)

% Function to solve for theta in Twu's correlation for MW of heavy hydrocarbons

% Called within Twu and PRG2\_PMV

f = (exp(5.71419 + 2.71579\*theta - 0.286590\*theta^2 - 39.8544/theta - 0.122488/theta^2) - 24.7522\*theta + 35.3155\*theta^2) - Tb;

---

## APPENDIX 6

---

## Equilibrium Calculations Using Tangent Plane Criterion

Calculations of vapour liquid equilibria (VLE) are one of the mainstays of chemical engineering and plant design. Bubble points are a class of VLE calculations where we are concerned with the temperature and pressure conditions of a liquid under which the first bubble of vapour is formed and the composition of the vapour. There are two types of bubble point calculations depending on which variable temperature or pressure is being sought given the other as input. Dew point VLE calculation is the opposite of bubble point calculation in that the temperature and pressure of the vapour at which the first drop of liquid is formed and the composition of this drop are important. Just as with bubble point, there are two types of dew point calculations depending on whether temperature or pressure is being sought. Isothermal flash calculation is one where the composition, temperature and pressure of a feed are known and we are interested in the composition of vapour and liquid, as well as, the fraction of vapour at some pressure.

There are three conditions that the above VLE and any other phase equilibrium calculations must satisfy for a system for  $n_c$  components:

(i) Material balance ( $n_c$  equation):

$$(1 - \xi)x_i + \xi y_i - z_i = 0 \quad (6A.1)$$

(ii) Chemical potential of species must be the same in each phase ( $n_c$  equations):

$$\mu_i^L(T, P, \bar{x}) = \mu_i^V(T, P, \bar{y}) \quad (6A.2)$$

(iii) Gibbs energy must be global minimum at given T and P for a stable system (1 equation):

$$\Delta G > 0 \quad (6A.3)$$

Typically, the first two conditions are usually the only criteria employed for solving VLE and other phase equilibria problems. While the first two conditions are often sufficient to solve such problems, Baker *et al.*<sup>1</sup> have shown that there are instances where this approach can lead to incorrect predictions of phase behaviour. An example of this is shown in Figure 6A - 1 for VLE of a binary mixture. The tangent to the Gibbs energy surface represents the chemical potential of the species at that mole fraction composition. Each of the tangents shown satisfies the condition that the chemical potential of the species is the same in each phase. However, only one tangent satisfies the stability condition that the Gibbs energy of the mixture must be a global minimum.

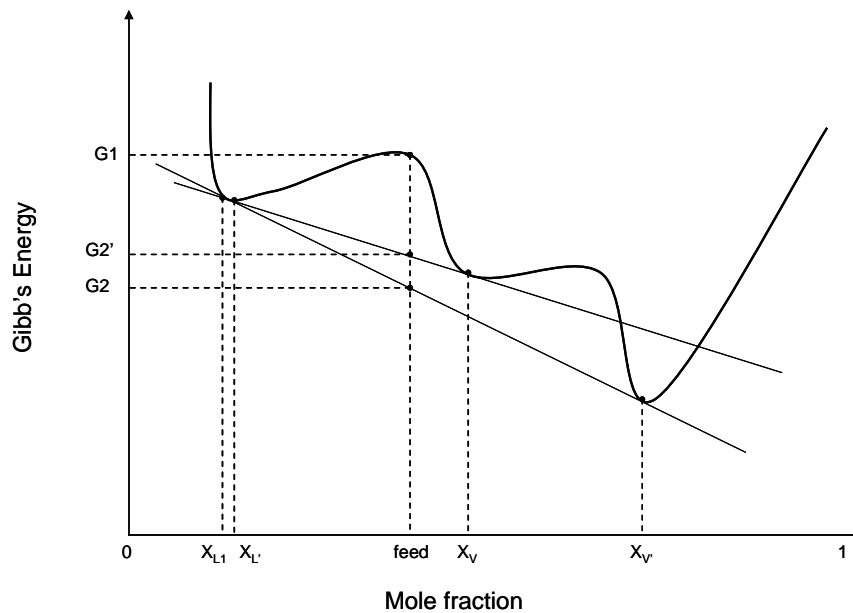


Figure 6A - 1 Gibbs energy diagram to a mixture for a system in a PT region of LV phase behaviour.

The third condition forms the basis of the so-called tangent plane criterion developed by Baker *et al.* and is expressed mathematically:

$$D_x(T, P, \bar{y}) = RT \sum_{i=1}^{n_c} y_i \ln \left[ f_i(T, P, \bar{y}) / f_i(T, P, \bar{x}) \right] \geq 0 \quad (6A.4)$$

This equation is a statement that at for a given temperature and pressure, a system with composition  $\bar{x}$  is stable if a tangent plane to the Gibbs free energy surface at composition  $\bar{x}$  lies below the Gibbs free energy surface, i.e., the Gibbs free energy for any composition  $\bar{y}$  is greater than the Gibbs energy at  $\bar{x}$ .  $D_x$  is the distance from the Gibbs free energy surface to the tangent plane. The equations necessary to apply the tangent plane criterion are summarized below.

$$g(y_i) = \ln K_i + \ln \phi_i(y, P_o, T_o) - \ln \phi_i(x, P_o, T_o) = 0 \quad (6A.5)$$

$$\phi_i(y, P_o, T_o) = \frac{f_i(y, P_o, T_o)}{(y_i P_o)} \quad (6A.6)$$

$$Y_i = K_i x_i \quad (6A.7)$$

$$y_i = \frac{Y_i}{\sum_{j=1}^k Y_j} \quad (6A.8)$$

$$\sum_{i=1}^k Y_i = 1 \quad (6A.9)$$

Note that equations 3, 4 and 5 mean that the solution must have  $y_i = Y_i$

**Solution Methodology:**

- Problem: We wish to find  $P_o$ , the bubble pressure, at a specified temperature,  $T_o$ , and composition,  $x_i$ .
- If K-values are independent of composition then solution is rather easy (solve Equation 5) and just depends on the form of  $K_i$ .
- In the case where K-values are functions of compositions related through an EOS, alternative approach to the solution have been discussed by, e.g., Nghiem and Michelsen. Nghiem discusses three applications of Newton's method which differ mainly in the choice of the independent variable:  $K_i$  or  $\ln P$  (or  $\ln T$ ). We have chosen to utilize the Quasi-Newton successive substitution (QNSS) method proposed by Nghiem where the independent variable is  $\ln K_i$ . The solution proceeds as follows:

1. Initial estimate for P and  $\ln K_i$ :  $P^{(0)}$  and  $\xi^{(0)}$  (a column vector of  $\ln K_i$ ):

$$\xi^{(0)} = (\ln K_1, \ln K_2 \dots \ln K_k)^T \quad \dots a$$

2. Using  $K_i$ , calculate  $Y_i$  and  $y_i$ . The  $x_i$ 's (feed compositions) and  $T_o$  are known.

$$Y_i = K_i x_i \quad \dots b$$

$$y_i = \frac{Y_i}{\sum_{j=1}^k Y_j} \quad \dots c$$

3. Using values of P,  $T_o$ ,  $K_i$ 's,  $y_i$ 's and  $x_i$ 's, calculate  $g(y_i)$  and target function  $g(y)$ :

$$g(y_i) = \ln K_i + \ln \phi_i(y, P_o, T_o) - \ln \phi_i(x, P_o, T_o) \quad \dots d$$

where:

$$\phi_i(y, P_o, T_o) = \frac{f_i(y, P_o, T_o)}{(y_i P_o)} \quad \dots e$$

$$g(y) = \sum_{i=1}^k [g(y_i)]^2 \leq 10^{-10} \quad \dots f$$

An expression is needed for fugacity coefficient,  $\phi_i$ , which depends on the derivatives of the mixing rules (see below). In the present case, the focus will be on the mixing rules for the  $b$  term while the quadratic, i.e., classical van der Waals mixing rule is used for the  $a$  term.

Change  $P$  using an appropriate method (e.g., Newton's methods such as `lsqnonlin.m` in Matlab) to minimize the target function  $g(y)$ . Note the required residual can be very small.

- If `lsqnonlin.m` in Matlab is used then the Jacobian ( $dg/dp$ ), need not be explicitly calculated. Instead, we define a Matlab function which computes  $g(y)$  using the current values of  $x$ ,  $y$ ,  $T$  and  $K$ .
- The Jacobian could be determined explicitly and  $p$  updated:  

$$p^{(k+1)} = p^{(k)} - [J^{(k)}]^{-1}g(y)^{(k)}$$

4. If target function is met then  $P_{bp} = P$ . If target function is not met then update  $K_i$  us QNSS.

$$\begin{aligned}\Delta\xi^{(m)} &= \xi^{(m+1)} - \xi^{(m)} = -\sigma^{(m)} g^{(m)} && \dots g \\ g^{(m)} &= (g(y_1), g(y_2) \dots g(y_k))^{(m)} && \dots h \\ \sigma^{(m)} &= -\frac{\Delta\xi^{(m-1)T} g^{(m-1)}}{\Delta\xi^{(m-1)T} (g^{(m)} - g^{(m-1)})} \sigma^{(m-1)} && \dots i\end{aligned}$$

Conditions :

$$\sigma^{(0)} = 1$$

$$|\sigma^{(m)}| \leq 30$$

5. Using new values of  $\xi^{(m+1)}$  and  $P^{(m)}$ , return to step 2. Repeat steps until  $g(y) \leq 1^{-10}$

### Fugacity coefficient

It can be shown that for the Peng-Robinson CEOS the fugacity coefficient is given by:

$$\begin{aligned}\ln \varphi_i &= -\ln(1 - b\rho) - \ln Z + \frac{n}{1 - b\rho} \cdot \left( \frac{\partial b\rho}{\partial n_i} \right) \\ &\quad - \frac{an^2}{nbRT\sqrt{8}} \left[ \frac{(1 + \sqrt{2})}{1 + (1 + \sqrt{2})b\rho} - \frac{(1 - \sqrt{2})}{1 + (1 - \sqrt{2})b\rho} \right] \cdot \left( \frac{\partial b\rho}{\partial n_i} \right) \\ &\quad - \ln \left( \frac{1 + (1 + \sqrt{2})b\rho}{1 + (1 - \sqrt{2})b\rho} \right) \left[ \frac{1}{nbRT\sqrt{8}} \cdot \left( \frac{\partial an^2}{\partial n_i} \right) - \frac{an^2}{(nb)^2 RT\sqrt{8}} \cdot \left( \frac{\partial nb}{\partial n_i} \right) \right]\end{aligned} \tag{6A.10}$$

Z and  $\rho$  will depend on P for the given x, y and T and can be found by solving the PREOS

Now we need only find the three derivatives which depend on the mixing rules we wish to employ for 'a' and 'b'.



## Jacobian of $g(\mathbf{y})$

$$g = D_x^*(y, p, T) = \sum_{i=1}^{nc} y_i \ln \left[ \frac{f_i(\vec{y}, p, T)}{f_i(\vec{x}, p, T)} \right] = 0$$

$g$  : distance of Gibbs free energy surface to tangent plane at  $\mathbf{x}$

Jacobian :

$$J = \frac{dg}{dp}$$

$$f_i(y, p, T) = y_i p \phi_i(\vec{y}, p, T)$$

Substituting :

$$g = \sum_{i=1}^{nc} y_i \ln \left[ \frac{y_i p \phi_i(\vec{y}, p, T)}{x_i p \phi_i(\vec{x}, p, T)} \right] = \sum_{i=1}^{nc} y_i \ln \left[ \frac{y_i \phi_i(\vec{y}, p, T)}{x_i \phi_i(\vec{x}, p, T)} \right] = \sum_{i=1}^{nc} y_i \ln \left[ K_i \frac{\phi_i(\vec{y}, p, T)}{\phi_i(\vec{x}, p, T)} \right]$$

$$g = \sum_{i=1}^{nc} y_i [\ln K_i + \ln \phi_i(y, p, T) - \ln \phi_i(x, p, T)]$$

$$\therefore \left. \frac{dg}{dp} \right|_{K, T} = \sum_{i=1}^{nc} y_i \left[ \frac{\partial}{\partial p} \ln \phi_i(\vec{y}, p, T) - \frac{\partial}{\partial p} \ln \phi_i(\vec{x}, p, T) \right]$$

$$\ln \phi_i = \left( \frac{\partial}{\partial n_i} \left( \frac{G - G^{ig}}{RT} \right) \right)_{T, P, n_{j \neq i}} = \frac{(\mu_i - \mu_i^{ig})}{RT}$$

$$\frac{\partial}{\partial p} (\ln \phi_i) = \frac{\partial}{\partial p} \left( \frac{\mu_i - \mu_i^{ig}}{RT} \right) = \frac{1}{RT} \left( \frac{\partial \mu_i}{\partial p} - \frac{\partial \mu_i^{ig}}{\partial p} \right) = \frac{1}{RT} (\bar{V}_i - \bar{V}_i^{ig})$$

where :

$\bar{V}_i$  = partial molar volume of component  $i$

Substituting :

$$\left. \frac{dg}{dp} \right|_{K, T} = \sum_{i=1}^{nc} y_i \left[ \frac{1}{RT} (\bar{V}_i - \bar{V}_i^{ig})_{y, p, T} - \frac{1}{RT} (\bar{V}_i - \bar{V}_i^{ig})_{x, p, T} \right]$$

$$= \sum_{i=1}^{nc} y_i \left[ \left( \frac{\bar{V}_i}{RT} \right)_{y, p, T} - \left( \frac{\bar{V}_i}{RT} \right)_{x, p, T} \right]$$

$$\therefore J = \frac{1}{RT} \sum_{i=1}^{nc} y_i [(\bar{V}_i)_{y, p, T} - (\bar{V}_i)_{x, p, T}] = \frac{\sum_{i=1}^{nc} y_i (\bar{V}_i)_{y, p, T}}{RT} - \frac{1}{RT} \sum_{i=1}^{nc} y_i [(\bar{V}_i)_{x, p, T}]$$

$$= \frac{V_{y, p, T}^-}{RT} - \frac{1}{RT} \sum_{i=1}^{nc} y_i (\bar{V}_i)_{x, p, T}$$

$$J = \frac{Z_{y, p, T}^-}{P} - \frac{1}{RT} \sum_{i=1}^{nc} y_i (\bar{V}_i)_{x, p, T}$$

### Partial Molar Volume from PREOS with General Mixing Rule

$$P = \frac{RT}{V-b} - \frac{a}{V^2 + 2bV - b^2}$$

$$V = \frac{V_t}{n_t}$$

$$\therefore P = \frac{RT}{\frac{V_t}{n_t} - b} - \frac{a}{\left(\frac{V_t}{n_t}\right)^2 + 2b\frac{V_t}{n_t} - b^2} = \frac{n_t RT}{V_t - n_t b} - \frac{n_t^2 a}{V_t^2 + 2bn_t V_t - n_t^2 b^2}$$

Differentiating wrt  $n_i$

$$0 = \frac{RT}{V_t - n_t b} \cdot (1) - \frac{n_t RT}{(V_t - n_t b)^2} \cdot \left[ \frac{\partial V_t}{\partial n_i} - \left( \frac{\partial n_t b}{\partial n_i} \right) \right] - \frac{\frac{\partial}{\partial n_i} (a n_t^2)}{V_t^2 + 2bn_t V_t - n_t^2 b^2} + a n_t^2 \frac{\frac{\partial}{\partial n_i} (V_t^2 + 2bn_t V_t - n_t^2 b^2)}{(V_t^2 + 2bn_t V_t - n_t^2 b^2)^2}$$

$$0 = \frac{RT}{V_t - n_t b} - \frac{n_t RT}{(V_t - n_t b)^2} \cdot \left[ \frac{\partial V_t}{\partial n_i} - \left( \frac{\partial n_t b}{\partial n_i} \right) \right] - \frac{\frac{\partial}{\partial n_i} (a n_t^2)}{V_t^2 + 2bn_t V_t - n_t^2 b^2} + \frac{2a n_t^2}{(V_t^2 + 2bn_t V_t - n_t^2 b^2)^2} \left[ V_t \frac{\partial V_t}{\partial n_i} + V_t \left( \frac{\partial n_t b}{\partial n_i} \right) + b n_t \frac{\partial V_t}{\partial n_i} - n_t b \left( \frac{\partial n_t b}{\partial n_i} \right) \right]$$

$$\frac{\partial V_t}{\partial n_i} = \bar{V}_i$$

$$\bar{V}_i \left[ \frac{n_t RT}{(V_t - n_t b)^2} - \frac{2a n_t^2 (V_t + b n_t)}{(V_t^2 + 2bn_t V_t - n_t^2 b^2)^2} \right] = \frac{RT}{V_t - n_t b} + \frac{n_t RT}{(V_t - n_t b)^2} \left( \frac{\partial n_t b}{\partial n_i} \right) - \frac{\frac{\partial}{\partial n_i} (a n_t^2)}{V_t^2 + 2bn_t V_t - n_t^2 b^2} + \frac{2a n_t^2}{(V_t^2 + 2bn_t V_t - n_t^2 b^2)^2} \left[ V_t \left( \frac{\partial n_t b}{\partial n_i} \right) - n_t b \left( \frac{\partial n_t b}{\partial n_i} \right) \right]$$


---

$$\frac{RT}{\underline{V}_t - n_t b} + \frac{n_t RT}{(\underline{V}_t - n_t b)^2} \left( \frac{\partial n_t b}{\partial n_t} \right) - \frac{\frac{\partial}{\partial n_t} (a n_t^2)}{\underline{V}_t^2 + 2b n_t \underline{V}_t - n_t^2 b^2} +$$

$$\frac{2a n_t^2}{(\underline{V}_t^2 + 2b n_t \underline{V}_t - n_t^2 b^2)^2} \left[ \underline{V}_t \left( \frac{\partial n_t b}{\partial n_t} \right) - n_t b \left( \frac{\partial n_t b}{\partial n_t} \right) \right]$$

$$\therefore \bar{V}_i = \frac{\left[ \frac{n_t RT}{(\underline{V}_t - n_t b)^2} - \frac{2a n_t^2 (\underline{V}_t + b n_t)}{(\underline{V}_t^2 + 2b n_t \underline{V}_t - n_t^2 b^2)^2} \right]}{\left[ \frac{n_t RT}{(\underline{V}_t - n_t b)^2} - \frac{2a n_t^2 (\underline{V}_t + b n_t)}{(\underline{V}_t^2 + 2b n_t \underline{V}_t - n_t^2 b^2)^2} \right]}$$

### References:

---

<sup>1</sup> Baker, L.E.; Pierce, A.C.; Liks, K.D. Gibbs Energy Analysis of Phase Equilibria. Society of Petroleum Engineering Journal 22 (1982) 731 - 742.

---

**APPENDIX 7**

---

Table A7 - 1 Matlab m-files used to calculate bubble point pressures at a set of temperature conditions for a mixture of a given composition.

Matlab Program	Description
bubblept.m	Script file to compute bubble point pressures for a given mixture composition and critical properties (mixpropABVB_C10.m) and temperatures (TmixABVB_C10.m). Bubble point pressure prediction are output with the corresponding liquid and vapour mass densities. For bubble point pressures at fixed temperature and variable composition change outer loop to update composition instead of temperature.
<u>PREOS.m</u>	Function to calculate compressibility and molar volume of phases at specified temperature, pressure and composition
<u>mixrule.m</u>	Function file to apply classical van der Waals mixing rule for energy term and choice of mixing rule to co-volume to a specified mixture
<u>dmix.m</u>	Function file to calculate derivatives of the chosen mixing rules for specified fluid mixture
<u>logephi.m</u>	Function file to calculate $\log_e$ of fugacity coefficient for a specified fluid
<u>Jvx.m</u>	Function file to calculate the second part of the Jacobian , $J = \frac{Z_{y,p,T}}{P} - \frac{1}{RT} \sum_{i=1}^{nc} y_i (\bar{V}_i)_{x,p,T}$
<u>mixprop ABVB_C10.m</u>	Function file with critical properties, mole fractions and molecular weight of components in a mixture
<u>Tmix ABVB_C10.m</u>	Function file with an array containing temperatures at which to return bubble point pressure.

**bubblept.m**

```
% bubblept.m calculates a bubble point pressure at various temperatures for
% a mixture having a specified composition.
%
% Inputs required for each component which are provided by mixprop.m are:
% Pc: critical pressure in kPa
% Tc: critical temperature in K
% Vc: critical volume in m3/mole
% omega: acentric factor
% z: mole fraction of component
% MW: molecular weight in g/mole
% Tmix: matrix of temperature for Pb calculation
%
% bubblept also requests the temperature and guessed pressure for the bubble point
% pressure calculation.
```

```
clear;
```

```

format long

% Constants
R = 8.314472; % Gas constant 8.31447 (m3_Pa/mole_K) from NIST
(http://physics.nist.gov/cuu/Constants/index.html)

% Initial guess of bubble pressure for first temperature (temperatures
% should increase monotonically). Initial guess for next temperature is
% bubble pressure for previous (lower) temperature.
% Input guessed pressure for calculating K-values
disp('Temperatures should increase monotonically');

%Pk = input('Pressure (kPa) for estimating initial K-value:');
Pk = 0.001; % start at 0.001

% Empty set to accumulate Pb, Tb, rho liq. and rho vap.
Pb = [];
Tb = [];
rho lb = [];
rho vb = [];

% _____
% Calculate temperature independent mixture properties

% Input Pc, Tc, Vc, omega, z and MW as matrix 'prop' from mixprop.m
[prop] = mixprop ABVB_C10;
[s,t] = size(prop); % size of prop matrix; s is number of components

% 'a' term for PREOS
ac = 0.4572355289213894*R^2.*prop(:,2).^2./(prop(:,1)*1e3);

% Improved PR-EOS (1978 version), Robinson et al., Fluid Phase Equil. 24,
% 25-41, 1985

for i = 1:s;
    if prop(i,4) < 0.491;
        m(i) = 0.37464 + 1.54226*prop(i,4) - 0.26992*prop(i,4).^2;
    else
        m(i) = 0.379642 + 1.48503*prop(i,4) - 0.164423*prop(i,4).^2 + 0.016666*prop(i,4).^3;
    end
end
m = m';

% Original PR-EOS (1976 version)
% m = 0.37464 + 1.54226.*prop(:,4) - 0.26992.*prop(:,4).^2;

```

```

k = zeros(s); % Pre-define matrix of zeros

% for i = 1:s;
%   for j = i+1:s;
%       k(i,j) = 1 - ((2.*prop(i,3).^(1/6).*prop(j,3).^(1/6))/(prop(i,3).^(1/3) +
prop(j,3).^(1/3))).^(1.2126);
%       k(j,i) = k(i,j);
%   end
% end

% z is matrix of component mole fractions
z = prop(:,5);

% Check mole fraction for consistency
sumz = sum(z);

if sumz ==1
else disp('Mole fraction summation error. Check input data');
    break
end

% Estimated ln(K0)
lnK0 = [0.855728363;
-3.085350615;
-3.926319282;
-4.63583398;
-5.041532082;
-5.962368281;
-6.931245373;
-7.856558096;
-8.911499056;
-9.731820113;
-10.86052992;
-4.033262137;
-4.063373772;
-3.125206145;
-4.045213694;
-4.858373685;
-5.044114244;
-5.187792414;
-4.563731889;
-5.964598973;
-9.168128063
];

% _____

```

```

% Import matrix of temperature for calculations
% T is obtained from a column matrix of temperature
[Tmix] = TmixABVB_C10;
[jt,jtt] = size(Tmix); % size of T matrix; jt is number of temperature inputs

for nt = 1:jt;
T = Tmix(nt,1);% T for bubble point pressure calculation

%
% _____
% Temperature dependent alpha for updating with new values of T(K)
alpha = (1 + m.*(1-(T./prop(:,2)).^0.5)).^2;

% Alpha function from Gasem et al., Fluid Phase Equil. 213, 19-37, 2003
% m = 0.134 + 0.508.*prop(:,4) -0.476.*prop(:,4).^2;
% alpha = exp(2.00 + 0.836*(T./prop(:,2)).*(1 - (T./prop(:,2)).^m));

a = ac.*alpha;

% 'b' term for PREOS
b = 0.07779607390389232*R.*prop(:,2)./(prop(:,1)*1e3);

% Calculation of k matrix of binary interaction parameter.
% These can all be set equal to zero or calculated using an appropriate
% method, e.g., the method of Reid, Prausnitz and Sherwood, The Properties of
% Gases and Liquids, 3rd Edition, McFraw-Hil, NY 1977.

RT = R*T; % Constant for calculation

%
% _____

% INITIAL ESTIMATE OF K-VALUES FOR BUBBLE PRESSURE CALCULATION

% To initiate bubble pressure calculation we need to provide good initial
% guesses for K-value and bubble pressure Pb. We use a stability test
% calculation (Michelsen 1982, Nghiem and Heidemann 1982 and Nghiem and Li
% 1984).
%
% The temperature for the stability test is the temperature for Pb
% calculation. The pressure for the calculated initial guess of K-value
% could be in the two phase region for the system

% Solve PR EOS with appropriate mixing rules, e.g., van der Waals mixing
% rules to obtain densities (or molar volumes = 1/density).
% Ideally we should use the same mixing rules for this estimate as that used for
% the bubble pressure calculation. The mixing rule is specified in PREOS.m
% Fugacity of liquid phase components are fixed for given T and P.
% The mixing rule for calculating the fugacity coefficient is specified in

```



```

% logephi.m

[Zliq,VL,amixL,bmixL] = PREOS(a,b,k,z,s,Pk,T);
logephi = logephi(a,b,amixL,bmixL,Zliq,VL,z,k,T,Pk);

% For normal hydrocarbons, use either Wilson or Michelsen equations to
% determine initial guess for K-value at initial guess for bubble pressure.
% For heavy hydrocarbons, it may be easier to specify some reasonable guess.

% Initial guess for lnK using Wilson equation
% lnK0 = 5.373*(1 + prop(:,4)).*(1 - prop(:,2)/T) + log(prop(:,1)/Pk); % initial guess ln K

% Initial guess for lnK using equation proposed by Michelsen 1982
% lnK0 = log(prop(:,1)/Pk) + 5.42*(1 - prop(:,2)/T);

% For 10 HVGO and 10 VTB components.

% Estimated ln(K0)
lnK0 = [0.855728363;
-3.085350615;
-3.926319282;
-4.63583398;
-5.041532082;
-5.962368281;
-6.931245373;
-7.856558096;
-8.911499056;
-9.731820113;
-10.86052992;
-4.033262137;
-4.063373772;
-3.125206145;
-4.045213694;
-4.858373685;
-5.044114244;
-5.187792414;
-4.563731889;
-5.964598973;
-9.168128063
];
% _____

% % First and second initial guesses (u) for vapor phase mole fraction and
% % normalized molefractions (x)
% ug1 = exp(lnK0).*z;
% ug2 = z./exp(lnK0);

```

```

% xg1 = ug1/sum(ug1);
% xg2 = ug2/sum(ug2);
%
% % Implement stability analysis using QNSS method proposed by Nghiem and
Li(1984)
% % Using the first initial guess
%
% for kiter = 1:2
%   if kiter == 1
%     u0 = ug1;
%     x0 = xg1;
%   else
%     u0 = z./exp(lnK0);
%     x0 = ug2/sum(ug2);
%   end
%
% [Zx0,Vx0,amixx0,bmixx0] = PREOS(a,b,k,x0,s,Pk,T);
% logephix0 = logephi(a,b,amixx0,bmixx0,Zx0,Vx0,x0,k,T,Pk);
% d0 = log(u0)+ logephix0' - log(z) - logephiz'; % Tangent plane criteria
% err = norm(d0); % Tolerance for convergence test
%
% sigma0 = 1; % initial step-size for QNSS
% dlnK0 = - sigma0*d0;
% lnK1 = lnK0 + dlnK0; % New value of lnK
%
% % Iterate to find new value of lnK
% tol = 1e-10;
% j = 0; % After 10 iterations we want to reset sigma = 1
% while err > tol
%   u1 = exp(lnK1).*z;
%   x1 = u1/sum(u1);
%   [Zx1,Vx1,amixx1,bmixx1] = PREOS(a,b,k,x1,s,Pk,T);
%   logephix1 = logephi(a,b,amixx1,bmixx1,Zx1,Vx1,x1,k,T,Pk);
%   d1 = log(u1)+ logephix1' - log(z) - logephiz';
%   dd0 = d1 - d0;
%   sigma1 = abs((-dlnK0*d0)/(dlnK0*dd0))*sigma0; % Sigma must be a positive
number
%
%
%   if abs(sigma1) > 6 % Limit step size at each iteration (max = 6)
%     if sign(sigma1)==1
%       sigma1 = 6;
%     else sigma1 = -6;
%     end
%   end
% end
%
%
%

```

```

%     dlnK1 = - sigma1*d1;
%     [maxdlnK1,i] = max(abs(dlnK1)); % Limit \dlnK\ <=/= 6 by reducing sigma if
necessary
%     if maxdlnK1 > 6
%         sigma1 = 6/abs(d1(i));
%     end
%
%
%     dlnK1 = - sigma1*d1;
%     lnK2 = lnK1 + dlnK1;
%     lnK1 = lnK2; % Update lnK1
%     err = norm(d1);
%     if err < tol, break, end
%     d0 = d1;
%     sigma0 = sigma1;
%     dlnK0 = dlnK1;
%     j = j + 1;
%     if j== 10
%         sigma0 = 1; % Reset sigma
%         j = 1; % Reset j
%     end
% end
% if kiter == 1
%     lnKguessa = lnK1;
% else
%     lnKguessb = lnK1;
% end
% end
%
% % If there are two different sets of lnK, select one
% ard = (lnKguessa - lnKguessb)./lnKguessa; % Absolute relative difference between
two lnK
% knorm = norm(ard); % Average absolute relative difference
% if knorm < 1e-6
%     lnK0 = lnKguessa;
%     disp('Identical pair of lnK found from stability analysis');
%     disp(lnKguessa);
% else
%     disp('Different lnK found from stability analysis');
%     lnKguessa
%     lnKguessb
%     select = input('Enter 1 to select 1st lnK or 2 for second lnK or 3 to break: ');
%
%     if select == 1
%         lnK0 = lnKguessa;
%     elseif select == 2
%         lnK0 = lnKguessb;

```

```

%     else break
%     end
% end

%


---


% INITIAL ESTIMATE OF Psat FOR BUBBLE PRESSURE CALCULATION

% First and second initial values (x) for normalized vapor phase
% molefraction
ug1 = exp(lnK0).*z;
ug2 = z./exp(lnK0);
yg(:,1) = ug1/sum(ug1);
yg(:,2) = ug2/sum(ug2);

% Use search with bisection to find initial guesses for saturation pressure
% at given T

step = 0.5; % Step size in kPa for search (default 10.0)
tol = 1e-6; % Convergence tolerance for bisection to find psat
Pmin = Pk/2; % Minimum pressure for search (default 0.05)
Pmax = 1000.0; % Upper limit for search (default 50001 kPa)
p0 = []; % Matrix for collecting estimates of psat
tag = [];

% For each y, find the zeros of d where x and z are known but logephiz and
% logephiy vary with pressure
for r = 1:2
y = yg(:,r);
pa = Pmin; % Initial pressure

% Initialize empty matrices to store p and d for Figure 1 and 2
p=[];
d=[];

while pa < Pmax
[Zza,Vza,amixza,bmixza] = PREOS(a,b,k,z,s,pa,T);
logephiza = logephi(a,b,amixza,bmixza,Zza,Vza,z,k,T,pa);
[Zya,Vya,amixya,bmixya] = PREOS(a,b,k,y,s,pa,T);
logephiya = logephi(a,b,amixya,bmixya,Zya,Vya,y,k,T,pa);

pb = pa + step; % End point of current pressure interval
[Zzb,Vzb,amixzb,bmixzb] = PREOS(a,b,k,z,s,pb,T);
logephizb = logephi(a,b,amixza,bmixzb,Zzb,Vzb,z,k,T,pb);
[Zyb,Vyb,amixyb,bmixyb] = PREOS(a,b,k,y,s,pb,T);
logephiyb = logephi(a,b,amixyb,bmixyb,Zyb,Vyb,y,k,T,pb);

```

```

daa = log(y) + logephiya' - log(z) - logephiza';
da = dot(y,daa);
dbb = log(y) + logephiyb' - log(z) - logephizb';
db = dot(y,dbb);
p = [p;pa];
d = [d;da];
rpa = pa;
rpb = pb;

% Check for root between pa and pb
if sign(da)==sign(-db) % There is a root since d changes sign
    % Begin bisection to locate psat within tolerance
    err = abs((rpa - rpb)/rpa);
    while err > tol
        pmid = (rpa + rpb)/2; % Bisection
        [Zzmid,Vzmid,amixzmid,bmixzmid] = PREOS(a,b,k,z,s,pmid,T);
        logephizmid = logephi(a,b,amixzmid,bmixzmid,Zzmid,Vzmid,z,k,T,pmid);
        [Zymid,Vymid,amixymid,bmixymid] = PREOS(a,b,k,y,s,pmid,T);
        logephiymid = logephi(a,b,amixymid,bmixymid,Zymid,Vymid,y,k,T,pmid);
        dmm = log(y) + logephiymid' - log(z) - logephizmid';
        dm = dot(y,dmm);
        if sign(da)==sign(-dm); % Then root in interval pa and pmid
            rpb = pmid;
        else
            rpa = pmid;
            [Zz1,Vz1,amixz1,bmixz1] = PREOS(a,b,k,z,s,rpa,T);
            logephiz1 = logephi(a,b,amixz1,bmixz1,Zz1,Vz1,z,k,T,rpa);
            [Zy1,Vy1,amixy1,bmixy1] = PREOS(a,b,k,y,s,rpa,T);
            logephiy1 = logephi(a,b,amixy1,bmixy1,Zy1,Vy1,y,k,T,rpa);
            daa = log(y) + logephiy1' - log(z) - logephiz1';
            da = dot(y,daa);
        end
        err = abs((rpa - rpb)/rpa);
    end
    p0 = [p0;rpa]; % Tag initial guess with D1* or D2*
    [sp,sd] = size(p0);
    tag = [tag;r];
end
pa = pb; % Update pa for the new p interval
end

% Plot D1* and D2* to locate all roots
subplot(1,2,r); plot(p,d);
title('Roots of D* for Initial Guess of Psat');
xlabel('Pressure (kPa)');
ylabel(['D',int2str(r),'*']);

```

```

end

disp('Initial guess for Psat(kPa)');
disp(p0); % Output initial guess for Psat

ps = [p0,tag]; % Tag initial guess so right value of lnK is used
ps = sortrows(ps,1); % Sort initial guesses of Psat from smallest to largest

% Review roots and decide whether new guess for Psat is required
% cont = input('1 to continue 0 to abort: ');
cont =1;
if cont == 0
    break
end

%NEED TO DISCARD SOLUTIONS WITH TOO MANY ROOTS
[ss,tt] = size(p0); % number of initial guesses for Pb </= 4?
if ss > 4
    disp('Too many roots. Check initial guess for Pk');
    break
end

% _____

% Apply QNSS method of Michelsen 1982, Nghiem and Heidemann 1982 and Nghiem
and Li
% 1984. An iteration for lnK is nested inside an iteration for Pbubble.

%  $dD^*/dp = J(\text{press}) = J_y - J_x = Z(y)/P - v_{ix}$ 

% Normally, tol1 < tol2 < tol3
tol1 = 1e-8; % Tolerance for QNSS iteration of lnK
tol2 = tol1*10; % Tolerance for Newton iteration for p
tol3 = tol2*10; % Tolerance for overall convergence norm(g)

Psat = []; % Initialize empty matrix to store results
tagstab = []; % Initialize empty matrix to tag Psat on stability limit
ysat = []; % Initial empty matrix to output y corresponding to Psat
Vsat = []; % Initial empty matrix to output V corresponding to Vsat

lnKguess1 = lnK0 ; % Convenient change of variable name

% Select each initial guess of pressure to find Pb
for jjj = 1:ss
    p = ps(jjj,1);
    if ps(jjj,2) == 1

```

```

    u = exp(lnKguess1).*z;
    y = u/sum(u);
else
    if ps(jjj,2)== 2
        u = exp(-lnKguess1).*z; % NEED -VE LNK FOR INITIAL GUESS FROM D2*
        y = u/sum(u);
    end
end

lnK1 = lnKguess1;

[Zy,Vy,amixy,bmixy] = PREOS(a,b,k,y,s,p,T);
logephiy = logephi(a,b,amixy,bmixy,Zy,Vy,y,k,T,p);
[Zz,Vz,amixz,bmixz] = PREOS(a,b,k,z,s,p,T);
logephiz = logephi(a,b,amixz,bmixz,Zz,Vz,z,k,T,p);

d0 = log(y)+ logephiy' - log(z) - logephiz'; % Tangent plane criteria
gnorm = norm(d0); % Tolerance for convergence test
errd = gnorm;

counterlnk = 0;

while gnorm > tol3 % Tolerance for outer loop updating lnK
    counterlnk = counterlnk + 1;
    if counterlnk == 100
        disp('Max iterations reached for inner loop updating Psat. Try relaxing tolerance
(tol3)');
        return, end
    [Zy,Vy,amixy,bmixy] = PREOS(a,b,k,y,s,p,T);
    logephiy = logephi(a,b,amixy,bmixy,Zy,Vy,y,k,T,p);
    [Zz,Vz,amixz,bmixz] = PREOS(a,b,k,z,s,p,T);
    logephiz = logephi(a,b,amixz,bmixz,Zz,Vz,z,k,T,p);

    dp = log(y)+ logephiy' - log(z) - logephiz'; % Tangent plane criteria

    Dstar = dot(y,dp);
    errp = abs(Dstar);
    gnorm = norm(dp);

    % Update p while lnK is fixed
    % Instead of an analytical Jacobian this p can be found using a
    % Newton method from Matlab

    counterp = 0;

    while errp > tol2 % Tolerance for inner loop updating p
        counterp = counterp + 1;

```

```

    if counterp == 50000
        disp('Max iterations reached for inner loop updating Psat. Try relaxing tolerance
(tol2) or reducing inverse relaxation');
        return, end
        Jy = Zy/(p); % Units are 1/kPa
        Jx = Jvx(Zz,Vz,T,k,a,b,y,z); % Units are same as V/RT = 1/P (1/Pa)

        invlambd = 1e2; % A reciprocal relaxation factor >= 1; default 1e2
        Jpress = invlambd*(Jy - 1e3*Jx); % Units are 1/kPa
        pnew = p - Dstar/Jpress; % Units are kPa

```

```

% A GTEST FAILURE PROBABLY IS A RESULT OF A NEGATIVE PRESSURE
CALCULATED SOMEWHERE LIKELY IN THE INNER LOOP FOR PSAT IN BUBBLEP
% CHANGE INITIAL GUESS OR DECREASE TOLERANCES FOR LNK, P AND
NORM(G) FOR TANGENT PLANE CRITERIA

```

```

[Zy,Vy,amixy,bmixy] = PREOS(a,b,k,y,s,pnew,T);
logephiy = logephi(a,b,amixy,bmixy,Zy,Vy,y,k,T,pnew);
[Zz,Vz,amixz,bmixz] = PREOS(a,b,k,z,s,pnew,T);
logephiz = logephi(a,b,amixz,bmixz,Zz,Vz,z,k,T,pnew);
dp = log(y)+ logephiy' - log(z) - logephiz'; % Tangent plane criteria

```

```

Dstar = dot(y,dp);
errp = abs(Dstar);
p = pnew;
end

```

```

% Update lnK using QNSS
d1 = log(u)+ logephiy' - log(z) - logephiz';
errd = norm(d1);
jj = 0;

```

```

while errd > tol1
    if jj == 0
        sigma1 = 1; % Initial step size
    else
        dd0 = d1 - d0;
        sigma1 = ((- (dlnK0*d0)/(dlnK0*dd0))*sigma0); % Sigma can be +ve or -ve
    end
    here
end

```

```

if abs(sigma1) > 6 % Limit step size at each iteration (max = 6)
    if sign(sigma1)==1
        sigma1 = 6;
    else sigma1 = -6;
    end
end

```



```

end

dlnK1 = - sigma1*d1;
lnK2 = lnK1 + dlnK1;

lnK1 = lnK2; % Update lnK1
d0 = d1;
sigma0 = sigma1;
dlnK0 = dlnK1;
jj = jj + 1;

if jj == 10 % Generally this is the same as number of components
    jj = 0; % Reset j
else
end

if ps(jjj,2) == 1
    u = exp(lnK1).*z;
    y = u/sum(u); % New value of y
else
    if ps(jjj,2) == 2
        u = exp(-lnK1).*z; % NEED -VE LNK FOR INITIAL GUESS FROM D2*
        y = u/sum(u); % New value of y
    end
end

[Zy,Vy,amixy,bmixy] = PREOS(a,b,k,y,s,p,T);
logephiy = logephi(a,b,amixy,bmixy,Zy,Vy,y,k,T,p);
[Zz,Vz,amixz,bmixz] = PREOS(a,b,k,z,s,p,T);
logephiz = logephi(a,b,amixz,bmixz,Zz,Vz,z,k,T,p);

d1 = log(u)+ logephiy' - log(z) - logephiz'; % Tangent plane criteria
errd = norm(d1);
end
tstab = abs(norm(z) - norm(y))/norm(z); % For convergencer on stability limit, y
= z
end

molarmass = y'*prop(:,6);
rho = molarmass*1e-3./Vz;

% Accumulate results for later output
Psat = [Psat;p];
tagstab = [tagstab;tstab];
ysat = [ysat,y];

```

```

Vsat = [Vsat;Vz];

end % Loop finding Pb for all p0
% _____

% Output results
format short g

% Update initial guess for P to start calculation at next temperature
Pk = max(Psat);

% Prepare output of Pb and T
Pb = [Pb;Pk];
Tb = [Tb;T];

% Psat in psia
Psatpsi = Psat*0.1450377439;

% Output mass density of liquid phase in kg/m3
molarmass = z'*prop(:,6);
rhoL = molarmass*1e-3./Vsat;

% Output mass density of liquid phase in kg/m3
molarmass = ysat'*prop(:,6);
rhoV = molarmass*1e-3./Vsat;

disp('Temperature (K)=');
T % display temperature corresponding to calculated pressures

Psat = [Psat,rhoL,rhoV,tagstab,ysat'];
Psatkpa = sortrows(Psat,1);
disp('Columns with Psat (KPa), liq. density (kg/m3), vap. density (kg/m3), abs(z-y)/z
and corresponding vapour mole fract. y');
disp(Psatkpa);
disp(Pb);

% Prepare output of rho liq. and rho vap.
[dz,eZ] = size(Psatkpa);
rhoL = Psatkpa(eZ,2);
rhoV = Psatkpa(eZ,3);
rhoLb = [rhoLb;rhoL];
rhoVb = [rhoVb;rhoV];

end % loop to update T for bubble pressure calculation

```

```

% Display results
disp('Temperature (K), Pbubble (kPa), rho liq (kg/ m3), rho vap (kg/ m3)');
Results = [Tb,Pb,rholb,rhovb];
disp(Results);
Results = [Pb];
disp(Results);
%

```

---

```

%End function bubblept

```

---

### **PREOS.m**

```

function [Zq,V,amix,bmix] = PREOS(a,b,k,x,s,Pk,T)

% Solve PR EOS with appropriate mixing rules, e.g., van der Waals mixing
% rules to obtain densities (or molar volumes = 1/density). Ideally we
% should use the same mixing rules for this estimate as that used for
% the bubble pressure calculation.

% From individual 'a' and 'b' terms obtain 'a mix' and 'b mix' by applying
% the appropriate mixing rule
[amix,bmix] = mixrule(a,b,k,x,s);

% Gas constant 8.31447(J/mole/K):
R = 8.314472; %from NIST (http://physics.nist.gov/cuu/Constants/index.html)

% Test for stable root will fail if Pk is negative
if Pk < 0
    disp('No stable root for PREOS. GTest will fail. Negative P calculated. Relax
tolerance for QNSS evaluation of lnK or increase inverse-relaxation factor or use new
initial guess for P');
    return, end

A = amix*Pk*1e3/(R^2*T^2);
B = bmix*Pk*1e3/(R*T);

c(1) = 1; % coeff for Z^3
c(2) = -(1-B); % a2, coeff for Z^2
c(3) = A-3*B^2-2*B; %a1, coeff for Z^1
c(4) = -(A*B-B^2-B^3); % a0, coeff for Z^0

% Solution method 1
Z = roots(c); % Solve for roots of CEOS

%

```

---

```

% Find real roots for case where R>0
Zss = [];
m = length(Z);

    for w = 1:m
        v(w,1) = isreal(Z(w,1));
        if v(w,1) == 1
            Zss= [Zss;Z(w,1)];
        end
    end

% Find all non-negative, real Z
Zs = [];
m = length(Zss);

for w = 1:m
    if Zss(w,1) > 0
        Zs= [Zs;Zss(w,1)];
    end
end

% Find the most stable root
% A GTEST FAILURE PROBABLY IS A RESULT OF A NEGATIVE PRESSURE
CALCULATED
% SOMEWHERE LIKELY IN THE INNER LOOP FOR PSAT IN BUBBLEP
numroots = length(Zs);
t1 = 1 + sqrt(2);
t2 = 1 - sqrt(2);
t3 = sqrt(8);

% Initial value for Zmin
Zmin = Zs(1);

for j = 1:numroots-1
    Gab = log((Zs(j+1) - B)/(Zmin - B)) - (Zs(j+1) - Zmin)+ A/(B*(t1 - t2))*log(((Zs(j+1) +
t1*B)*(Zmin + t2*B))/((Zmin + t1*B)*(Zs(j+1) + t2*B)));
    if Gab > 0
        Zmin = Z(j+1);
    end
end

Zq = Zmin; % Z corresponding to lowest Gibbs free energy

V = Zq*R*T/(Pk*1e3); % Molar volume of phase required for fugacity of phase

```

End

---

### mixrule.m

```
function [amix, bmix] = mixrule(a,b,k,x,s)
```

```
% mixrule applies the van der Waals mixing rules to calculate the mixture  
% 'a mix' and 'b mix' terms for use with the PREOS. It is invoked from  
% within propcomp.m
```

```
% _____
```

```
% van der Waals mixing rule
```

```
suma = 0;
```

```
% sumbvdw = 0;
```

```
% sumblor = 0;
```

```
% sumbgh = 0;
```

```
% sumbls = 0;
```

```
% sumbvdwlor = 0;
```

```
% sumbvdwgh = 0;
```

```
% sumbvdwls = 0;
```

```
for i = 1:s;
```

```
    for j = 1:s;
```

```
        suma = suma + x(i)*x(j)*(1-k(i,j))*(a(i)*a(j))^0.5;
```

```
    end
```

```
end
```

```
amix = suma;
```

```
% Binary mixing parameter term for combined mixing rule
```

```
% Form A
```

```
% for i = 1:s;
```

```
%     for j = 1:s;
```

```
%         l(i,j) = ((b(i) - b(j))^2)/(b(i)^2 + b(j)^2);
```

```
%     end
```

```
% end
```

```
% Form B
```

```
% for i = 1:s;
```

```
%     for j = 1:s;
```

```
%         l(i,j) = 1 - 2*(b(i)*b(j))^0.5/(b(i)+b(j));
```

```
%     end
```

```
% end
```

```
% Form C
```

```

% for i = 1:s;
%   for j = 1:s;
%     l(i,j) = abs(b(i) - b(j))/(b(i) + b(j));
%   end
% end

% Form D
% for i = 1:s;
%   for j = 1:s;
%     l(i,j) = ((b(i) - b(j))^2)/(b(i) + b(j))^2;
%   end
% end

% Form E
% for i = 1:s;
%   for j = 1:s;
%     l(i,j) = 1 - (((b(i) - b(j))^2)/(b(i)^2 + b(j)^2));
%   end
% end

% Form F
% for i = 1:s;
%   for j = 1:s;
%     l(i,j) = (((a(i) - a(j))^2)/(a(i)^2 + a(j)^2));
%   end
% end

% l = 1 - l;

% l = l.^1.5;

% l = zeros(s);

%%%%%%%%%%%%%%%%%%%%%%%%%%%%%%%%%%%%%%%%%%%%%%%%%%%%%%%%%%%%%%%%%%%%%%%% Choose a mixing
rule%%%%%%%%%%%%%%%%%%%%%%%%%%%%%%%%%%%%%%%%%%%%%%%%%%%%%%%%%%%%%%%%%%%%%%%%

% Individual mixing rules
bmix = rulevdw(b,x,s); % van der Waals
% bmix = rulelor(b,x,s); % Lorentz
% bmix = rulegh(b,x,s); % Good and Hope
% bmix = rulels(b,x,s); % Lee and Sandler
% bmix = rulesad(b,x,s); % Sadus

% Combined mixing rules
% bmix = rulevdwlor(b,x,s,l); % vdW + Lorentz
% bmix = rulevdwgh(b,x,s,l); % vdW + Good and Hope
% bmix = rulevdwls(b,x,s,l); % vdW + Lee and Sandler

```

```
% bmix = rulevdwsad(b,x,s,l); % vdW + Sadus
```

```
% bmix from van der Waals  
% sumb=0;  
% for i = 1:s;  
%   sumb = sumb + x(i)*b(i);  
% end  
% bmix = sumb;
```

```
end
```

```
% _____
```

```
function [bmix] = rulevdw(b,x,s)
```

```
% van der Waals mixing rule
```

```
sumbvdw = 0;
```

```
for i = 1:s;  
    for j = 1:s;  
        bvdw(i,j) = 0.5*(b(i) + b(j));  
        sumbvdw = sumbvdw + x(i)*x(j)*bvdw(i,j);  
    end  
end  
bmix = sumbvdw;
```

```
end
```

```
% _____
```

```
function [bmix] = rulelor(b,x,s)
```

```
% Lorentz mixing rule
```

```
sumblor = 0;
```

```
for i = 1:s;  
    for j = 1:s;  
        blor(i,j) = 0.125*(b(i)^(1/3) + b(j)^(1/3))^3;  
        sumblor = sumblor + x(i)*x(j)*blor(i,j);  
    end  
end  
bmix = sumblor;
```

```
end
```

```
% _____
```

```

function [bmix] = rulegh(b,x,s)

% Good and Hope mixing rule

sumbgh = 0;

for i = 1:s;
    for j = 1:s;
        bgh(i,j) = (b(i)*b(j))^0.5;
        sumbgh = sumbgh + x(i)*x(j)*bgh(i,j);
    end
end
bmix = sumbgh;

end
% _____
function [bmix] = rulels(b,x,s)

% Lee and Sandler mixing rule

sumbls = 0;

for i = 1:s;
    for j = 1:s;
        bls(i,j) = (0.5*(b(i)^(2/3) + b(j)^(2/3)))^(3/2);
        sumbls = sumbls + x(i)*x(j)*bls(i,j);
    end
end
bmix = sumbls;

end
% _____
function [bmix] = rulesad(b,x,s)

% Sadus mixing rule

sumbsad = 0;
coeffsad = 1/(4*2^(1/3)); % Coefficient for Sadus mixing rule

for i = 1:s;
    for j = 1:s;
        bsad(i,j) = coeffsad*(b(i)^(1/3) + b(j)^(1/3))^2*(b(i) + b(j))^(1/3);
        sumbsad = sumbsad + x(i)*x(j)*bsad(i,j);
    end
end
bmix = sumbsad;

```



```

end

%_____

function [bmix] = rulevdwlor(b,x,s,l)

% vdW with Lorentz

sumbvdwlor = 0;
for i = 1:s;
    for j = 1:s;
        bvdw(i,j) = 0.5*(b(i) + b(j));
        blor(i,j) = 0.125*(b(i)^(1/3) + b(j)^(1/3))^3;
        sumbvdwlor = sumbvdwlor + (1 - l(i,j))*x(i)*x(j)*bvdw(i,j) + l(i,j)*x(i)*x(j)*blor(i,j);
    end
end
bmix = sumbvdwlor;

end

```

```

%_____

function [bmix] = rulevdwgh(b,x,s,l)

% vdw with Good and Hope

sumbvdwgh = 0;
for i = 1:s;
    for j = 1:s;
        bvdw(i,j) = 0.5*(b(i) + b(j));
        bgh(i,j) = (b(i)*b(j))^0.5;
        sumbvdwgh = sumbvdwgh + (1 - l(i,j))*x(i)*x(j)*bvdw(i,j) + l(i,j)*x(i)*x(j)*bgh(i,j);
    end
end
bmix = sumbvdwgh;

end

```

```

%_____

function [bmix] = rulevdwls(b,x,s,l)

% vdw with Lee and Sandler

sumbvdwls = 0;
for i = 1:s;

```

```

    for j = 1:s;
        bvdw(i,j) = 0.5*(b(i) + b(j));
        bls(i,j) = ((0.5*(b(i)^(2/3) + b(j)^(2/3)))^(3/2));
        sumbvdwls = sumbvdwls + (1 - l(i,j))*x(i)*x(j)*bvdw(i,j) + l(i,j)*x(i)*x(j)*bls(i,j);
    end
end
bmix = sumbvdwls;

end
% _____
function [bmix] = rulevdwsad(b,x,s,l)

% vdw with Sadus

sumbvdwsad = 0;
coeffsad = 1/(4*2^(1/3)); % Coefficient for Sadus mixing rule

for i = 1:s;
    for j = 1:s;
        bvdw(i,j) = 0.5*(b(i) + b(j));
        bsad(i,j) = coeffsad*(b(i)^(1/3) + b(j)^(1/3))^2*(b(i) + b(j))^(1/3);
        sumbvdwsad = sumbvdwsad + (1 - l(i,j))*x(i)*x(j)*bvdw(i,j) + l(i,j)*x(i)*x(j)*bsad(i,j);
    end
end
bmix = sumbvdwsad;

end
% _____

```

### **dmix.m**

```

function [db, dnb, da] = dmix(a,b,rho,n,x,k,s)

% Get the derivative terms for calculation of Loge(fugacity coeff) and the
% Jacobian (dg/dp) based on the selected mixing rule

% _____

% da for van der Waals mixing rule (d(n^2a)/d(ni))
for i = 1:s
    sum = 0;
    for j = 1:s
        nj(j) = x(j)*n;
        sum = sum + 2*nj(j)*(1-k(i,j))*(a(i)*a(j))^0.5;
    end
    da(i) = sum;
end

```

```

end

% Binary interaction term for combined mixing rule

% Form A
% for i = 1:s;
%   for j = 1:s;
%     l(i,j) = ((b(i) - b(j))^2)/(b(i)^2 + b(j)^2);
%   end
% end

% Form B
% for i = 1:s;
%   for j = 1:s;
%     l(i,j) = 1 - 2*(b(i)*b(j))^0.5/(b(i)+b(j));
%   end
% end

% Form C
% for i = 1:s;
%   for j = 1:s;
%     l(i,j) = abs(b(i) - b(j))/(b(i) + b(j));
%   end
% end

% Form D
% for i = 1:s;
%   for j = 1:s;
%     l(i,j) = ((b(i) - b(j))^2)/(b(i) + b(j))^2;
%   end
% end

% Form E
% for i = 1:s;
%   for j = 1:s;
%     l(i,j) = 1 - (((b(i) - b(j))^2)/(b(i)^2 + b(j)^2));
%   end
% end

% Form F
% for i = 1:s;
%   for j = 1:s;
%     l(i,j) = (((a(i) - a(j))^2)/(a(i)^2 + a(j)^2));
%   end
% end

% l = 1-l;

```

```

% l = 1.^(1.5);

% l=zeros(s);

%%%%%%%%%%%%%%%%%%%%%%%%%%%%%%%%%%%%%%%%%%%%%%%%%%%%%%%%%%%%%%%%%%%%%%%% d(b*rho/dnk and d(nb)/dnk for individual mixing
rules%%%%%%%%%%%%%%%%%%%%%%%%%%%%%%%%%%%%%%%%%%%%%%%%%%%%%%%%%%%%%%%%%%%%%%%%

[db, dnb] = rulevdw(b,x,s,rho,n); % van der Waals
% [db, dnb] = rulelor(b,x,s,rho,n); % Lorentz
% [db, dnb] = rulegh(b,x,s,rho,n); % Good and Hope
% [db, dnb] = rulels(b,x,s,rho,n); % Lee and Sandler
% [db, dnb] = rulesad(b,x,s,rho,n); % Sadus

%%%%%%%%%%%%%%%%%%%%%%%%%%%%%%%%%%%%%%%%%%%%%%%%%%%%%%%%%%%%%%%%%%%%%%%% d(b*rho/dnk and d(nb)/dnk for combined mixing
rules%%%%%%%%%%%%%%%%%%%%%%%%%%%%%%%%%%%%%%%%%%%%%%%%%%%%%%%%%%%%%%%%%%%%%%%%

% [db, dnb] = rulevdwlor(b,x,s,rho,n,l); % vdW + Lorentz
% [db, dnb] = rulevdwgh(b,x,s,rho,n,l); % vdW + Good and Hope
% [db, dnb] = rulevdwls(b,x,s,rho,n,l); % vdW + Lee and Sandler
% [db, dnb] = rulevdwsad(b,x,s,rho,n,l); % vdW + Sadus

% bmix from van der Waals
% sumb = 0;
% for i = 1:s;
%   sumb = sumb + x(i)*b(i);
% end
% bmix = sumb;

% van der Waals mixing rule
%db for van der Waals mixing rule
% db = b*rho/n; % d(b*rho)/d(ni)
% dnb = b; % % dnb(d(nb)/d(ni))for van der Waals mixing rule

end

% _____

function [db, dnb] = rulevdw(b,x,s,rho,n)

% van der Waals mixing rule
% Term 1, bmix
sumbvdw = 0;

for i = 1:s;
    for j = 1:s;

```

```

        bvdw(i,j) = 0.5*(b(i) + b(j));
        sumbvdw = sumbvdw + x(i)*x(j)*bvdw(i,j);
    end
end
bmix = sumbvdw;

% Term 2, sum xi*bik
sumbvdw = 0;

for i = 1:s;
    for j = 1:s;
        sumbvdw = sumbvdw + x(j)*bvdw(i,j);
    end
    bk(i,1) = sumbvdw;
    sumbvdw = 0;
end

db = 2*(rho/n)*bk - bmix*(rho/n);
dnb = 2*bk - bmix;

% db = b*rho;
% dnb = b;

end

% _____

```

```

function [db, dnb] = rulelor(b,x,s,rho,n)

```

```

% Lorentz mixing rule
% Term 1, bmix
sumblor = 0;

for i = 1:s;
    for j = 1:s;
        blor(i,j) = 0.125*(b(i)^(1/3) + b(j)^(1/3))^3;
        sumblor = sumblor + x(i)*x(j)*blor(i,j);
    end
end
bmix = sumblor;

% Term 2, sum xi*bik
sumblor = 0;

for i = 1:s;
    for j = 1:s;
        sumblor = sumblor + x(j)*blor(i,j);
    end
end

```

```

    end
    bk(i,1) = sumblor;
    sumblor = 0;
end

```

```

db = 2*(rho/n)*bk - bmix*(rho/n);
dnb = 2*bk - bmix;

```

```

end

```

```

% _____
function [db, dnb] = rulegh(b,x,s,rho,n)

```

```

% Good and Hope mixing rule
sumbgh = 0;

```

```

for i = 1:s;
    for j = 1:s;
        bgh(i,j) = (b(i)*b(j))^0.5;
        sumbgh = sumbgh + x(i)*x(j)*bgh(i,j);
    end
end

```

```

end
bmix = sumbgh;

```

```

% Term 2, sum xi*bik
sumbgh = 0;

```

```

for i = 1:s;
    for j = 1:s;
        sumbgh = sumbgh + x(j)*bgh(i,j);
    end
    bk(i,1) = sumbgh;
    sumbgh = 0;
end

```

```

db = 2*(rho/n)*bk - bmix*(rho/n);
dnb = 2*bk - bmix;

```

```

end

```

```

% _____
function [db, dnb] = rulels(b,x,s,rho,n)

```

```

% Lee and Sandler mixing rule
% Term 1, bmix
sumbls = 0;

```

```

for i = 1:s;
    for j = 1:s;
        bls(i,j) = (0.5*(b(i)^(2/3) + b(j)^(2/3)))^(3/2);
        sumbls = sumbls + x(i)*x(j)*bls(i,j);
    end
end
bmix = sumbls;

% Term 2, sum xi*bik
sumbls = 0;

for i = 1:s;
    for j = 1:s;
        sumbls = sumbls + x(j)*bls(i,j);
    end
    bk(i,1) = sumbls;
    sumbls = 0;
end

db = 2*(rho/n)*bk - bmix*(rho/n);
dnb = 2*bk - bmix;

end
%_____
function [db, dnb] = rulesad(b,x,s,rho,n)

% Sadus mixing rule
% Term 1, bmix
sumbsad = 0;
coeffsad = 1/(4*2^(1/3)); % Coefficient for Sadus mixing rule

for i = 1:s;
    for j = 1:s;
        bsad(i,j) = coeffsad*(b(i)^(1/3) + b(j)^(1/3))^2*(b(i) + b(j))^(1/3);
        sumbsad = sumbsad + x(i)*x(j)*bsad(i,j);
    end
end
bmix = sumbsad;

% Term 2, sum xi*bik
sumbsad = 0;

for i = 1:s;
    for j = 1:s;
        sumbsad = sumbsad + x(j)*bsad(i,j);
    end
    bk(i,1) = sumbsad;

```

```

    sumbsad = 0;
end

db = 2*(rho/n)*bk - bmix*(rho/n);
dnb = 2*bk - bmix;

end
%_____

function [db, dnb] = rulevdwlor(b,x,s,rho,n,l)

% vdw with Lorentz mixing rule
% Term 1, sum xixbj
sumbvdwlor = 0;
for i = 1:s;
    for j = 1:s;
        bvdw(i,j) = 0.5*(b(i) + b(j));
        blor(i,j) = 0.125*(b(i)^(1/3) + b(j)^(1/3))^3;
        sumbvdwlor = sumbvdwlor + (1 - l(i,j))*x(i)*x(j)*bvdw(i,j) + l(i,j)*x(i)*x(j)*blor(i,j);
    end
end
bmix = sumbvdwlor;

% Term 2, sum xi*bik
sumbvdwlor = 0;

for i = 1:s;
    for j = 1:s;
        sumbvdwlor = sumbvdwlor + (1 - l(i,j))*x(j)*bvdw(i,j) + l(i,j)*x(j)*blor(i,j);
    end
    bk(i,1) = sumbvdwlor;
    sumbvdwlor = 0;
end

db = 2*(rho/n)*bk - bmix*(rho/n);
dnb = 2*bk - bmix;

end

%_____

function [db, dnb] = rulevdwgh(b,x,s,rho,n,l)

% vdw with Good and Hope mixing rule
% Term 1, sum xixbj
sumbvdwgh = 0;
for i = 1:s;
    for j = 1:s;

```



```

    bvdw(i,j) = 0.5*(b(i) + b(j));
    bgh(i,j) = (b(i)*b(j))^0.5;
    sumbvdwgh = sumbvdwgh + (1 - l(i,j))*x(i)*x(j)*bvdw(i,j) + l(i,j)*x(i)*x(j)*bgh(i,j);
end
end
bmix = sumbvdwgh;

% Term 2, sum xi*bik
sumbvdwgh = 0;

for i = 1:s;
    for j = 1:s;
        sumbvdwgh = sumbvdwgh + (1 - l(i,j))*x(j)*bvdw(i,j) + l(i,j)*x(j)*bgh(i,j);
    end
    bk(i,1) = sumbvdwgh;
    sumbvdwgh = 0;
end

db = 2*(rho/n)*bk - bmix*(rho/n);
dnb = 2*bk - bmix;

end
% _____
function [db, dnb] = rulevdwls(b,x,s,rho,n,l)

% vdw with Lee and Sandler mixing rule
% Term 1, sum xixbj
sumbvdwls = 0;
for i = 1:s;
    for j = 1:s;
        bvdw(i,j) = 0.5*(b(i) + b(j));
        bls(i,j) = ((0.5*(b(i)^(2/3) + b(j)^(2/3)))^(3/2));
        sumbvdwls = sumbvdwls + (1 - l(i,j))*x(i)*x(j)*bvdw(i,j) + l(i,j)*x(i)*x(j)*bls(i,j);
    end
end
bmix = sumbvdwls;

% Term 2, sum xi*bik
sumbvdwls = 0;

for i = 1:s;
    for j = 1:s;
        sumbvdwls = sumbvdwls + (1 - l(i,j))*x(j)*bvdw(i,j) + l(i,j)*x(j)*bls(i,j);
    end
    bk(i,1) = sumbvdwls;
    sumbvdwls = 0;
end
end

```

```

db = 2*(rho/n)*bk - bmix*(rho/n);
dnb = 2*bk - bmix;

end
% _____
function [db, dnb] = rulevdwsad(b,x,s,rho,n,l)

% vdw with Sadus mixing rule
% Term 1, sum xixbjij
sumbvdwsad = 0;
coeffsad = 1/(4*2^(1/3)); % Coefficient for Sadus mixing rule

for i = 1:s;
    for j = 1:s;
        bvdw(i,j) = 0.5*(b(i) + b(j));
        bsad(i,j) = coeffsad*(b(i)^(1/3) + b(j)^(1/3))^2*(b(i) + b(j))^(1/3);
        sumbvdwsad = sumbvdwsad + (1 - l(i,j))*x(i)*x(j)*bvdw(i,j) + l(i,j)*x(i)*x(j)*bsad(i,j);
    end
end
bmix = sumbvdwsad;

% Term 2, sum xi*bik
sumbvdwsad = 0;

for i = 1:s;
    for j = 1:s;
        sumbvdwsad = sumbvdwsad + (1 - l(i,j))*x(j)*bvdw(i,j) + l(i,j)*x(j)*bsad(i,j);
    end
    bk(i,1) = sumbvdwsad;
    sumbvdwsad = 0;
end

db = 2*(rho/n)*bk - bmix*(rho/n);
dnb = 2*bk - bmix;

end

```

---

### **logephi.m**

```
function logephi = logephi(a,b,amix,bmix,Z,V,x,k,T,Pk)
```

```

% logephi.m calculates loge fugacity coefficient of component i in a mixture of
% known composition, temperature and pressure. logephi is based on the
% Peng-Robinson EOS. The variables a, b, Z, V and x have their standard
% meanings and refer to the mixture. k is the binary interaction

```

```

% coefficients for the mixture.
%
% logephi.m is set up such that variable mixing rules can be used to calculate
% loge fugacity coefficient of the ith component.

rho = 1/V;
R = 8.314472; % Gas constant 8.31447(m3_Pa/mole_K)from NIST
(http://physics.nist.gov/cuu/Constants/index.html)

% n is a dummy variable and is the total number of moles in the mixture.
n = 1;

[s,t] = size(k); % size of k matrix; s is number of components

% _____

[db, dnb, da] = dmix(a,b,rho,n,x,k,s); % Derivative of appropriate mixing rule

% _____

% Loge Fugacity coefficient
t1 = 1+sqrt(2);
t2 = 1+t1*bmix*rho;
t3 = 1-sqrt(2);
t4 = 1+t3*bmix*rho;
t5 = (t1/t2)-(t3/t4);
t6 = t2/t4;

for j = 1:s
p1 = -log(1-bmix*rho) - log(Z) + n*db(j)/(1-bmix*rho); % This is correct
p2 = -db(j)*(amix*n/(bmix*R*T*sqrt(8)))*t5; % This is correct
p3 = -log(t6)*((da(j)/(n*bmix*R*T*sqrt(8))) -(amix*dnb(j))/(bmix^2*R*T*sqrt(8))); % This
is correct
logephi(j) = p1 + p2 + p3;
end

```

---

### **Jvx.m**

```
function viyi = Jvx(Z,V,T,k,a,b,y,x)
```

```

% This function evaluates one part of the Jacobian required for calculation
% of bubble pressures using bubblep.m In this case, the Jacobian is the
% derivative of g, the normalized distance from the tangent plane, to
% pressure

```

```

R = 8.314472; % Gas constant 8.31447(m3_Pa/mole_K)from NIST
(http://physics.nist.gov/cuu/Constants/index.html)
RT = R*T;

nt = 1; % Dummy variable representing total number of moles of mixture
Vt = V*nt; % Total volume of mixture of nt moles
rho = 1/V;

% Mixture parameters
[s,t] = size(k);
[amix, bmix] = mixrule(a,b,k,x,s);

% Derivatives of mixing rules
[db, dnb, da] = dmix(a,b,rho,nt,x,k,s);

% Calculation of partial molar volume of component i, V(i) with generalized
% mixing rule
ta = (Vt - nt*bmix); % Scalar
tb = (Vt^2 + 2*bmix*nt*Vt - nt^2*bmix^2); % Scalar
t1 = RT/ta; % Scalar
t2 = nt*RT*dnb/ta^2; % Vector
t3 = da/tb; % Vector
t4 = 2*amix*nt^2*(Vt*dnb - nt*bmix*dnb)/tb^2; % Vector
t5 = nt*RT/ta^2; % Scalar
t6 = 2*amix*nt^2*(Vt + nt*bmix)/tb^2; % Scalar

Vm1 = (t1 + t2 - t3 + t4)/(t5 - t6); % Vector

viyi = dot(y,Vm1)/RT; % scalar

% _____
% Partial molar volume for vdW mixing rules
% tta = (Vt -bmix); % Scalar
% ttb = (Vt^2 + 2*bmix*Vt - bmix^2); % Scalar
% tt1 = RT*(Vt - bmix + b)*ttb^2; % Vector
% tt2 = da*ttb; % Vector
% tt3 = 2*amix*tta*b; % Vector
%
% Vm2 = (tt1 - (tt2 - tt3)*tta^2)./(RT*ttb^2 - 2*amix*(Vt+bmix)*(Vt-bmix)^2);
% viyi = dot(y,Vm2)/RT;
% _____

end

```

**mixprop ABVB C10.m**

function prop = mixpropABVB\_C10

% Critical properties and composition of 10 molecular model representing  
% ABVB and 10 psuedo-components representing HVGO (from HYSYS). The  
% properties are molar averages computed from those estimated for  
% 60 molecular models using the Marrero-Gani group contribution methods.  
% Acentric factors were calculated from critical properties using the  
% correlation developed by Ambrose and Walton. Critical properties for  
% n-decane are taken from the DIPPR database. Function file to provide  
% critical properties (Pc, Tc, Vc, omega), z (composition of mixture) and  
% MW (molecular weights of components in the mixture). One row is used for  
% each component and rows are separated by ";" The units of each variable  
% are as follows:

% Pc: critical pressure in kPa  
% Tc: critical temperature in K  
% Vc: critical volume in m3/mole  
% omega: Pitzer acentric factor, unitless  
% z: molefraction of component  
% MW: molecular weight (g/mole)

% n-decane 10 components for HVGO and 10 components for VTB

prop = [  
2110 617.7 0.000617 0.4923 0.421626 142.282;  
1206.64910.21 0.001326 1.0306 0.002406 344.32;  
1082.17948.50 0.001506 1.1161 0.006138 393.15;  
994.63 978.34 0.001662 1.1804 0.070056 433.04;  
946.08 993.92 0.001759 1.2165 0.061024 452.79;  
846.10 1026.810.001992 1.2939 0.014107 495.94;  
751.19 1057.810.002267 1.3715 0.005703 533.30;  
684.39 1087.730.002520 1.4325 0.005503 578.79;  
618.88 1120.120.002826 1.4959 0.007842 628.68;  
570.04 1143.320.003095 1.5446 0.005826 660.03;  
507.16 1173.250.003515 1.6104 0.003263 695.72;  
865.04 1054.870.002579 0.4959 0.102259 560.39;  
810.79 1070.260.002836 0.4473 0.055352 798.96;  
860.26 1038.590.002465 0.2664 0.049246 696.84;  
815.62 1104.690.002819 0.3379 0.058326 820.22;  
770.46 1103.600.003153 0.5509 0.032236 910.05;  
778.76 1115.920.003153 0.5596 0.021768 912.78;  
692.99 1203.680.004400 0.3589 0.011538 1292.56;  
704.47 1187.590.004156 0.2690 0.009635 1218.28;  
697.52 1214.370.004401 0.4879 0.007256 1309.27;  
617.30 1522.120.012142 0.4014 0.048890 3730.88  
];

end

---

**Tmix ABVB\_C10.m**

function Texp = TmixABVB\_C10

% Temperatures for bubble pressure data of ABVB mixtures

% Mixture temperatures in Kelvin

Texp = [  
313.13;  
323.23;  
333.33;  
343.20;  
353.07;  
363.09;  
373.11;  
383.12;  
393.12;  
403.29;  
413.45;  
423.51;  
433.56;  
443.33;  
453.10;  
463.17;  
473.24;  
483.22;  
493.20;  
503.18;  
513.15;  
523.17;  
533.18;  
543.18;  
553.18;  
563.12;  
573.06;  
583.34;  
593.61;  
603.44;  
613.27;  
633.24;  
653.20];  
end